THE MELTING OF POLYMERS IN SINGLE SCREW EXTRUDERS

by Ian Ronald Edmondson

July 1973

A Thesis presented for the degree of Doctor of Philosophy of the University of London

Department of Mechanical Engineering,
Imperial College of Science and Technology
Exhibition Road,
London S.W.7.



Summary

The present work describes an experimental and theoretical investigation into the melting process that occurs in single screw extruders that are used to process thermoplastic materials.

The aim of the investigation was to develop a theoretical analysis of this melting process. This was thought desirable for three reasons; to aid in extruder design; to aid the improvement of the processibility of thermoplastics; to help to optimise the operating performance of extruders.

An experimental investigation into the melting process was carried out with the aid of an experimental extruder that was equipped with a split barrel and a set of pressure transducers. A series of screw extraction experiments were performed so that the pattern of melting could be observed and also so that the melting pattern could be correlated with the detail pressure recordings that were taken during the experiments.

The knowledge gained by observing these melting patterns was used to formulate the present theoretical melting model. The experimental results were also used to evaluate the accuracy of the subsequent theoretical predictions.

Although the experimental results showed that the pattern of melting agreed with that hitherto reported the present theoretical melting model based in this pattern differs somewhat from the usual interpretation. The main difference are the inclusion of a melt film between the solid bed and the screw root and the fact that the solid bed is allowed to accelerate.

A comparison between the present experimental results and the theoretical simulations of those experiments showed good agreement between the melting profiles but not such good agreement between the pressure profiles. In addition the experimentally observed phenomenon of solid bed break-up correlated well with the theoretical prediction of a region of high acceleration of the solid bed. Since the experimental results show fairly conclusively that solid bed break-up causes pressure cycling of periodicity between five and fifteen seconds, the ability of the model to predict the likely occurrence of such surging may be of considerable use.

Some theoretical results are presented to indicate how the theory may be used as

a tool in extruder design, in improving material processibility and in improving the operating performance of extruders.

Lastly an explanation of the occurrence of solid bed break-up is proposed. It is suggested that although solid bed break-up is in general dependent on the strength of the compacted and heated solid granular bed and on the boundary stresses on the bed it is the nature of the boundary stresses that essentially determines whether or not the solid bed fractures.

Further, the results indicate that the more Newtonian the molten thermoplastic is the more conducive these boundary stresses are to solid bed break-up, all other things being the same.

Acknowledgements

I would like to express my appreciation to I.C.I. Plastics Division for their generous financial and technical support during this project.

I would also like to thank both the Polymer Supply and Characterisation Centre of RAPRA for the materials they supplied and the thermal property measurement section of RAPRA for the data they supplied concerning these materials.

I would like to thank the staff of the Mechanical Engineering Department of Imperial College for their assistance during the course of the project, in particular S. Watts and G. Williamson.

Lastly I wish to thank my supervisor, Dr.R.T. Fenner, for his help and encouragement throughout this project.

I R Edmondson

Contents

	page
Summary	2
Acknowledgements	4
Chapter 1 Introduction	7
Chapter 2 Experimental Investigation	
2.1 Extruder Screw Geometry	14
2.2 Experimental Literature Review	17
2.3 Present Experimental Work	
2.3.1. Introduction	30
2.3.2. Experimental Apparatus and Materials	33
2.3.3. Preliminary Experiments and Experimental Procedure	49
2.3.4. Preparation and Presentation of the Experimental Results	62
2.4. Discussion of the Experimental Results	81
2.5. Conclusions	131
Chapter 3 Theoretical Analysis of the Melting Process	
3.1 Introduction	132
3.2 Theoretical Literature Review	133
3.3 Discussion of the Basic Assumptions made in the present Melting Model	143
3.4 The Derivation of the Mathematical Equations Describing the Melting Model	150
3.5 The Solution of the Governing Equations of the Model	175
3.6 Experimental and Theoretical Correlations	
3.6.1. Introduction	186
3.6.2. The Data Requirements of the Melting Analysis	187
3.6.3. Presentation of the Results	193
3.6.4. Conclusions	234
Chapter 4 Theoretical Simulations and Conclusions	
4.1 Introduction	235
4.2 Theoretical Simulations concerning Extruder Design	236

4.3 Theoretical Simulations of the effect of Material Properties on Melting Performance 249

4.4 Theoretical Simulations of factors affecting the Performance of Extruders in operation 256

4.5 Concluding Discussion 259

Plates 267

Notation 283

References 291

Appendices

Appendix A 294

Appendix B 297

Appendix C 303

Chapter 1 : Introduction

Extrusion is a forming process of great importance to the plastics industry. There are two main reasons for this. Firstly the inherent nature of thermoplastic materials lends itself to the process in that these materials have relatively low melting temperatures, 100°C to 400°C, and when molten require a relatively low force to extrude; several thousand Newtons being usually adequate. Further, the high viscosity of most thermo plastics enables the extrudate to maintain the shape imparted to it by the extrusion die until it is cooled. The second reason for the extensive use of extrusion in processing thermoplastics is the continuous nature of the process itself. This inevitably makes it economically attractive in what is essentially a mass production industry, and also one in which the cost of the raw material is relatively high, putting greater emphasis still on cheap processibility. The continuous nature of the extrusion process is valuable also in some stages of the manufacture of raw polymers.

To extrude thermoplastics optimally one needs a continuous supply of the material at the die in a processible state, that is under suitable conditions of temperature; pressure, and homogeneity. One also desires these supply conditions to be steady. If for any reason they are not then the condition known as surging arises, which manifests itself as a variation in output rate. This is undesirable as it leads to variation in product quality and can upset the smooth continuous operation of the haul-off systems.

Clearly to have a positive flow through the die there must be a positive pressure in the supplied material, the higher this pressure is, the greater will be the flow rate. To ensure adequate quality of the extrudate, if this is a processing criterion, the supply material must have thermal and physical homogeneity, a uniform shear and thermal history, and must be supplied under steady conditions. The supply temperature must be above the materials melting or softening point and below its decomposition temperature. One further requirement of the supply material is that it

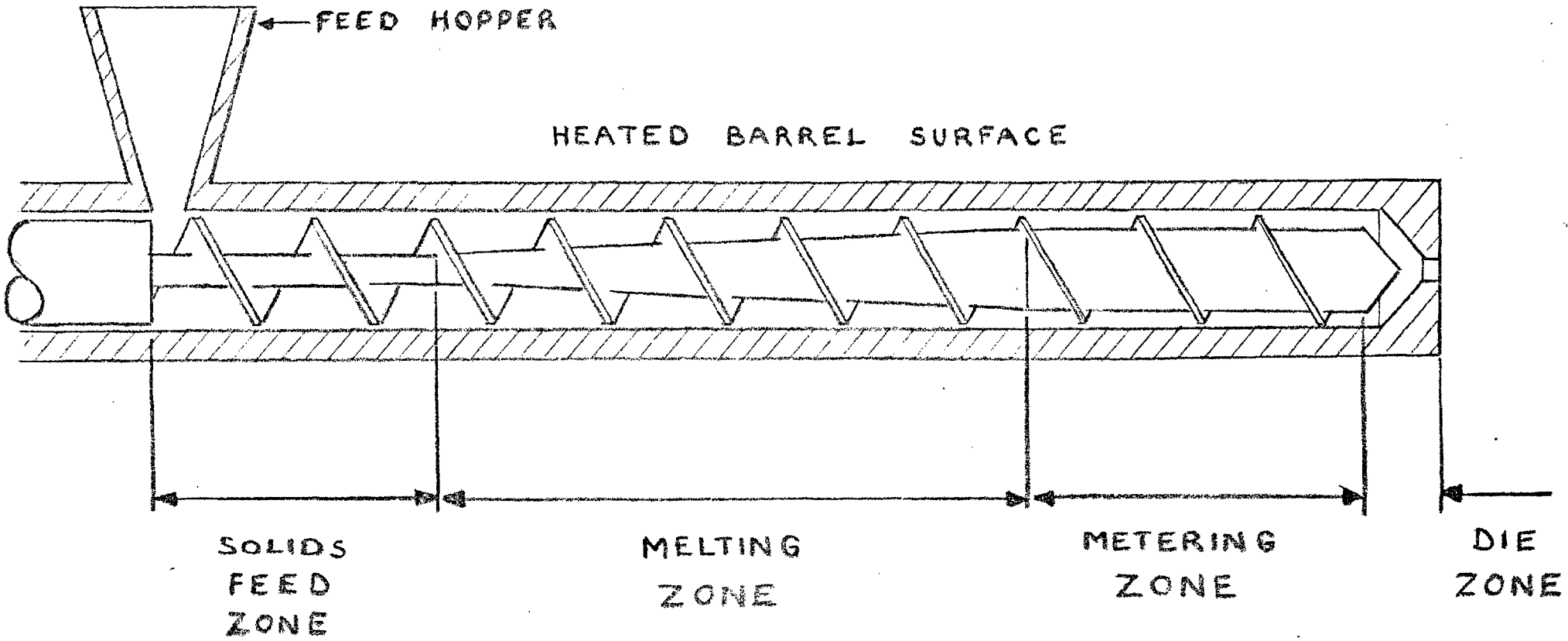


Figure 1.1

Diagram of a Single Screw Extruder.

be free from impurities of any sort. With most thermoplastics the most troublesome impurities are gaseous, either air that has become entrapped or other gases which may have been given off by the material itself.

The machine most usually used to fulfill these supply requirements is the single screw extruder, as it is normally called. In fact the extrusion process only takes place through the die, the rest of the machine is concerned with supplying the material to the die. A schematic diagram of such a machine is shown in figure 1.1. It consists of a helical screw which rotates in a heated barrel. The die assembly is fitted at one end of the barrel after the tip of the screw. The screw itself may be, in general, heated, cooled, or left neutral. The barrel is usually heated though exceptionally part or all of it may be cooled to prevent overheating which may be caused by high viscous dissipation in the molten thermoplastic. Solid material in granular or powder form is supplied through the feed hopper at the opposite end to the die. The material is transported along the screw melting or softening as it does so and becoming pressurised so that ideally the material entering the die zone fulfills the previously outlined requirements for extrusion. The increase in energy the material acquires during its passage along the screw comes from two sources; from thermal energy supplied by the barrel heaters by means of conduction through the barrel inside wall, and from the mechanical energy supplied to the screw by its drive motor. This mechanical energy is used to generate pressure in the material and to increase its temperature by transformation into thermal energy by means of viscous dissipation in the plastic when it becomes molten or softened.

The machine described briefly above is more correctly termed a single screw plasticating extruder in that it is required to melt the plastic as well as pressurise it. Another type of machine is often used in the manufacture of raw polymer, this may be called a single screw melt pump extruder. This machine differs from the plasticating extruder in that it is supplied with molten material and its purpose is to mix the polymer and pressurise it in readiness for extrusion. This type of machine is not considered in the present work.

As has been said one requires the plastic entering the extrusion die to be sufficiently molten or softened, sufficiently mixed thermally and physical, of uniform thermal and shear history, having sufficient pressure to flow through the die at a reasonably rate, and that these conditions be steady. These requirements form a basis for judging the performance of the single screw plasticating extruder, hereafter called the extruder.

There are many reasons why one would like to be able to predict how well a particular extruder fulfills these requirements. Firstly the capital cost of such machines is high and therefore a considerable amount of expense on theoretical work is economically justifiable in that once the initial theoretical simulations have been set up the cost of performing theoretical experiments is low in comparison with the cost of building a machine or part of a machine. This is the machine design incentive. Then there is the problem of material processibility. Here again it could be more economical to simulate the processing of new grades of plastics or even new types, then to perform actual experiments, which would of necessity be of limited range. Lastly theoretical simulations would be of value in optimising the processing conditions of existing materials in existing machines.

One must now look at the different parts of the single screw extruder in more detail to define more precisely what has to be analysed. Before doing so however it is useful to point out some important properties of plastic materials which are of relevance to their processing behaviour in extruders. Plastics are highly viscous, pseudoplastic or shear thinning fluids which also exhibit visco-elasticity. Their viscosity is also highly sensitive to temperature. They have generally low thermal conductivity and hence are good practical insulators. It should be pointed out that for any theoretical simulation to be of value one needs accurate information about the properties of the material.

Firstly then one can consider the die flow problem. The most important information that one needs to know is the relationship between flow rate through the die and pressure drop across it. After this a knowledge of the

temperature distribution through the plastic, and how this is affected by the flow rate, is required. This is so that one can prevent overheating of the material and help in predicting the elastic recovery of the extrudate. Clearly the final requirement is that the flow properties, in particular the elastic effects and the thermal properties of the plastic be known. In die design the elastic recovery the material undergoes on exit from the die has a significant effect on the final dimensions of the extrudate and hence must be included in the design calculations. There are several comprehensive analyses of die flow in the literature (21,22).

The rest of the extruder is usually thought of as having three distinct sections. This is a useful concept to employ at this stage. The first is termed the solids flow zone. This is characterised by the complete absence of molten material. Transport along the screw of the solid material is due to surface stresses produced by coulomb friction between the metal surfaces and the plastic. An analysis of this zone should provide information about the relationship between flow rate and pressure gradient and the thermal developement of the material. The literature provides a number of analyses of this zone (23,24,25,26).

The second section is called the transition or melting zone. This zone follows the solids flow zone and starts at the point of appearance of molten material. Usually molten material appears first adjacent to the barrel surface. As soon as this molten material appears the transport mechanism changes and viscous stresses become important. The zone ends when the material has become completely molten. Again in this zone the pressure gradient flow rate relationship needs to be known as well as the final thermal state of the material and the degree of physical mixing . One other piece of information that is of vital importance is the length of the zone and its starting point. Clearly it is essential that the end of the zone comes before the physical end of the screw. The literature relevant to this zone is considered in the next chapter.

The third section of this part of the extruder is the metering zone which

follows the melting zone, occupying the rest of the length of the screw and consisting of fully molten material. The length of the zone is obviously dependent on the previous zones. This fact stresses the importance of being able to predict the length of the previous zones. The requirements of the metering zone analyses are as before; the pressure gradient flow rate dependence, the thermal developement of the material and the degree of physical mixing that takes place. This zone of the extruder has perhaps been more comprehensively analysed than the other two and there is a wealth of literature concerning it (15,27,28,29).

Usually the screw is divided into three physical sections, a constant channel depth section starting at the feed hopper end followed by a decreasing channel depth or tapered section, which in turn is followed by another constant channel depth section. These sections of the screw do not, however, automatically correspond to the three processing zones described above. The vast majority of screws used in extruders conform to this basic pattern, though in some cases certain of these screw sections may be absent, for example, the screw may taper continuously along its whole length. In more recent years various fundamentally different screw designs have been tried with some success. In particular are these screws with mixing devices of different sorts such as smear tips, mixing rings or longitudinal flutes on the screw (30). Also the use of tapered grooves in the feed end of the barrel coupled with various mixing devices on the screw has been tried (31). However consideration of any such screw geometries does not fall within the scope of the present work which confines its attention to the more normal type of screw design.

As can be seen from the foregoing there are several different component processes which plastic materials are subject to in the rather imprecisely termed process of single screw extrusion. Of these different component processes the present work is concerned with that occurring in the transition zone; this process one may term the melting process. It is hoped that this contribution in conjunction with analyses of the other relevant processes

in the extruder will enable useful theoretical predictions to be undertaken. In addition a qualitative explanation of certain forms of surging which can be particularly troublesome in extruding plastics and which are believed to originate in the melting zone is proposed.

To be able to undertake an analysis of the melting process one needs some basic information as to how the process of phase change manifests itself in this particular environment. The importance of such a knowledge of the pattern of melting becomes more apparent later. To obtain this information one needs to perform experiments. Therefore it is appropriate now to present a review of past experiments and then to consider the present experimental contribution prior to the theoretical work.

Chapter 2: Experimental Investigation

2.1: Extruder Screw Geometry

It is important at this stage to present a thorough description of the geometry of the extruder screw and the important simplifications to this geometry that will be made use of in both the experimental and theoretical results what follow. It is also an opportunity to introduce some terminology. Figure 2.1 shows the important geometrical quantities associated with a single start screw, that is, a screw with one continuous channel only. Multiple start screws are less usual though they do occur. The present work deals consistently with single start screws only. It should be noticed that the channel width, W, the flight land width, w, and the helix angle, θ, are functions of the radial coordinate, r. The helix angle normally quoted for a screw is that at its nominal outside diameter, D, which is calculated as

$$\theta(D/2) = \tan^{-1}(P/\pi D) \qquad (2.1)$$

Where P is the pitch of the single start screw.

For a square pitch screw, that is, one in which the pitch equals the diameter, this angle is 17.6°.

The channel depth, H_c, usually varies linearly in the compression or tapered section of the screw and a coefficient of channel taper is defined as the change in channel depth per unit axial length, A, or per unit helical length measured at the mean channel depth, B.

Thus if the feed section channel depth is H_o,

$$H_c(l) = H_o - A.l \qquad (2.2)$$

where l is the axial length

or,

$$H_c(z) = H_o - B.z \qquad (2.3)$$

where z is the helical length

The channel width is expressed in terms of the pitch as

$$W(r) = P.\cos\theta(r) - w(r) \qquad (2.4)$$

Finally the relation between helical length, and axial length is

$$z(r) = l / \sin\theta(r) \qquad (2.5)$$

Figure 2.1

The Extruder Screw Geometry

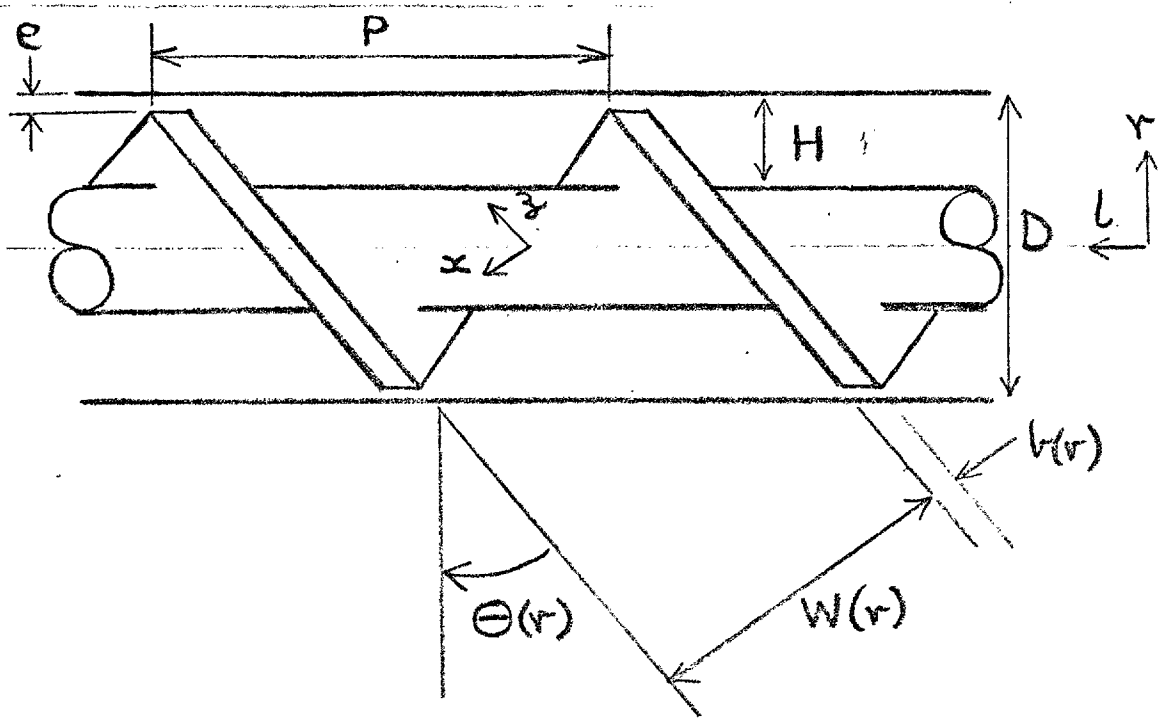
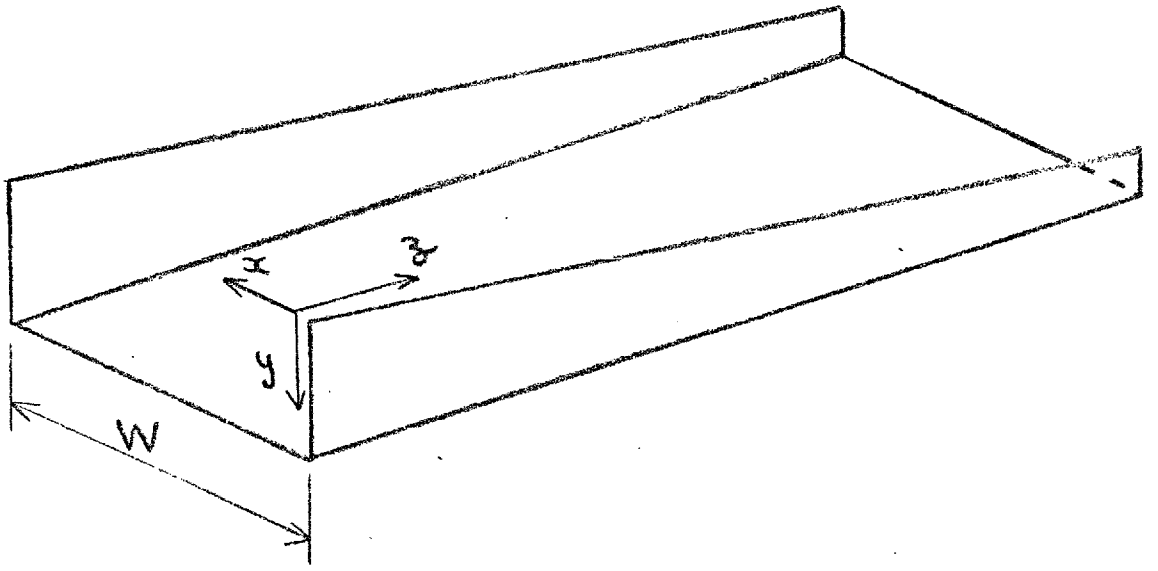


Figure 2.2

The Cartesian coordinate system for the screw channel



It is often useful to define position along the screw in terms of a number of "turns" or pitch lengths from the feed hopper. Thus the beginning of the tapered zone may be after, say,5 turns. For a square pitch screw this position is defined as

$$L = 5P = 5D \qquad (2.6)$$

The helical position may be computed from equation (2.5).

Two important assumptions will now be introduced. The first is that one may treat the system as consisting of a stationary screw and a rotating barrel rather than the actual case of a rotating screw and stationary barrel. The obvious objection to this concept is that one is thereby neglecting the effect of contrifugal forces on the radial pressure distribution. However, because plastics are highly viscous and the flow in the extruder is slow, the Reynolds number is low and the flow is laminar. In such a case this effect is reasonably insignificant.

The second assumption is that of imposing a geometrical simplification on the flow domain. The now stationary screw channel will be thought of as having been unwound into a long parallel sided channel. In other words a cartesian coordinate system is to be defined in place of the true helical coordinate one; this cartesian system is defined in figure 2.2. The channel cross-section is now rectangular and hence the width is not a function of the depth. These two assumptions are essentially made to simplify the visualisation of the flow behaviour and the mathematical formulation of the theory. A fuller treatment of these assumptions is given in Reference 15.

2.2: Experimental Literature Review

The earliest published work on the melting process was naturally experimental. The now classical cooling experiment was first performed by Maddock (2) and he was soon followed by Street (3). This experiment has formed the basis of most experimental work concerned with the melting process in single screw extruders and the technique has changed remarkably little over the years. It consists primarily of removing from the extruder barrel the screw whilst completely full of material. The technique is to run the extruder until it has settled down at the desired operating conditions and then to cool the barrel and screw as rapidly as possible after switching off the drive to the screw. The idea is to solidify rapidly the material in the screw channel for later observation. Once the barrel has been cooled to room temperature the screw is pushed out by a suitable technique, and the now solid plastic removed from the screw channel.

The two basic experimental problems involved are achieving a sufficiently rapid rate of cooling to prevent the material in the screw channel melting by the conduction of residual heat in the metal and the mechanical difficulty of over coming the surface stresses between the barrel wall and solid plastic in the screw channel.

It is usually found necessary to employ water cooling both of the screw and more importantly of the barrel to achieve a sufficient cooling rate. This was the method Maddock used. To extract the cold screw in general requires a relatively large force depending obviously on the area of contact between the barrel and the plastic. Normal extraction systems for screws are only meant to be employed to extract a screw that is essentially devoid of material achieved by running the machine with the feedstock cut off until output from the die ceases. In this case the extraction force is much reduced, the more so since the extraction may be performed at normal processing temperatures. Thus specially designed extraction systems are usually needed to perform cooling experiments with the extruder. In addition it is clear that the difficulty of performing such experiments is, approximately speaking,

directly proportional to the square of the screw diameter, all other things includung the length to diameter, L/D, ratio being the same.

The extraction force required for a particular size of extruder is difficult to estimate for several reasons. The nature of the contact between the metal and plastic is something about which little information is available and the proportion of the total area of the bore of the barrel that is bonded in this manner to the plastic is uncertain. One can calculate an upper bound on this extraction force if one assumes the strength of the plastic metal bond to be equal to the ultimate strength of the plastic and that this bond extends over the whole surface area of the barrel bore. However such a calculation yields what turn out to be ridiculously high forces and as such is of no practical use.

Thus the size of the extraction force available even in a specially designed system is a guess and is perhaps limited by, and therefore chosen because of, the restraints on the mechanical size and strength of the transmission system. For these reasons it has often been the case that the extraction force has been inadequate to extract the screw in its cold state. In such cases the normal procedure is to reheat the extruder barrel as much as is required for the extractor to function. Clearly if a lot of reheat is necessary the point in rapidly cooling the extruder beforehand is lost. Notwithstanding the foregoing it is possible to perform a hot extraction with useful results provided that the hot plastic does not adhere to the barrel surface. If this is possible it is a much simpler task in that no barrel water coolers are needed (they are not necessarily standard equipment on an extruder), and the extraction force is much reduced. Street(3) was able to employ a hot extraction procedure in his experiments with polystyrene.

Having extracted the screw with the solidified plastic around it, the material is removed and the different regions observed. The aim of this observation is to identify the areas that consisted of molten plastic and those that consisted of unmolten plastic while the extruder was operating. Normal practice is to cut thin sections out of the ribbon of plastic removed from

the screw at regular intervals along its length, normal to the flights. To aid in viewing these sections and in particular to discriminate between regions that had been solid and those that had been molten, pigment is often added to the feedstock of the extruder during the operation. The pigment may be added in one of two ways; either by obtaining a supply of granules or powder, of the particular experimental material, which has had the pigment homogenised within it during the final stage of manufacture, and then simply mixing a certain proportion of this pigmented material with the natural feedstock material, or, the raw pigment itself may be mixed by hand with the granules or powder immediately prior to being fed into the hopper of the extruder. The differences between these two pigmentation techniques will be discussed further in a later section.

That concludes the present description of the experimental technique usually employed in investigations of the melting process. As has been said Street(3) employed a hot extraction technique when working with polystyrene. He performed his experiments on a 2 inch (50.8 millemetre) diameter machine with a 20:1 L/D ratio. Maddock(2) on the other hand extracted cold, though usually he found some reheating to be necessary. The extruder he used was also a 2 inch diameter machine but having a 15:1 L/D ratio. He performed experiments with both low density polyethylene and plasticised polyvinylchloride. The sections of plastic obtained in such experiments show a pattern of compatible displacements in a single-phase stress-free system. From observation of these patterns and a knowledge of the actual thermo-mechanical boundary conditions one attempts to visualize a compatible set of displacement rates which could occur in the real two phase non-isothermal system within the extruder. The observations these two workers made of the plastic removed from the screw led to essentially similar conclusions as to the manner in which the material melted in the extruder.

A photograph of a typical cross-sectional specimen together with a schematic representation of it are shown in figure 2.3. This photograph is actually taken from the authors experimental results but serves to illustrate the

Figure 2.3

A Typical Observed Melting Pattern

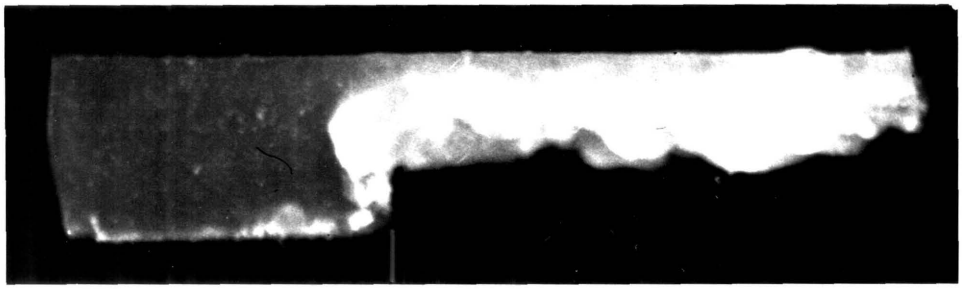
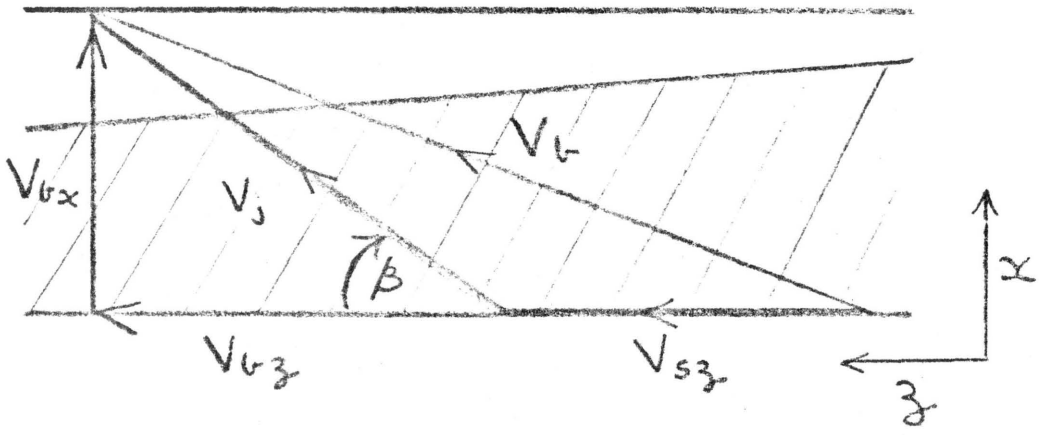


Figure 2.4

Velocity diagram for the solid bed



results of earlier work to which it is similar.

The demain can be divided into three regions shown in the figure; the melt pool consisting of re-circulating molten material between the trailing or pushing flight and the solid bed; the solid bed made up of the unmolten granules or powder situated between the leading flight and the melt pool; and the melt film which is a thin layer of molten material between the upper surface of the solid bed and the barrel. Street (3) observed a fourth region; part of the solid bed adjacent to the melt pool differed from the remainder of the solid bed in that the granules had become softened and had partially fused together. In addition Street noted that melting occurred at the interface between the melt pool and this region of the solid bed. Other experimenters including Maddock (2) have not mentioned this fourth zone and study of published cross-sectional photographs, see for example Tadmor (5) or Martin(9), do not seem to support Streets original observation. It may well be that this subdivision of the solid bed into two regions was a consequence of a lack of compaction of the solid bed due to the constant pitch, constant channel depth screw used by Street. Certainly all the other published experimental results with one exception (13) have come from extrusion trials using tapered screws, albeit of different designs. Maddock (2) noted one other secondary aspect of the pattern. At later stages of melting he observed a film of material between the screw root and the solid bed, and between the leading flight and the solid bed, forming a circulating flow path around the solid bed.

This then was the observed pattern of melting. The qualitative explanation of the mechanism which resulted in this observed pattern was given as follows. Melting essentially takes place by the solid plastic receiving, from the hot barrel surface, conducted heat, which originates from the barrel heaters. Initially the molten material will form a layer coating the barrel surface and in addition filling in the gaps between the solid granules. As soon as the first molten layer is formed shearing within it leads to the conversion of mechanical energy by viscous dissipation. The presence of this extra thermal energy within the melt film will in general increase the thermal gradient at

the interface of the melt film with the solid bed and hence increase the rate of melting at this interface. When the thickness of the film becomes greater than the flight clearance the trailing flight will act as a wiper and this action leads to the collecting of the molten plastic in the melt pool. Thus the mechanism consists of material melting off the top of the solid bed being entrained in the melt film and then discharging into the melt pool; the melt pool increasing in width at the expense of the solid bed width until the whole channel is full of molten material.

Experimental results obtained by Martin (9) show partial agreement with this melting mechanism. Martin employed a cold extraction technique though it appears that the extruder barrel was air cooled, and hence cannot have been particularly rapid. He carried out experiments with one short and one long compression screw on low density polythylene granules and powder. His results show agreement with the model of Maddock and Street during the early stages of melting. With the short compression screw and granular material the rapid compression section caused the solid bed to fracture with the result that individual granules or groups of granules were dragged along in the melt. However the behaviour of the powder material agrees with the previously stated model even after the compression zone. With granular material processed on the long compression screw the results agreed with the model until the width of the melt pool was between 30% and 50 % of the channel width. At this point the solid bed underwent a gross deformation, spreading itself across the channel, and molten material appeared all around the granules.

Perhaps the most comprehensive set of melting experiments reported to date is that of Tadmor et al (5,8,15). They carried out a series of experiments on a 2.5 inch (76.2 millemetre) diameter extruder having a 26.1 L/D ratio. The machine was not fitted with barrel water cooling jackets but a system of water jets was arranged around the barrel to cool it reasonably quickly. Most of the experiments were performed with low density polyethylene granules under a variety of operating conditions. However individual experiments were also performed with polypropylene, high density polyethylene, rigid polyvinylchloride (PVC), Nylon , and acrylonitrile butadiene styrene (ABS).

Additionally experiments were performed with plasticised PVC on a 3.5 inch (88.9 millemetre) diameter extruder and with low density polyethylene on an 8 inch (203.2 millemetre) diameter extruder.

These experiments were primarily performed to obtain results with which to test the accuracy of the melting theory that Tadmor (4) had developed. For this reason the information concerning the experimental conditions and the particular materials used is much more comprehensive than for other reported melting experiments. Also, because of this primary function of the experiments some interesting features which the plastic cross-sections show that differ from the simple model were not discussed in the original publication (5). The first of these being the presence of a melt film around three sides of the solid bed as noted earlier by Maddock (2). In some cases towards the end of melting the film between the solid bed and screw root increased in thickness and could no longer be considered a thin film. The second feature of note is the regular occurrence of a phenomenon called solid bed break-up or fracture. At some point during the melting zone the solid bed can be seen to fracture in the plane of the channel cross-section. There is thus a series of separate pieces of solid bed at different locations along the channel, separated by parts of the channel totally full of melt. These separate pieces of solid bed would appear to melt by the same mechanism as that applying before fracture occurs.

This solid bed break-up shown in the results of Tadmor et al (5) is not the same as that observed by Martin (9) which was referred to earlier. The fracture of the solid bed in the latter's experiments was produced by the short compression section of the screw and in effect the metal wedge formed by the barrel and screw root continuously separated the bed into small segments. In the former's experiments the break-up of the solid bed does not appear to be caused directly by screw taper, which in this case, is gradual extending over about ten "turns" of the screw. Further, the occurrence of this break-up is periodic.

Overall the results of Tadmor et al (5) agree with the earlier work of

Maddock and Street and that proposed melting mechanism can be applied to them with the differences mentioned above.

As these experimental results were to be used to check with theoretical predictions, certain relevant measurements were made. The most important was the measurement of the ratio of mean solid bed width to channel width at regular intervals down the channel. From these figures a graph was drawn of this ratio, called the reduced solid bed width, against channel position, usually for convenience expressed in terms of the number of "turns" along the screw. These curves were termed experimental solid bed profiles and were compared to solid bed profiles predicted by the melting theory.

The extruder used to perform these experiments was equipped with a series of pressure transducers at a range of locations along the barrel. With these, records of the operating pressures were made. Again these were later used to check theoretical predictions of pressure in the melting zone (8).

Additional experiments were reported for which pressure records were made but no cooling experiment performed (8,15), these included a series on an 8 inch diameter extruder.

Donovan (10) reported a series of experiments performed on 2.5 inch (76.2 millemetre), 4.5 inch (127 millemetre) and 8 inch (203.2 millemetre) diameter extruders. The plastics used were low density polyethylene, PVC, ABS and polypropylene. As with the previously described experiments, these by Donovan were primarily intended to check theoretical predictions. For this reason pressure measurements were taken at several points along the barrel (12).

Although Donovan has not published any photographs of his experimental cross-section he confirms that during the earlier stages of melting the observed pattern supports the proposed mechanism. However as with Tadmors results he notes the appearance of melt films, on the sides of the solid bed in contact with the screw, at a later stage of the melting process. In addition he comments on the regular occurrence of solid bed break-up.

Donovan presented a new piece of experimental information of great significance, namely evidence of acceleration of the solid bed in the down channel direction.

Figure 2.4 shows a plan view of part of the unwound screw channel. V_b is the barrel velocity and its direction is at an angle Θ, the helix angle, to the channel wall, having components V_{bx} and V_{bz} in the x and z coordinate direction respectively. The velocity of the solid bed is V_{sz} in the z direction. The relative velocity between the barrel and the solid bed is V_j at an angle β to the channel wall. Clearly if the solid bed is not moving then β becomes equal to Θ. The maximum value of β is likely to be $\pi/2$ at which V_{sz} becomes equal to V_{bz}. Donovan observed smear lines on some of his experimental specimens, the angle of which he was able to measure. These measured smear angles were an indication of the angle β defined above. Donovan observed that these smear angles increased as the solid bed moved further along the screw indicating acceleration of the solid bed.

There is one difference in the form in which Donovan presents his experimental solid bed profiles. Instead of measuring the ratio of mean solid bed width to channel width he measured the ratio of the area of the solid bed to the channel cross-sectional area at each section, thus taking into account any significant amount of molten material between the solid bed and the screw. Either approach is valid provided any theoretically predicted profiles are expressed in a consistent fashion.

Vermeulen et al (13) obtained results from a short series of cooling experiments on a 60 millemetre diameter 15:1 L/D ratio extruder. The screw used here was a constant pitch and constant channel depth design and the material was low density polyethylene. The results as with those of Donovan and Tadmor, showed agreement with the basic model of Maddock and Street up to approximately half way through the melting process. Thereafter appeared a molten film between the solid bed and the screw root and the solid bed fractured.

Tadmor and Klein (15) discussed the occurrence of solid bed break-up in the experiments reported in the work of Tadmor et al (5) and which have been previously described. They noted the regularity of the phenomenon and that the severity of it seemed to be much influenced by the material, granule size and screw geometry rather than the operating conditions. They also noted

that bed break-up could explain the temperature fluctuations observed in the screw mounted thermo-couple probes of the experiments of Marshall et al (18). The alternating of solid plug and melt plug passed the probes was suggested as the cause of these fluctuations. The passage of a melt plug passed the probe was recorded as a period of rising temperature and the passage of the solid plug as a period of falling temperature. Tadmor and Klein also proposed that pressure and output surging of frequency 1 to 15 cycles / min was due to bed break-up.

Comment was also passed on the beneficial effect of screw cooling on stability of pressure and output rate. Maddock (2) first reported results that showed that screw cooling could prevent bed break-up and Tadmor and Klein suggested this to be the reason for lack of surging.

Maddock (30) observed pressure variations along the length of the extruder in experiments performed with a negative pressure gradient in the metering zone. He suggested that surging arose as a result of excessive pressure developement in the feed and transition zones and a resultant tendency to over supply the metering zone.

A recent paper by Klein (19) dealt in more detail with surging and its relationship with themelting process. He made a distinction between two forms of bed break-up . The first he described as being due to excessive rapidity of taper such that the solid bed is deformed to fill an increased area of the channel cross-section with the result that it tended to jam and block the channel. The channel only became unblocked after sufficient pressure had been generated behind it to cause the bed to fracture and the broken piece to move forward down the channel. The second form of bed break-up Klein described, what he termed "melting instability", is essentially that phenemenon that has been described as bed break-up in the present review.

Bed break-up was also observed in a series of model experiments reported by Stevens(20). These were performed utilizing a transparent extruder barrel made of polymethylmethacrylate (PMMA) and a model fluid. He recorded the fact that bed break-up occurred only after the solid bed had become surrounded

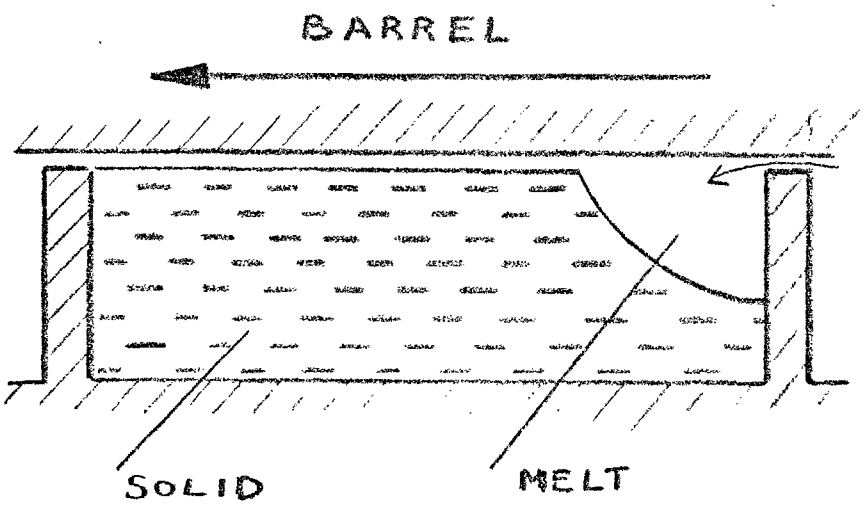
by melt. However he did not connect this phenomenon with surging.

Rousselet (16) carried out a number of novel experiments using a 60 millemetre diameter 20:1 L/D ratio extruder. The materials were powder PVC, crystal polystyrene and a PVC / vinyl acetate copolymer. The method of extracting the screw was unusual. Instead of the normal procedure of pushing the screw out of the die end of the barrel, he employed a longitudinally split barrel. In other words the barrel was opened up after the experiment and the screw lifted out. It is not clear what form of barrel cooling was used in these experiments. Rousselet reports agreement with the earlier findings of Maddock and Street. He also gives a detailed explanation of the nature of the pressure traces obtained in his experiments. The particular pressure transducers used were of a sufficiently fast response time to allow the recordings to show the variation of pressure that occurred within one revolution of the screw. Discussion of these results in the light of the present experimental work will be given in the appropriate section later.

Cooling experiments reported by Menges and Klenk (6) on rigid PVC powder showed a completely different melting pattern from anything observed elsewhere. This pattern is shown schematically in figure 2.5. Essentially "melting" of the PVC only takes place between the flight land and the barrel. Powder is dragged into this gap and is intensely sheared as it does so and becomes "molten". Clearly this is a very slow process and rarely can all the material become molten by this means. The remaining solid bed becomes compacted and sintered but the results showed a considerable proportion is not mixed at all by the time it gets to the end of the screw. Menges and Klenk concluded that the PVC did not follow the pattern of Maddock and Street because it was a highly viscous non-wetting plastic. However a subsequent paper by Gale (32) which reports cooling experiments on rigid PVC powder, has shown that the melting pattern of rigid PVC powder is highly dependent on the lubricant used and its concentration. The melting pattern of Maddock with melt films all around the solid bed was observed for rigid PVC by Gale if a suitable choice of lubricant was made.

Figure 2.5

Diagram of the trailing flight melting mechanism



This concludes the literature review of the experimental work. The general conclusion to be drawn is that the basic pattern first observed by Maddock would seem to apply fairly generally during approximately the first half of the melting process. Thereafter it can become modified in a number of ways. The following sections describe the present experimental work and discuss the present results and how they agree or not with the work discussed in this section.

2.3 Present Experimental Work

2.3.1: Introduction

Experimental investigations into the melting process occurring in single screw extruders can have three primary functions, not entirely connected. Firstly, experiments can yield information which gives insight into the physical mechanism of the process. Into this category falls the work of Maddock (2), Street (3), Menges and Klenk (6), Gale (32), and Martin (9). Secondly, the effects of different extruder operating conditions and screw geometry on the melting process can be studied in what is essentially an empirial fashion. Typical examples of this are Maddock (2) and Martin (9). Thirdly, experiments can provide sets of results which can be compared with the predictions of a theoretical analysis of the melting process. The work of Tadmor et al (5), Donovan (10) and Vermeulen et al (13) comes under this heading. The second and third functions are perhaps served by experiments which set out to imitate practical operating conditions. The first function, however, may also be served bydeliberately operating the extruder under extreme conditions which would never be used in practice.

The present experimental work was undertaken with the aim of fulfilling functions one and three but not two. It was thought necessary to do basic experiments on the nature of the melting mechanism for two reasons. Firstly early experience of the author of performing cooling experiments with rigid PVC powder produced results which were not consistent with the Maddock model. Unfortunately these experiments were performed on an extruder set up that did not permit the ideal experimental technique of a cold extraction, nor was the machine equipped with instrumentation above that normal for a production machine. In particular there were no pressure transducers or gauges and no barrel water coolers. Hence there was an incentive to repeat the experiments with an experimental extruder specifically designed to perform cooling experiments. In addition to this, other early cooling experiments performed by the author had shown that the mechanism of extraction of the screw by pushing it out of the end of the barrel furthest from the feed hopper could, if reheat of the barrel was necessary, produce a set of thermo-mechanical

boundary conditions on the material in the screw channel that partially simulated those thermo-mechanical boundary conditions occurring during operation of the extruder. Hence there could be produced a melting pattern during the extraction process that was not there during operation of the extruder. The potential effect of this was twofold. Firstly the part of the channel that was, during operation, completely full of solid could become molten to a certain extent during extraction. Secondly the region where melting was taking place during operation of the extruder could melt even more during extraction. The overall effect being to distort the true melting region and perhaps, though less likely, the pattern of melting.

At the time of setting up the present experimental extruder the paper by Rousselet (16) had not been published. Therefore there had not appeared any detailed examination of the pressure variation across the width of the channel in the melting region and it was thought important to perform such a study to aid in the visualization of the melting mechanism.

These then were the reasons for wishing to perform some fundamental experiments into the melting process. As has been stated earlier the eventual aim of the present work is to produce a theoretical analysis of the melting process. Therefore some detailed experimental results would be useful to compare with the theoretical predictions. It would, of course, have been possible to utilise the already available experimental results of Tadmor et al (5) to this end as has been done before (11). However it was thought preferable to produce a new set of such results.

In the first place it was thought possible to combine the requirements of both the functions of the present experimental work into one comprehensive set of experiments. Secondly the results produced by Tadmor et al (5) have a number of limitations. In the first place the majority of the experiments were performed with low density polyethylene granules, only single experiments being performed with other materials. Further, although a seemingly wide range of operating conditions were chosen for the different runs with the polyethylene they all, in a non-dimensional characterization proved to be similar. In every experiment bar one the non-dimensional flow rate,

π_Q, as evaluated in the melting zone, was greater than one half, and the non-dimensional pressure gradient in the metering section, π_P, negative, that is

$$\pi_Q = Q/(W \cdot H_c \cdot V_{bz}) > 0.5 \qquad (2.7)$$

where Q is the dimensional volumetric flow rate and,

$$\pi_P = \frac{\partial p}{\partial z} \cdot \frac{H_c}{\bar{\tau}} < 0 \qquad (2.8)$$

where $\bar{\tau}$ is the shear stress at the mean shear rate V_{bz}/H_c .

The reason for this similarity may well be the particular screw design employed.

The last reason for performing a completely new set of melting experiments is that one vital part of the data required for a theoretical simulation is that relating to the thermal and flow properties of the material being used. The information concerning these properties that Tadmor et al (5) supplies appears to be primarily based on information received from the material manufacturers and the accuracy of it is not quoted. In other words the data used was at best based on bulk average measurements. It was thought desirable and possible to perform at least some of the contemplated experiments with material for which the flow and thermal data could be obtained by measurements made on samples out of the same bags of material that were used in the extrusion experiments.

Then there were the reasons for extending the scope of the experimental work to fulfil the first and third functions mentioned earlier. No attempt was made to fulfil the second function as one of the overall aims of the work presented here is to be able to perform theoretical simulations to take the place of such empirical expermentation.

Such then is the background to the present experimental work. The following section describes the specific experimental equipment used in performing the experiments. It also discusses the choice of experimental materials and the particular range of operating conditions employed.

2.3.2: Experimental Apparatus and Materials.

From the literature it can be seen that several techniques have been employed to follow the melting process in the single screw extruder. These may be divided into two basic methods; direct and indirect. The direct methods are by means of the cooling experiment (2,3,5,9) or by employing suitable viewing windows in the extruder barrel (9). The indirect methods consist of interpreting either detailed pressure traces taken from barrel mounted transducers (16) or interpreting detailed temperature traces taken from thermo-couple probes mounted on the screw but reading the temperature of the plastic rather than that of the screw (18).

All these methods in one form or another have been employed previously. However the only one which is usually sufficient when employed on its own is the cooling experiment. This is because it provides a continuous record of the melting process where as the others at best only give a representation of the process at discrete intervals. In addition the cooling experiment gives a three-dimensional representation whilst the others only provide a two-dimensional one. The main disadvantage of the cooling experiment as compared to the other methods is that it involves a lot of extra work and hence time, in performing each experiment. It also can involve the design of special apparatus. However it was felt that the extra effort involved in performing such experiments was justified in the light of the previous comments on the validity of the hitherto observed melting patterns.

Having decided to design the extruder set-up for cooling experiments it was not thought worthwhile to equip it with screw mounted thermo-couples. This decision was taken on two counts. Firstly it was thought that having decided to perform cooling experiments the information concerning the melting mechanism provided by such thermo-couples was virtually redundant. Secondly the equipment and the modifications required to so equip the extruder would have been considerable.

Experience of fitting viewing windows into extruder barrels is limited and little of what has been done has been reported in any detail in the literature.

In the context of the overall aims of this work it was not thought that the results obtainable from developing a system of optical viewing probes for the extruder barrel would be adequate return for the time and effort involved. It was, however, thought desirable to equip the extruder barrel with pressure transducers. One reason for this has been mentioned, namely to attempt to provide correlation between the cross-channel pressure profile and melting pattern to confirm the interpretation of melting patterns from such pressure profiles. Secondly, of course, this enables axial pressure profiles to be obtained which are of importance in the theoretical comparisons. Lastly a study of pressure recordings over longer periods of time than the periodicity of the screw rotation is a good way of studying and characterising surging behaviour in extruders.

The extruder that was to be used to perform the experiments was a 1.5 inch (38.1 millemetre) diameter Bone Brothers machine with a 20:1 L/D ratio. A specially built screw extractor was available for this machine powered by an electric a.c. motor.

In view of the suspicion of the extraction technique discussed in the previous section it was decided to build a new barrel for this extruder that could be split into two halves thus allowing the screw to be removed from the barrel without it being subjected to heat or shear forces. At the time this barrel was designed the existence of Rousselet's split barrel extruder (16) was not known. The barrel was also equipped with six transducer ports and nine thermo-couple mounting holes to measure the barrel temperature. The drawings of the barrel are reproduced in figures 2.6 and 2.7, whilst figure 2.8 gives two illustrations of it.

It was also necessary to obtain water cooling jackets for the extruder; it was already equipped with facilities to water cool the screw. The barrel heaters were split into two control zones only, each occupying about half of the overall length. This made it easy to fit water coolers. These consisted of copper cooling tubes cast into an aluminium jacket that fitted round the extruder barrel. Provision was made in these jackets for the various pressure and thermo-couple ports. They were cast in two pairs, one pair for each

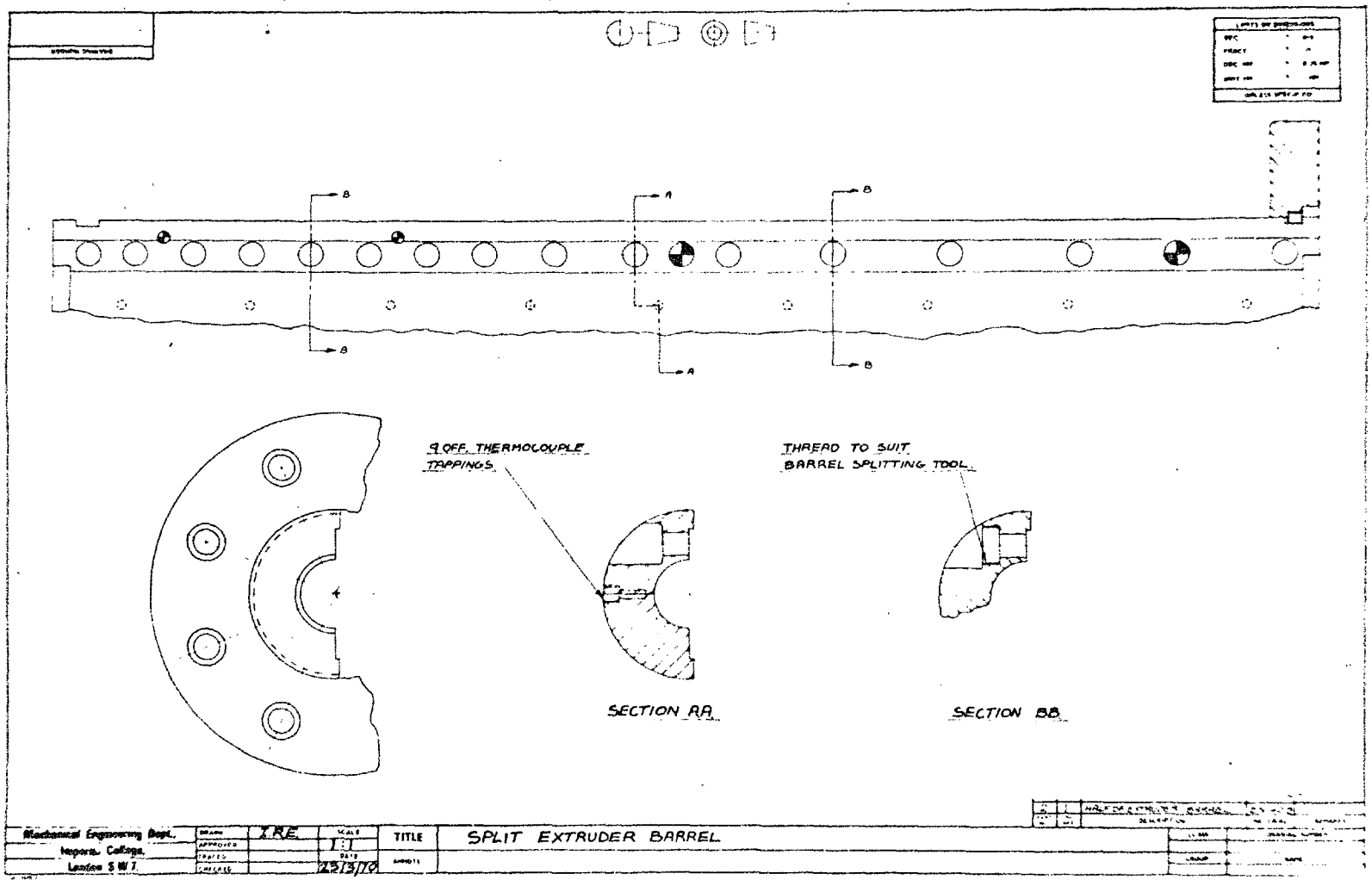


Figure 2.6

Drawing of the 'upper' half of the split extruder barrel

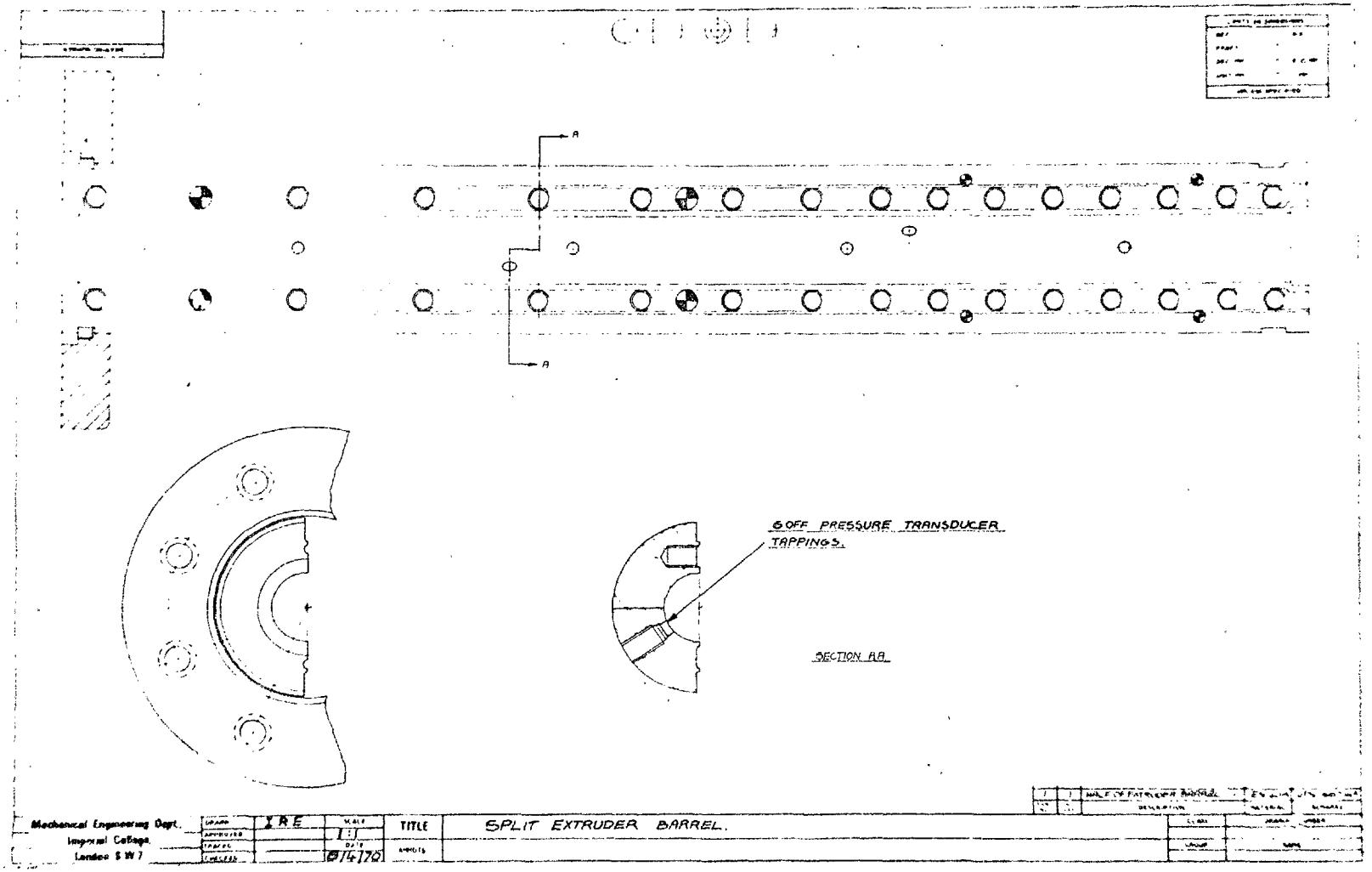
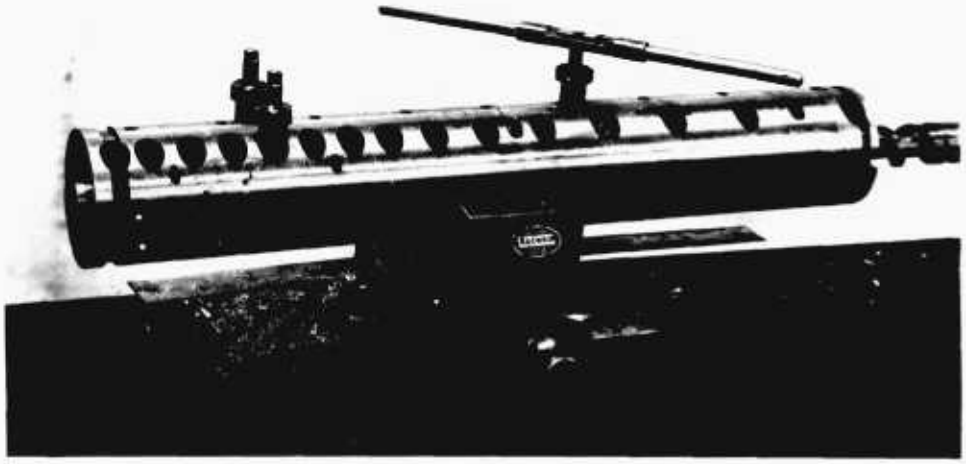


Figure 2.7

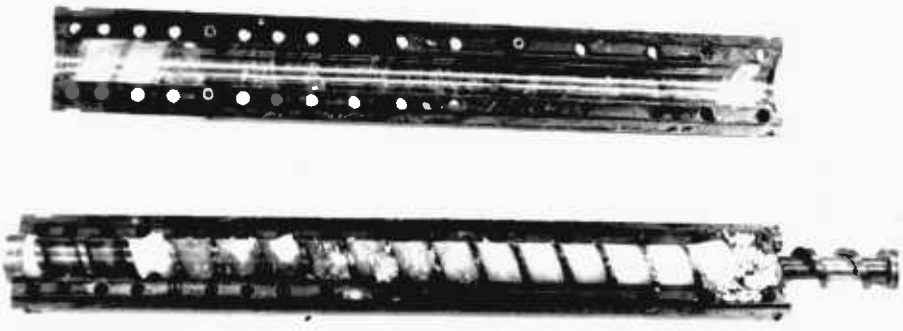
Drawing of the 'lower' half of the split extruder barrel

Figure 2.8

Two views of the split extruder barrel



(a) Showing the splitting tools in use



(b) Showing the two split halves

heating zone of the barrel. New electrical resistance heaters were obtained to clamp around the outside of the coolers.

The two heater zones of the barrel were controlled by thyristor units. The water jackets were not used as part of the barrel temperature control system, the original air fans being more than adequate, but only for rapid cooling of the barrel as required by the cooling experiment technique. The head and die assembly were fitted with a separate heater and conventional proportional control unit. No provision for cooling these units was made as they could be relatively easily removed from the barrel as indeed they had to be before the screw could be removed.

The head unit was fitted with a grease filled bourdon pressure gauge which by virtue of its direct reading of pressure gave a quick visual check to the state of operation of the extruder.

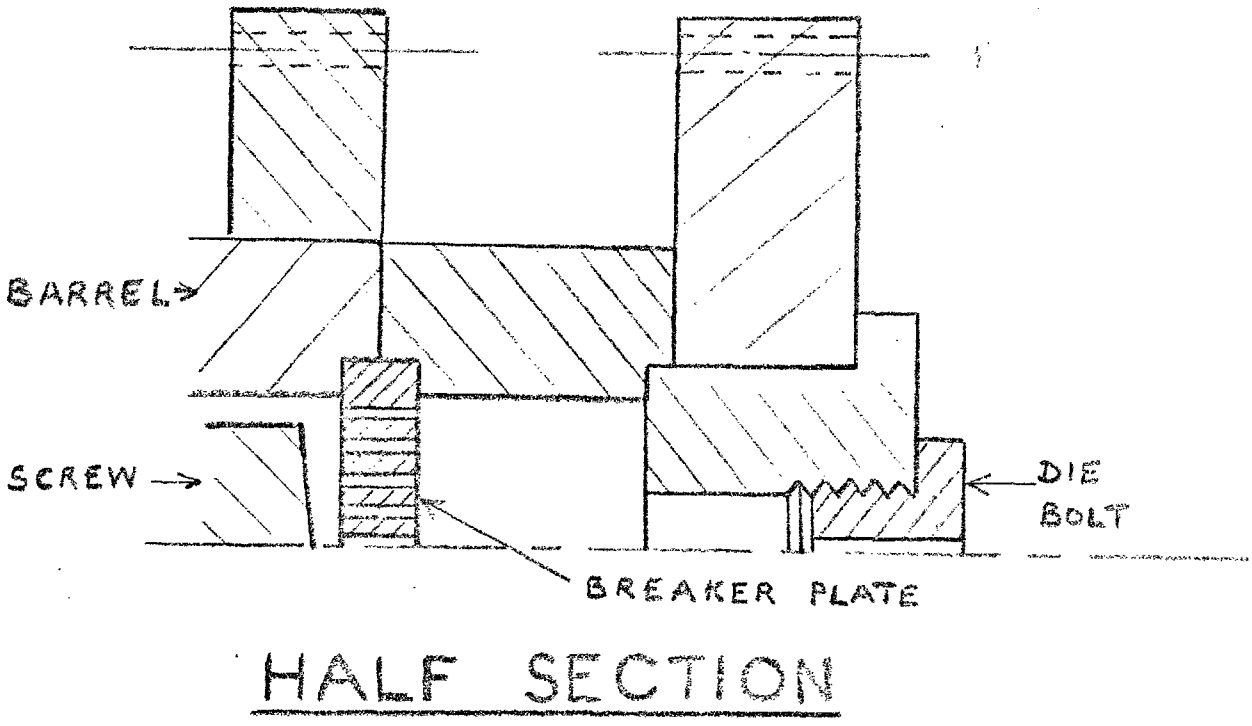
The die used on this machine was of the utmost simplicity. The layout is shown diagrammatically in figure 2.9. The essential part being a bolt with a drilled hole down the centre which was screwed into the main die assembly. This system allowed for a variety of back pressures to be generated in the machine by simply changing the die bolt for ones of different diameters.

The extruder control panel provided information about the motor current, motor speed, which was continuously variable between 24 r.p.m. and 84 r.p.m., and the barrel and head unit control temperatures. The barrel thermo-couples not used as part of the controlling system were conected via a Data Transfer Unit (DTU) into a Digital Volt Meter (DVM) which was equipped with a visual display panel. A small printer was connected to the DVM to enable a permanent record of the millevolt readings from the thermo-couples to be made. The purpose of the DTU was to control the cycling of up to 20 different input channels into the DTU, and to control the frequency of operation of the printer.

Dynisco pressure transducers were used on the extruder barrel. These are American made units that have several important advantages over comparable British made units, although their cost is about twice that of a British transducer. The principle of operation of most pressure transducers intended for

Figure 2.9

Diagram of the die assembly.



use in plasticating extruders is essentially the same. The tip of the transducer is in contact with the plastic by virtue of being mounted flush with the barrel wall. The pressure of the material causes the cap to deform. This deformation is then transmitted within the stem of the transducer to the bulb where it produces a strain in a strain gauge which is one of four resistances arranged in a Wheatstone Bridge network. The outcome of this straining is an e.m.f. which is essentially proportional to the applied pressure. In the case of the Dynisco transducers the deflection of the cap is transmitted to the strain gauge by a thin capillary of mercury. The usual alternative to this is a thin metal tube providing a mechanical link. The advantages of the Dynisco units are as follows. The shift of its zero point is much less sensitive to changes of surrounding temperature, that is, the extruder barrel, than other units. In addition to this it does not require any air or water cooling for the strain gauge bridge. It can withstand mechanically a 200% full scale overload, although the readings are not accurate at this level. It has the smallest cap diameter that is available, 0.303 inch (7.7 millemetre), though this is not to imply that it is the only make with this particular cap diameter. This last point is all the more important when dealing with such a comparatively small diameter machine as the present one. Lastly this type of transducer employs, along with some other makes, a bonded strain gauge bridge, which gives an extra degree of robustness to it. This is important for the particular experimental work envisaged in that the transducers will have to be handled much more than perhaps would be usual due to the frequency of removal of the screw from the extruder. One final practical point in the authors experience is that, provided the mounting ports for the transducers are made to the specified tolerances then complete interchangeability between different transducers and different ports presents no problems. Figure 2.10 shows a schematic outline of the experimental extruder indicating the relative positions of the transducer ports, the thermo-couple probes and the heating zones. In addition the geometry of the two experimental screws is shown. The 2.25:1 compression ratio screw was used for the experiments with PVC, all the other experiments being performed on the 4:1 compression

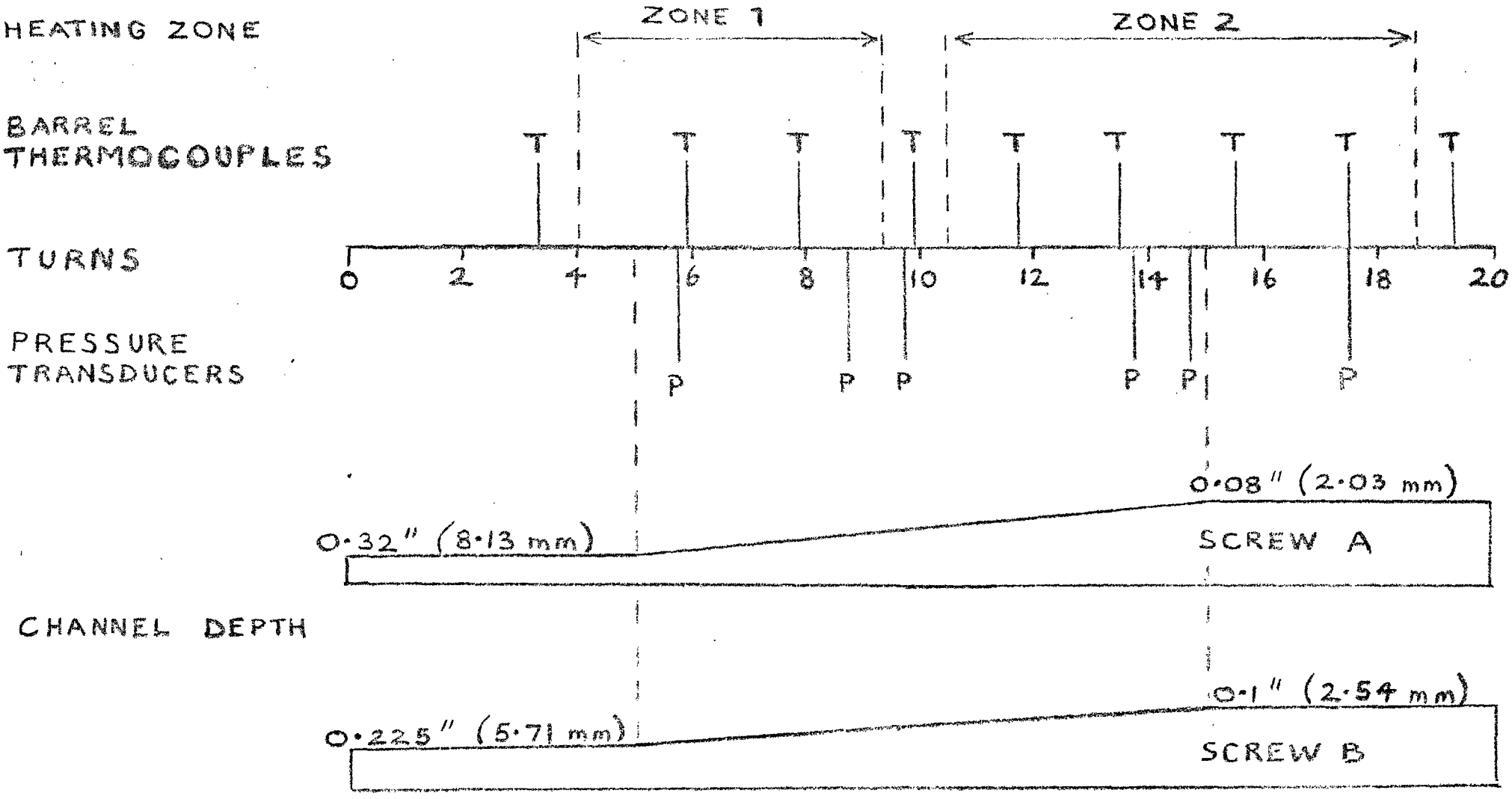


Figure 2.10

Diagram of the experimental extruder and screws showing the positions of the various instrument and control equipment.

ratio screw. The compression of a screw is defined as the ratio of the channel cross-sectional area in feed zone to that in the metering zone.

To make best use of the ability of the transducers to follow the changes of pressure that occur within each revolution of the screw an Ultra-Violet (UV) chart recorder was used. This type of recorder employs a beam of ultra-violet light that is directed by the rotation of a galvanometer mirror on to suitable sensitive chart paper. The movement of the galvanometer mirror is dependent on the input signal. The movement of the chart paper is controlled over a more than adequate range of speeds by an electric motor and gearbox.

This type of recorder was prefered to a pen-type chart recorder for several reasons. Firstly and perhaps, most importantly, the fastest full scale response time of the best pen systems is no less than perhaps 0.5 seconds which is barely adequate to follow the detailed changes of pressure that may occur. In addition a pen recorder tends to be a messy machine especially if several channels are used on one machine. A U.V. recorder may have anything from 12 to 20 channels whereas more than 6 on a pen recorder is exceptional. Finally the U.V. recorder is no more expensive than a pen recorder or set of them with the same number of channels.

Although it is possible to connect the output of a transducer to the U.V. recorder input directly, it is more flexible to insert an amplifier between the two. This enables one to use galvanometers of faster response time in the U.V. recorder and to have a separate control over the amplitude of the pressure variation as recorded on the chart paper. This is due to the variable gain control fitted to the amplifiers.

A view of the instrumented extruder, control cabinet and recording equipment is shown in figure 2.11.

Figure 2.12 shows the screw extractor on its own and as it appears fitted to the extruder ready for operation.

The extractor consists of a threaded bar whose length is approximately the same as the extruder screw. This bar is driven axially forwards or backwards by a gear wheel which is threaded on its internal surface to mesh with the thread

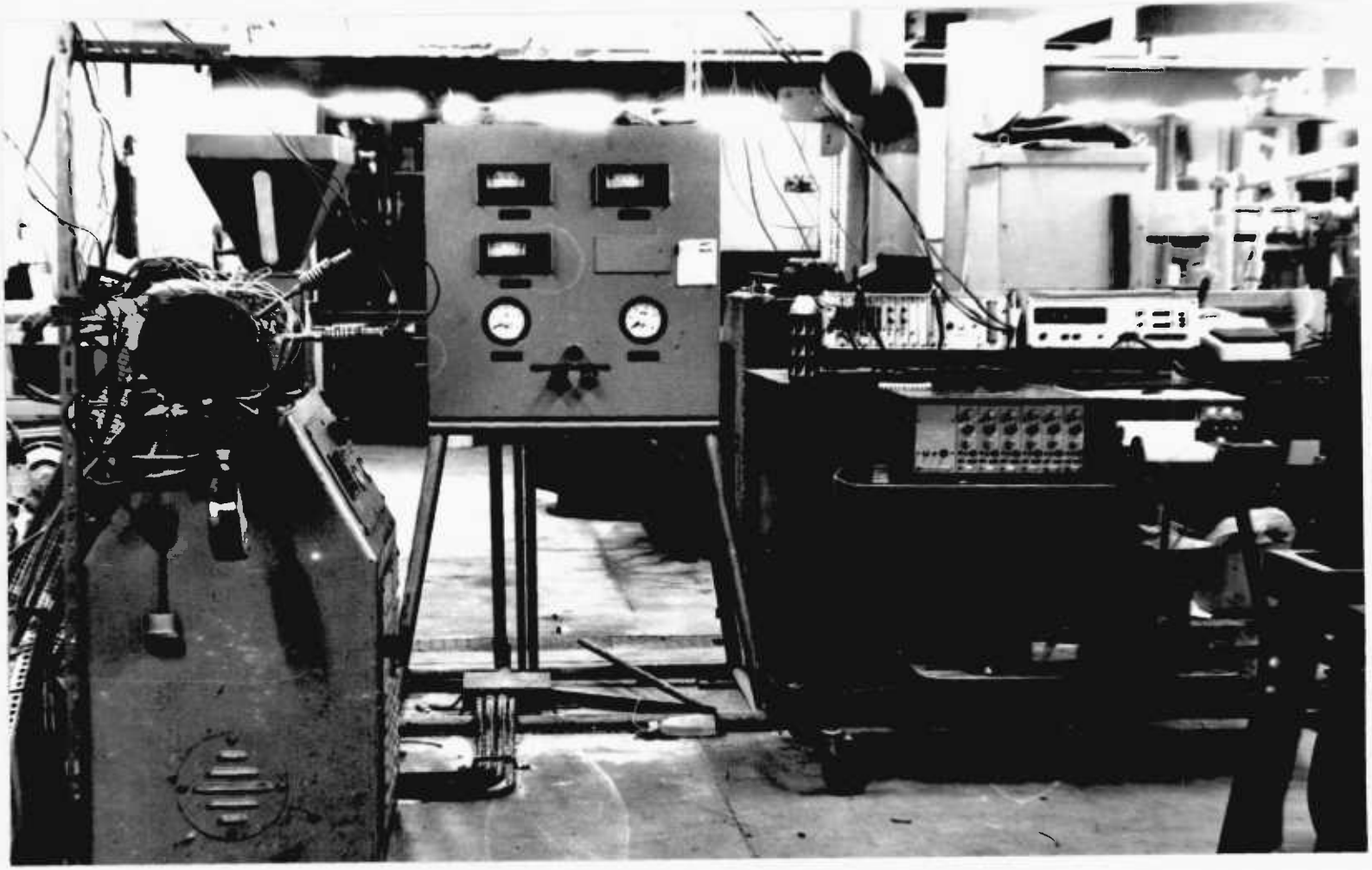
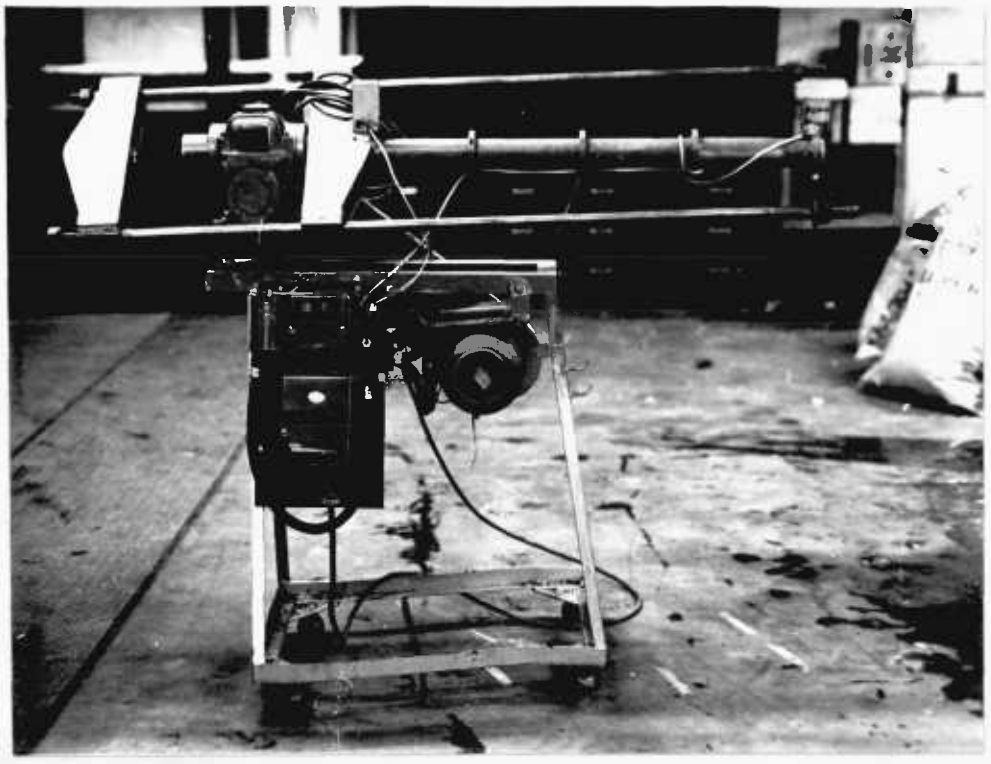


Figure 2.11

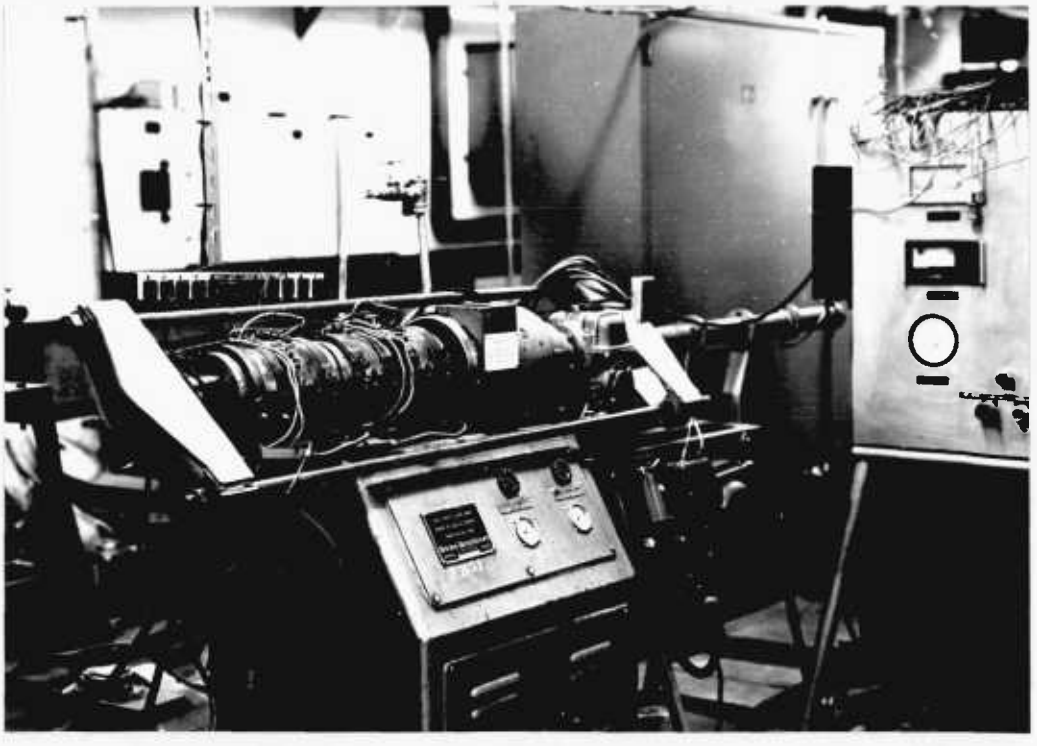
A general view of the experimental extruder

Figure 2.12

Two views of screw extractor



(a) The unit in isolation



(b) The unit fitted to the extruder

on the bar around which it fits. This gear wheel is caused to rotate by the transmission of power from the electric drive motor via suitable reduction gearing. Whilst this rotates it cannot move axially, therefore the threaded bar moves axially, it being prevented from rotating by a key fitted at its rear end which isconstrained to move axially by a slot in the tubular casing around the bar. It is the forward movement of this bar that forces the screw out of the barrel. To do this the extractor is mounted on the back of the extruder and held in position by two tie-bars that stretch between a collar on the extractor and a separate collar located on the front face of the barrel, that is, the die end. Thus the thrust in the extractor bar pushing on the screw is reacted against by tension in these tie-bars.

This concludes the description of the experimental extruder and instrumentation equipment.

It was thought desirable to perform experiments on as large a range of materials as possible. This was done in the first place to see whether different materials displayed different melting patterns, and secondly to provide as comprehensive a set of experimental data as possible with which to check out the theoretical analysis. The particular materials chosen are listed in Table 2.1.

The first three materials were specially obtained from the Polymer Supply and Characterization Centre (PSCC) of the Rubber and Plastics Research Association (RAPRA). These materials were taken from the batches that had been specially mixed to ensure identical material in each bag. The original supplier of the material is not known. These materials are made available on request for research activities in the general field of plastics. The idea being that a comprehensive wealth of data, about a few particular materials is potentially more useful for research purposes than a little information about a lot of different materials. The importance of this in the present work is that it meant that very detailed knowledge of the flow and thermal properties of these materials would be or would become available.

The low density polyethylene powder was chosen as it was a material with which

Table 2.1

The Experimental Materials and the Extruder Barrel Set Temperature used for each Material.

Material and code	Material Supplier	Barrel Temperature °C
Low density polyethylene granules - LDPE 1	P.S.C.C.	150
High density polyethylene granules - HDPE 1	P.S.C.C.	170
Polypropylene granules	P.S.C.C.	250
Low density polyethylene powder - WNC 71	I.C.I.	150
Plasticised PVC granules - GDC/542	I.C.I.	160
Crystal polystyrene - KLP	B.P.	200
Polyethylene Teraphalate 'Melinex'	I.C.I.	300
Rigid PVC powder - PC8/038	I.C.I.	160

a lot of experimental work had been done by other workers in the College laboratory and for which, therefore, property data was already available. Similarly the particular grade of plasticised PVC chosen was one for which I.C.I. (Plastics Division) were able to provide comprehensive property data. Crystal polystyrene was chosen because of it being an extremely brittle material unlike most of the other experimental materials.

Those six materials were used in the main experimental program. Later additional experiments were performed with two other materials.

The polyethylene teraphalate ('Melinex') was used because of the particular surging problems that can arise in its extrusion.

The rigid powder blend PVC was used to check out the earlier results with rigid PVC powder that showed extreme disagreement with the usual melting model of Maddock.

The last area that needs reviewing in this section concerns the choice of operating conditions for the experiments. Under this heading are included choice of screw speed, of barrel and die temperatures, of the die and hence back pressure and the use of screw cooling. To help decide on specific operating conditions a number of trial experiments were performed on the extruder. The results of some of these early experiments will be discussed further in the next section. Only those observations drawn from these experiments which are relevant to the choice of operating conditions will be presented here.

It was found that at the maximum speed of the extruder, namely 84 r.p.m., it was well capable of completely melting the maximum output rate achievable, which was with the largest diameter die both with and without screw cooling. Because of the aims of the experiments it was thought desirable to cause the melting region to extend over as long a length of channel as possible. It was essentially for this reason that the decision was made not to use screw cooling for the experimental runs. Of course, in practice the use of screw cooling is avoided if at all possible and therefore the decision is justifiable from a practical point of view. For each material the barrel temperature settings were different and are given in Table 2.1. Advice was sought as to typical processing temperatures for each material. In the interests of simplicity both experimentally

and theoretically it was decided to set both barrel zones to the same temperature, though sometimes the die was set to a different temperature.

In view of the number of different materials being used, six initially, it was thought that four experiments per material, giving a total of 24 experiments, would be a manageable number. The operating settings that varied between the four experiments on each material were screw speed and die bolt diameter; barrel and die temperatures were not altered. Two screw speeds were used, 40 r.p.m. and 80 r.p.m., and three die bolts each of the same length but having different diameters; 1/16 inch(1.59 millemetre); 3/32 inch(2.38 millemetre); 5/32 inch (3.97 millemetre), respectively. The four experiments were as follows.

1: 40 r.p.m.; 1/16 inch.

2: 40 r.p.m.; 3/32 inch.

3: 80 r.p.m.; 3/32 inch.

4: 80 r.p.m.; 5/32 inch.

This choice of experiments fulfills the following desirable criteria. Firstly a reasonable range of back pressures and output rates is covered. Secondly an adequate range of screw speeds is used. Thirdly and most importantly the criticism levelled against the experiments of Tadmor et al (5), namely that they all had a non-dimensional metering zone pressure gradient that was negative, in other words there was always a pressure maximum somewhere before the end of the screw, does not apply to the present experiments. That is, the present choice of experimental operating condition gives a good range of non-dimensional flow rates.

In the next section the preliminary trial experiments are discussed with regard to the contribution they made to the final experimental procedure which is then itself described.

2.3.3 Preliminary Experiments and Experimental Procedure

Preliminary experiments were performed for several reasons. The new split extruder barrel had to be tested as did the new heaters and cooler units. Similarly the instrumentation systems had to be checked through and the overall operation of the extruder familiarised. More explicitly the experimental procedure had to be established.

The most important aspect of procedure in the beginning was the operations involved in splitting the extruder barrel, this was the more so since the barrel with the screw inside it had to be removed from the base of the machine for this to be done. The sequence of operations involved here started with the removal of the die and head unit and the associated barrel flange. The screw water cooling coupling and reed were removed and all the various thermo-couple probes in the barrel taken out. The electrical connections to the heaters were then removed and the water piping disconnected from the cooling jackets. The pressure transducers were always removed before the plastic in the barrel had solidified so as to avoid damage to their caps due to the solid plastic. This practice is recommended by the manufacturers.

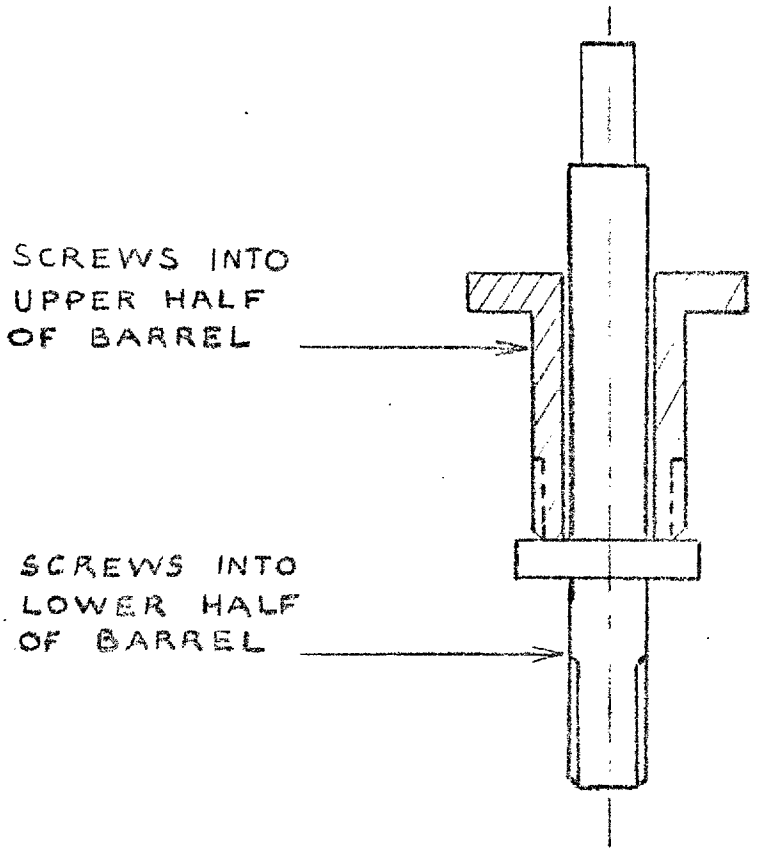
Having removed all connections between the barrel and the machine except the locating and clamping flange at the feed hopper end the metal bands clamping the heaters and cooling jackets to the barrel were loosened so that these units could be slid off the end of the barrel which was lubricated with high temperature silicon grease to facilitate this.

The barrel was located by means of a spigot in the feed hopper casting and was held in place by a flange which is separate from the barrel, the clamping force being exerted through a split ring locating in a circumferential rectangular section groove around the end of the barrel. This can be seen in figure 2.7. The Allen screws holding the barrel to the hopper assembly were then removed and the barrel and screw pulled away.

In general the solidified material in the screw adhered to the barrel inner surface with the result that the two halves of the barrel were effectively stuck together. Therefore, even after removing the set of Allen screws holding the two halves together the barrel did not come apart. This was forseen and

Figure 2.13

Diagram of the barrel splitting tool.



and special splitting tools were designed and built for this purpose; the design is shown in figure 2.13 and they can be seen in position in figure 2.8. The inner part is first screwed into the barrel at one of the four special locations designed for this purpose, shown in figure 2.6, using the thread in the 'lower' half of the barrel used also by the clamping screw. The outer part of the splitting unit is then fitted over the inner and screwed into the thread in the 'upper' half of the barrel. This thread in the 'upper' half of the barrel is peculiar to these four special locations. A tap wrench is then used to unscrew the inner part. As it unscrews out of the lower half of the barrel the shoulder on it bears up on to the outer part which is rigidly attached to the 'upper' half of the barrel and hence the two halves are caused to separate. Because of the dowel pins locating the two halves of the barrel together, the two halves must remain square to each other during splitting to prevent any tendency to jam. This means in practice that three splitting tools at least were employed simultaneously.

Having split the barrel it usually happened that the screw and plastic would still be stuck to the 'lower' half of the barrel. Sometimes the screw could be separated by simply clamping the barrel half in a vice and pushing the protruding end of the screw away from the barrel. If this failed the barrel was locally and gently heated on the outside surface with an oxy-acetylene burner. Normally the screw stuck to the half of the barrel in which the transducer ports were located. The reason for this being that the transducers were removed before solidification of the material and so some molten material had flowed into the part before solidifying. Because of this it was normally only necessary to direct the flame of the burner up these parts to soften these plugs before the screw could be separated from the barrel half. Conveniently the plastic usually remained stuck to the screw channel and not the barrel surface. It was found that material at certain points tended to leak through the inner sealing surface of the barrel and to collect in the trough in the 'lower' half of the barrel, between the inner and outer sealing surfaces, and even to pass down the thread of the screws although it did not leak past the outer sealing surface. This leakage was not particularly serious and presumably was self

stopping as there was no path to the outside of the barrel. However this stagnant material was liable to decompose and in the case of PVC the hydrogen chloride given off during decomposition could be harmful to the metal. For this reason a solution to the leakage problem was sought. The most convenient way of making the seal good was found to be placing a layer of polytetraflorethylene (PTFE) tape along the inner sealing surface. This material was ductile so that it naturally was extruded into the points of potential leakage as the barrel halves were screwed together. It could also withstand the processing temperatures required by most of the materials used in the experiments.

The method of removal of the screw from the barrel using a screw extractor was, in contrast, a much simpler operation. Having removed the die and head unit and the screw water cooling parts, the extractor could be fitted to the machine. If all went well the extractor would then push the screw out cold. This obviously is a much quicker method. It was found that three complete experiments using the extraction procedure could be performed in the time taken to do one using the splitting technique. For this reason early experiments were performed to compare the results obtained from extraction experiments and otherwise identical ones using the splitting technique.

The experiments showed, as one would expect, that if extraction was performed without any reheating of the extruder barrel then the two techniques gave identical results. Also it was found possible using some skill to apply reheat and still preserve the true melting patterns. The essential requirement for success in such a case was to obtain a sufficiently high surface temperature on the barrel inner surface without having too large a quantity of residual heat in the barrel and heater units.

The extraction force available for these early experiments was about 6 Tons (about 60kN). The conclusion from these comparative runs was that an increase in this force would enable virtually all the extractions to be performed cold and hence without producing inaccurate results. Therefore a more powerful electric motor was fitted to the extractor which increased the extraction force to 10 Tons (about 100kN), and it was decided to employ the extraction technique

as the standard procedure in the main experimental work. In fact several of the experiments in the main series were performed using the splitting technique. There were two reasons for this. Firstly it was thought advisable to split the barrel for a thorough inspection and clean before commencing each set of four experiments with a new material. Secondly it proved impossible to extract some materials without resorting to excessive reheating and in these cases also the barrel was split.

These initial experiments were all performed using unpigmented material, mostly low density polyethylene granules. It was found possible to distinguish the regions of solid granules and of molten plastic successfully. However it was not possible to adequately distinguish between material that had been molten during operation of the extruder and that that had melted during cooling due to conduction of residual heat from the barrel. The result of this conduction melting was to give the impression that the melt film was thicker than it really had been during operation of the extruder.

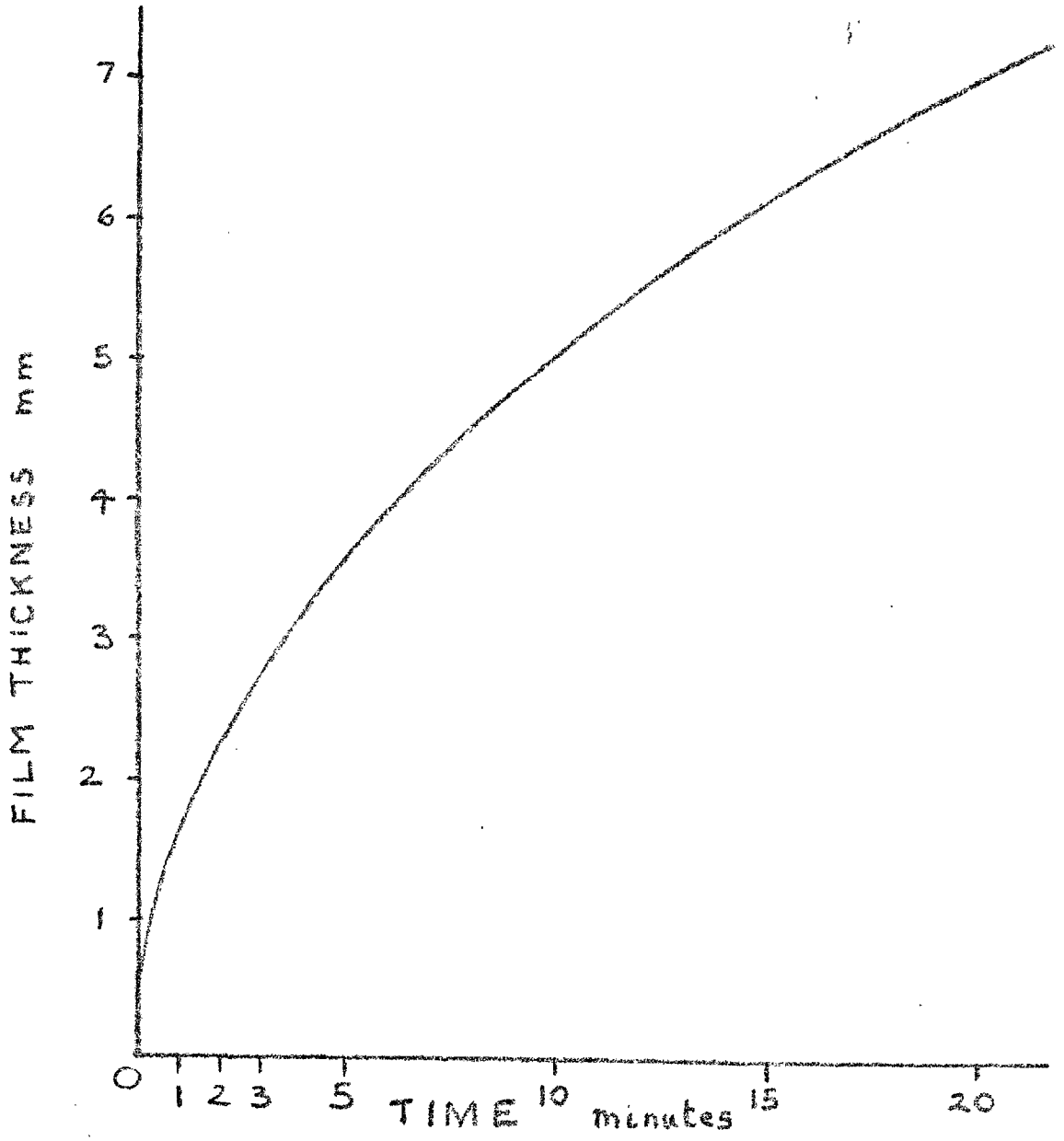
To confirm this observation two comparative experiments were performed. The difference between the two being that in the first the usual maximum cooling rate was used whilst in the second the barrel assembly was allowed to 'cook' for five minutes after the heaters and drive motor had been turned off before the cooling was applied. The results showed what appeared to be a significantly thicker melt film in the second case than in the first.

A simple order of magnitude calculation was performed to investigate the effect of cooling rate on the thickness of this conduction melted layer. The details of the calculation are given in Appendix A. Figure 2.14 shows the relevant results of this calculation. The thickness of the molten layer, δ , in millemetres is plotted against the time taken to reduce the barrel surface temperature from its operating value to the melting temperature of the plastic. These particular results were calculated for the extrusion of low density polyethylene.

In practice the minimum time taken from the moment rotation of the screw ceased to the barrel thermo-couples recording the barrel temperature as being at the

Figure 2.14

The variation of melt film thickness due to heat conducted from the barrel whilst the extruder cools down against the cool down time.



melting point of the plastic for the polyethylene experiments was about 3 minutes. Figure 2.14 shows a predicted thickness of about 2.75 millemetre. A typical measure value for such a case was found to be about 2 millimetre. The most significant point arising from the results of figure 2.14 is that even if cooling could be achieved in one minute the thickness of the molten layer would be about 1.5 millemetre which is still about an order of magnitude larger than the later experimental and theoretical evidence suggests the melt film thickness to be. The conclusion then is that it is impractical to attempt to prevent the formation of any significant conduction melted material. Rather the procedure should be to identify it separately from the other molten material.

This can be adequately done by using pigment. Two ways of using pigments were mentioned in an earlier section. It was decided that the method of physically mixing the pigment with the natural granules or powder just before putting the material in the hopper was preferable on several counts. Firstly it was much simpler and more convenient than mixing a proportion of coloured granules or powder in with the natural material. Also it showed up more clearly the outline of the individual granules in the solid bed. This was because each granule had some particles of pigment on its surface which effectively marked the surface out. This point is really a result of the general advantage of this method which is that for a given proportion of pigment it is possible to achieve a more uniform dispersion of discrete particles of the pigment in the initial solid plastic, which considerably aids later observation of the process.

A blue dye was chosen for the present experimental work. It was a very intense dye requiring only the minutest quantities to be added to the feedstock. Experiments showed that a proportion of one part dye to 50,000 parts plastic, by mass, was sufficient to give adequate colouring of the extruded material. This proportion varied somewhat between materials. The more opaque the material the higher the concentration of dye needed to be. This was because the dye itself was transparent when mixed in with the molten plastic and therefore if the plastic was reasonably transparent the intensity of the colouration

was a function of the thickness of the section of material being viewed as well as the overall concentration of the dye.

Experiments were also performed to see if the addition of the dye had any effect on the extrusion process. Results proved negative, that is, no noticeable differences were observed that were outside the limits of experimental error.

It is now appropriate to describe the experimental procedure adopted throughout the main series of experiments.

The correct screw for the material to be processed was selected and fitted into the barrel and drive keyway behind the hopper. The die and head unit were fitted and their heater and control thermo-couple connected up. The screw cooling coupling was then fitted to the back of the screw. The hopper cooling water was turned on, the temperature controllers set to the correct temperature according to the plastic being used and the heaters switched on. At this stage the pressure transducers were lightly screwed into the barrel so that they could heat up with it. While the machine was heating up the thermo-couples were checked out and DVM system tested.

Once the barrel had reached its set temperature each transducer was unscrewed so that any molten plastic on the thread or on the cap could be wiped off. They were then screwed back into the barrel and tightened up sufficient to form an adequate seal. The leads were then connected up to the transducers so that the recording system could be tested and zeroed. It was important that the transducers should be at the barrel set temperature before they were zeroed so that thermal drift of the zero was minimised.

The zeroing operation consisted of three operations. Firstly the UV recorder inputs were disconnected so that the galvanometers could be mechanically adjusted to give the desired position for the zero of each transducer channel. Then the UV inputs were connected to the amplifier outputs. The amplifier inputs were effectively disconnected by setting a switch on the control panel of each unit to the 'zero' position. Having done this the galvanometer beams were re-set if necessary to the chosen zero positions by turning an adjusting screw on the amplifier control panel. The amplifier switch was then put to the 'run'

position which connected up the transducer electrical output to the amplifier input thus completing the system. With the amplifier gain control set to the desired value the Wheatstone bridge zero control was adjusted to once again bring the UV beams back onto the required zero points.

Having thus set up the zero points a record was made of them and the calibration traces. Each transducer was supplied with a calibration resistor. This resistor was wired into the circuit between the transducer and its amplifier and could be switched into the circuitry of the transducer. When switched into this circuit the resistor had the effect of simulating, nominally an 80% of full scale load on the transducer. Thus as long as there was no actual load on the transducer inclusion of the calibration resistance circuit produced a deflection on the UV recorder representing 80% of full scale for each particular transducer. This then served as the calibration trace. It is important to realise that because this resistor is situated prior to the amplifier input, reliance on the accuracy of the settings of the amplifier is automatically bypassed. The only information that needs to be accurately known is exactly what percentage of full scale load each particular resistor represents. To ascertain this accurately a dead weight pressure tester was used. Because of the excellent linear response of the transducers a continuous calibration chart was not necessary and the one figure provided by the calibration resistance was sufficient to calculate the conversion constant for the corresponding transducer, from centimetres of deflection, as read on the UV chart, to pressure.

The last operation performed before the machine could be started up was to check that bourdon pressure gauge on the head unit was functioning properly. Silicon grease was pumped through a nipple into the gauge until the gauge recorded zero and all the plastic that had penetrated the gauge during the previous experiment had been removed.

Usually the machine was left for about 30 minutes after being started up to settle down before any readings were taken. When the machine had settled down readings of motor current, output rate, head pressure and barrel temperatures were made. In addition comprehensive pressure recordings were taken. These fell into three categories. Firstly with the amplifier settings untouched a

low chart speed trace was made of all six transducers simultaneously. The chart speed was too slow to allow study of the pressure variation within one revolution of the screw but it did show up longer period variations of pressure that one may call surging. This indeed was the intention. Such traces would be taken over a period of several minutes or more. Secondly a recording was made of all six pressure traces simultaneously at a higher chart speed, again without altering the amplifier settings. This chart speed was chosen so that observation of the pressure variation over one revolution could be made, but the chief reason for taking this trace was to use it to take measurements of the pressures. The third sort of trace that was taken consisted of individual detailed recordings of each transducer in turn. For each of these the chart speed and amplifier gain were increased to give as big a trace as was thought necessary. While any one of these was being taken, the other five traces were suppressed by switching their amplifier switches from 'run' to 'zero' which then sent these traces to their zero positions. As the amplifier gain was increased the physical amplitude of the variation of the pressure trace increased which was the desired effect. However in addition the mean deflection of the trace increased and often this meant that the trace went off the edge of the chart paper. To bring it back on again meant altering the Wheatstone bridge zero control on the amplifier so that the zero was offset. This worked well but had one disadvantage; it was not then possible to re-align the zero on its original point without stopping the extruder. Hence these pressure recordings were the last to be taken.

Once all readings had been taken preparation was made for the cool down. The transducer leads were disconnected from the transducers and the hopper cooling water switched off so as to provide the maximum flow rate for screw cooling. The cool down procedure was to simultaneously turn on the water supply to the barrel coolers and the screw with the machine still running. Then as soon as the temperature of the barrel, as indicated by the controller units, began to drop the motor and heaters were switched off.

When the screw had stopped rotating all the transducers were unscrewed and completely removed from the machine as quickly as possible. The die and head unit were then removed while still hot, along with the breaker plate. When using PVC it was most important to remove these units as quickly as possible so that they could be cleaned out before the PVC had cooled down. If this was not done it meant burning the PVC out later, an unpleasant job due to the Hydrogen Chloride gas given off, this being the reason why the units had to be clean before re-assembly and heat up.

When the indicated barrel temperature was down to below 30 C the screw cooling was terminated and the coupling removed from the end of the screw so that the extractor could be fitted and operated. Usually the barrel water coolers were left on whilst extraction took place. However if the extractor was unable to move the screw as happened on occasions the cooling water was turned off and the heaters switched back on. In this situation care had to be taken as has been explained earlier. It was found useful to switch the front or metering zone heaters on first as the plastic is more likely to adhere to the barrel in this region compared to the melting and solids flow zones. Once the indicated temperatures had reached about 60% of the melting temperature of the plastic the extractor was tried out. As soon as it began to push the screw out the heaters were switched off and the barrel cooling jackets turned on. This usually prevented excessive reheating of the plastic as it passed through the barrel.

When the screw had been removed the plastic in the channel was marked and numbered at half turn intervals starting from the hopper end. This was done by simply sticking masking tape to the plastic. The material was then removed from the screw. With the flexible materials it could normally be unwound in one continuous length. Brittle or tough materials sometimes had to be chipped off in a number of separate pieces. Having removed the material from the screw the experiment was essentially over and the machine could be re-assembled in preparation for the next experiment.

In this fashion the first 20 experiments were satisfactorily performed. Difficulty was experienced with the experiments performed on crystal polystyrene. This

concerned the screw extraction which was found to be extremely difficult, and the splitting technique was employed twice in three experiments, the fourth experiment was not performed. Only two experiments were performed on rigid PVC due to the nature of the results of these two experiments, which will be discussed later. Similarly only two experiments were performed with 'Melinex'. This was because of the special difficulties encountered with this material. These were mainly associated with the fact that the extruder was operating at 300°C and consequently the violence of the cooling operation was extreme and the PTFE seals on the barrel of limited life only. Finally three experiments were performed using screw cooling; one each with low density polyethylene, high density polyethylene, and polypropylene. These were done, after examination of the results of the first 23 experiments, to study the effect of water cooling of the screw on surging. This will be discussed in detail in a later section. Details of all experiments are shown in Table 2.2. It should be noted that the numbering system used for the experiments in this work does not correspond to the order in which they were performed.

The techniques involved in preparing the specimens of plastic from the experiments are dealt with in the next section.

Table 2.2

The Experimental Numbering Scheme and Main Results.

No.	Material	N r.p.m.	Q gm/min	D inch	
1	Plasticised PVC	80	360	3/32	.384
2	" "	40	200	3/32	.426
3	" "	80	367	5/32	.391
4	" "	40	201	1/16	.429
5	Low density polyethylene granules	80	191	3/32	.442
6	" " " "	40	97	3/32	.449
7	" " " "	80	215.5	5/32	.498
8*	" " " "	80	140	3/32	.324
9	" " " "	40	83	1/16	.384
10	Polypropylene	40	80	1/16	.387
11	"	80	179	3/32	.422
12	"	40	93	3/32	.439
13	"	80	189	5/32	.446
14*	"	80	143	5/32	.337
15	High density polyethylene granules	80	187	3/32	.392
16	" " " "	40	94	3/32	.392
17	" " " "	80	206	5/32	.432
18*	" " " "	80	137	3/32	.289
19	" " " "	40	81.5	1/16	.34
20	Crystal polystyrene	80	266	5/32	.449
21	" "	40	110	3/32	.372
22	" "	40	128	1/16	.433
23	Melinex	80	319	3/32	.408
24	"	40	164	3/32	.420
25	Low density polyethylene powder	80	203	3/32	.470
26	" " " "	40	115	3/32	.533
27	" " " "	80	221	5/32	.511
28	" " " "	40	78	1/16	.361
29	Rigid PVC powder	80	419	3/32	.448
30	" " "	40	185	3/32	.396

* Denotes screw cooling experiment.

2.3.4: Preparation and Presentation of the Experimental Results

The preparation of the plastic specimens obtained from each experiment took up a large part of the overall time involved in performing the experiment. It was decided to cut out sections of plastic at half turn intervals to give a sufficiently detailed representation of the developement of the melting patterns without involving excessive preparatory effort.

A small table-top band saw was used to initially cut the strip of plastic into approximately half turn lengths, such that one face of each piece was to be prepared for visual observation. With the amorphous materials it was found adequate to use a fine grinding stone to prepare this surface, this was done for rigid and plasticised PVC, low and high density polyethylene and polypropylene It was found that as the crystallinity of the polymer increased this technique became more and more difficult. The grinding stone, instead of physically removing discrete particles of material, tended to melt the material and tear it. This did not leave such a uniform surface on the specimen. However it was judged to be adequate even for polypropylene in the absence of suitable alternatives. Having prepared the viewing face on one end of the half turn long pieces this was then cut off at about $\frac{1}{8}$ inch (about 3 millemetres) behind the face using the band saw again. With some materials the surface of the specimens at this stage was improved by rubbing lightly with a very fine wet and dry paper.

Some of the polypropylene and polystyrene specimens were prepared using a sledge microtome. Great difficulty was experienced preparing the polystyrene because of its extremely brittle nature. Preparation of the 'Melinex' however was even more difficult due to its amporphous state. Because 'Melinex' is a highly crystalline polymer it has virtually no strength at all in the amorphous state, unlike polymers of low crystallinity. The rapidity of barrel cooling was not sufficient to solidify the 'Melinex' into a crystalline state which would perhaps have been preferable. In this amorphous state it was not possible to grind the samples because they would shatter being unable to withstand the shear force put on them by the grinding surface. The problem was due to the difficulty of gripping the specimens sufficiently evenly to allow them to withstand the

grinding force. This was overcome by mounting the specimens in black 'Bakelite' moulding powder as used for mounting metallurgical samples. Because of the relatively high melting temperature of Melinex (265°C) it was not affected by the temperature involved in the process (150°C), which would have excluded the use of this technique on most of the other materials, though the pressure, about 1500 p.s.i.(about 10 MN/m), did cause some slight deformation of the specimens. This, however was insufficient to cause any real problem. Having mounted each specimen in this fashion the viewing surface was ground using a rotating grinding wheel fitted with fine wet and dry grinding paper.

Without doubt the best way of recording these results is to take individual photographs of each specimen on 35 millemetre size negatives. This, however, would have been much too long a process in view of the large number of specimens involved in the present work, totalling something over 600. Instead it was decided to lay out on a suitable marked card all the specimens for each experiment and to photograph them together. This was initially done on 35 millemetre negatives. However when the final enlarged prints were prepared it was found impossible to obtain sufficient quality due to the grain problem and the sort of detail required from the prints. This was overcome by using a 5 inch by 4 inch plate camera, with a cut film pack. The final prints in this case were made by contact printing from the negatives, the quality proving satisfactory. These melting cross-sections so obtained in the present experiments are shown in Plates 1 to 15. The experiments are characterised by the following code set out beneath each illustration.

Experiment 24: N(80); Q (179); D (3/32) -

where the figure in brackets after the N is the screw speed in r.p.m.; that after the Q is the output rate in gram/minute; that after the D is the die bolt diameter in inches.

The axial pressure profiles for each experiment are shown in Figures 2.15 to 2.29 inclusive.

Other experimental results of importance are presented where appropriate in the following discussion of the results. To facilitate comparison of the melting

cross-sections for any particular experiment with the corresponding pressure profile or any other experimental or theoretical results presented in the present work. Table 2.3 provides a quick reference as to where to find all such information concerning each experiment.

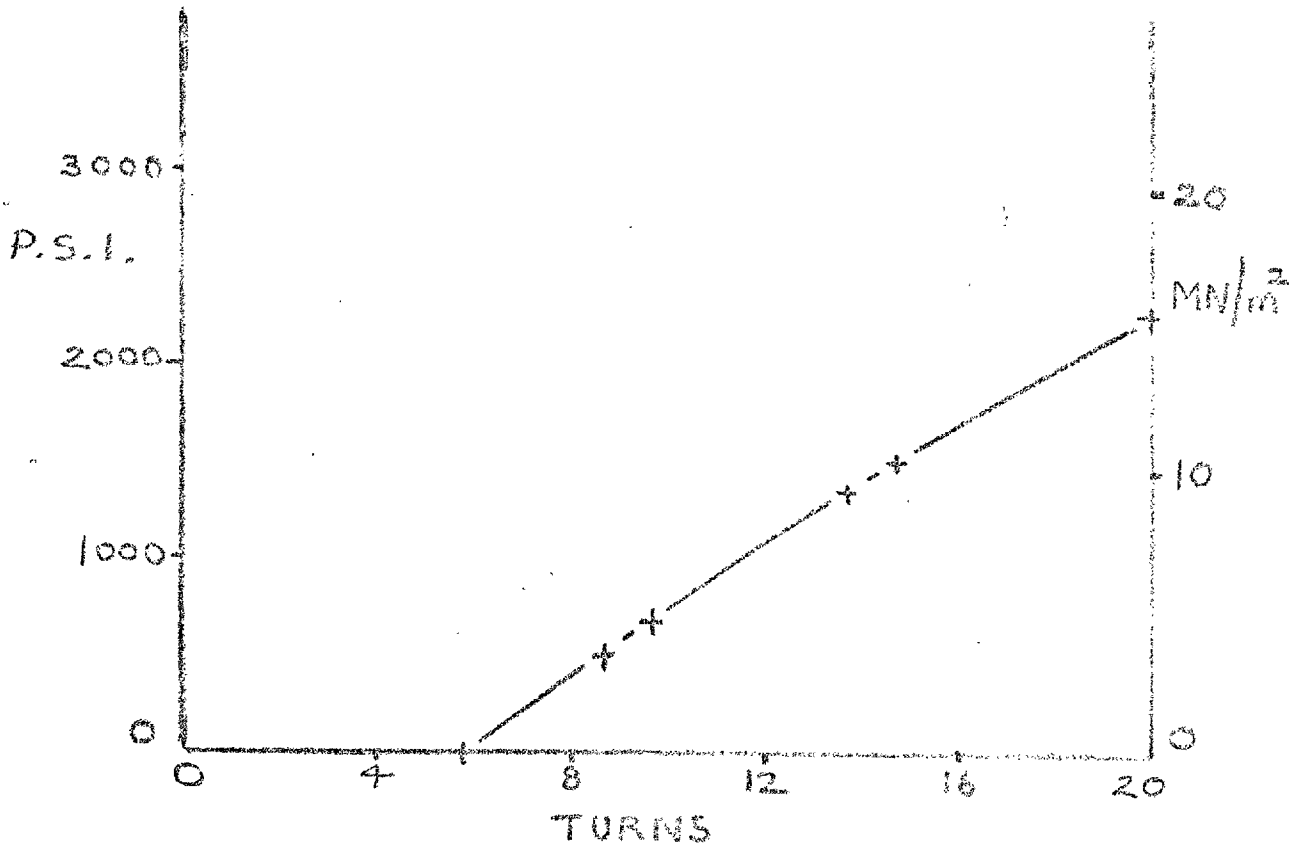
Table 2.3

Reference Table showing which experimental and theoretical results are presented in the present work for each experiment.

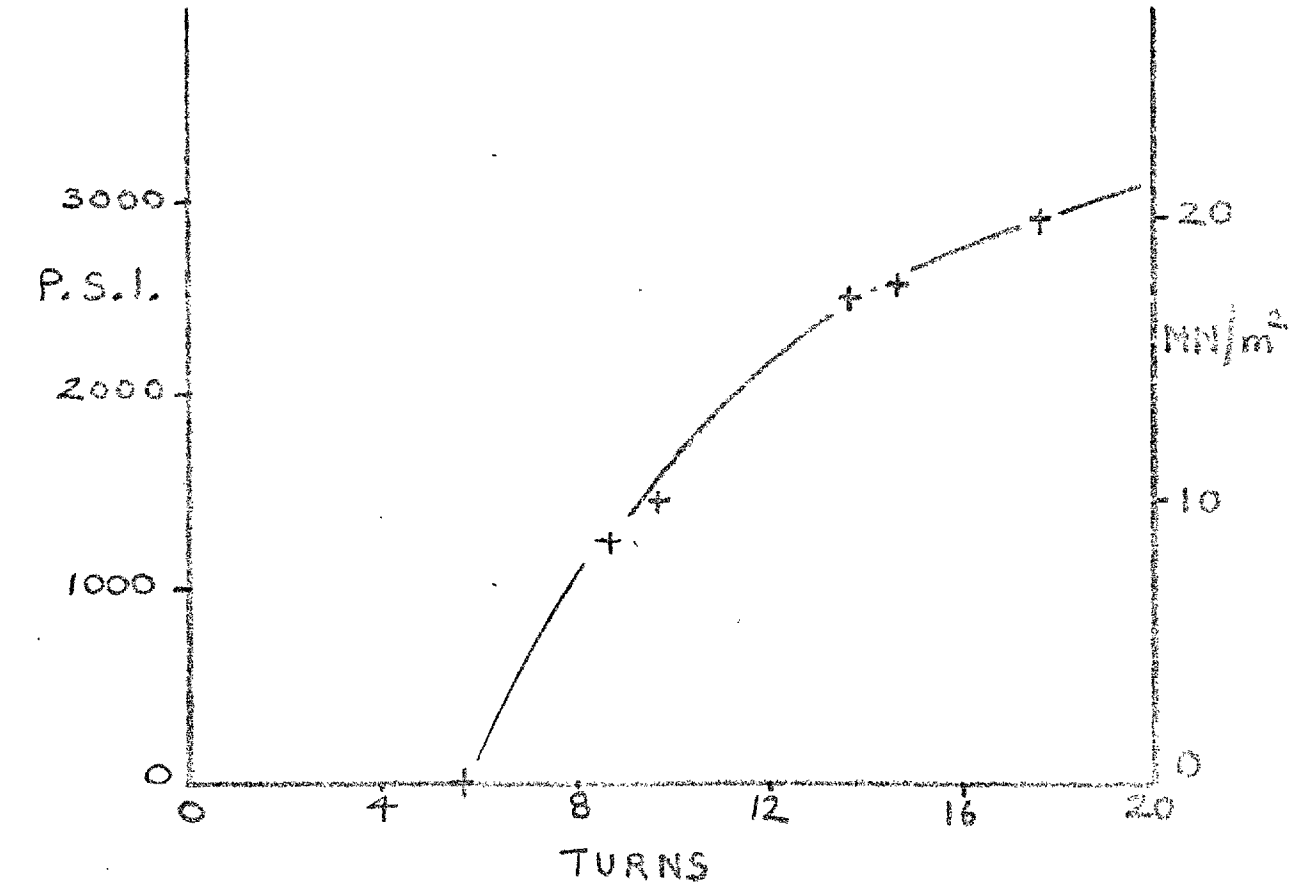
Expt No.	Material	Experimental figures				Theoretical Figures		
		Press Profile	Detail press traces	Low speed press traces	X sect photos plate no.	Solid bed profile	Press profile	Solid bed velocity profile
1	PVC	2.15(a)			1(a)	3.17		3.44
2	"	2.15(b)			1(b)	3.18		
3	"	2.16(a)	2.32-34		2(a)	3.14	3.14	3.14
4	"	2.16(b)			2(b)	3.19		3.45
5	LDPE 1	2.17(a)			3(a)	3.20	3.38	
6	"	2.17(b)			3(b)	3.21		
7	"	2.18(a)			4(a)	3.22		
8	"	2.18(b)			4(b)	3.23	3.42	
9	"	2.19(a)			5(a)	3.15	3.15	3.15
10	PP 1	2.19(b)			5(b)	3.24		
11	"	2.20(a)	2.57-58	2.54	6(a)	3.25	3.39	3.48
12	"	2.20(b)			6(b)	3.26		
13	"	2.21(a)		2.51	7(a)	3.27		
14	"	2.21(b)	2.35-38		7(b)	3.28		3.49
15	HDPE 1	2.22(a)	2.45-46 2.59	2.50	8(a)	3.29	3.41	
16	"	2.22(b)			8(b)	3.30	3.40	
17	"	2.23(a)			9(a)	3.13(b)		
18	"	2.23(b)		2.55	9(b)	3.31	3.43	
19	"	2.24(a)			10(a)	3.32		
20	Styrene	2.24(b)			10(b)			
21	"	2.25(a)			11(a)			
22	"	2.25(b)			11(b)			
23	Melinex	2.26(a)	2.63	2.61	12(a)	3.33		3.46
24	"	2.26(b)	2.64	2.62	12(b)	3.34		3.47
25	LDPE	2.27(a)			13(a)	3.35		
26	"	2.27(b)			13(b)	3.36		
27	"	2.28(a)	2.39-44		14(a)	3.16	3.16	3.16
28	"	2.28(b)			14(b)	3.13(a)		
29	PVC	2.29(a)			15(a)			
30	"	2.29(b)			15(b)	3.37		

Figure 2.15

Experimental Axial Pressure Profiles



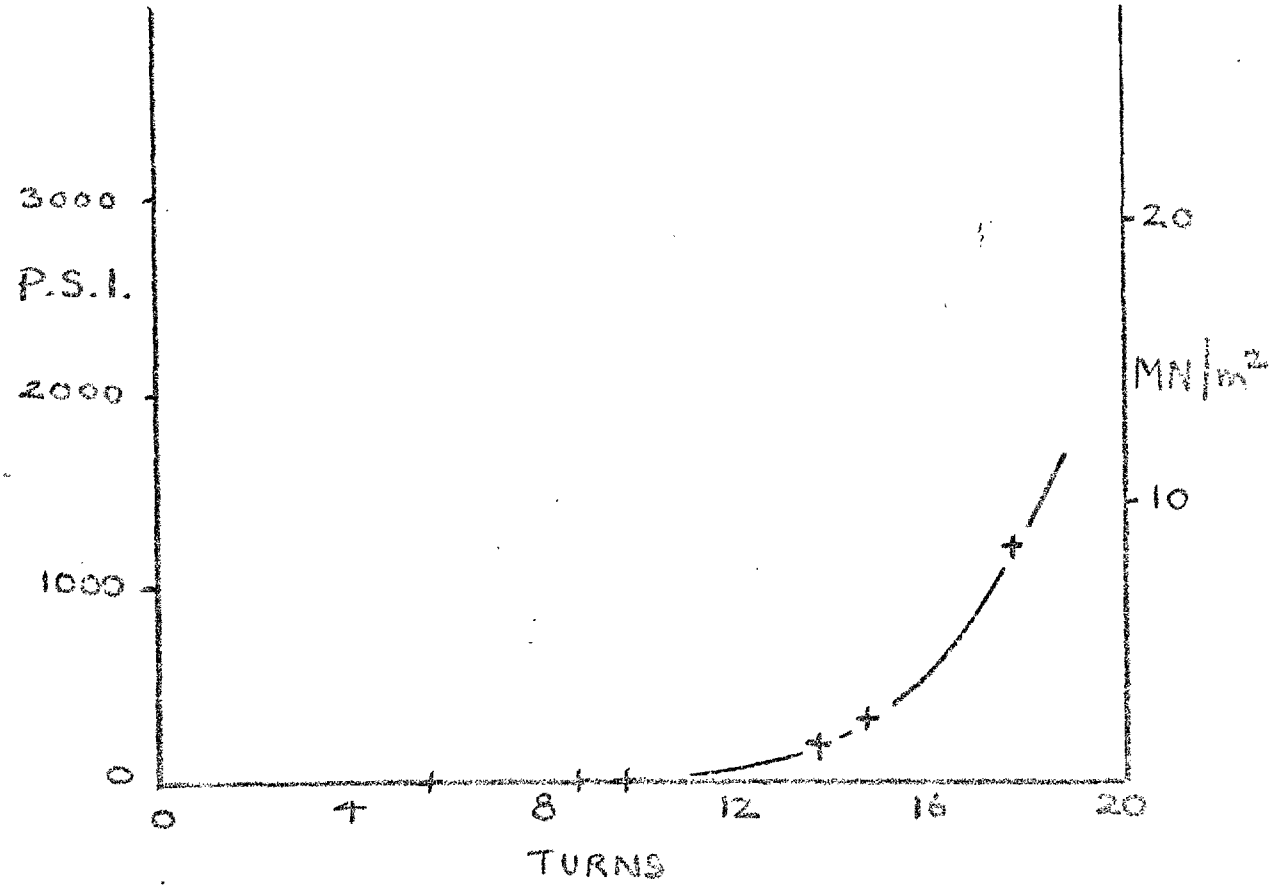
(a) Experiment 1, Plasticised PVC. N(80); Q(360); D(3/32)



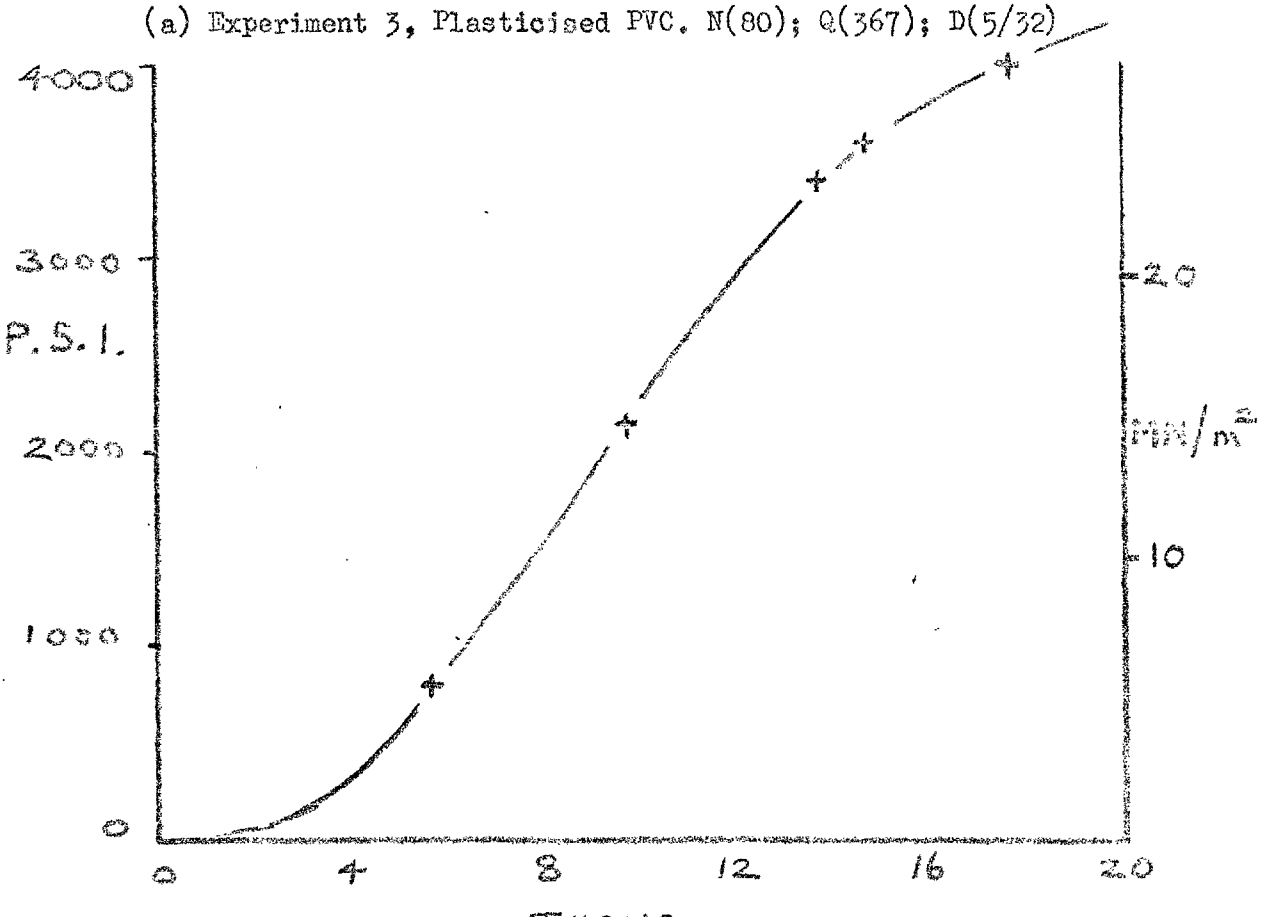
(b) Experiment 2, Plasticised PVC N(40); Q(200); D(3/32)

Figure 2.16

Experimental Axial Pressure Profiles



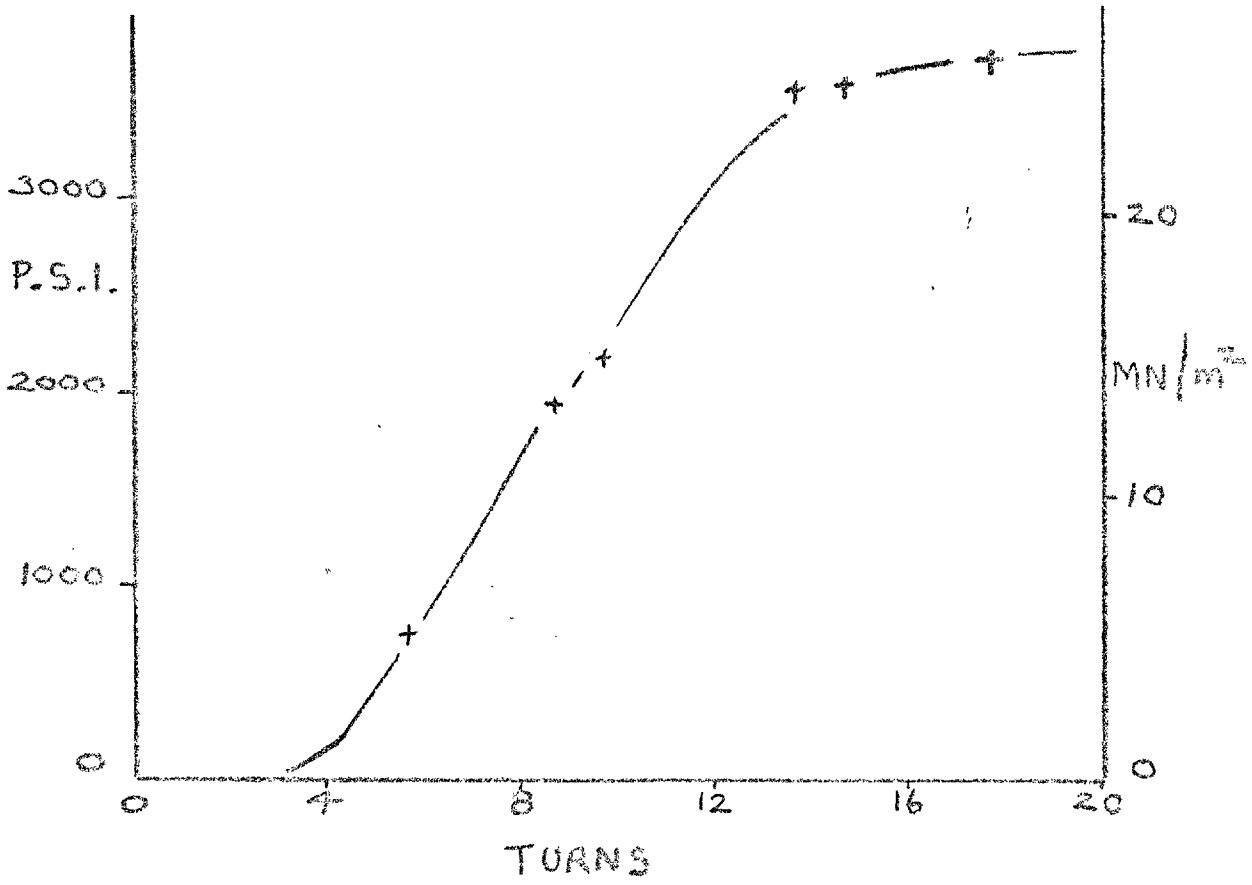
(a) Experiment 3, Plasticised PVC. N(80); Q(367); D(5/32)



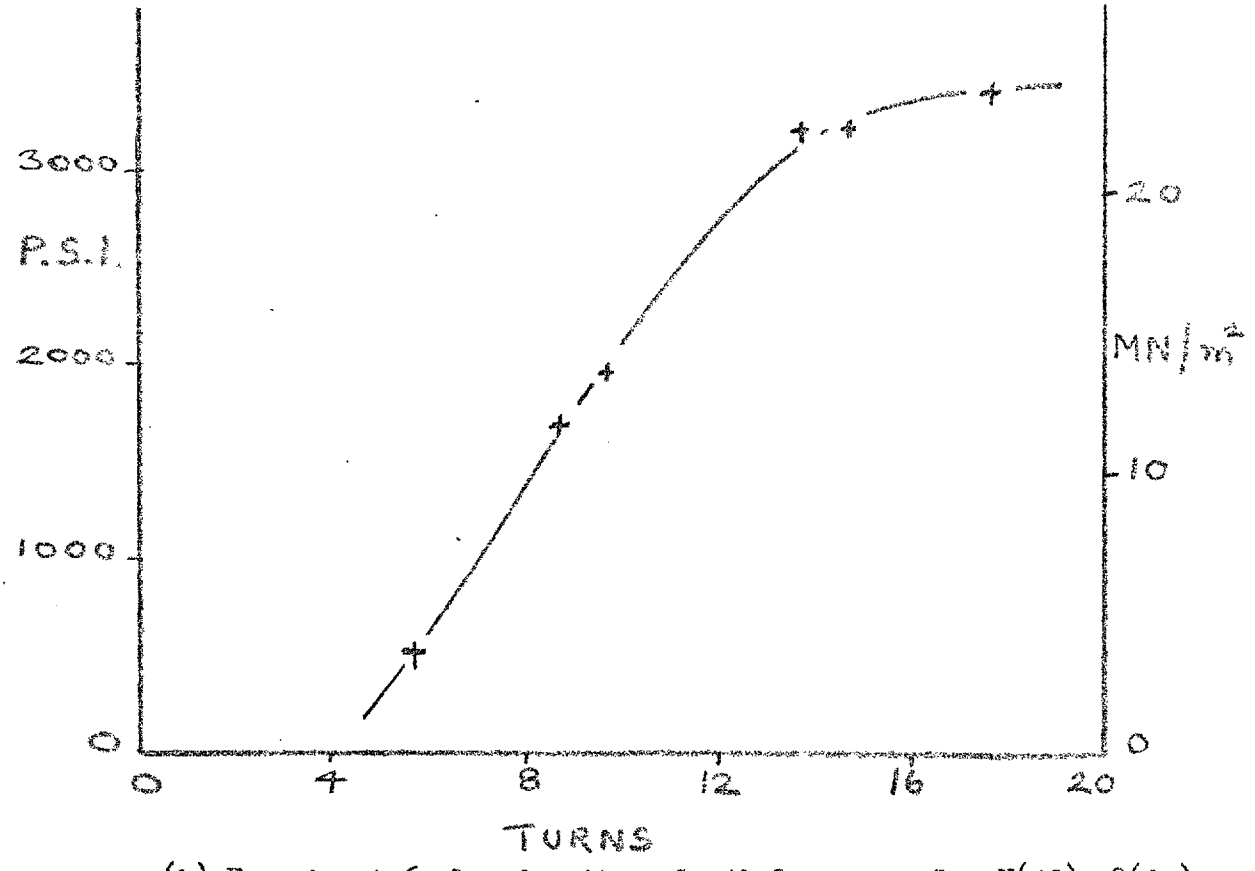
(b) Experiment 4, Plasticised PVC. N(40); Q(201); D(1/16)

Figure 2.17

Experimental Axial Pressure Profile



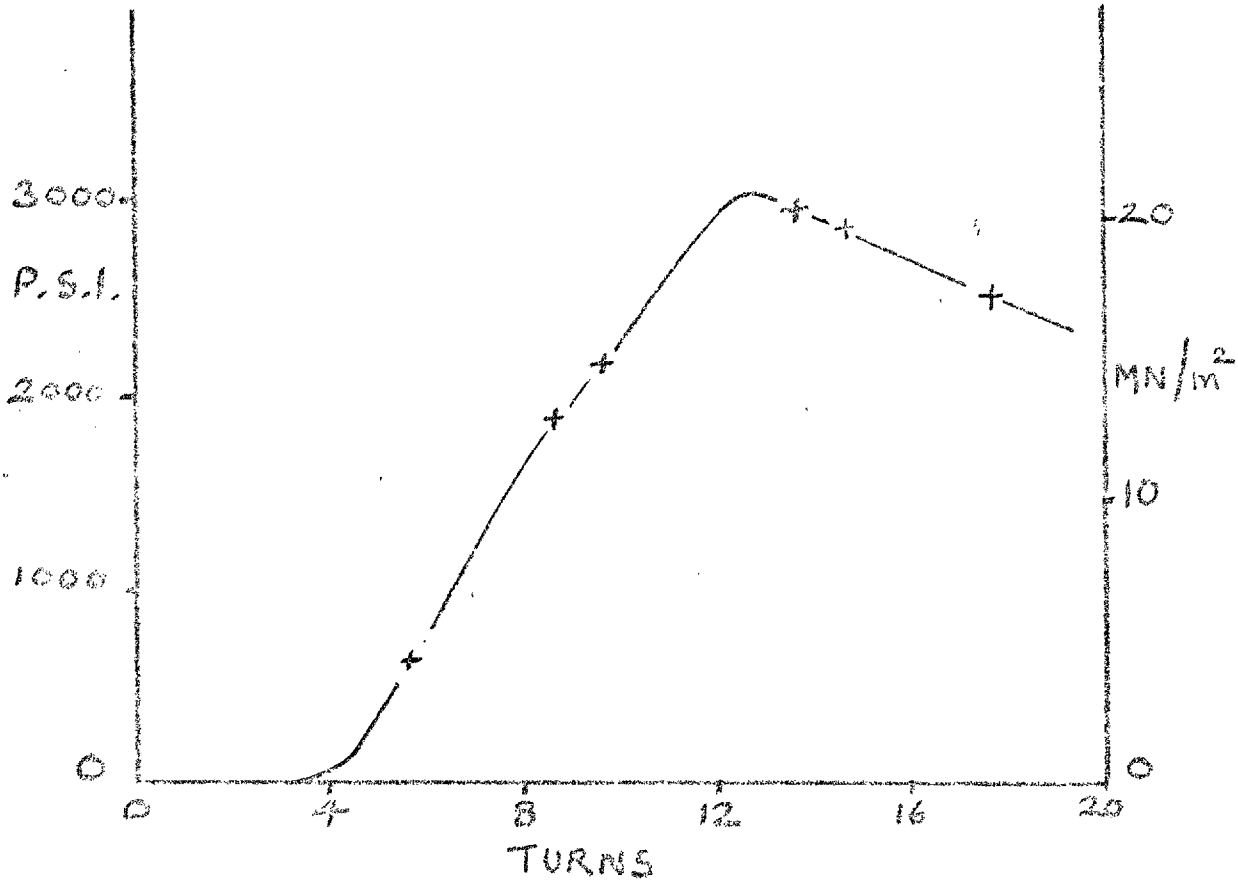
(a) Experiment 5, low density polyethylene granules N(80); Q(191); D(3/32)



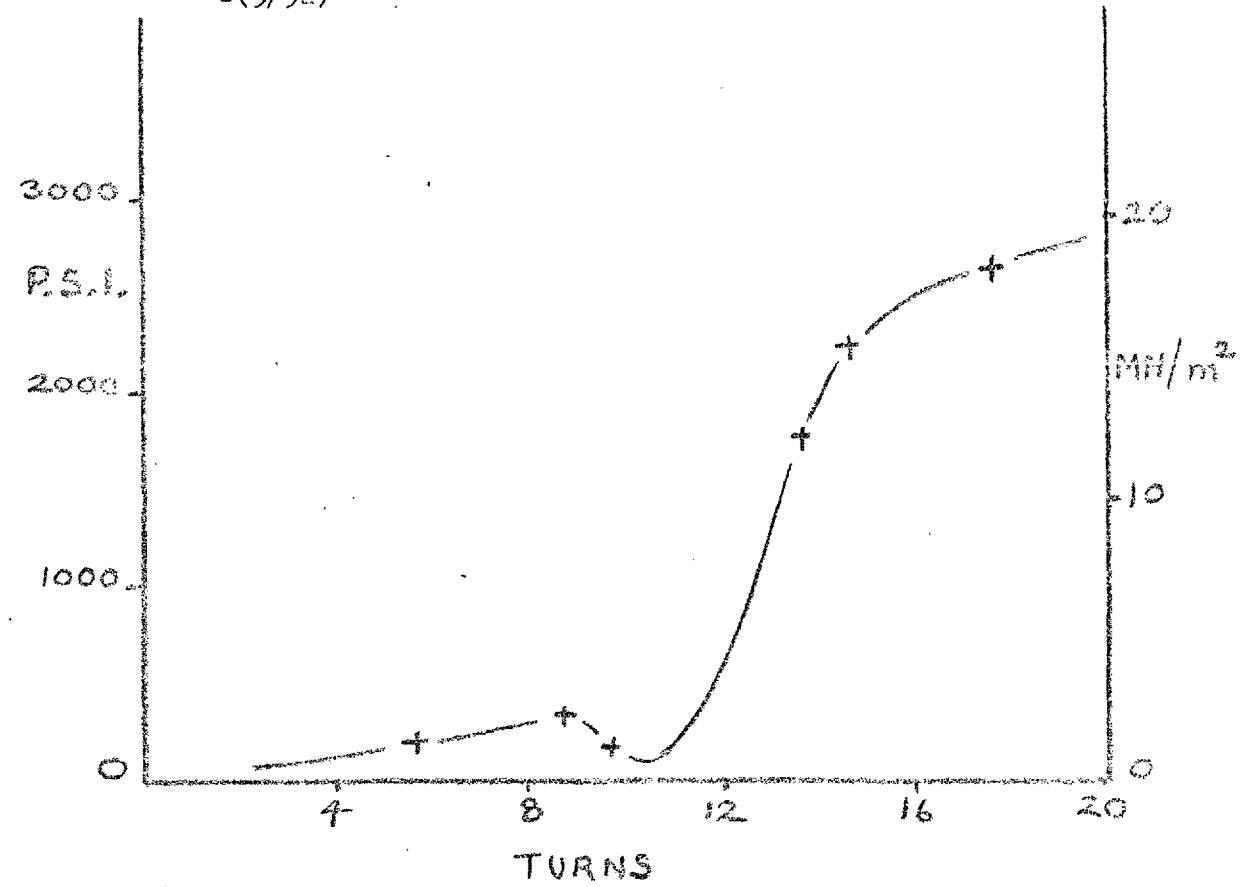
(b) Experiment 6, low density polyethylene granules N(40); Q(97); D(3/32)

Figure 2.18

Experimental Axial Pressure Profiles



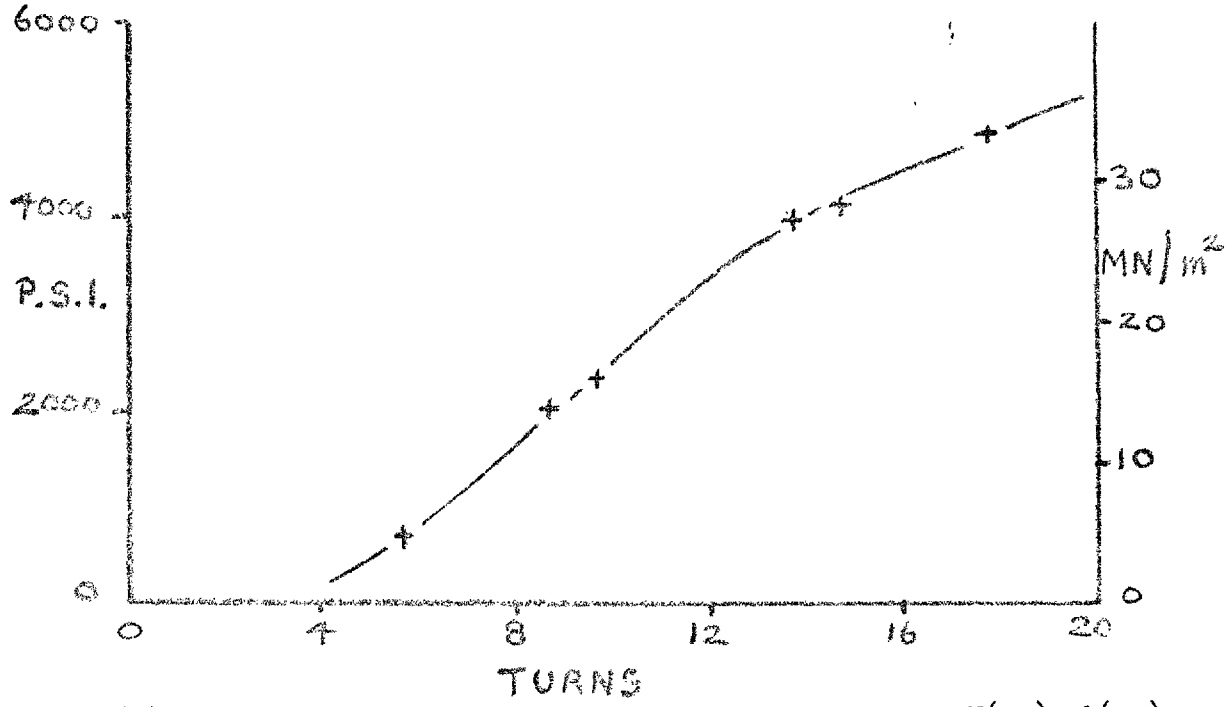
(a) Experiment 7, low density polyethylene granules. N(80); Q(215); D(5/32)



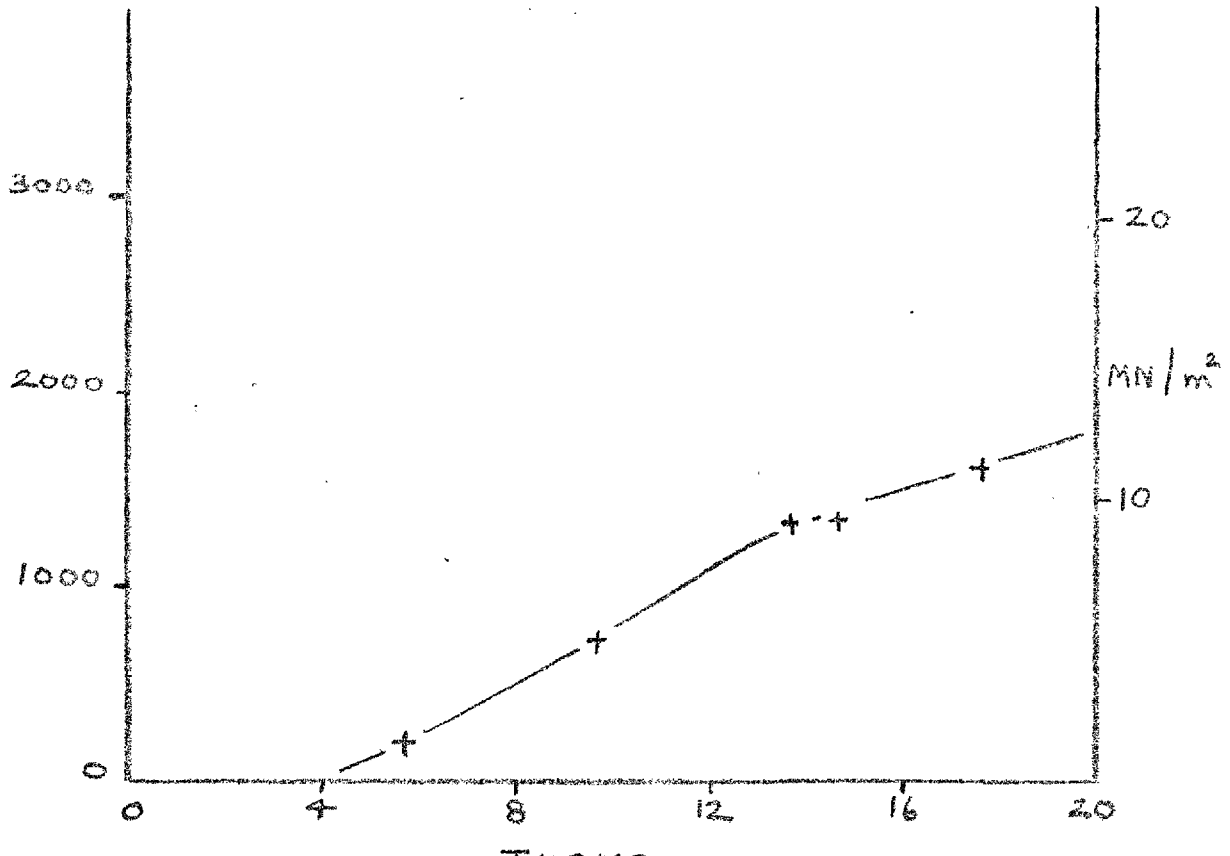
(b) Experiment 8, low density polyethylene granules, with screw cooling. N(80); Q(140); D(3/32)

Figure 2.19

Experimental Axial Pressure Profiles



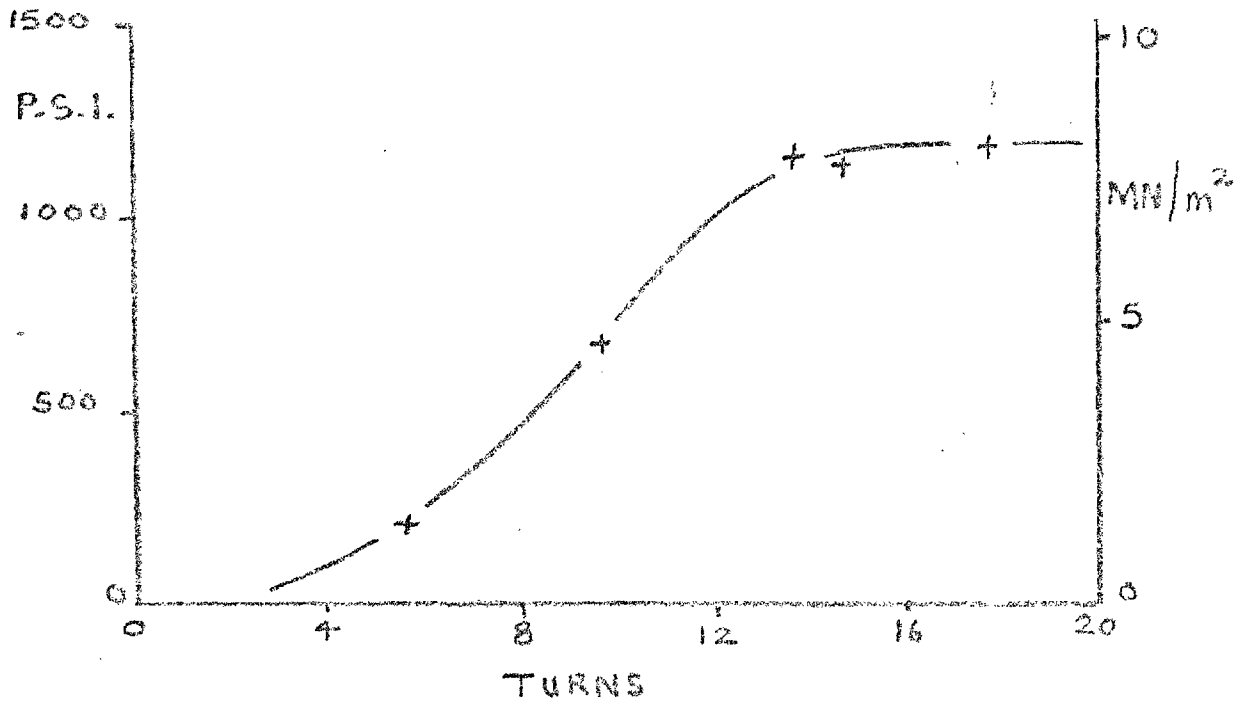
(a) Experiment 9, low density polyethylene granules. N(40); Q(83); D(1/16)



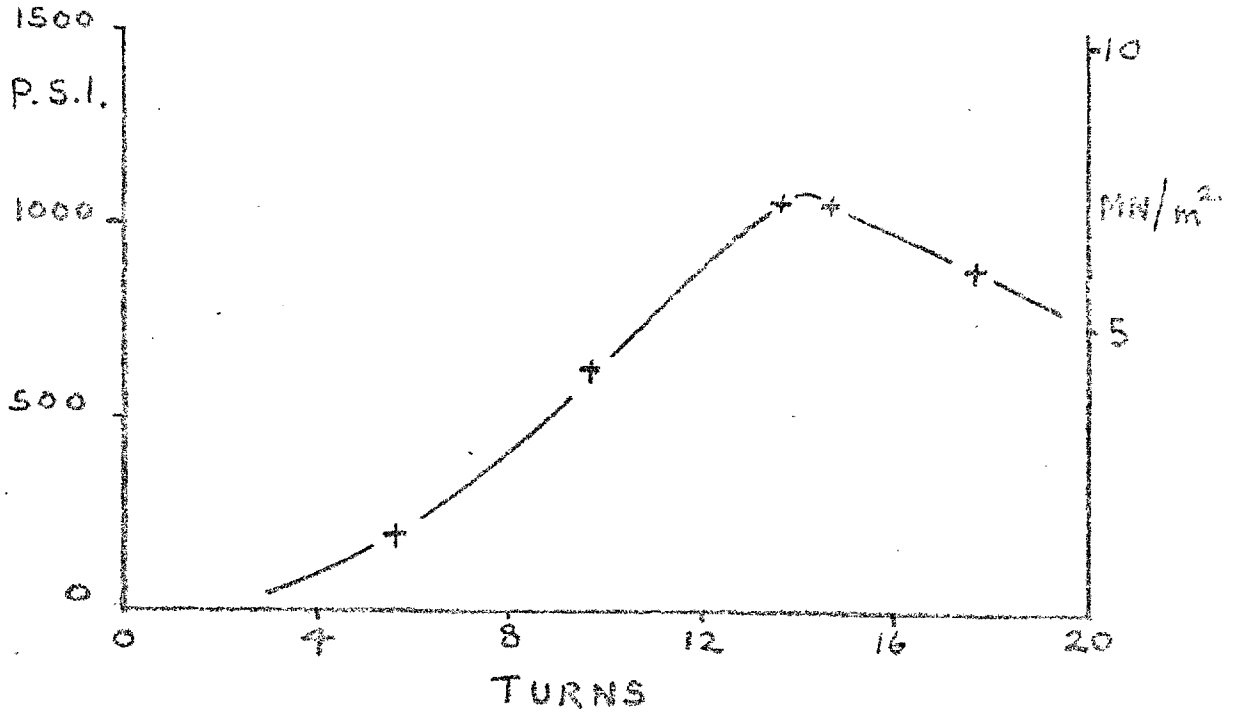
(b) Experiment 10, polypropylene N(40); Q(80); D(1/16)

Figure 2.20

Experimental Axial Pressure Profiles



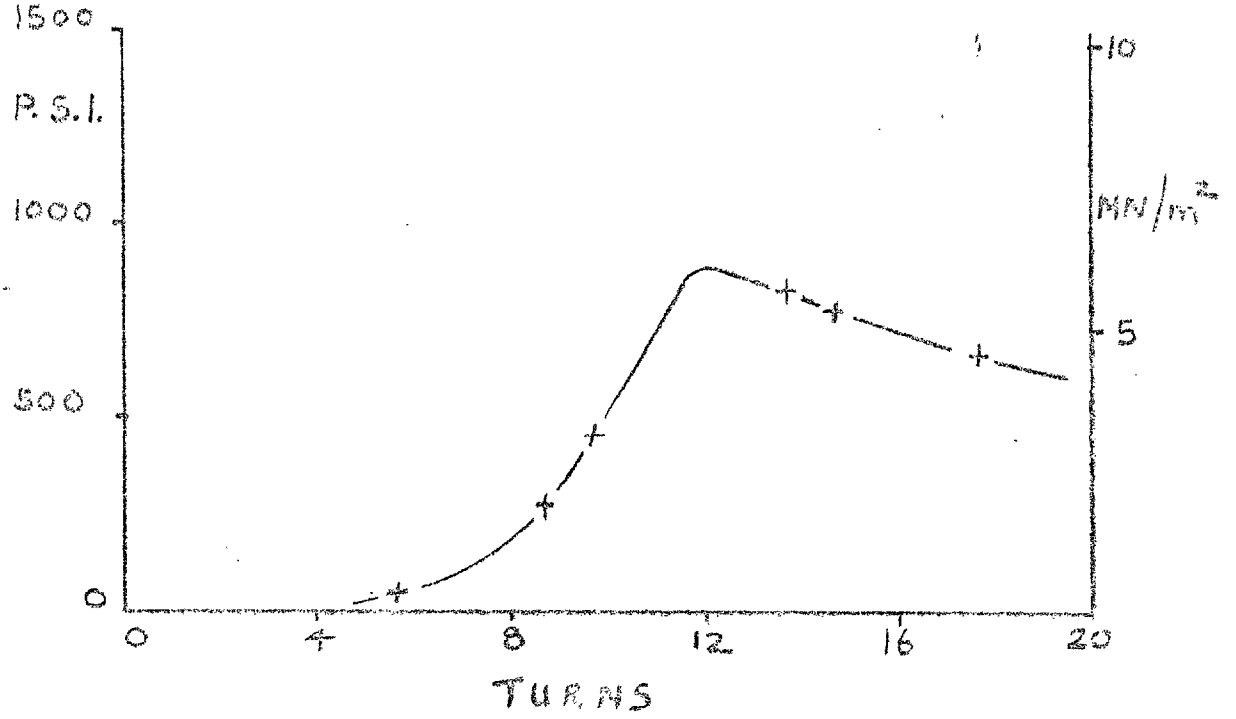
(a) Experiment 11, polypropylene. N(80); Q(179); D(3/32)



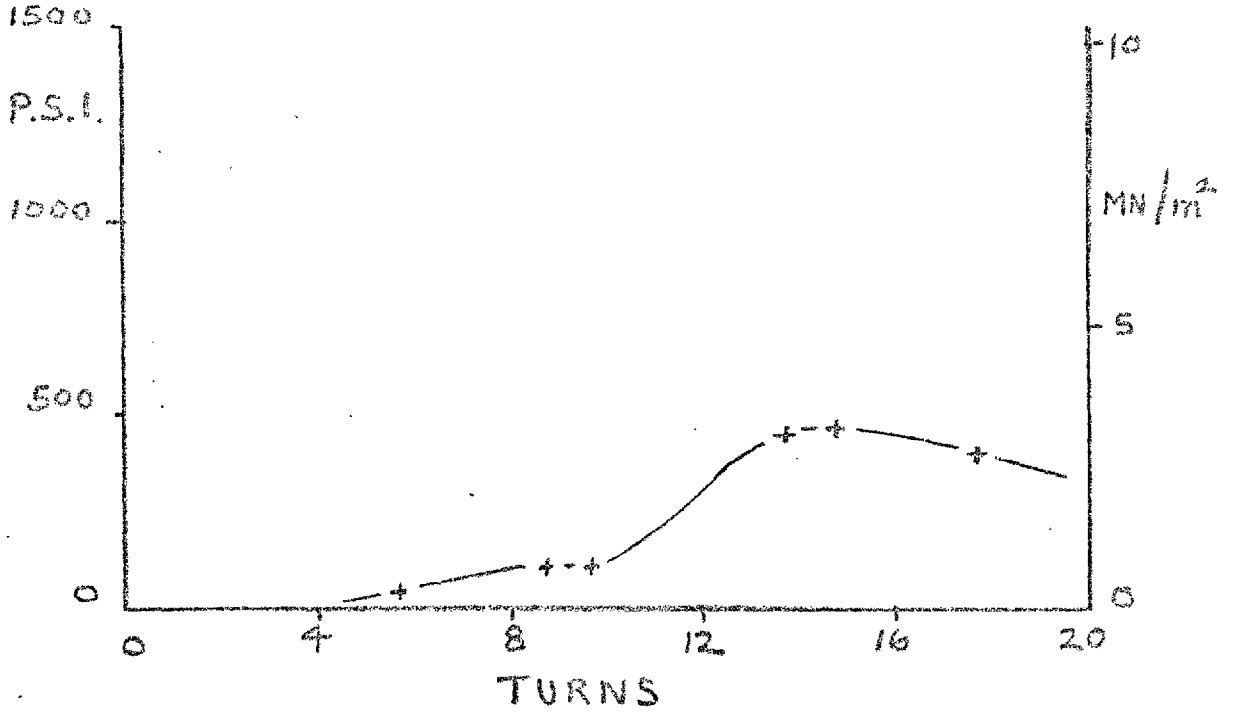
(b)Experiment 12, polypropylene. N(40); Q(93); D(3/32)

Figure 2.21

Experimental Axial Pressure Profiles



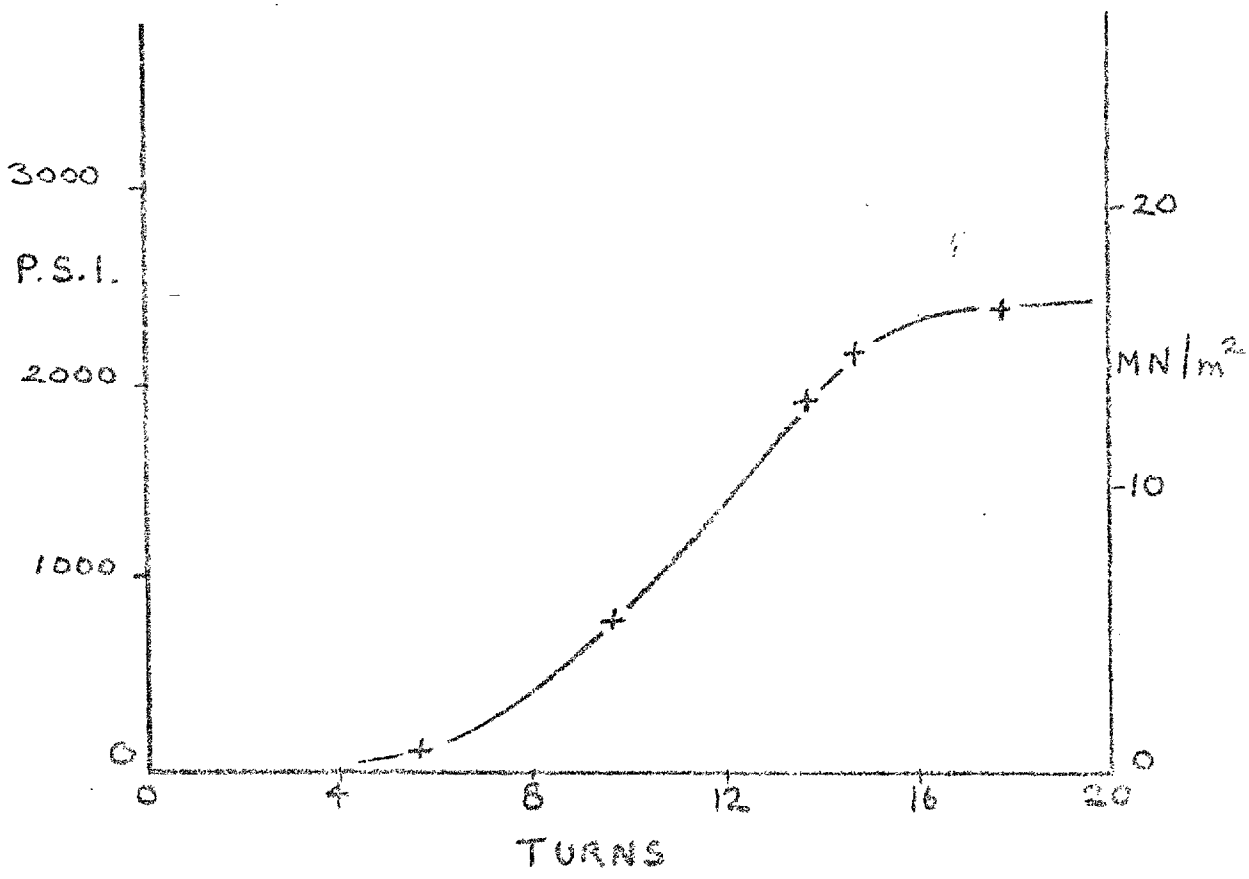
(a) Experiment 13, polypropylene. N(80); Q(189); D(5/32)



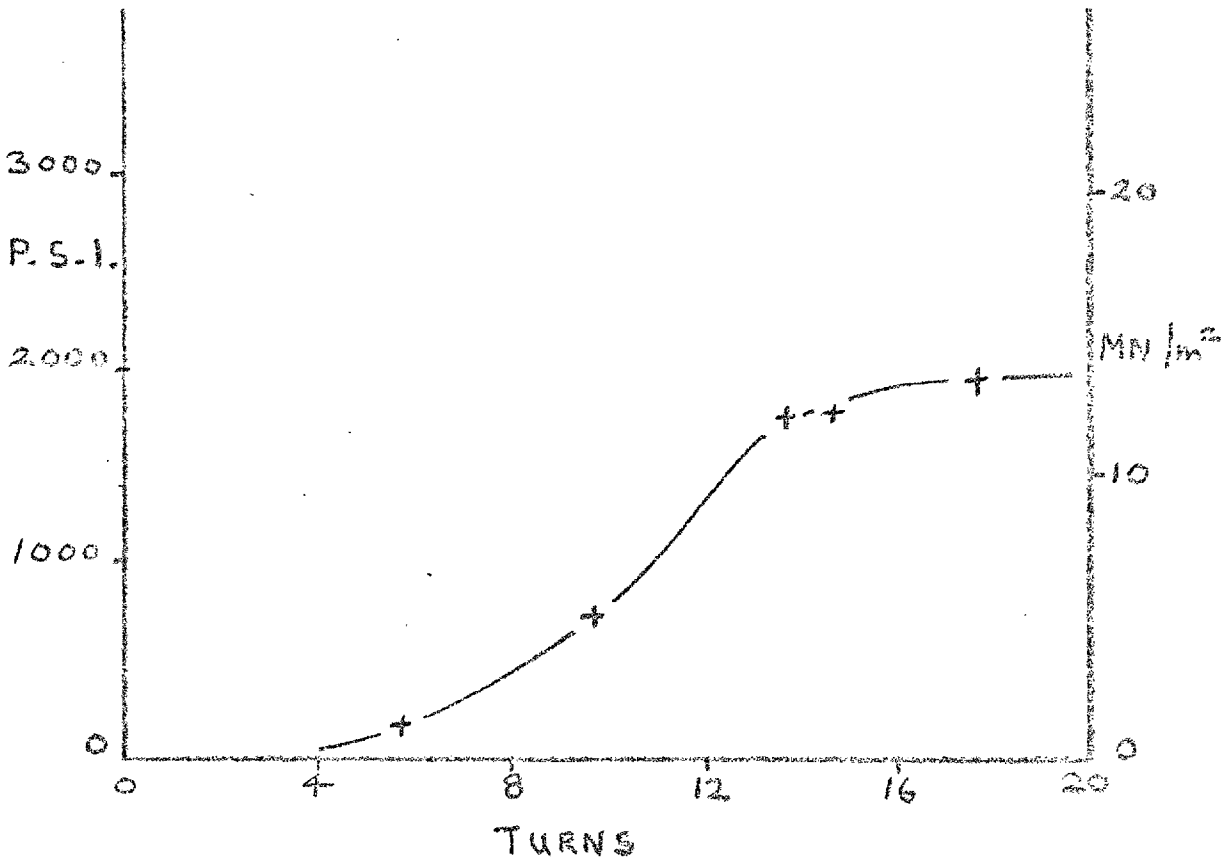
(b) Experiment 14, Polypropylene with screw cooling N(80); Q(143); D(5/32)

Figure 2.22

Experimental Axial Pressure Profiles



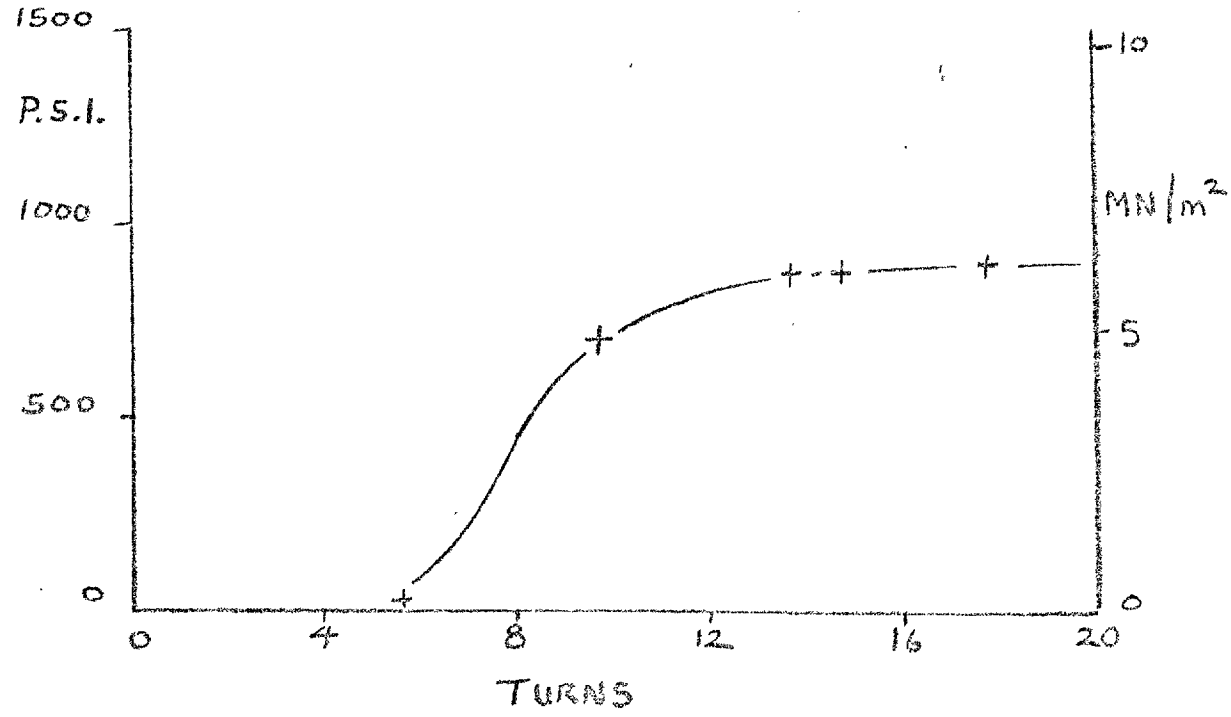
Experiment 15, High Density Polyethylene N(80); Q(187); D(3/32)



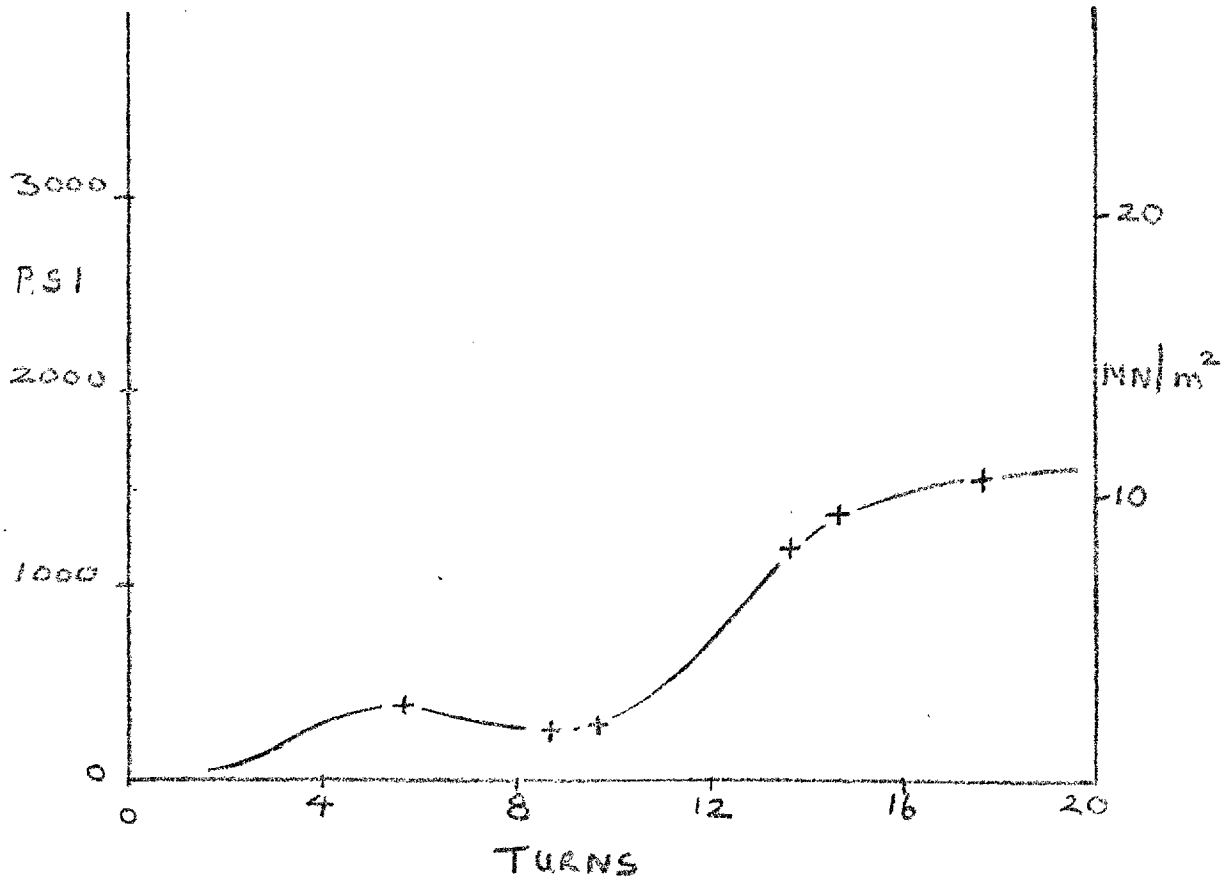
Experiment 16, High Density Polyethylene N(40); Q(94); D(3/32)

Figure 2.23

Experimental Axial Pressure Profiles



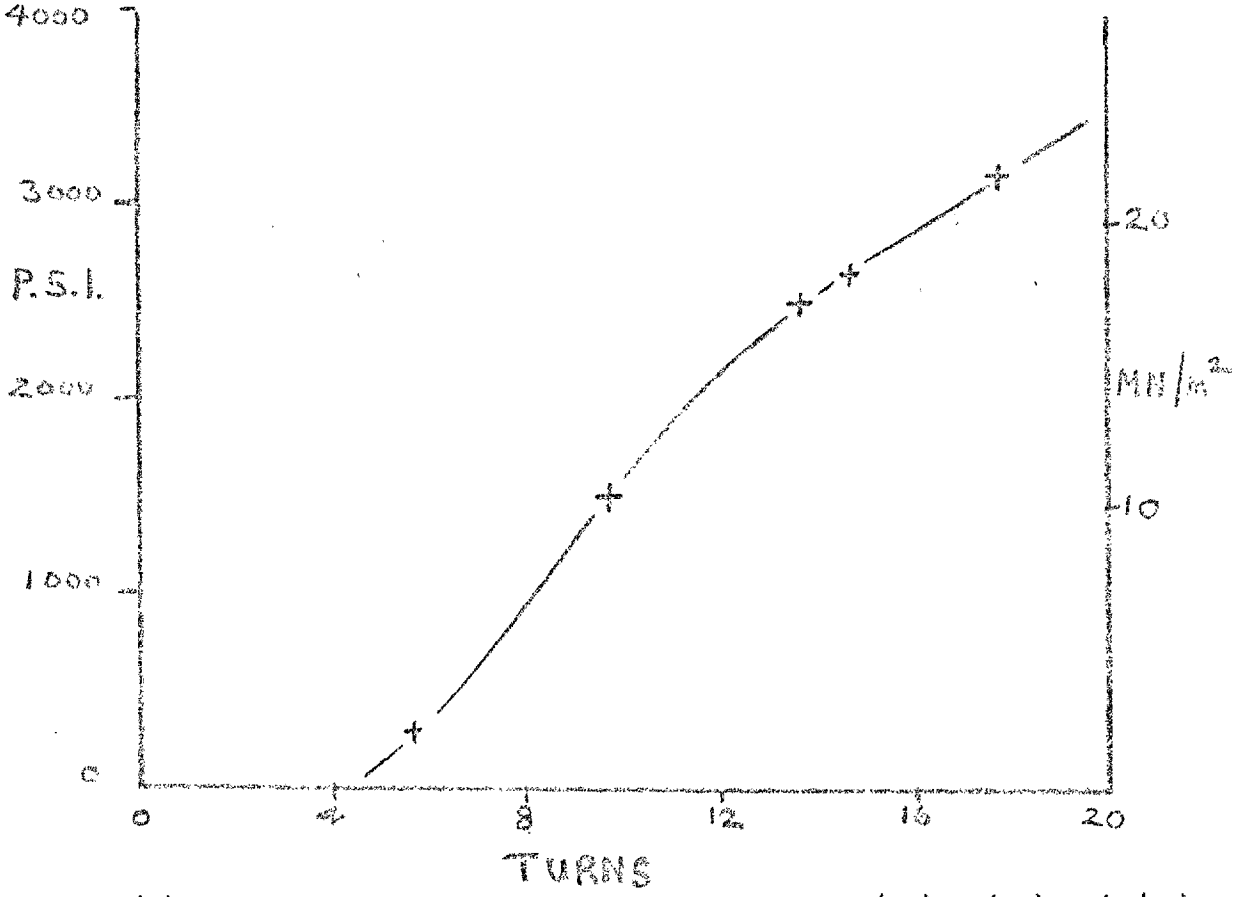
(a) Experiment 17, High Density Polyethylene N(80); Q(206); D(5/32)



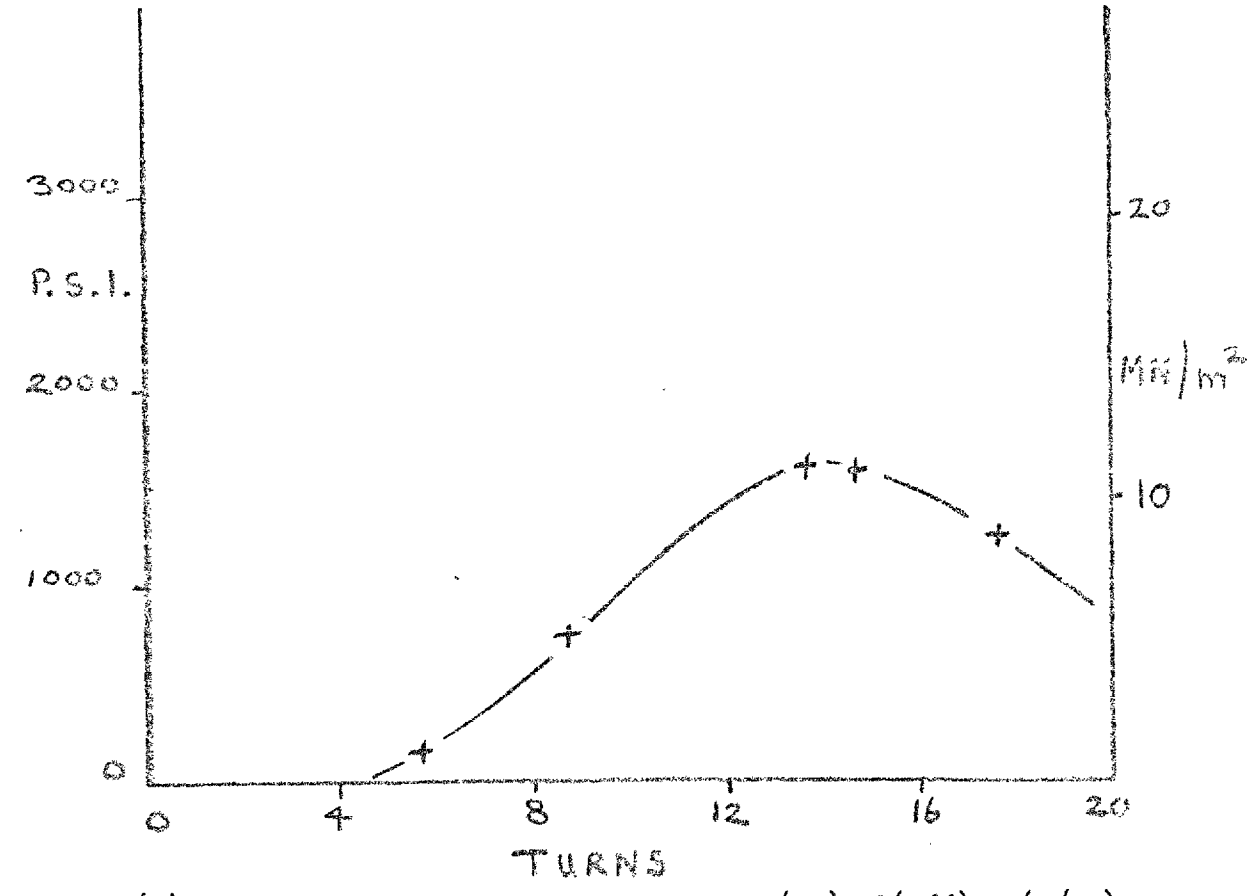
(b) Experiment 18, High Density Polyethylene with screw cooling N(80); Q(137); D(3/32)

Figure 2.24

Experimental Axial Pressure Profiles



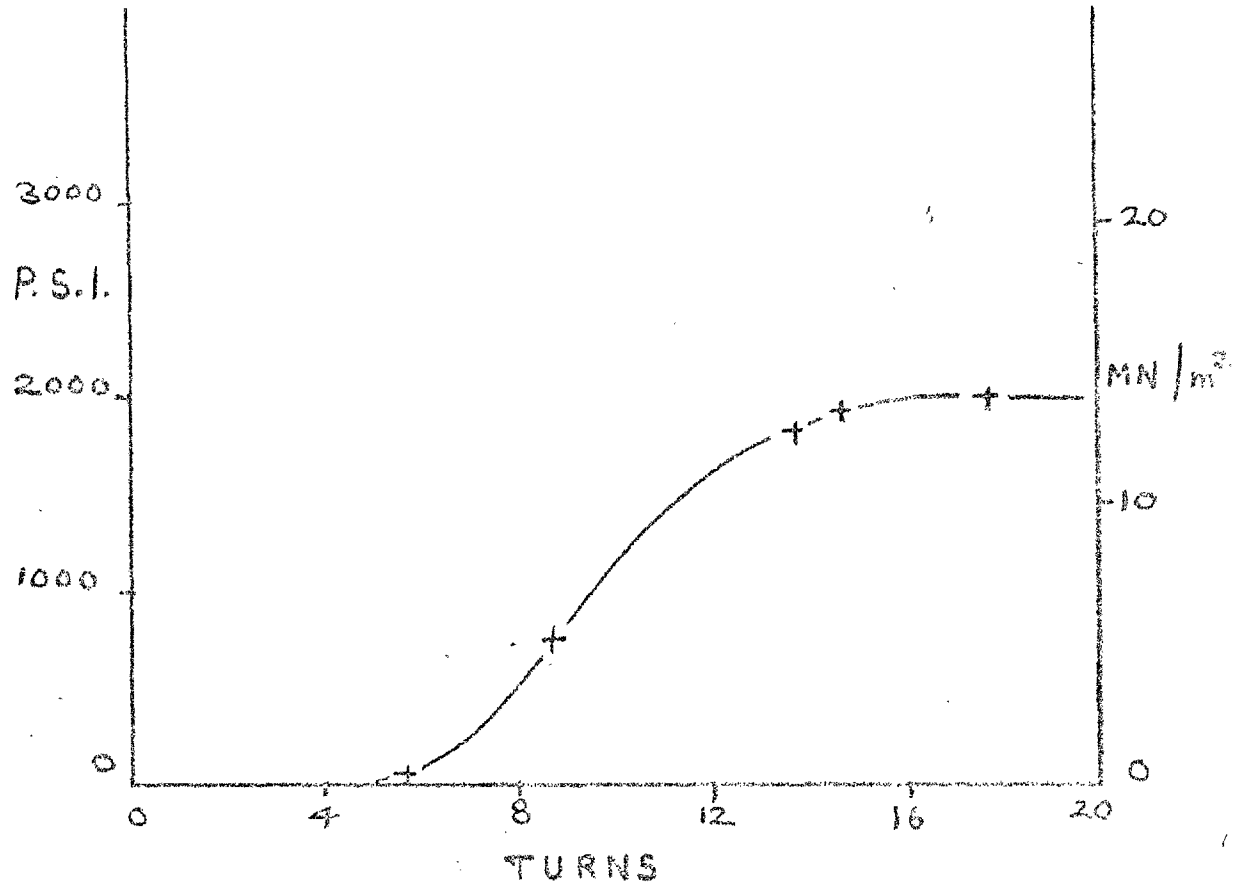
(a) Experiment 19, High Density Polyethylene N(40); Q(81); D(1/16)



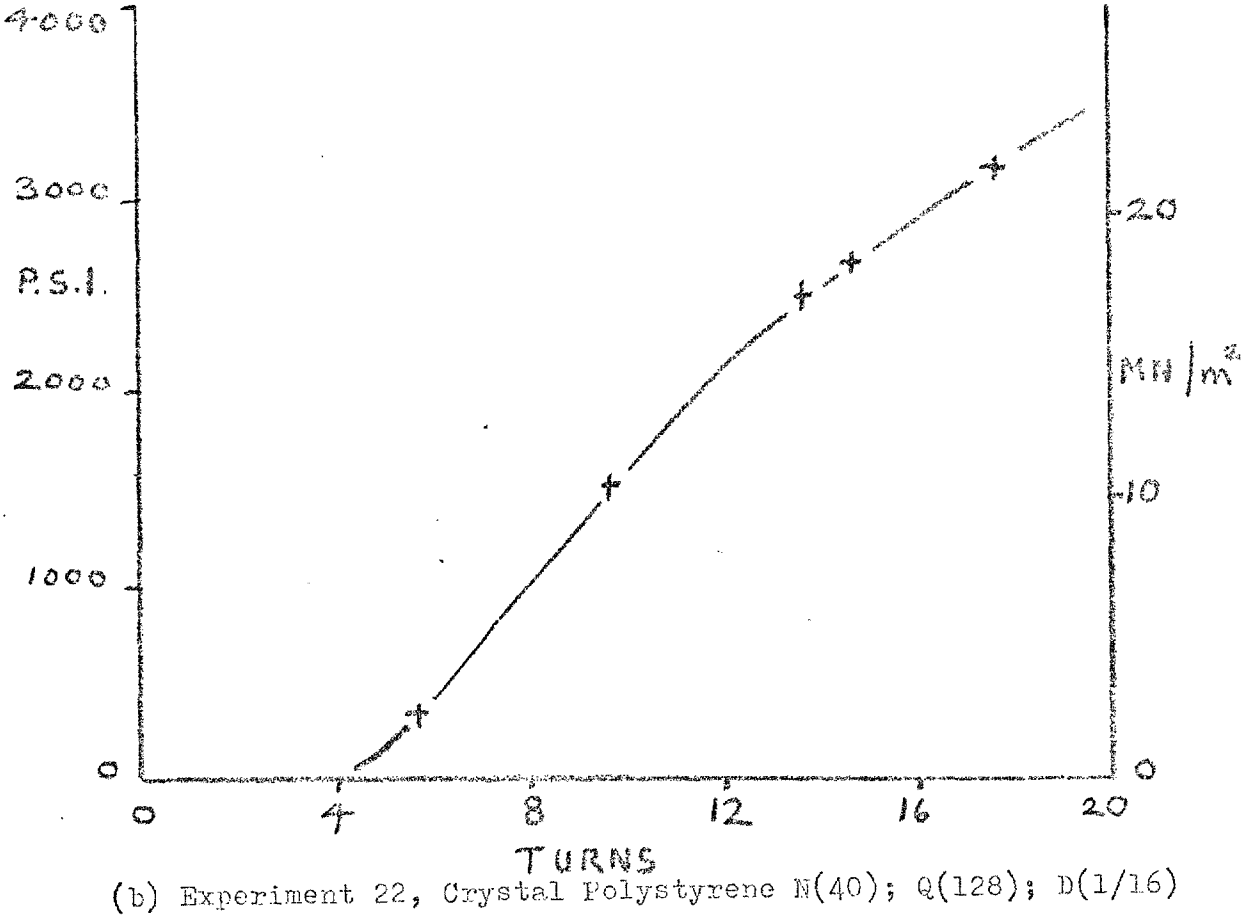
(b) Experiment 20, Crystal Polystyrene N(80); Q(266); D(5/32)

Figure 2.25

Experimental Axial Pressure Profiles



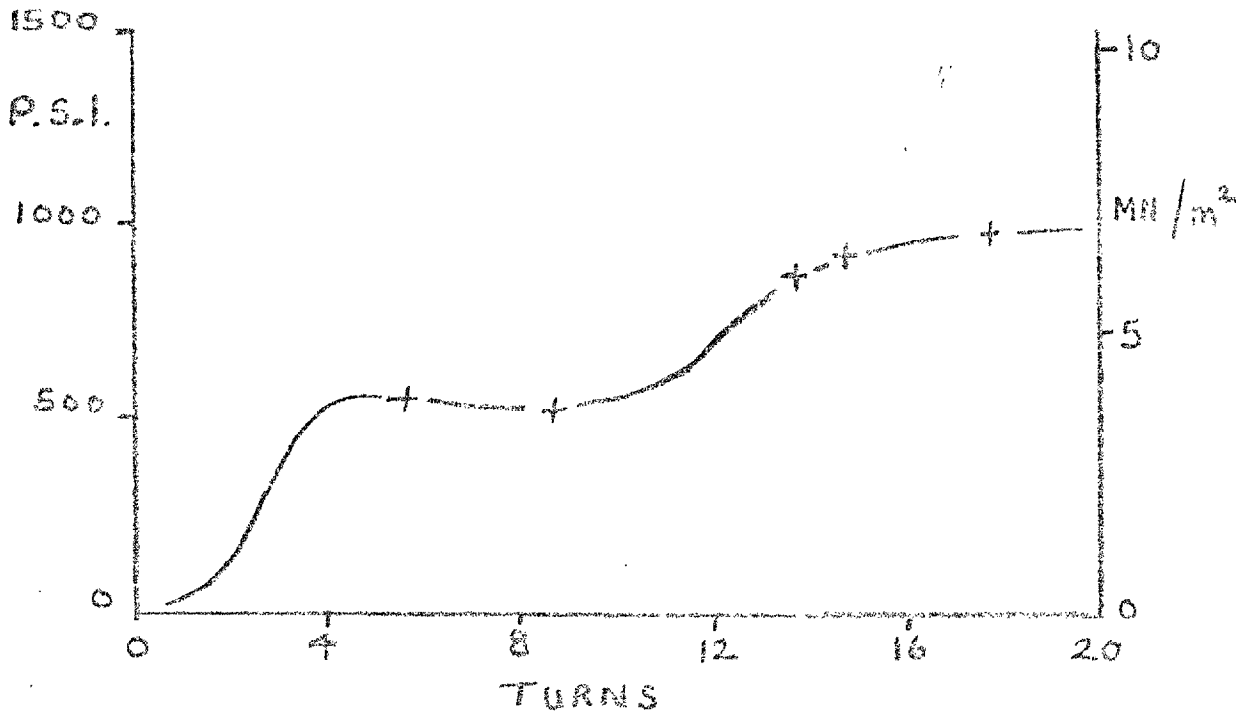
(a) Experiment 21, Crystal Polystyrene N(40); Q(110); D(3/32)



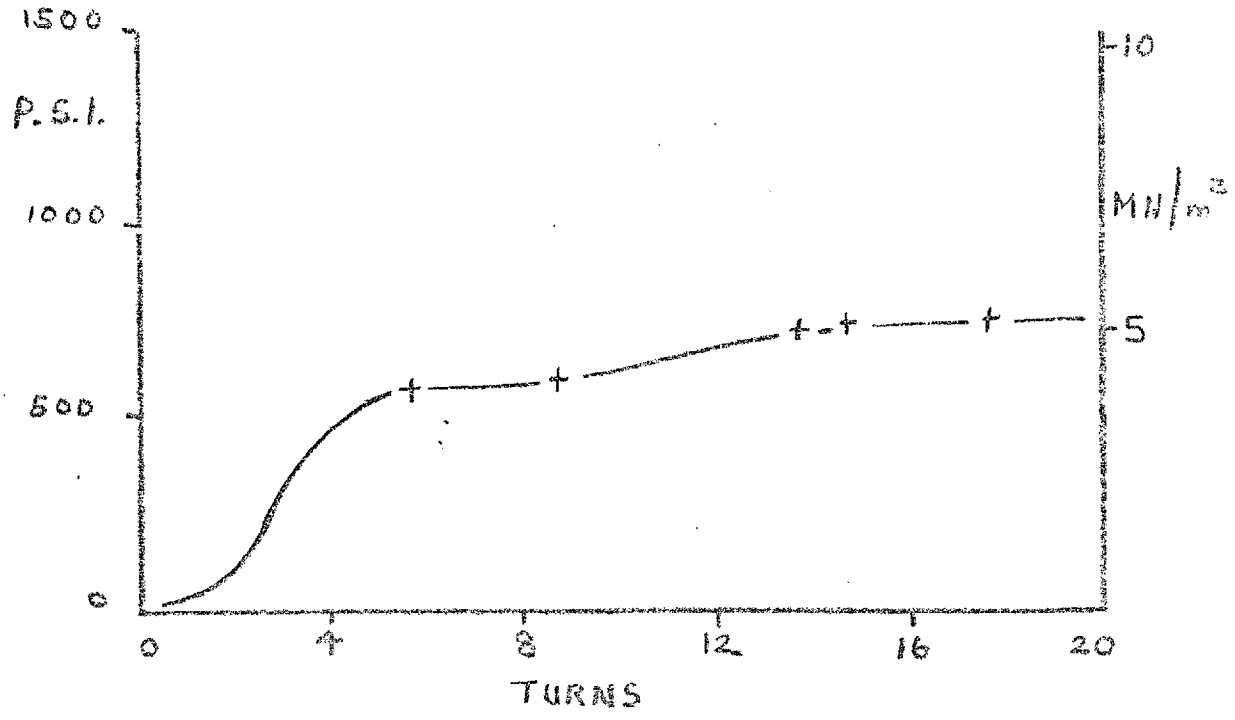
(b) Experiment 22, Crystal Polystyrene N(40); Q(128); D(1/16)

Figure 2.26

Experimental Axial Pressure Profiles



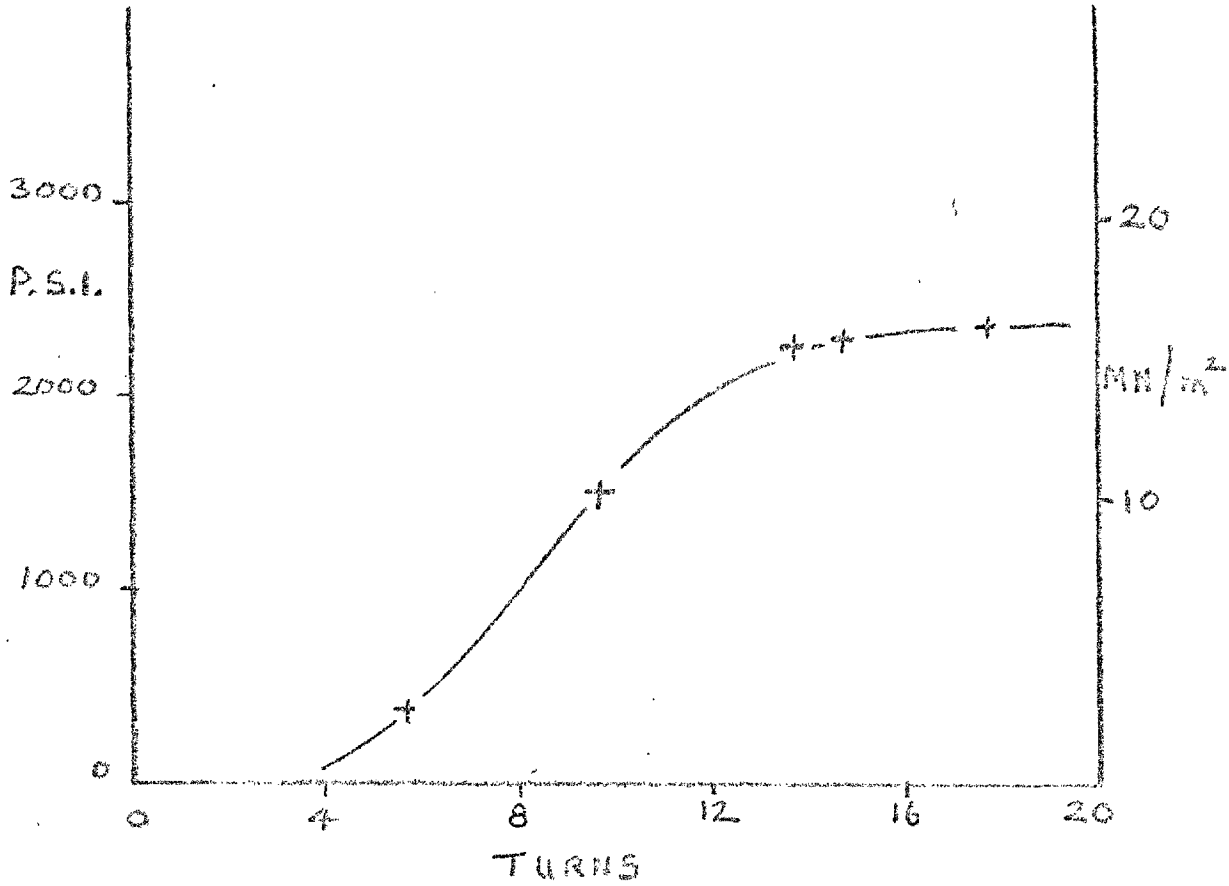
(a) Experiment 23, Melinex N(80); Q(319); D(3/32)



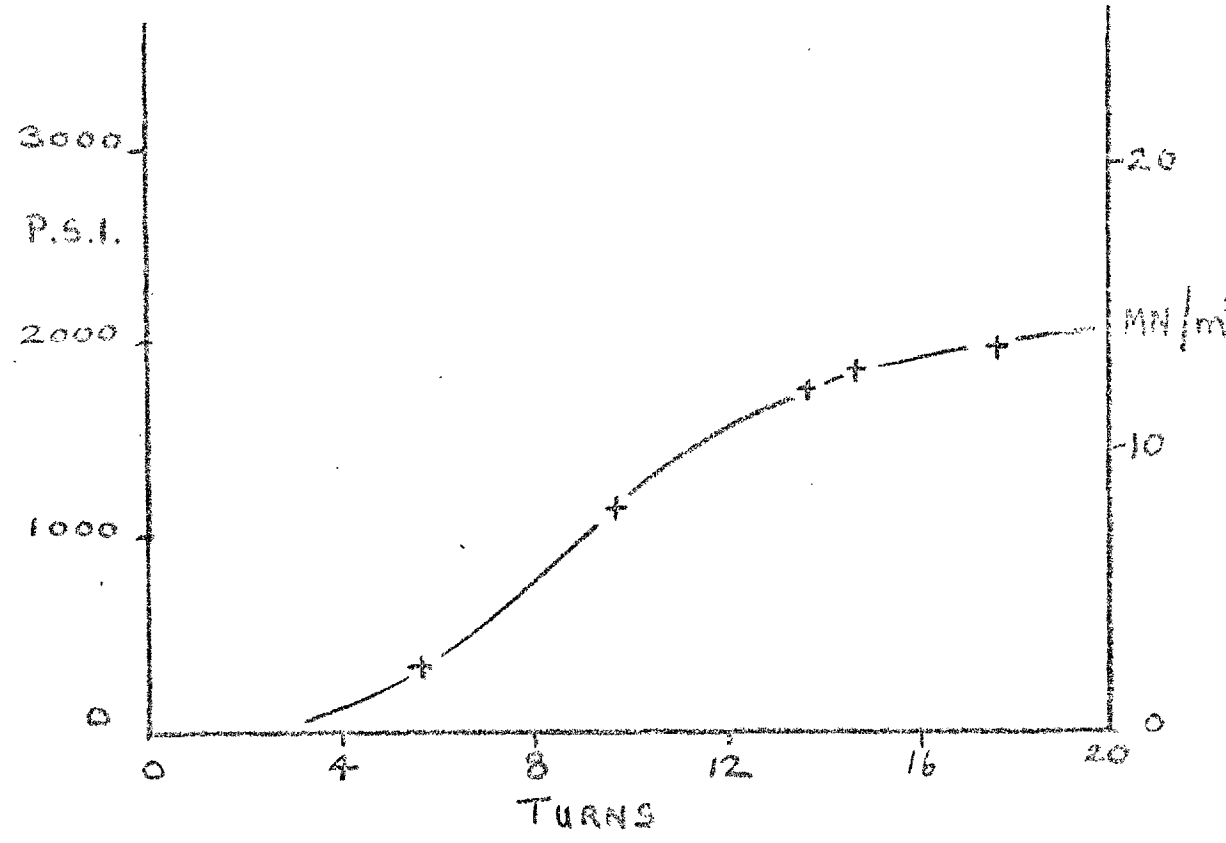
(b) Experiment 24, Melinex N(40); Q(164); D(3/32)

Figure 2.27

Experimental Axial Pressure Profiles



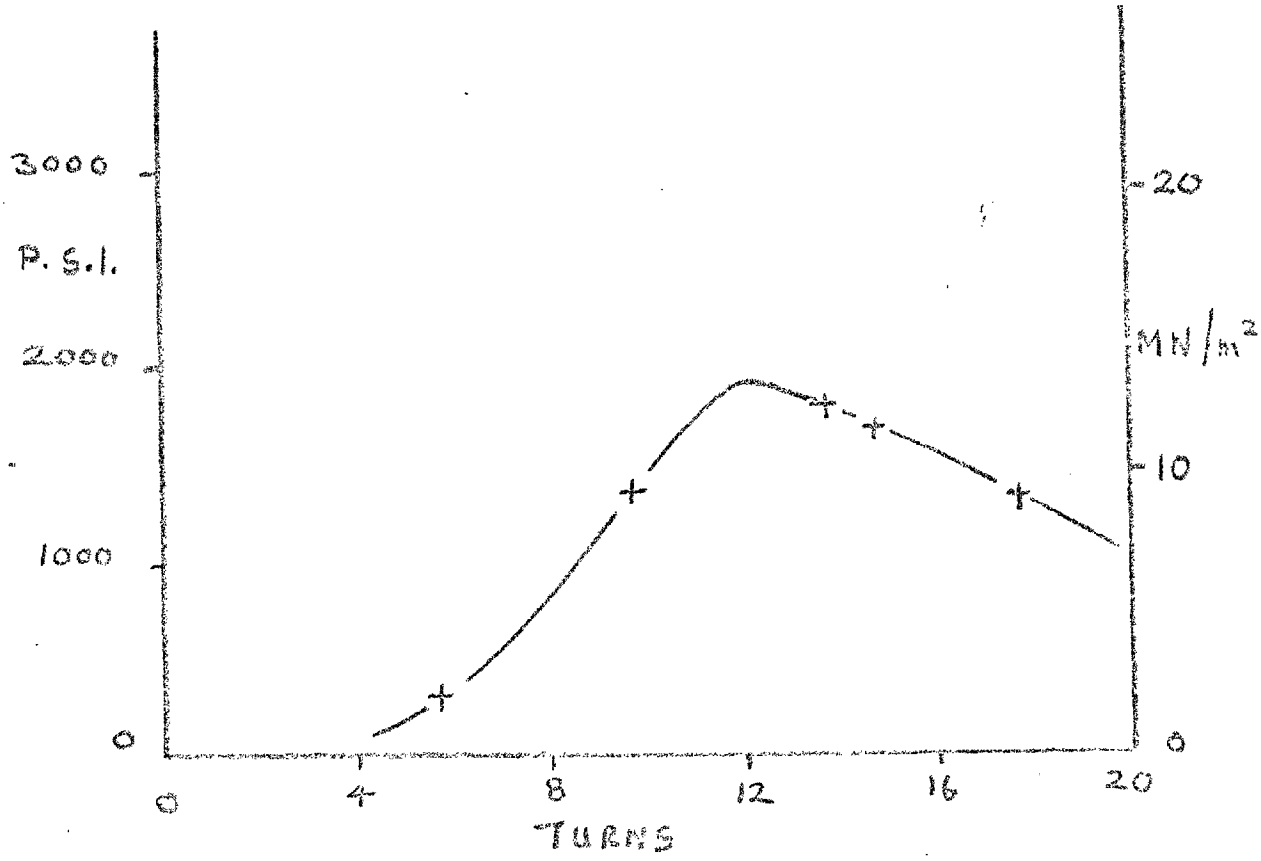
(a) Experiment 25, Low Density Polyethylene Powder N(80); Q(203); D(3/32)



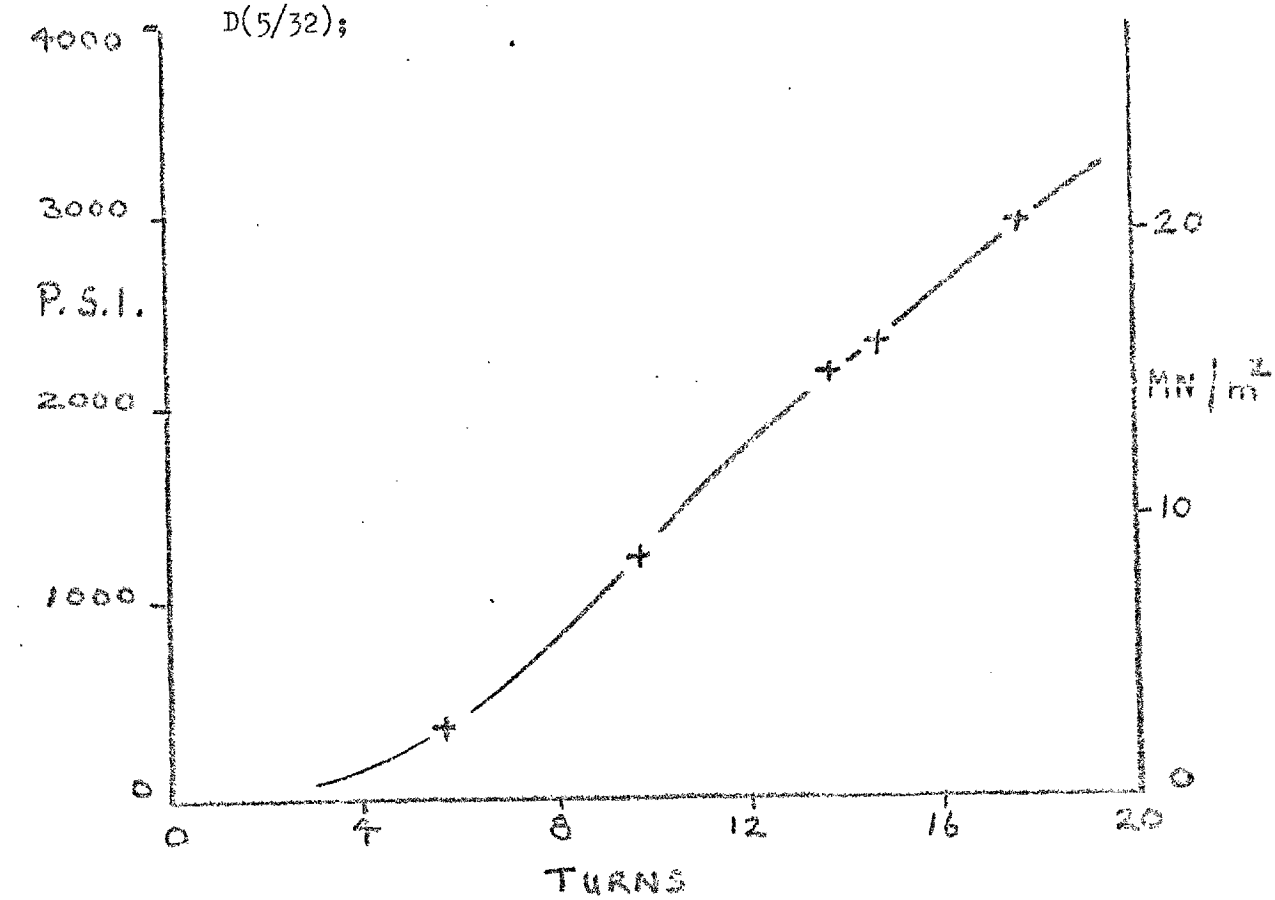
(b) Experiment 26, Low Density Polyethylene Powder N(40); Q(115); D(3/32)

Figure 2.28

Experimental Axial Pressure Profiles



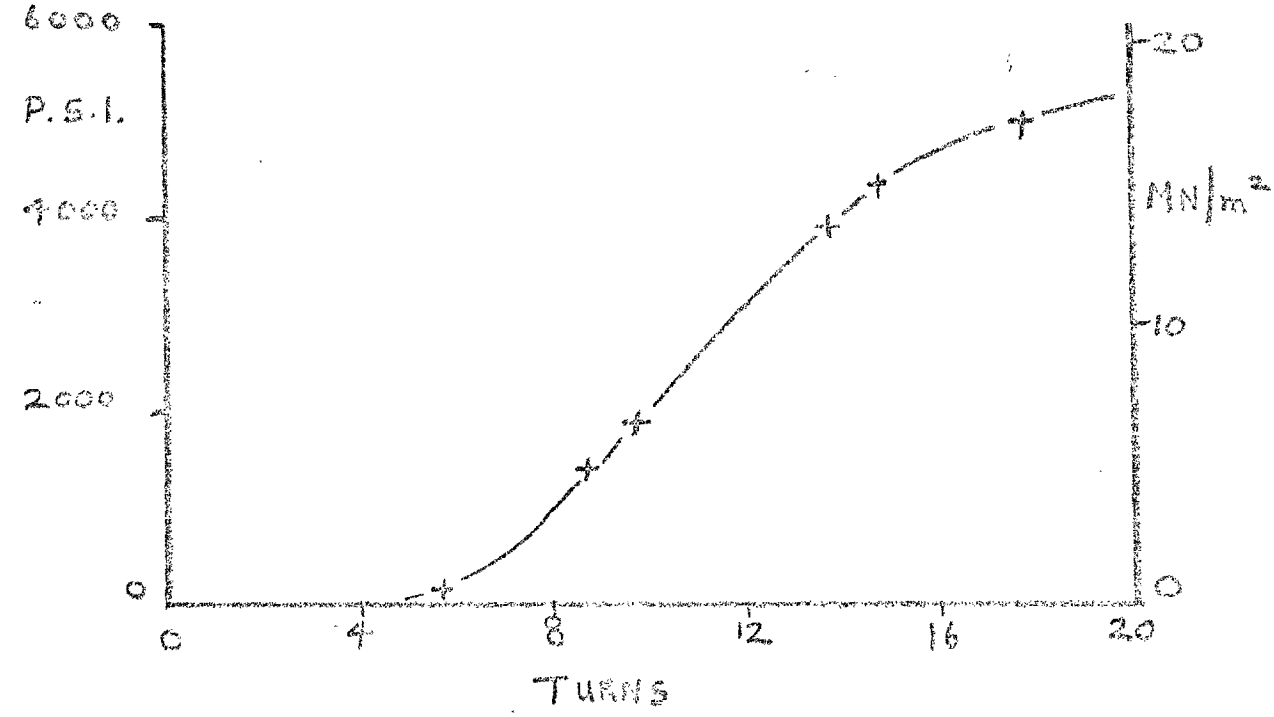
(a) Experiment 27, Low Density Polyethylene Powder N(80); Q(221); D(5/32);



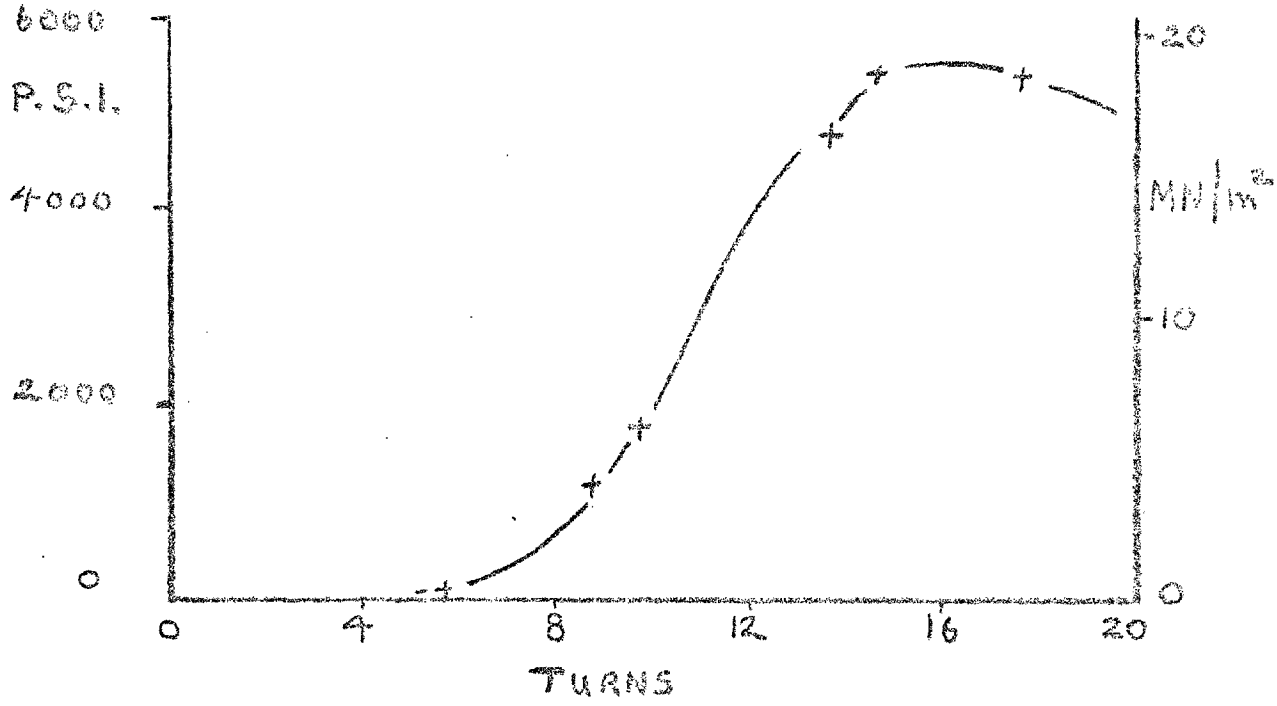
(b) Experiment 28, Low Density Polyethylene Powder N(40); Q(78); D(1/16)

Figure 2.29

Experimental Axial Pressure Profiles



(a) Experiment 29, Rigid PVC Powder N(80); Q(419); D(3/32)



(b) Experiment 30, Rigid PVC Powder N(40); Q(165); D(3/32)

2.4 Discussion of the Experimental Results

It has been stated that the aims of the present experiments were twofold; to obtain more qualitative information concerning the pattern of melting and the mechanisms operating with the extruder which produce these patterns, and secondly to obtain quantitative information of the melting process to be used in comparison with theoretical predictions. This latter specific data will be presented in the later chapter dealing with this comparison and does form part of the contents of this section.

Essentially then the present section deals with the observation and interpretation of the results with a view to obtaining, initially, a basic qualitative understanding of the melting process. Such an understanding will then provide the background against which to develop the theoretical analysis. The more complete an understanding one has of the process the better able one should be to make the necessary simplifications which allow the setting up of an analysis for which one can readily find the solution.

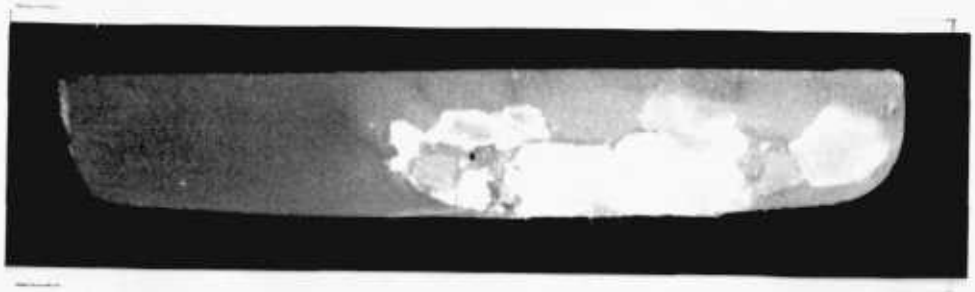
Initial observation of the melting cross-sections illustrated in the Plates shows that break-up of the solid bed is by no means uncommon. If, for the moment only, the melting behaviour prior to the bed break-up is considered, then it can be seen that the melting patterns conform to that observed by Maddock (2) and others. One typical such melting cross-section for each of the experimental materials is shown in figures 2.30 and 2.31.

A few simple observations concerning the presence or not of a melt film between the solid bed and the screw root can be made. For those experiments which do not exhibit bed break-up and did not have screw cooling, such a melt film always appeared during the later stages of melting. In some cases developing a significant thickness such that it could no longer be considered a film. For those experiments which did exhibit bed break-up this film was consistently observed and it can be seen in the Plates that bed break-up never occured before this melt film had formed and further that the break occured soon after the formation of this film. The experiments performed with water cooling of the screw did not display either a melt film beneath the solid bed or bed break-up.

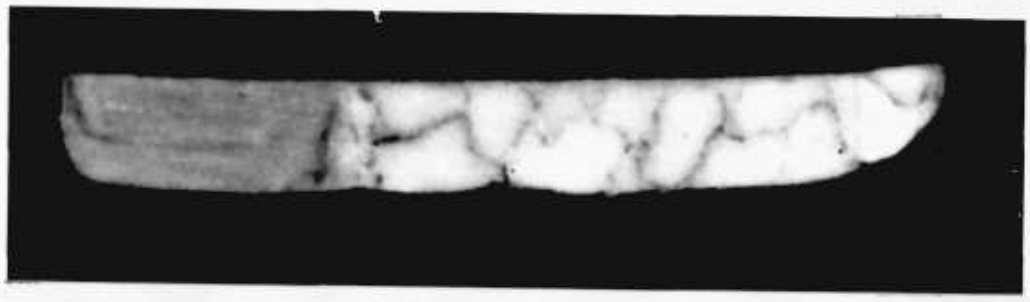
The initial conclusions that are drawn from the foregoing are that the hitherto

Figure 2.30

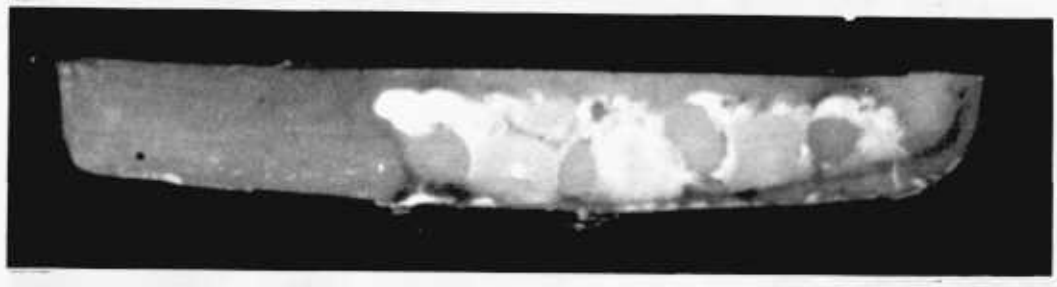
Typical Experimental Cross-Sections obtained in the present Experiments



(a) Experiment 7, Low density polyethylene, 9½ turns along the screw



(b) Experiment 2, Plasticised PVC, 11 turns along the screw



(c) Experiment 16, High density polyethylene, 10 turns along the screw



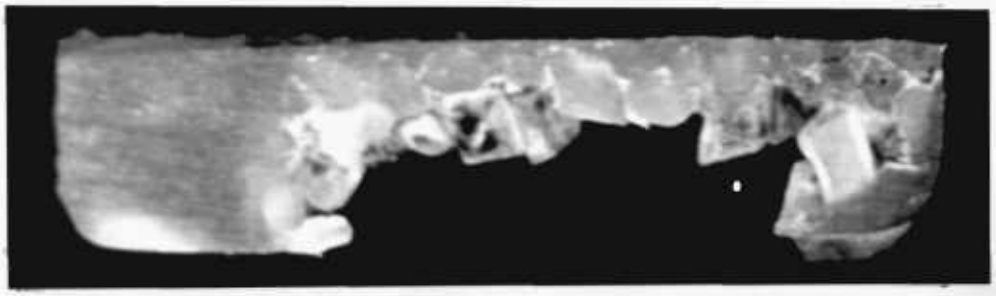
(d) Experiment 11, Polypropylene, 8 turns along the screw

Figure 2.31

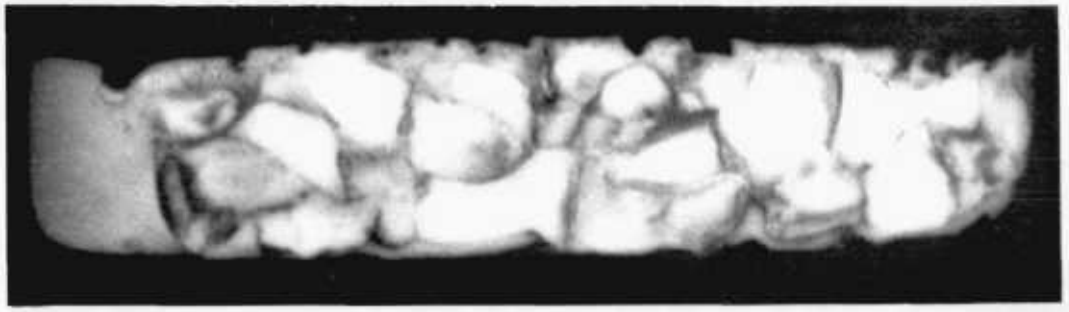
Typical Experimental Cross-Sections obtained in the present Experiments



(a) Experiment 27, Low density polyethylene powder, 7 turns along the screw



(b) Experiment 20, Polystyrene, $6\frac{1}{2}$ turns along the screw



(c) Experiment 24, Melinex, 8 turns along the screw



(d) Experiment 29, Rigid PVC, $7\frac{1}{2}$ turns along the screw

observed melting pattern is verified but that the occurrence of the phenomenon known as solid bed break-up, which has been observed and reported before (5,10) is fairly common and that its importance and its implications may have been ignored. It is appropriate before discussing this phenomenon in more detail to describe and discuss the detailed pressure traces taken during the experiments. Figures 2.32 to 2.46 show a selection of detail pressure traces together with, in relevant cases, the corresponding cross-sectional specimens, for a range of experiments. The traces are numbered from 1 to 6 from the feed hopper to the die respectively. Thus the number of each trace identifies its position along the barrel uniquely.

Figure 2.47 shows a sketch of part of the straightened out extruder channel with its solid bed melt pool interface marked out. It also shows the path along which the transducers record the pressure variation which is not at right angles to the channel walls. Therefore the cross-sections presented below the detail pressure traces in the above mentioned figures are approximations to and not an accurate representation of the state of the actual material in the channel whose pressure the transducer was recording.

It is also important to realise that the finite cap area of the transducers has an effect on the pressure recordings taken. Figure 2.48 illustrates a possible likely effect. Below the regular outline of the channel, with the transducer cap above it, is shown what might be the true pressure variation occurring. Below this is the trace that would be recorded by the UV recorder assuming that the transducer measures the average pressure over its cap area. It can be seen that given this assumption the transducer can only accurately measure the pressure at any point in its path when the actual pressure gradient is constant over the area of its cap. If the pressure gradient is changing the transducer effectively reduces this rate of change and hence smooths out pressure maximums or minimums.

Referring firstly to figures 2.32 to 2.34, these show the results for plasticised PVC granules from experiment 3. It can be seen that when the channel is completely full of molten, or gelled material in the case of PVC, trace 6 shown in figure 2.34, the trace is a smooth one exhibiting a 'saw tooth' shape. That

Figure 2.32

'Cross channel' pressure profile and corresponding specimen cross-section for plasticised PVC from experiment 3 at the 14 turn position

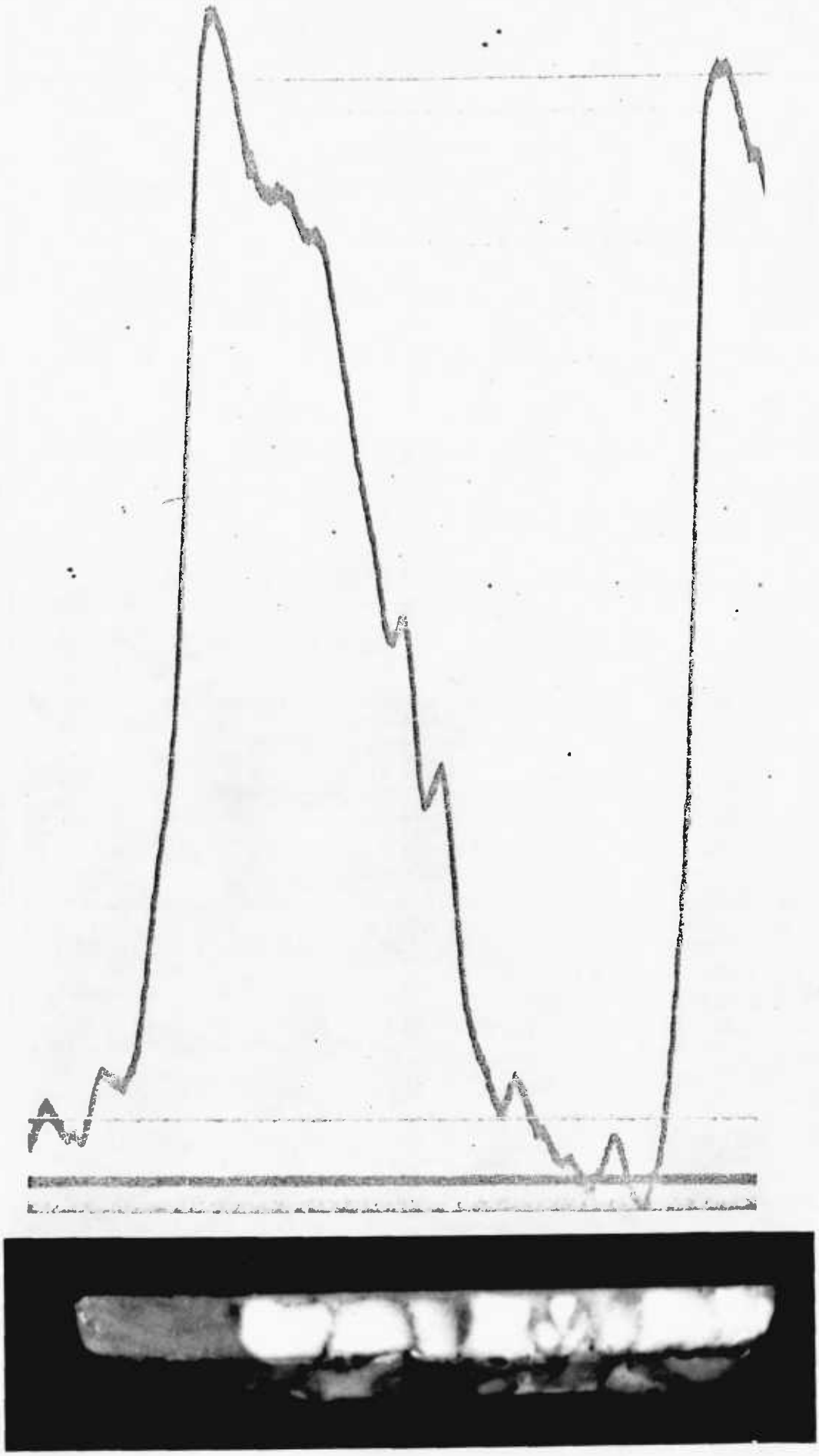


Figure 2.33

'Cross channel' pressure profile and corresponding specimen cross-section for plasticised PVC, from experiment 3, at the 15 turn position

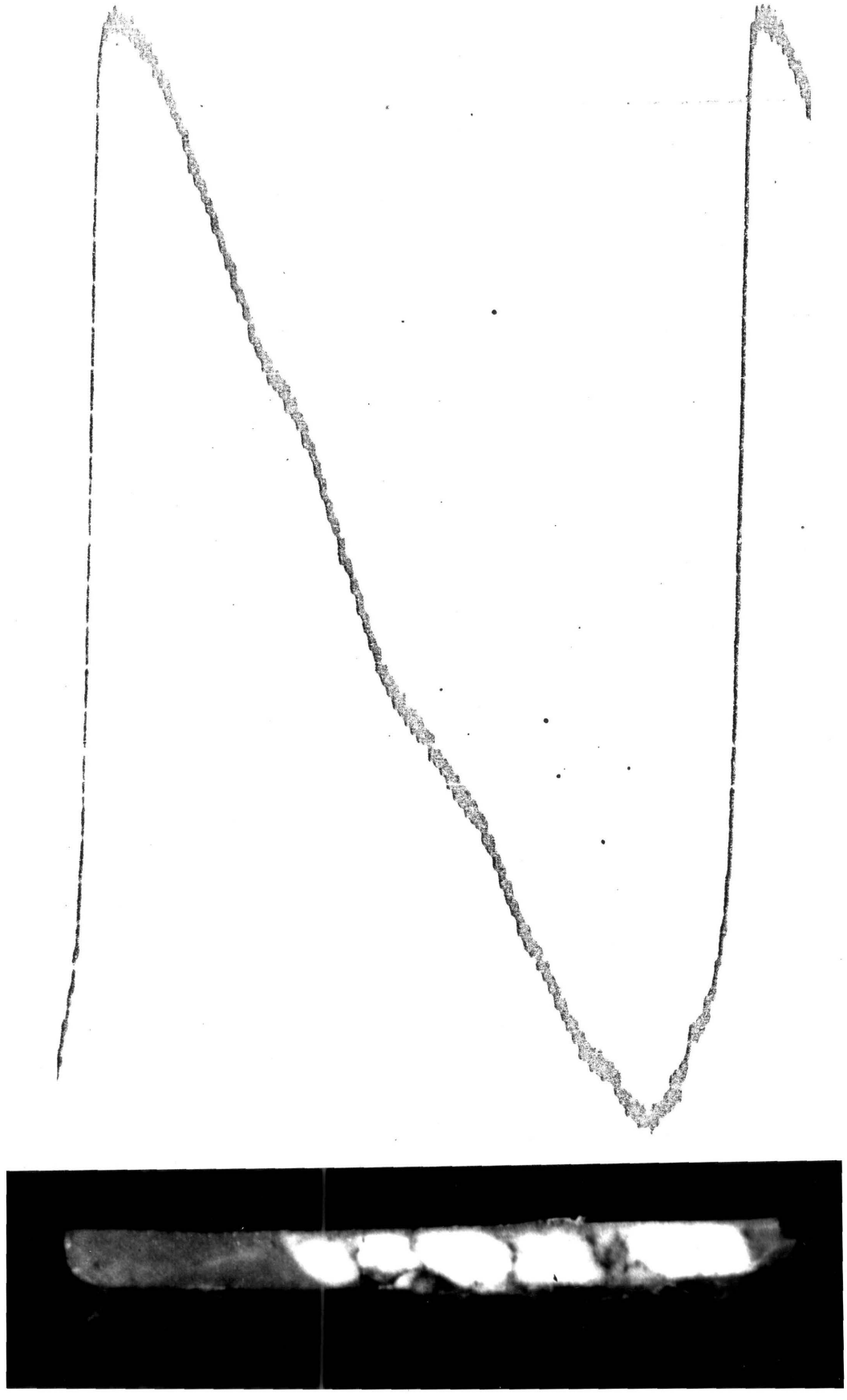


Figure 2.34

'Cross channel' pressure profile and corresponding specimen cross-section for plasticised PVC from experiment 3 at the 18 turn position

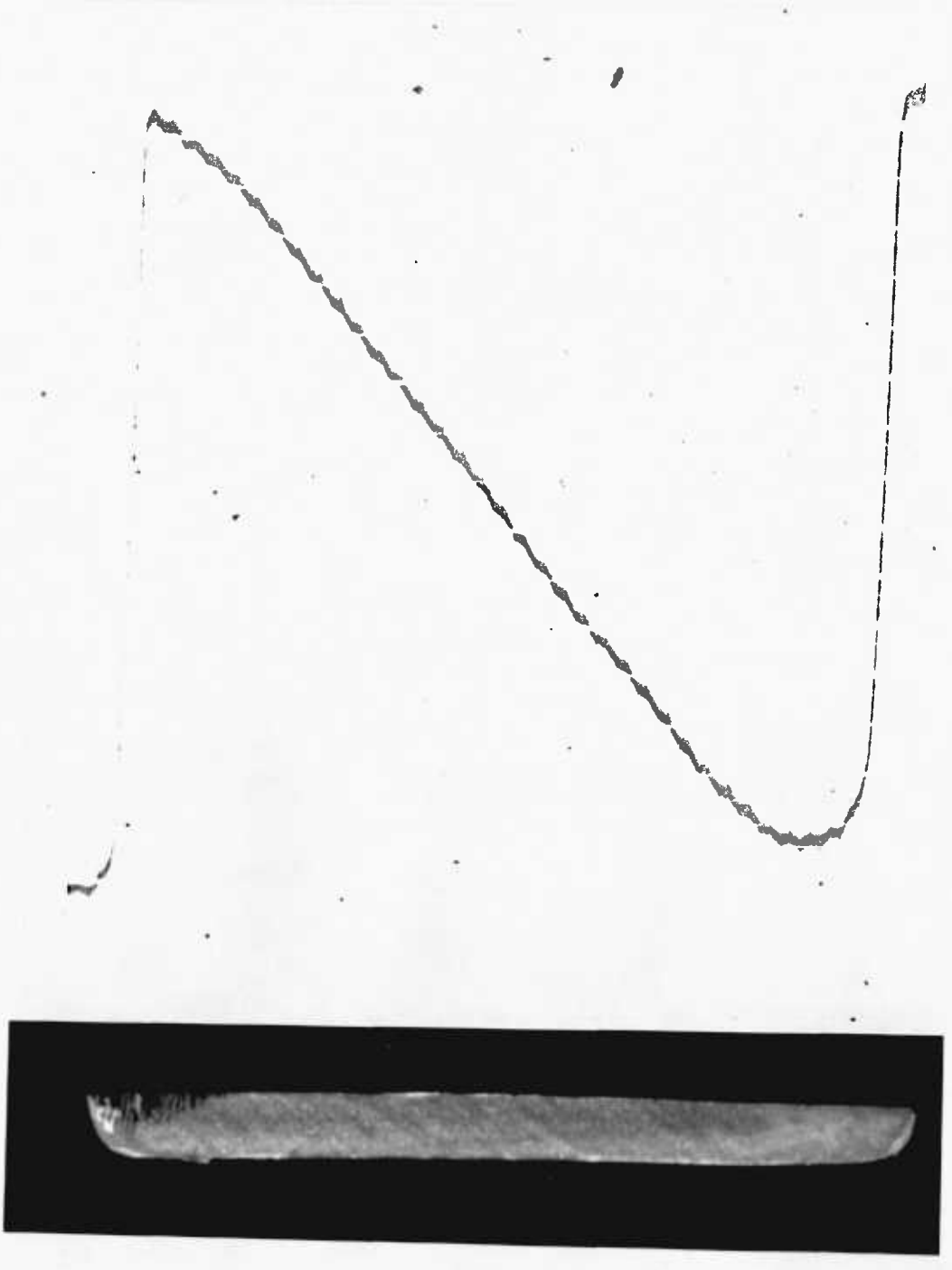


Figure 2.35

'Cross channel' pressure profile and corresponding specimen cross-section for polypropylene, from experiment 14 with screw cooling; at the 6 turn position

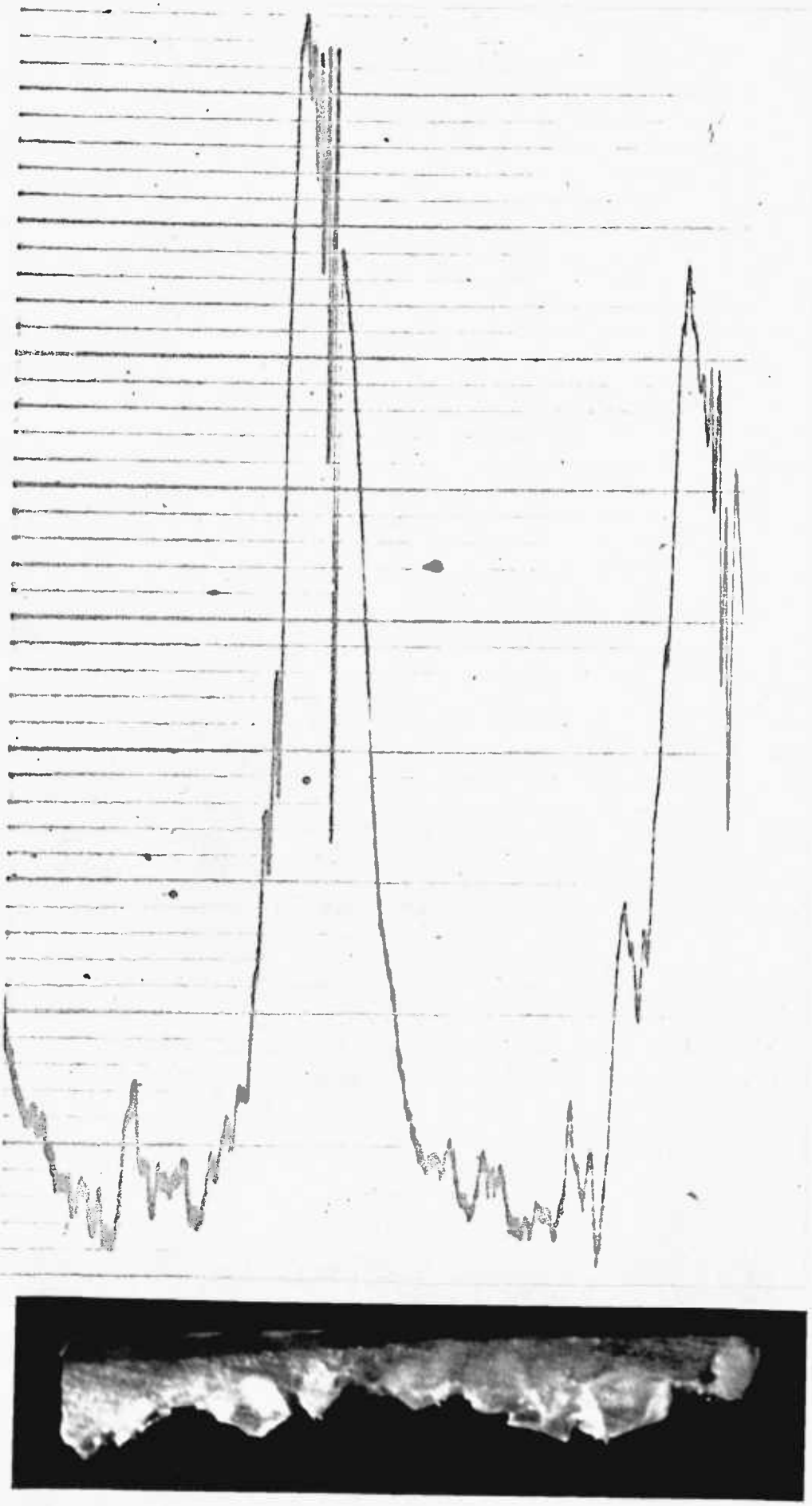


Figure 2.36

'Cross channel' pressure profile and corresponding specimen cross-section for polypropylene, from experiment 14 with screw cooling; at the 9 turn position

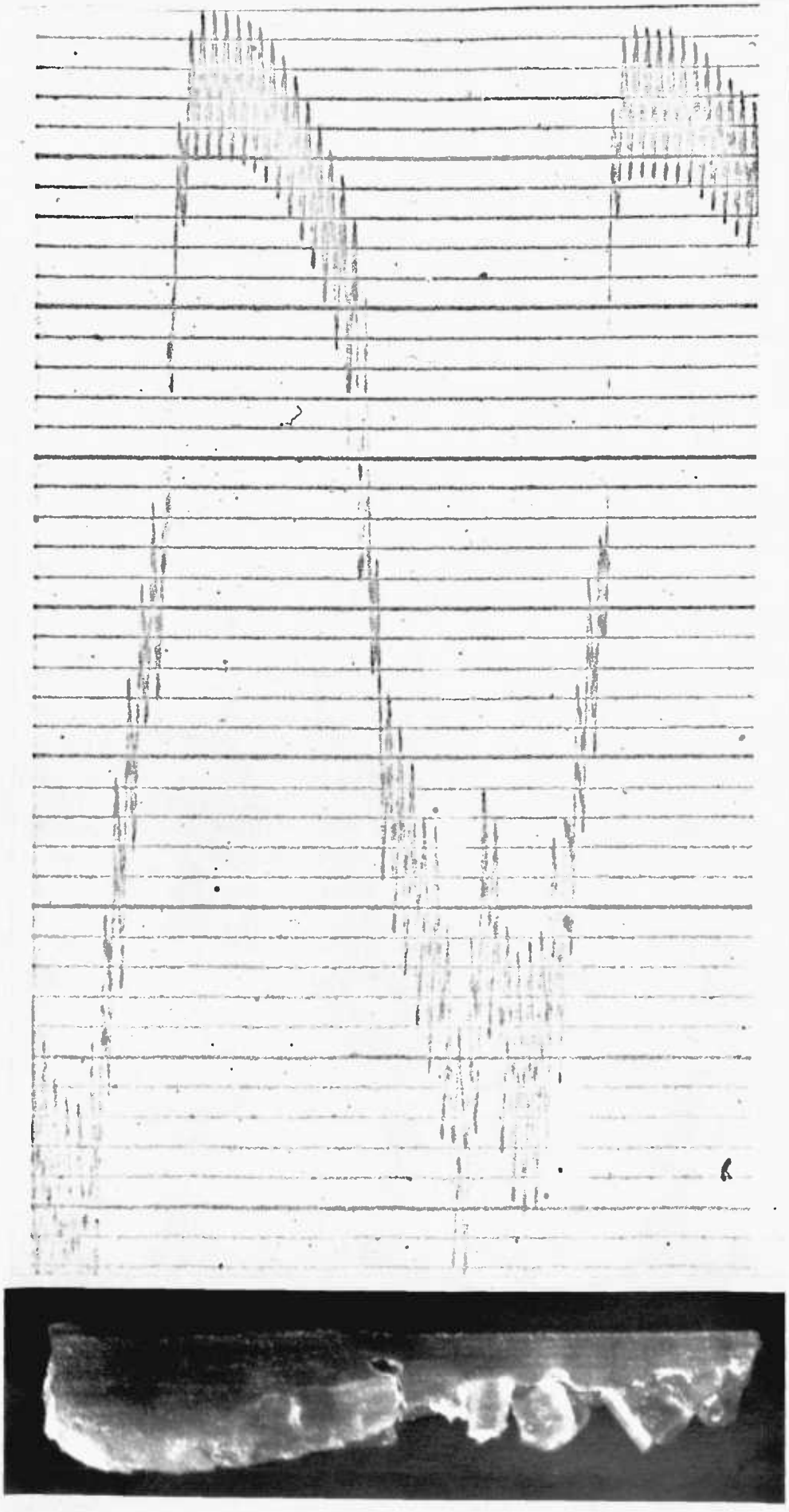


Figure 2.37

'Cross channel' pressure profile and corresponding specimen cross-section for polypropylene, from experiment 14 with screw cooling; at the 10 turn position

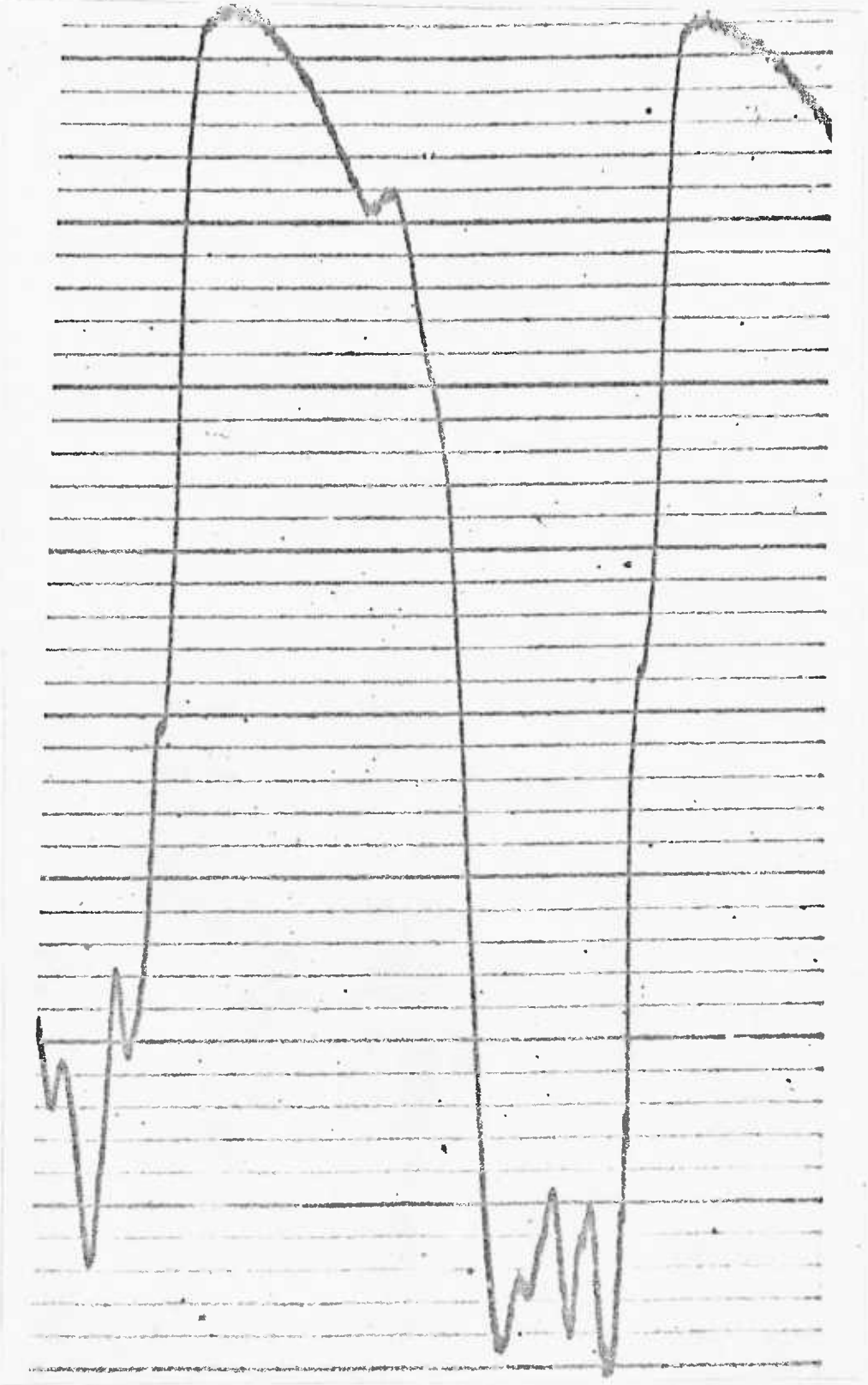


Figure 2.38

'Cross channel' pressure profile for polypropylene, from experiment 14 with screw cooling, at the 14 turn position

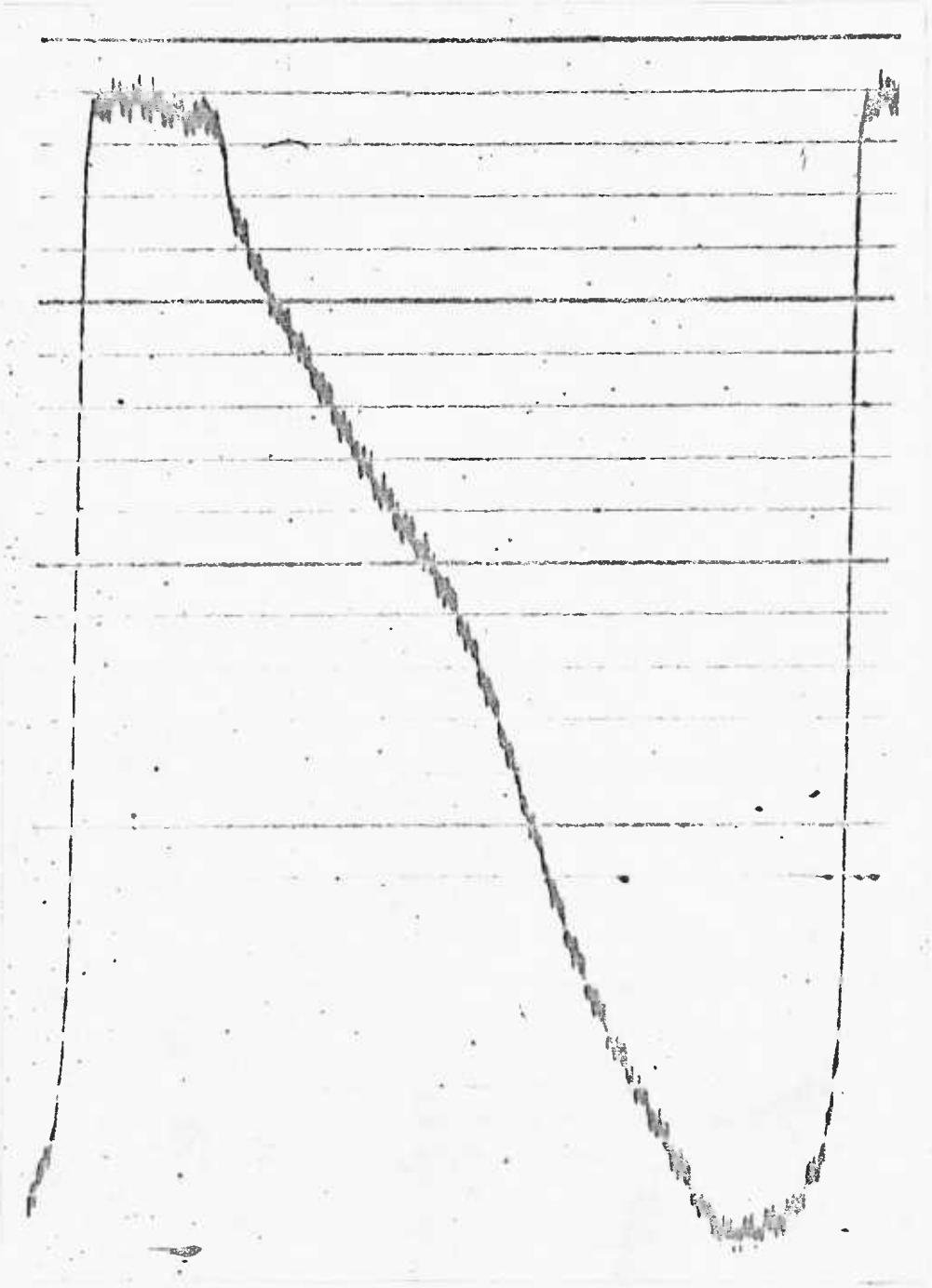


Figure 2.39

'Cross channel' pressure profile and corresponding specimen cross-section for low density polyethylene powder, experiment 27, at the 6 turn position

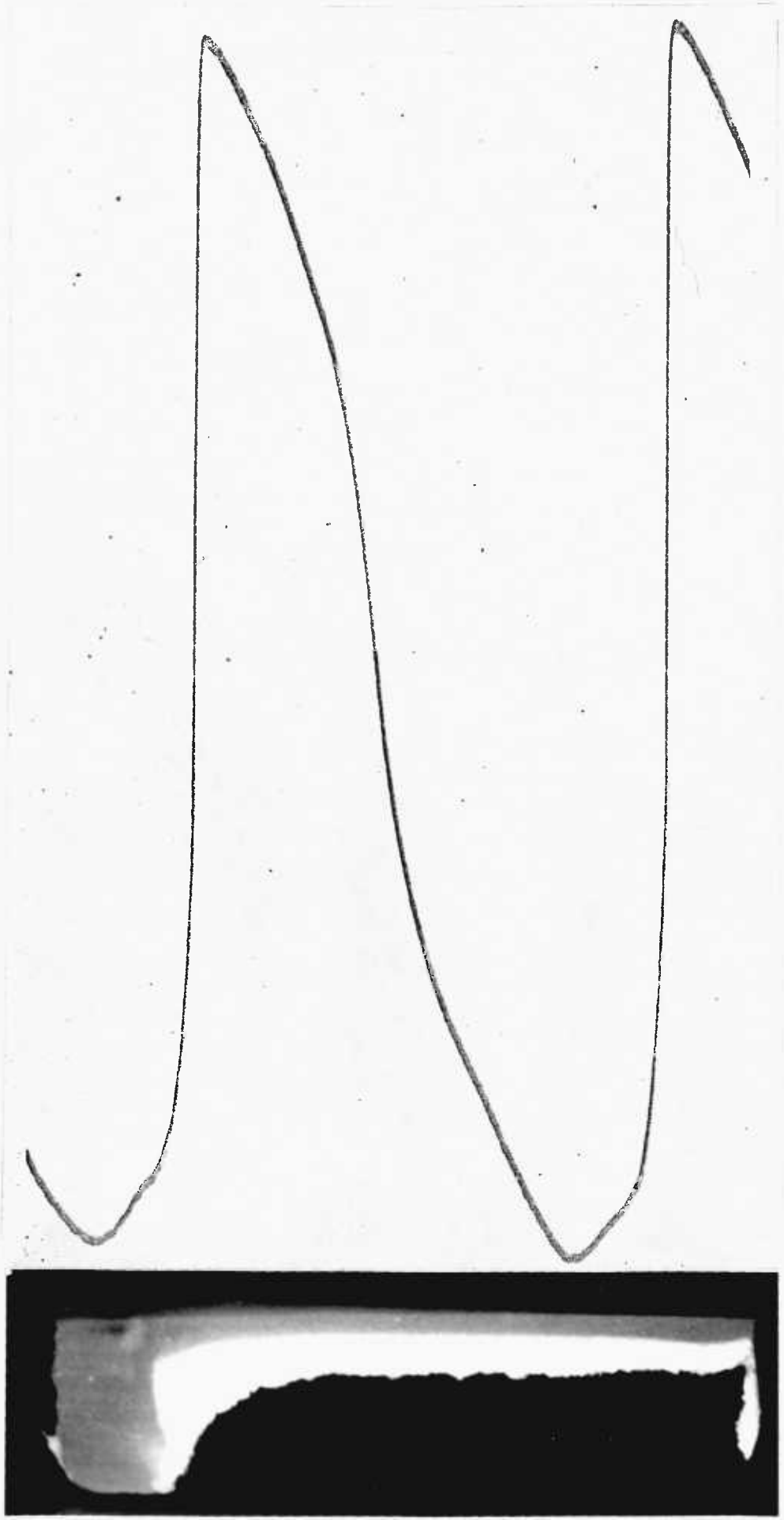


Figure 2.40

'Cross channel' pressure profile and corresponding specimen cross-section for low density polyethylene powder, experiment 27, at the 9 turn position

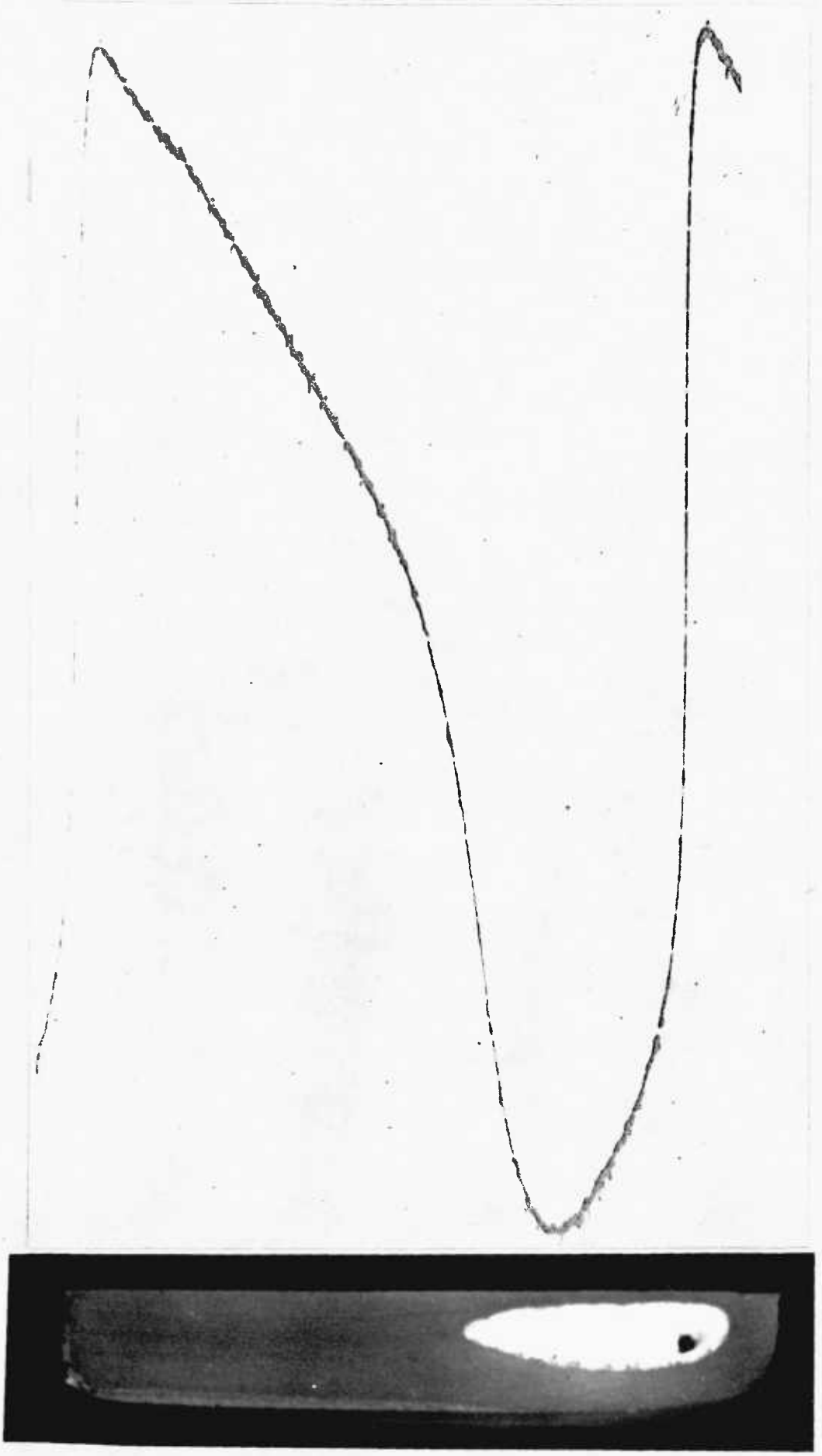


Figure 2.41

'Cross channel' pressure profile and corresponding specimen cross-section for low density polyethylene powder, experiment 27, at the 10 turn position

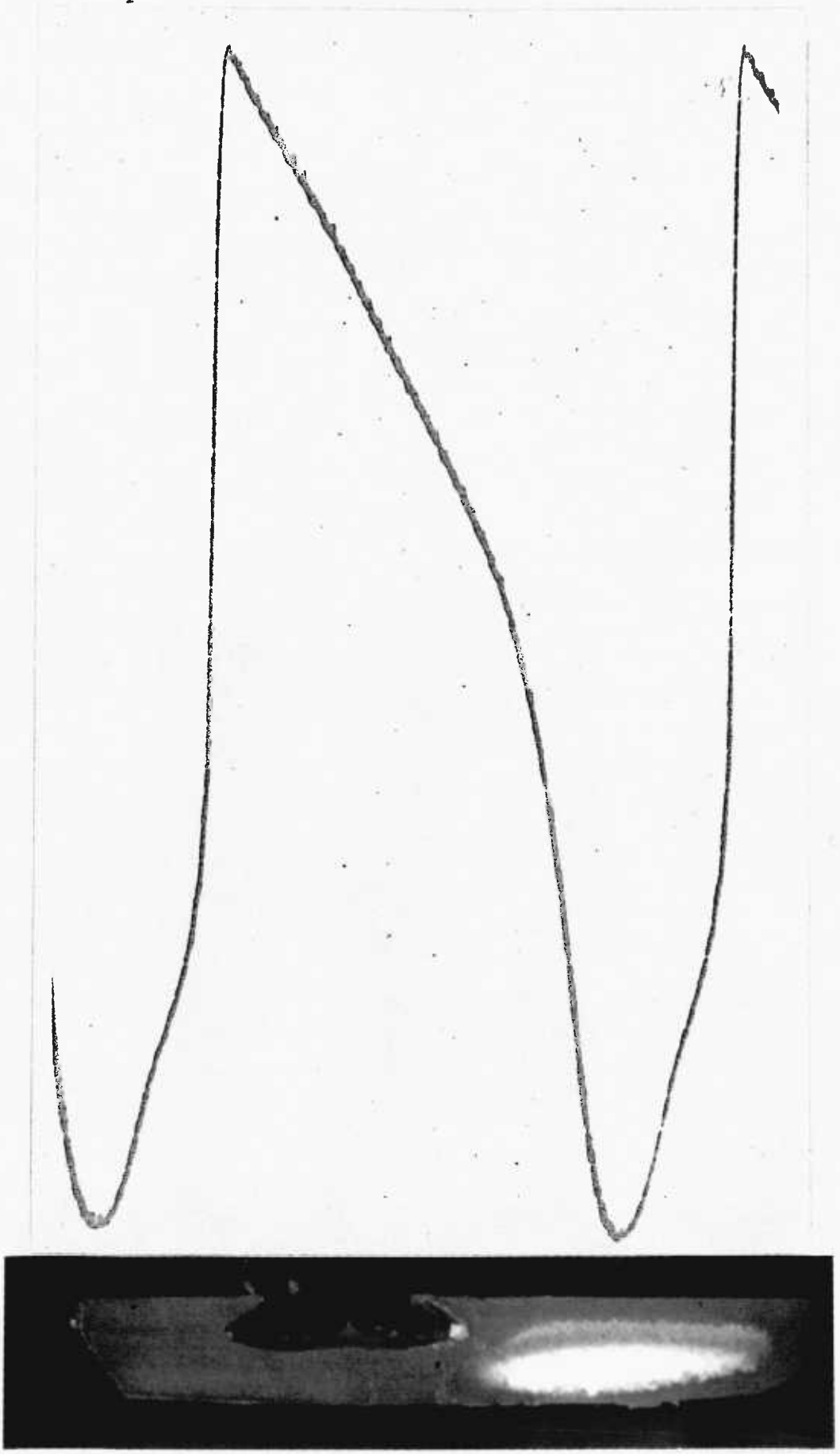


Figure 2.42

'Cross channel' pressure profile for low density polyethylene powder, experiment 27, at the 14 turn position



Figure 2.43

'Cross channel' pressure profile for low density polyethylene powder, experiment 27, at the 19 turn position

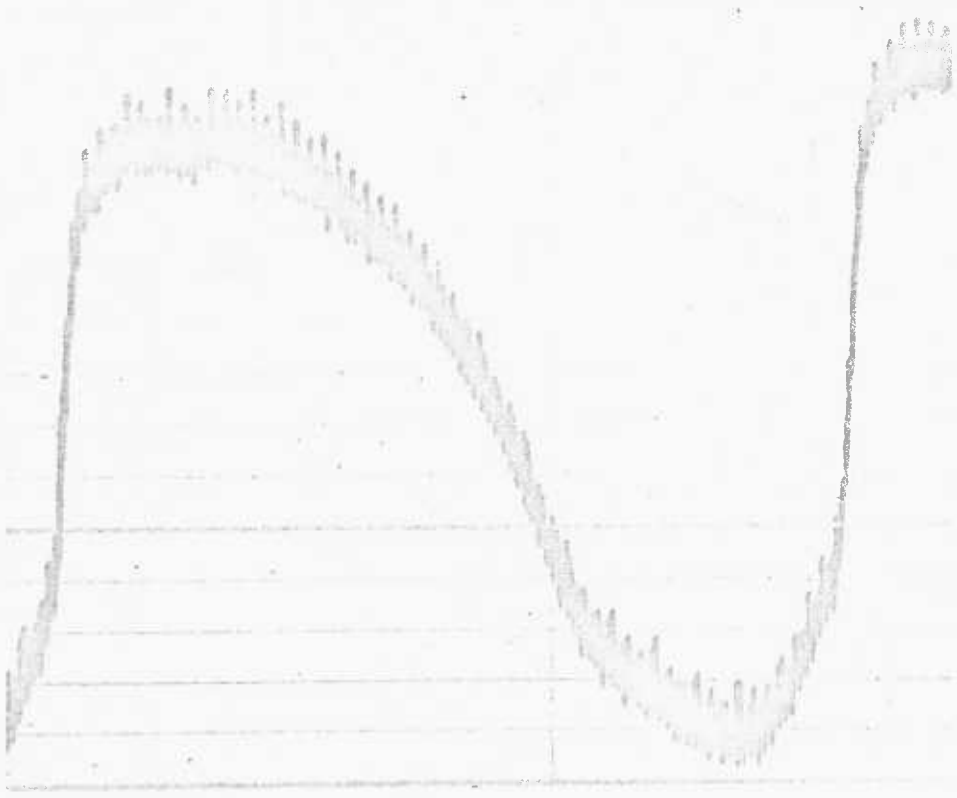


Figure 2.44

'Cross channel' pressure profile for low density polyethylene powder, experiment 27, at the 18 turn position

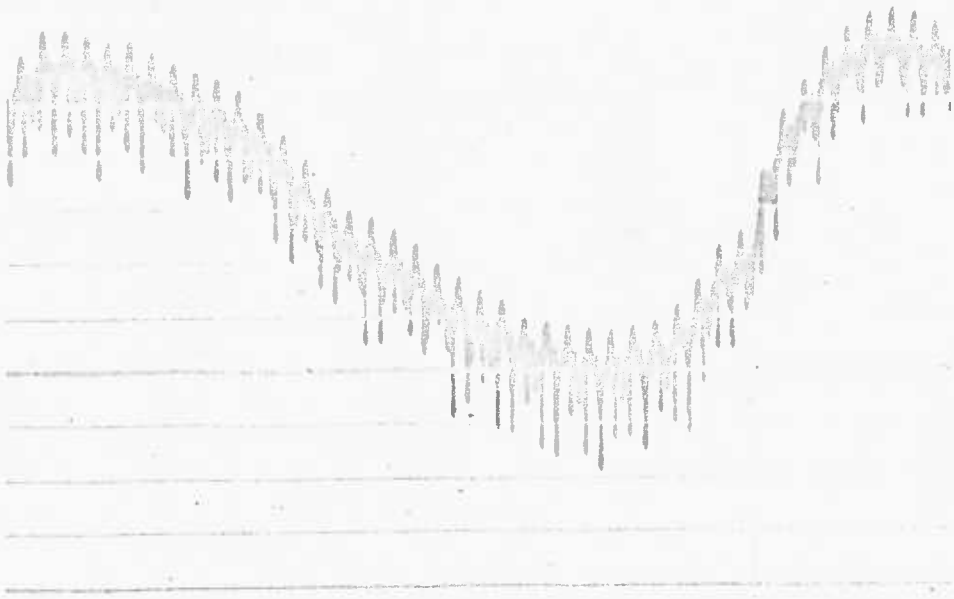


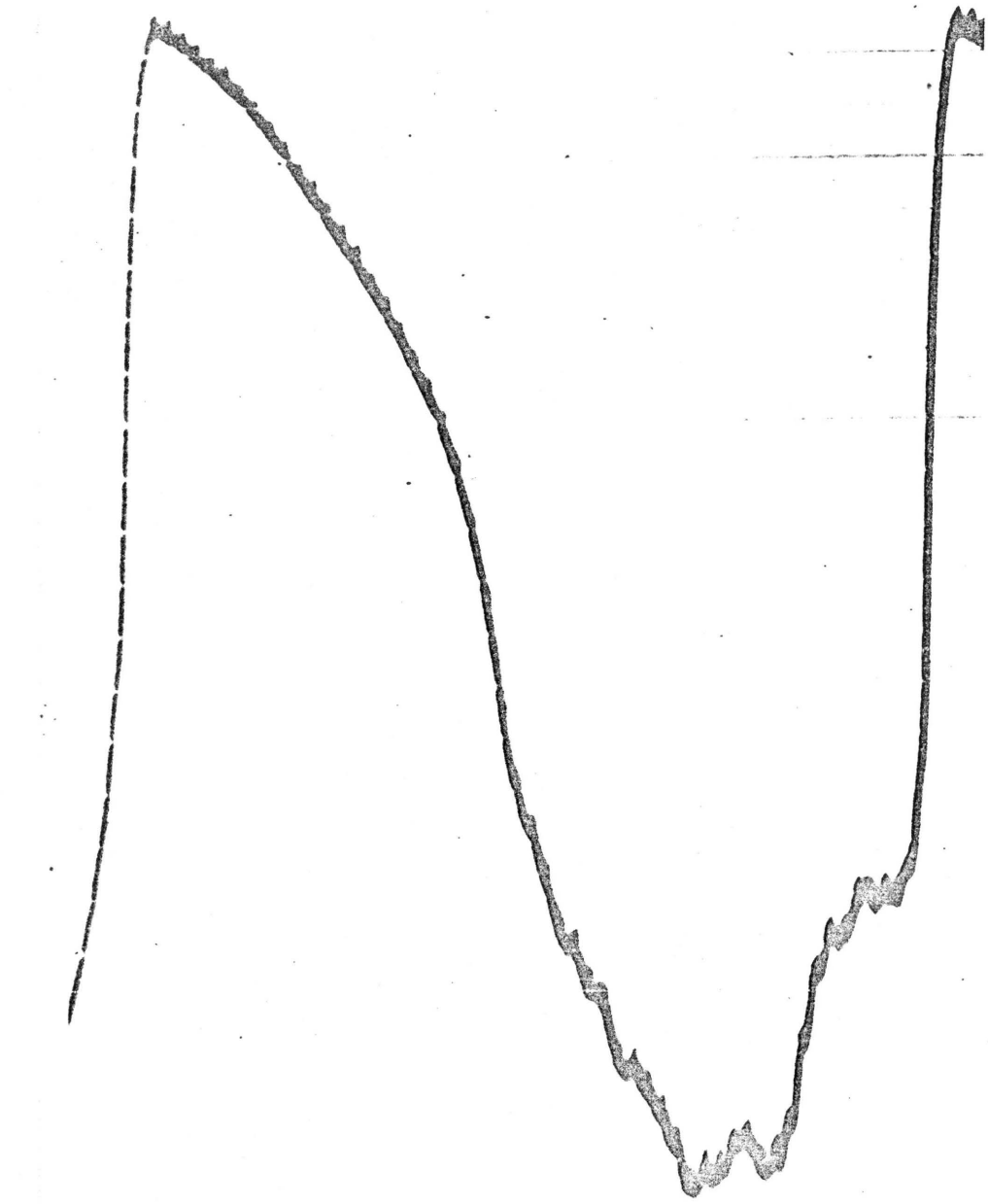
Figure 2.45

'Cross channel' pressure profile and corresponding specimen cross-section for high density polyethylene, experiment 15, at the 6 turn position



Figure 2.46

'Cross channel' pressure profile and corresponding specimen cross-section for high density polyethylene, experiment 15, at the 10 turn position



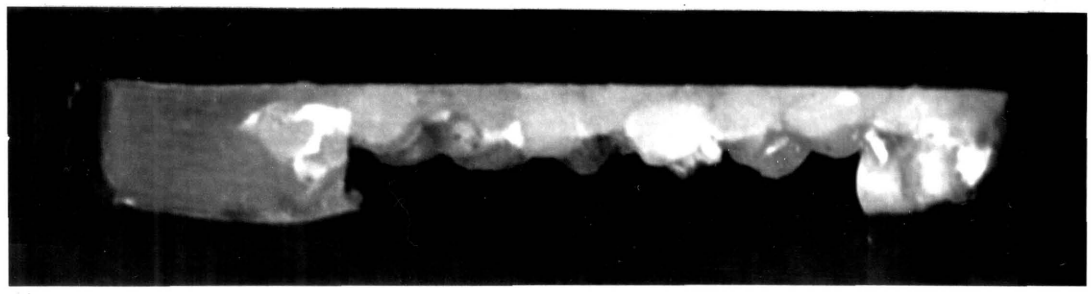


Figure 2.47

Sketch showing path along which the pressure transducers record

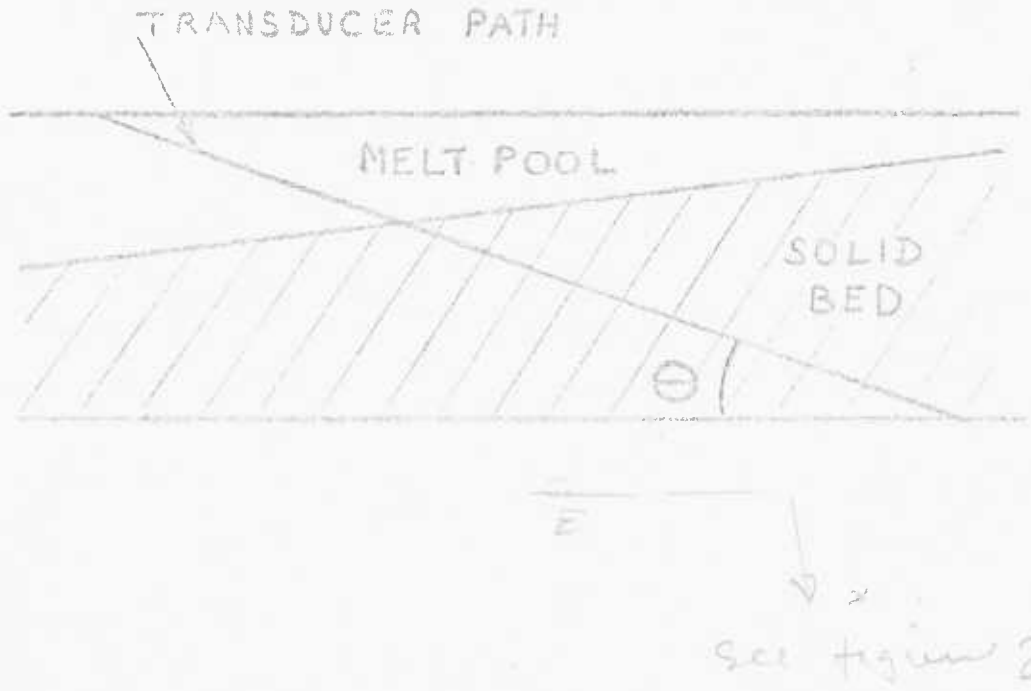
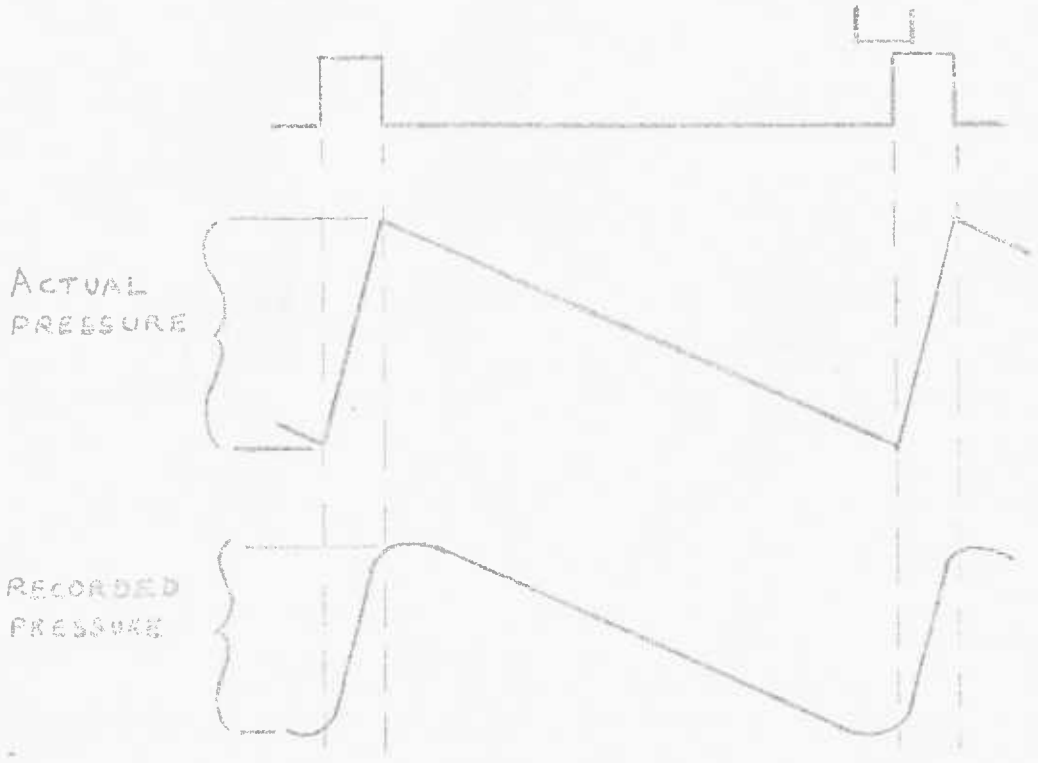


Figure 2.48

Illustration of the effect of the finite area of the cap of the pressure transducer on the recorded pressure trace



is, the pressure steadily increases across the width of the channel due to the drag from the barrel and then as the flight passes across the cap of the transducer the pressure drops off rapidly, as effectively the transducer is displaced to a point further up-channel towards the feed end of the screw. Trace 5 shown in figure 2.33 shows a partially molten case and it can be seen that pressure is generated in the solid bed across most of its width, and that this gradient is similar to that in the melt pool. This is perhaps due to the fact that these two regions of the channel contain material which is essentially in the same state. Traces for other materials do not in general show such a similarity of pressure gradients. Trace 4 shown in figure 2.32 shows an earlier stage in melting and here part of the solid bed next to the flight has a noticeably lower pressure gradient than the part adjacent to the 'melt' pool. In both traces 4 and 5 the 'melt' pool is identified by the smooth portion of the trace whereas the solid bed exhibits a more irregular trace.

Figures 2.35 to 2.38 show similar results for polypropylene, experiment no. 14, which was performed with water cooling of the screw. Examination of traces 1,2 and 3 shown in figures 2.35 to 2.37 respectively, shows very dramatically how the increase in width of the melt pool manifests itself in the pressure recordings as a smooth curve of relatively low pressure gradient compared to the gradient that exists in the region of the solid bed adjacent to the melt pool. It is noticeable here that the pressure in the solid bed does not increase very much as it travels down channel. Trace 4 of figure 2.38 shows the saw tooth trace typical of a melt filled channel. Examination of the axial pressure profile for this experiment shown in figure 2.21(b) shows that a negative down channel pressure gradient exists in the metering zone for this experiment. This fact explains the variation of the pressure gradient evident in trace 4, the trace being taken at very nearly the point of maximum pressure along the channel. This point will be discussed further later.

Turning now to figures 2.39 to 2.44, these show traces and specimens from experiment no. 27 for low density polyethylene powder. The first thing that is noticeable here is that, apart from amplifier noise, all the traces are

completely smooth. This is typical of powder material, in that the thickness of the melt film above the solid bed and the small particle size of the powder are such that movement of the solid beneath the melt film does not cause the solid to penetrate the film and hence cause a local momentary increase in pressure which is what would seem to happen with granular material causing the irregular pressure variation recorded above the solid bed.

Pressure trace no. 4 in figure 2.42 shows an interesting phenomenon. A sudden upward blip can be seen, occurring as the pressure is dropping rapidly over the flight. Corresponding to this is a downward blip in pressure in trace no.5. This cannot easily be seen in figure 2.43 due to amplifier noise. However a study of all the various pressure traces showed that this phenomenon occurred consistently. That is, it was observed that the upward blip in pressure of trace 4 was always accompanied by a downward blip in trace 5, at the same instant of time. Similarly there was observed an upward blip in trace 2 which was accompanied by a downward blip in trace 3. Additionally no such sudden blip in the pressure trace was ever recorded for numbers 1 and 6. The implication of this is that the occurrence of these blips was in part due to the relatively short distance between transducers 2 and 3 and between 4 and 5. Also study of the pressure traces shows that these pairs of blips occur at that point when part of the caps of both the transducers are simultaneously over the flight. The suggestion is that there could be some sort of pressure equalisation taking place along the top of the flight in that at the point when the blips occur there is a direct path along the top of the flight between the two transducer caps. Also it is the transducer recording the higher pressure of each pair that has a downward blip in the pressure trace and that recording the lower pressure that exhibits the upward blip in the pressure trace. However the mechanism by which this pressure equalisation takes place is a little difficult to visualize.

Refering now to traces 1,2 and 3 of figures 2.39 to 2.41, the regions of solid and melt can be distinguished readily from the pressure traces. Traces 4, 5 and 6 of figures 2.42 to 2.44 are all recording melt flow pressure variations.

Inspection of the axial pressure profile for this experiment shown in figure 2.28 (a) shows the existence of a comparatively large negative down channel pressure gradient starting in the tapered part of the screw after completion of melting, see also Plate 14. Trace 4, figure 2.42, was taken at around the region of maximum pressure where the gradient is changing from positive to negative and this explains the 'hump' in the middle of the trace.

The overall pressure difference recorded by the transducer over each cycle is a function of the cross channel pressure gradient and the downchannel pressure gradient. In a simple minded approach let the former be called G_x the later G_z and the overall pressure gradient measured by the transducer G. Now the transducer measures pressure along the path at Θ degrees, that is the helix angle, to the channel wall or z coordinate direction, see figure 2.47. Thus,

$$G = G_z \cdot \cos\Theta + G_x \sin\Theta \qquad (2.9)$$

Now because of the requirement that the net flow rate across the channel be zero, neglecting leakage flow through the flight clearance, G_x must always be positive. Therefore one can state that for G to be negative one must have

sign G_x negative and $|G_z| > G_x \tan\Theta$

Similarly for G to be positive one must have either

sign G_z positive

or, sign G_z negative and $|G_z| < G_x \tan\Theta$

This simple exercise supports the experimental findings that a negative down channel pressure gradient is not a sufficient condition for the pressure gradient recorded by a transducer to be negative.

These results do not agree with the interpretation recently put forward by Rousselet (16) who suggests that the shape of the pressure trace at the pressure peak is approximately sinusoidal and that in regions of negative downchannel pressure gradients the normal saw tooth melt flow trace is in a sense reversed in that the pressure is a minimum not a maximum at the point corresponding to the furthest downchannel position

recorded by the transducer, which can be called the 'pushing' flight side of the channel.

Trace 6 of figure 2.44 is approximately sinusoidal in form and corresponds to a region of negative pressure gradient well past the peak. A pressure trace taken by the author from a 2.5 inch (63.5 millimetre) diameter 25:1 L/D ratio experimental extruder is shown in figure 2.49. This trace exhibits the reversed saw tooth form and was taken in the metering zone of the screw whilst operating with a negative pressure gradient. The magnitude of the gradient in this case however being much larger than that for experiment 27. It would seem that in the experiments performed by Rousselet and in the experiment of figure 2.49 $\left|\frac{G_2}{2}\right|$ was sufficiently large to make G negative whereas in the results of experiments 27 and 14 this was not the case.

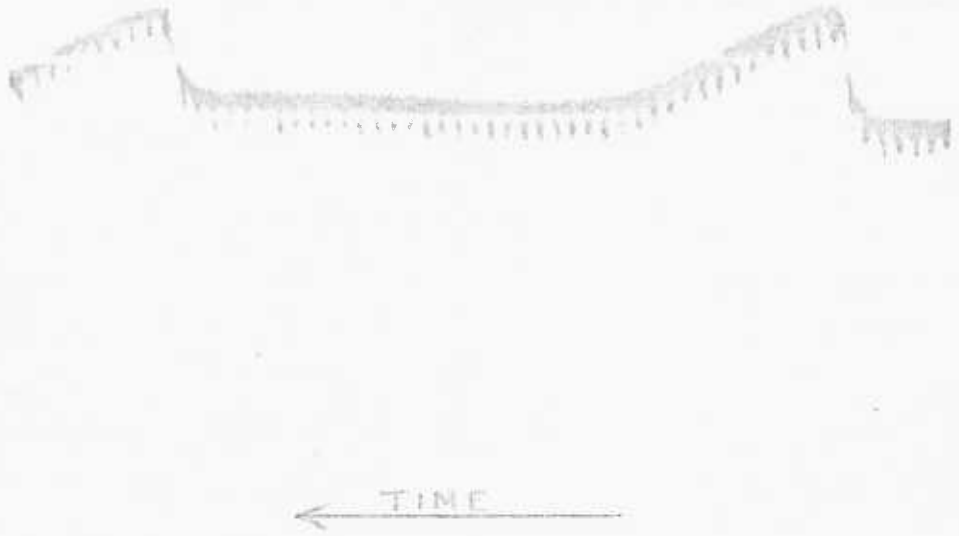
Figure 2.45 and 2.46 show some results for experiment 15 with high density polyethylene. Trace 1 in figure 2.45 shows what is a typical solid flow section trace, there being no molten material other than the beginnings of the melt film. The exponential pressure build-up typical of solids flow is apparent. Trace 3 in figure 2.46 shows the usual melting zone pressure variation; irregular low pressure over the solid bed and a smooth higher and increasing pressure over the melt pool. The melt traces for this experiment are not included as they add nothing to the discussion, being of a regular saw tooth form with a positive down channel pressure gradient.

All the above pressure traces were selected for comment as typical of steady-state melting behaviour, that is, in the absence of solid bed break-up. Although solid bed break-up did occur in experiments 15 and 27 it was possible to ignore, for simplicity and convenience, its effects in discussing the various sorts of pressure traces that can be developed in the steady state extrusion of different materials. However attention must now be paid in detail to the phenomenon of bed break-up and its relationship to processing instability or surging.

Bed break-up was observed to occur in at least one experiment for each material used except the two types of PVC. This is in agreement with the experimental results of Tadmor et al (5) and Donovan (10) who also did not observe bed break-up in PVC experiments. The occurrence of solid bed break-up varied with

Figure 2.49

Detail pressure trace taken in the melting zone of a $2\frac{1}{2}$ inch (63.5 millimetre) extruder



operating conditions for the other material. Contrary to the observations of Tadmor and Klein (15) the effect of the size of the granules on bed break-up was negligible. In particular no significant differences were detected between powder polyethylene and granular polyethylene.

The present results convincingly support the idea that surging of frequency 1 to 15 cycles/min is due to solid bed break-up, as proposed by Tadmor and Klein (15). Justification for this conclusion is to be found in the experimental pressure traces which will be presented now.

It has already been shown how the pressure in the extruder channel varies over the width of the channel and, clearly, the period of this variation is the time taken by the screw to rotate through 360 degrees. A study of the experimental pressure traces taken over a period of time, orders of magnitude greater than this show that in those experiments for which solid bed break-up was observed there was a low frequency cycling of pressure. The frequency was lower than that of the screw's rotation yet higher than could have been produced by the variation of the barrel temperature due to the nature of its control system. Figure 2.50 shows such a low speed recording of pressure traces 1,2,3 and 4 for experiment 15. Traces 1 and 3 correspond to those in figures 2.45 and 2.46. The irregular fluctuations of trace 1 may be ignored since they are essentially due to pressure generated in solids flow. Trace 2 is virtually steady. Trace 3 is steady except for the occasional but marked drop in pressure. Trace 4 is cycling continually and fairly regularly. The dramatic drop in pressure in trace 3 is linked with a much smaller drop in pressure in trace 2. Also it could be argued that this pressure drop produces a little time later a few cycles of low pressure on trace 4.

Figure 2.51 shows a similar recording of all six traces for experiment 13. Here it is seen that the pressure cycling is present from trace 2 and thereafter is seemingly transmitted along the extruder.

The suggestion is that when the bed breaks there is a pressure drop due to the flow of molten material between the two fracture surfaces.

Figure 2.52 shows a sketch of the unwound screw channel with the position of

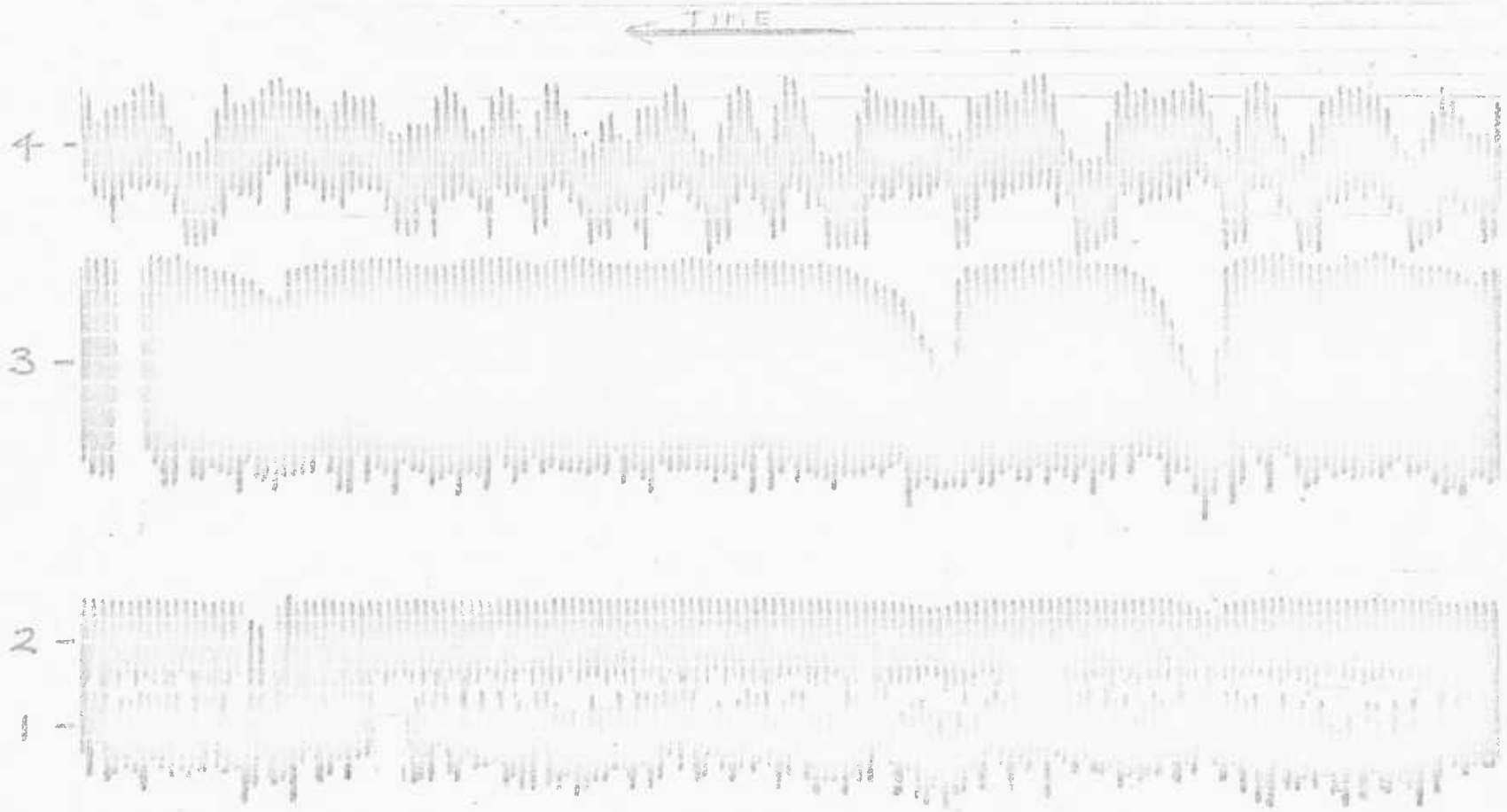


Figure 2.50

Low speed pressure recordings for high density polyethylene, experiment 15. Traces 1,2,3 and 4 are shown. Bed break-up is detected by trace 3 and the resulting surging shown also in trace 4.

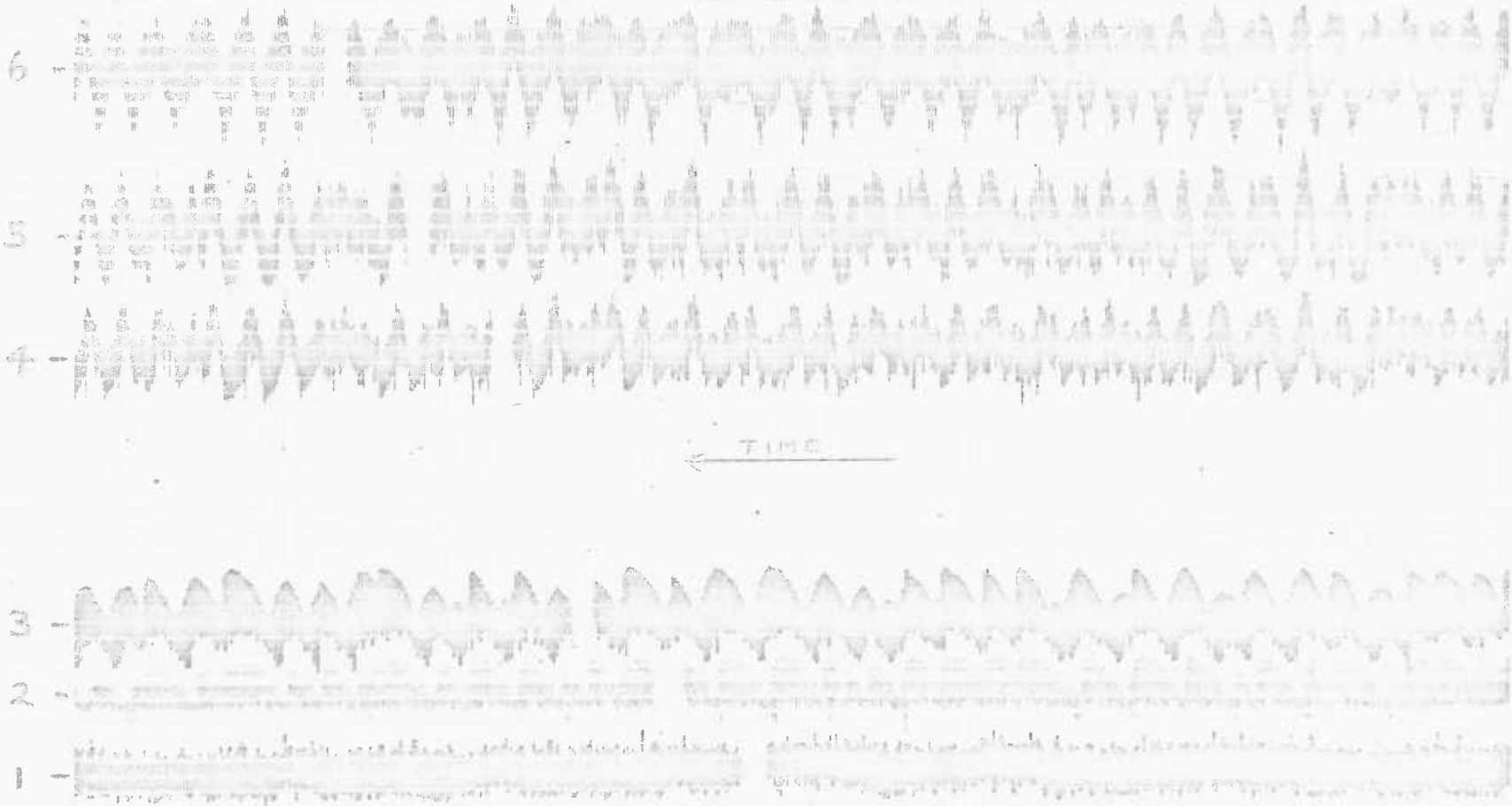
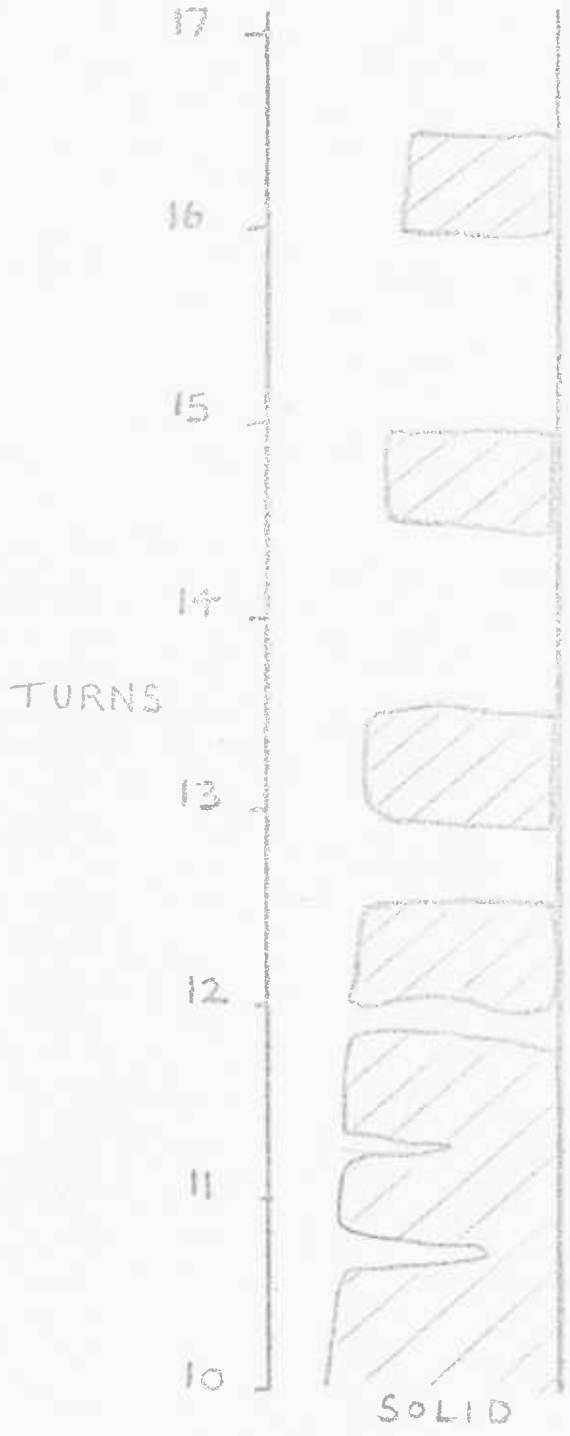


Figure 2.51

Low speed pressure recordings for polypropylene, experiment 13. All six traces are shown. Surging can be seen on traces 2 to 6.

Figure 2.52

Sketch of unwound screw channel showing position of broken pieces of solid bed, for experiment 15 with high density polyethylene



the broken pieces of bed marked, for experiment 15. It can be seen that the bed breaks at least partially sometime before the 10.5 turn position and presumably if the fracture is not complete it will become so at some later point. Refering to trace 3 of figure 2.50 again shows support for this in that the large drops in pressure may be due to the occurrence of complete fracture at around the 9.5 to 10.5 turn position, whilst the smaller drops may correspond to partial fractures.

These observations taken together suggest that bed break-up causes an initial pressure drop which is transmitted in the direction of flow along the screw, hence the cycling of trace 4 of figure 2.50, but has little effect on the preceding part of the flow, hence the very small pressure drops of trace 2 of figure 2.50.

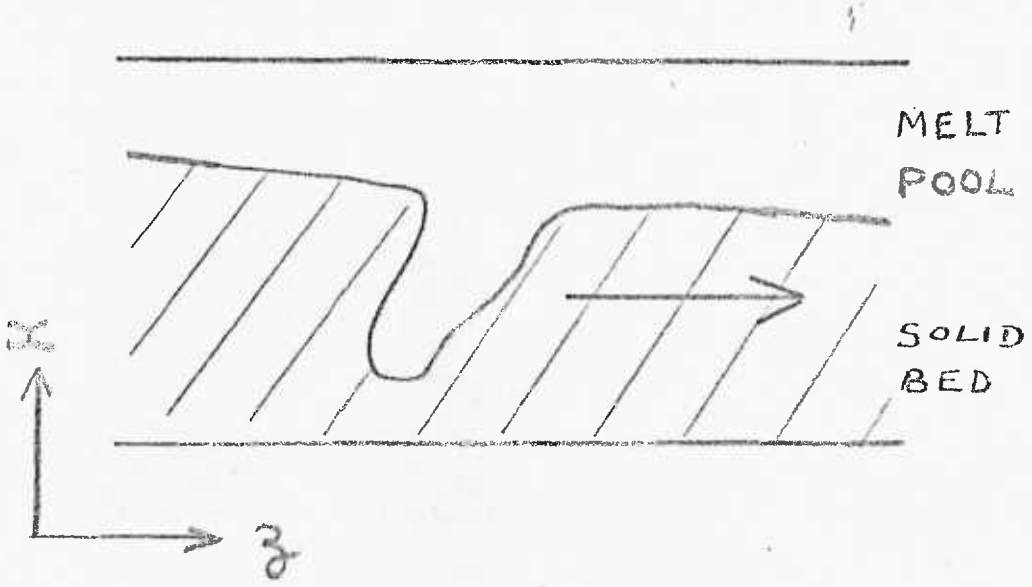
In this light figure 2.51 suggests that bed break-up occurs at approximately the 9 turn position in experiment 13. Inspection of the plastic pieces removed from the screw show that bed break-up occurred somewhere just before the 10 turn position.

Additional experimental evidence to support the idea that bed break-up initiates low frequency pressure cycling is to be found in the results of experiment 11. Figure 2.53 shows a photograph of a piece of plastic removed from the screw between the 9 and 10 turn position. It shows an almost complete bed break-up. The position of the break being at 9.25 turns, so that its effect would be picked up almost directly by transducers 2 and 3. Figure 2.54 shows the variation of trace no.2 for experiment 11 over a comparatively long period of time. The fairly regular drop in pressure seen here can only be due to the fracture of the solid bed.

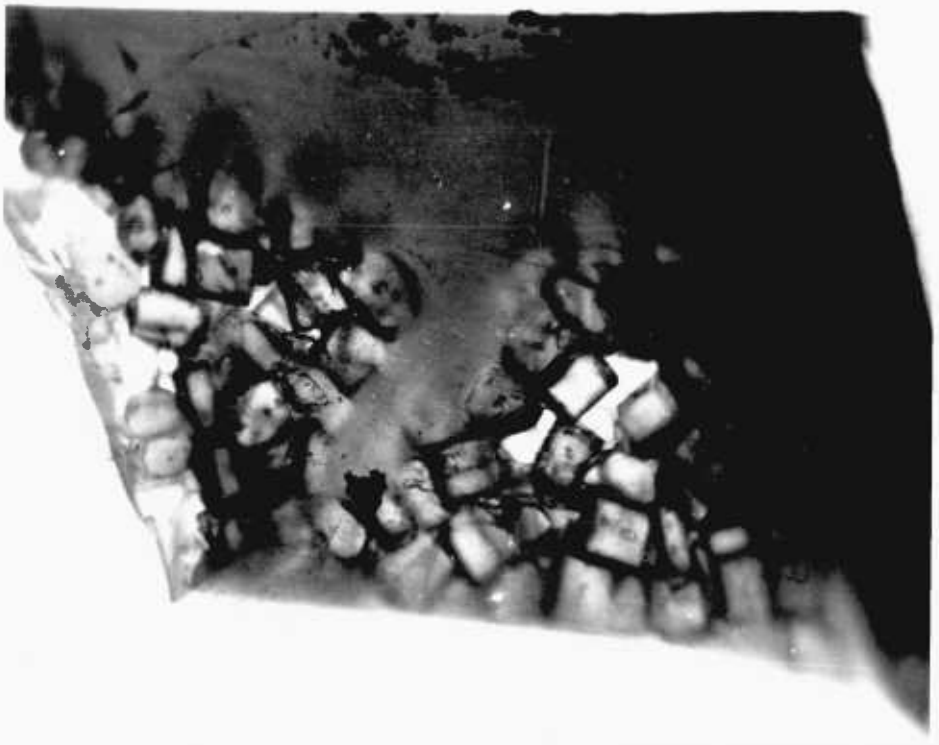
On re-examination of the results of the preliminary experiments it was noted that those performed with screw cooling did not exhibit bed break-up. This was in agreement with the results of Maddock (2). Therefore the three experiments 8,14 and 18 were performed to check these earlier observations. These three experiments were performed under identical control conditions as experiments 5,13 and 15 respectively save for the use of screw cooling. The results showed among other things that bed break-up did not occur and that there was no pressure

Figure 2.53

The occurrence of bed-break in experiment 11 at the $9\frac{1}{4}$ turn position



(a) Sketch



(b) Photograph

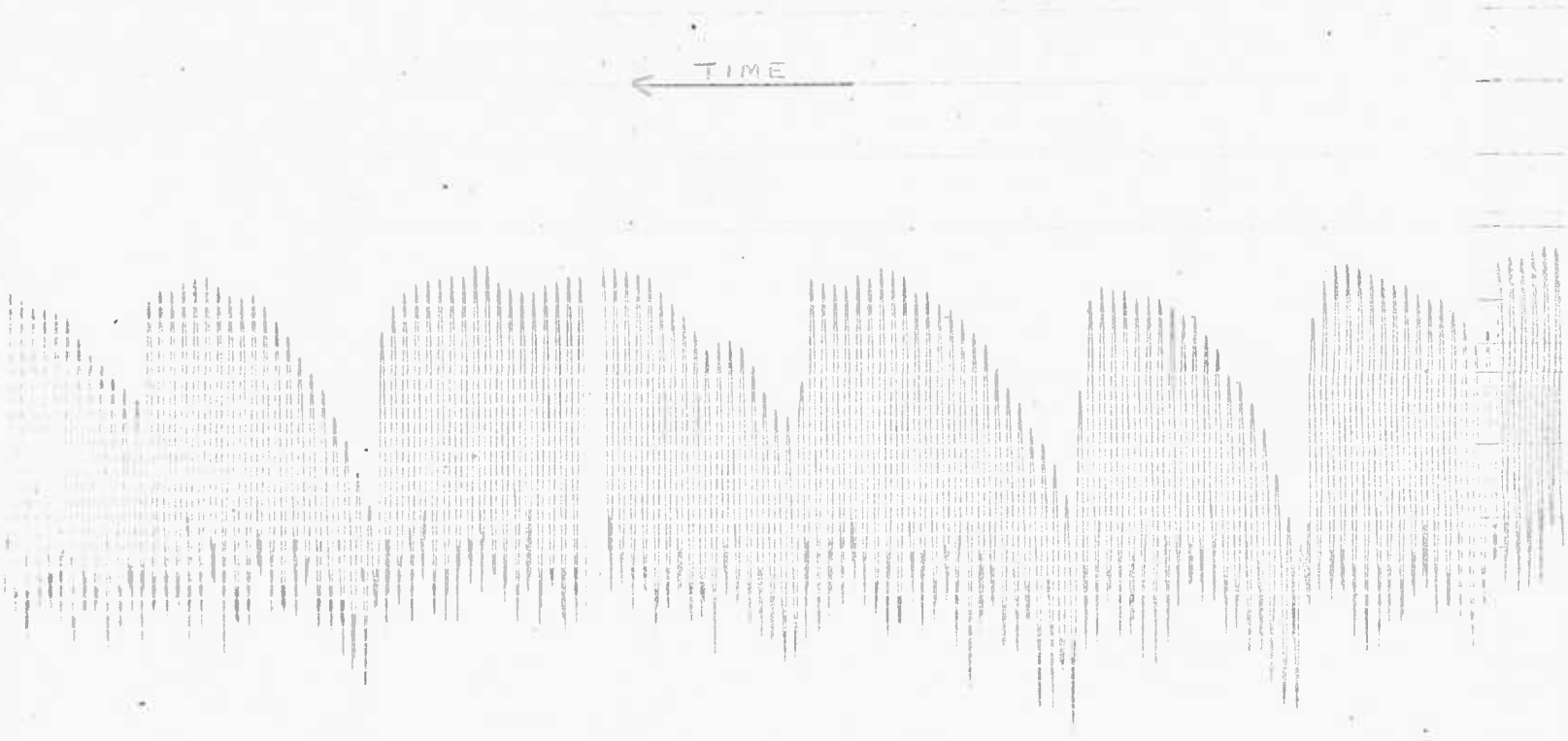


Figure 2.54

Low speed pressure recording showing the occurrence of bed break, trace 2 of experiment 11 with polypropylene

surging. Figure 2.55 shows the low speed recordings made of the pressures for experiment 18 and can be compared to figure 2.50. Although the magnitude of the pressures are indeed lower in the water cooled experiment the trace zeroes and transducer gains are similar for the two experiments so that the lack of pressure surging in the water cooled experiment is genuine.

It is also possible to look at and explain in terms of bed break-up the changes that occur to the pressure variation over one revolution of the screw. Figure 2.56 shows a series of sketches illustrating the various idealised forms of pressure traces to be expected. Diagram (a) illustrates the typical steady state type of trace in the melting zone. Diagram (b) shows a likely trace resulting if the bed break-up occurs directly beneath the transducer cap, and (c) shows the recording to be expected a short time after fracture. The difference between (a) and (c) is that the pressure in the melt pool in (c) is lower than that in (a) due to the flow of material between the fracture surfaces of the solid bed. Thus the repeated sequence would be (a),(b),(c), (a), etc., not at equal time intervals of course. One would expect several revolutions of the screw exhibiting the transition from (c) to (a) but relatively fewer to exhibit the actual break, that is, the transition from (a) to (b) to (c). An actual pressure trace showing this sort of behaviour is shown in figure 2.57 which is trace 3 of experiment 11.

At a point further down channel from the break point one would expect a slightly different sequence to be recorded. In this case the sequence would be (a), (d), (b), (c), (a), etc. Diagram (d) of figure 2.56 is the additional variation here, corresponding to the passage of the back face of the solid plug past the transducer. An actual example of this sequence is shown in figure 2.58 which is again taken from transducer 3 of experiment 11. The difference between the traces of figures 2.57 and 2.58 is that the point of fracture of the solid bed was presumably earlier in the latter than the former. In other words in the trace of figure 2.57 the fracture occurred within the physical space of the screw channel spanned by the transducer whilst in that of figure 2.58 it occurred in part of the channel not spanned by the transducer but nearer to the feed

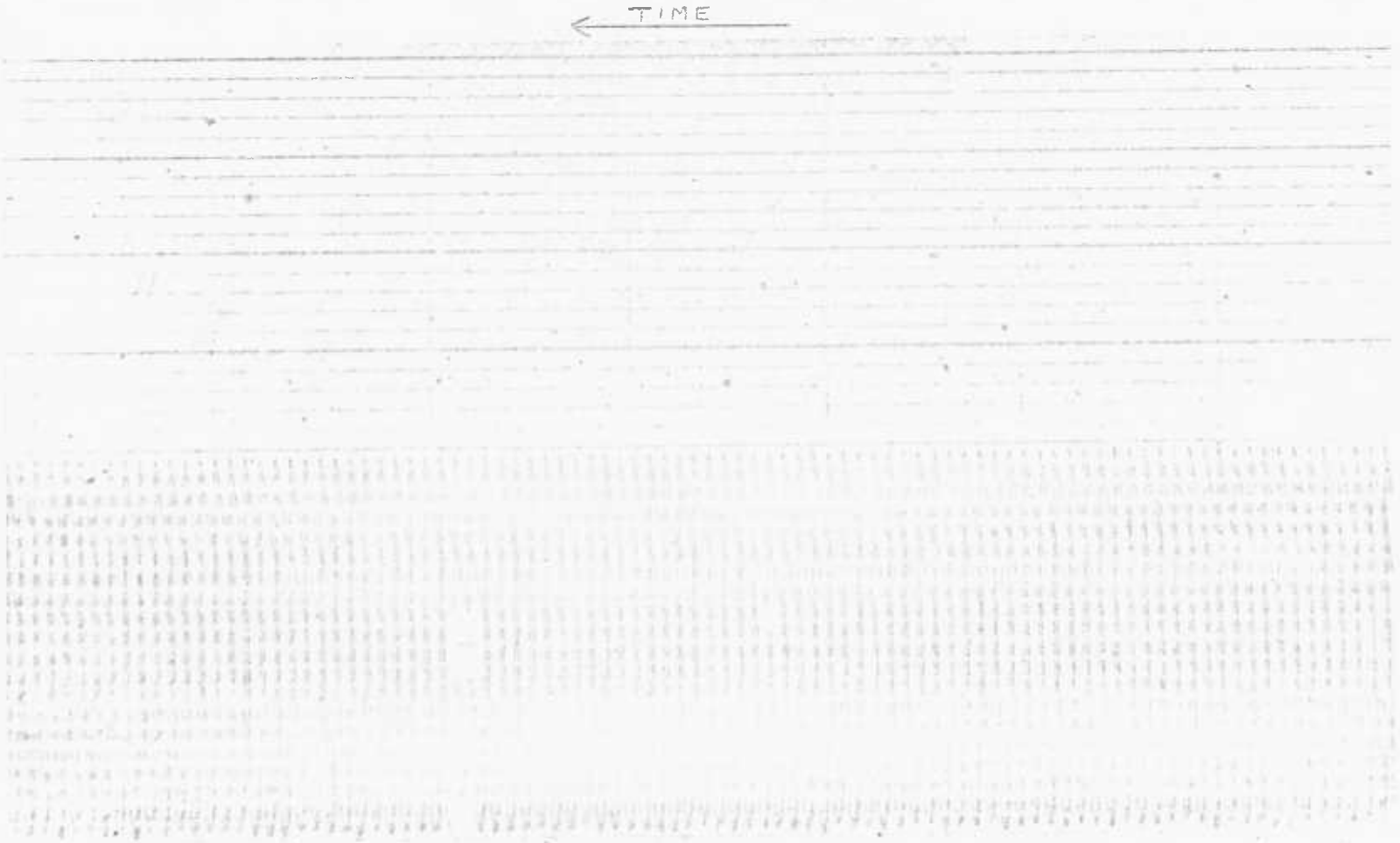
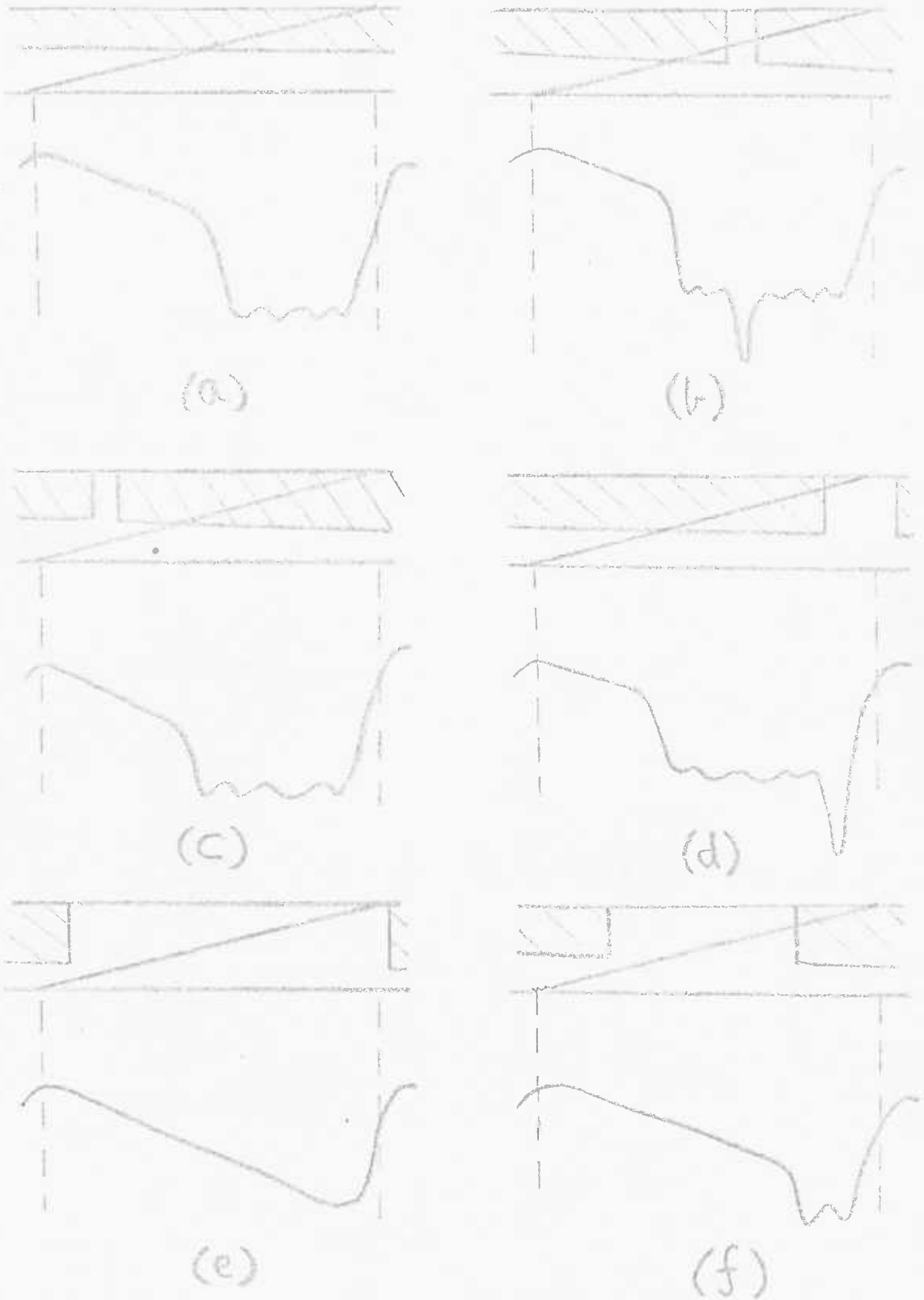


Figure 2.55

Low speed pressure recording from experiment 18 with high density polyethylene and screw cooling. Traces 1 to 6 shown overlapping each other

Figure 2.56

Sketches showing the form of the detail pressure traces that are seen when bed break-up occurs



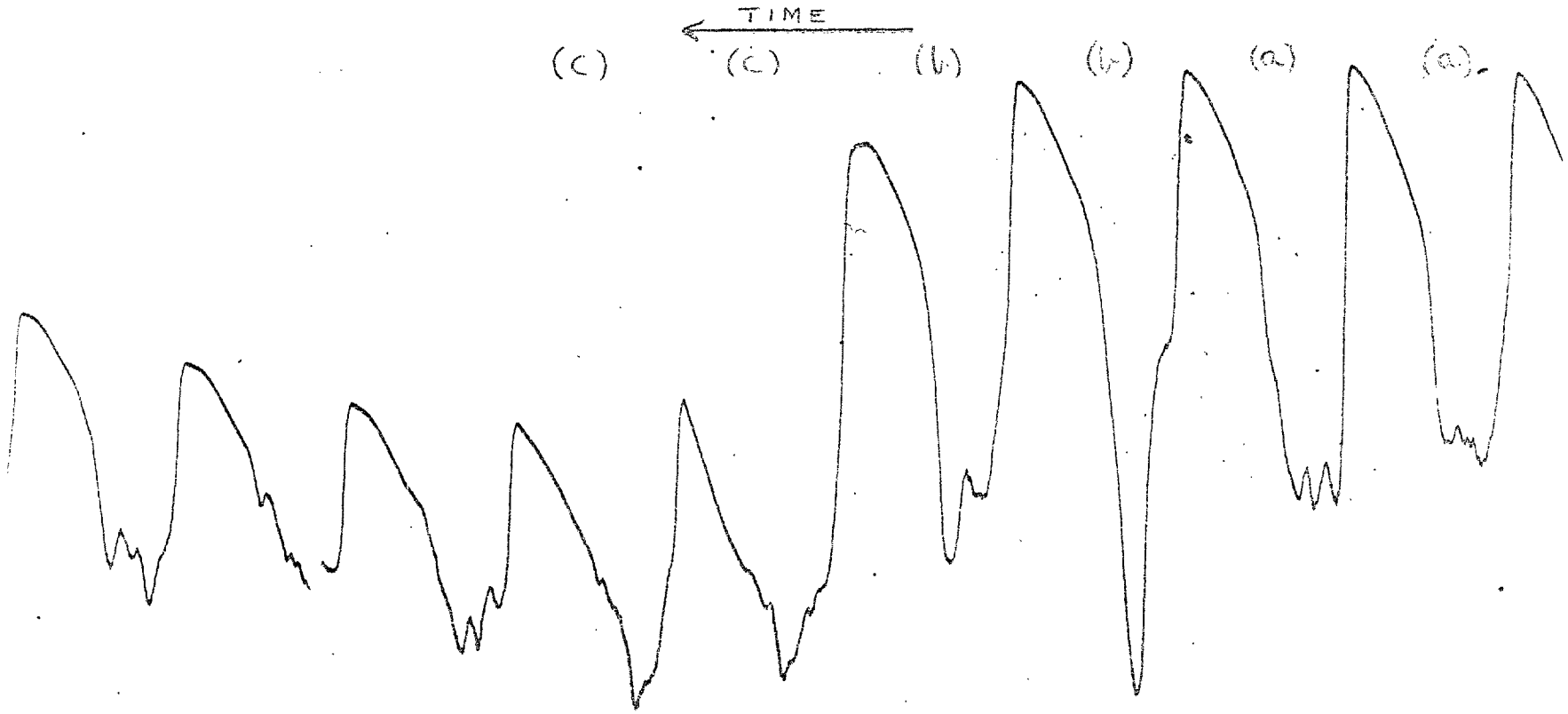


Figure 2.57

Series of detail pressure traces from experiment 11, trace number 3, showing the situation where bed break-up occurs at the transducer location

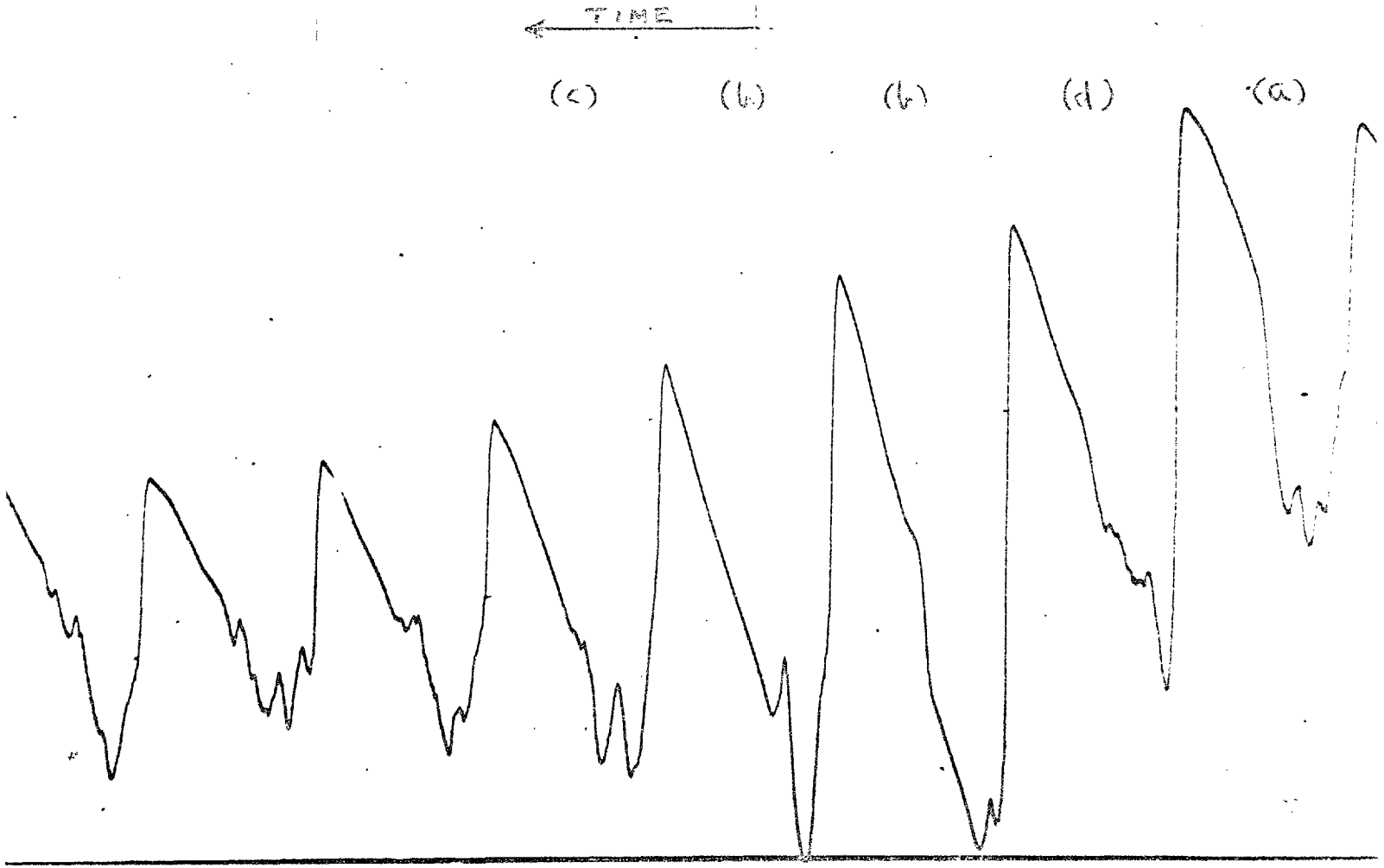


Figure 2.58

Series of detail pressure traces from experiment 11, trace number 3, showing the situation where bed break-up occurs just upstream of the transducer location

hopper. From this and other results presented earlier it is clear that the point of bed break and its frequency vary somewhat around their mean values. Nevertheless the effect of different extruder operating conditions and different types of plastic on the bed break up can still be detected.

Yet another sequence of pressure variations may occur at points far removed from the initiation of bed break, this is defined by (a), (d), (e), (f), (c), (a), etc. Diagram (e) of figure 2.56 is seen when there is a considerable melt plug between the solid plugs and is the normal saw tooth melt filled channel type of trace. Diagram (f) shows a last possible trace which may occur and gives the impression that the width of the solid bed is less than it, in fact, is. It should be noted that one does not necessarily expect to pick up all the traces in these sequences because of the rapidity of certain parts of the cycle. In particular, traces corresponding to diagrams (d) and (f) may not be recorded. Figure 2.59 shows an example of this third sequence, it is trace 5 from experiment 15. In fact, an example corresponding to diagram (f) is not recorded here.

One other type of trace not illustrated before has been observed in the pressure recordings made on the 2.5 inch diameter extruder mentioned earlier. Figure 2.60 shows this. It is an example that should correspond to the third sequence of variations described above. It does to the extent that there are well defined periods when the channel beneath the transducer is full of melt and when it is full of solid and melt. However it can be seen that the pressure in the solid bed is generally higher than the melt pressure. It should be remembered that in the metering zone flow of this experiment a large negative pressure gradient existed. It would seem that the taper of the screw is such that the solid is being 'pinched' between the screw root and the barrel surfaces and this pressure peak is some indication of the force required to deform the solid. In another experiment performed on this 2.5 inch extruder by a colleague, thermo-couple probes were mounted on the screw to record the temperature of the plastic. These were mounted at axial positions corresponding to the pressure transducers on the barrel. Simultaneous traces of pressure and temperature at several axial positions were made. These showed that during the period of peak pressure of

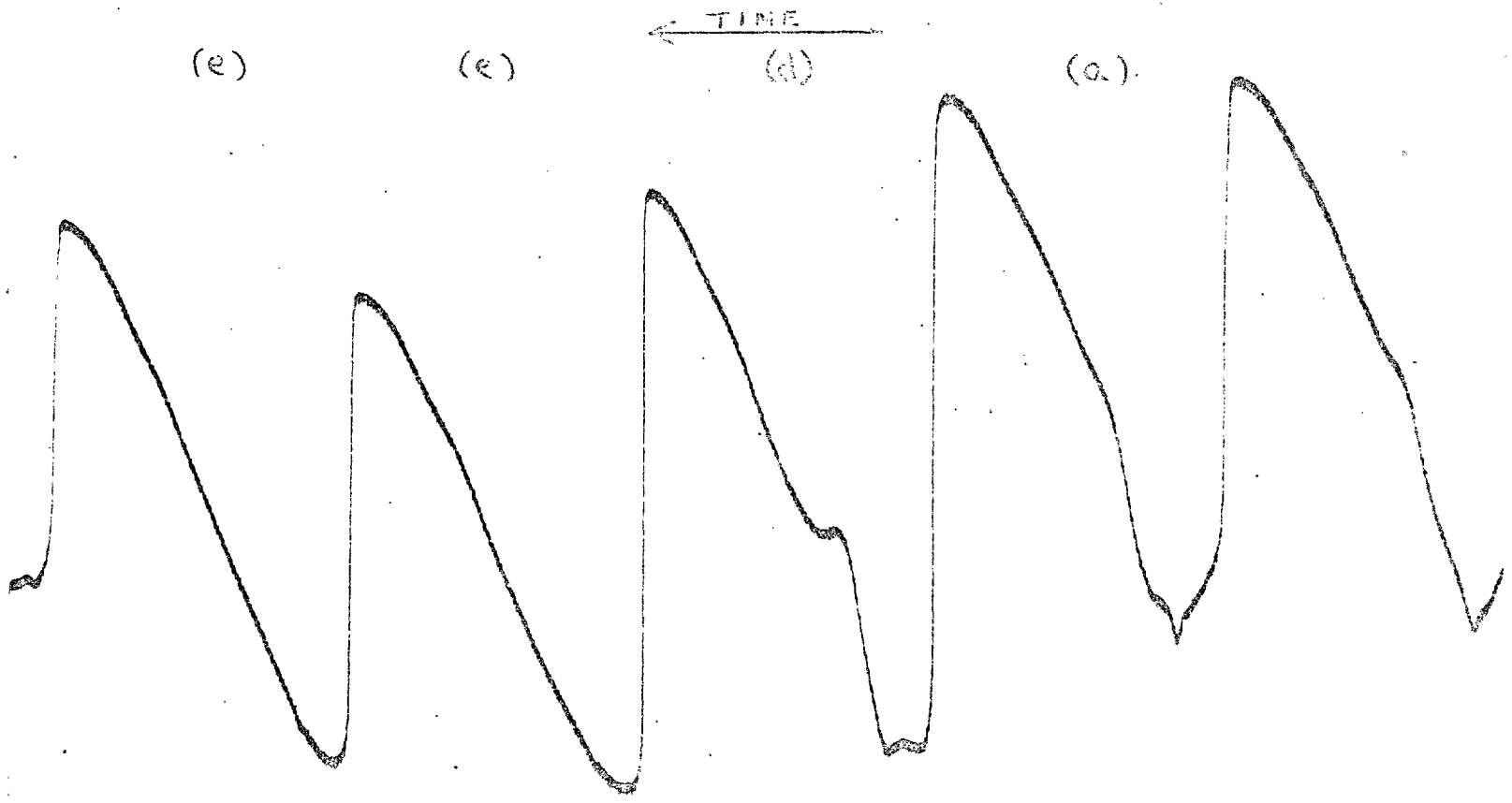


Figure 2.59

Series of detail pressure traces from experiment 15, trace number 5, showing the situation where bed break-up occurs a long way up stream of the transducer location

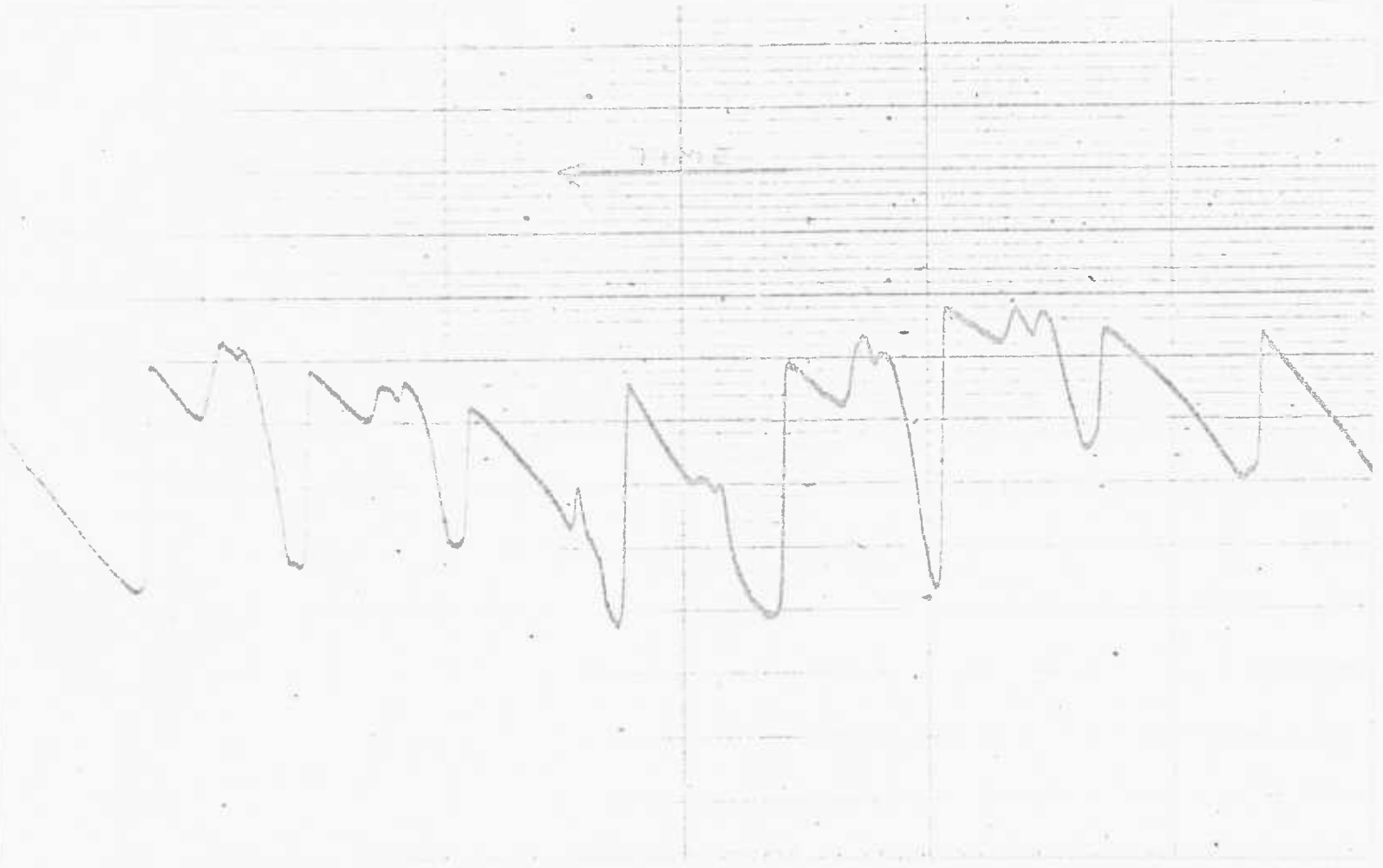


Figure 2.60

Series of detail pressure traces from an experiment on a 2.5 inch (63.5 millemetre) extruder, showing the situation where bed break-up occurs a long way upstream of the transducer location

the cycle variation the temperature was falling and conversely during the period of low pressure the temperature was rising, doubly reflecting the alternating passage of solid and melt plugs along the channel. These results are in agreement with Tadmor and Klein's(15) explanation of the temperature cycling along the screw observed by Marshall et al (18).

One important observation apparent from the foregoing description and illustration of the development of solid bed break-up both as a function of time at a particular position along the screw and as a function of position along the screw, has yet to be explicitly stated. It is that the length of the melt plug between any two pieces of the solid bed increases as the solid bed pieces travel down-channel. The implication of this observation when coupled with the observation that the length of the solid bed pieces does not seem to vary significantly is that the solid bed is accelerating. It is possible from the experimental results to make some simple quantitative measurements to illustrate this point. Defining the mean length of the solid plug as LS, the maximum length of the melt plug as LM and the mean periodicity of bed break-up as T, leads to the following simple relationships

$$W = LS / T \qquad (2.10)$$

where W is the velocity of the solid bed in the down channel direction at the point of bed break. Also

$$U = (LS + LM) / T \qquad (2.11)$$

where U is the maximum velocity in the downchannel direction reached by the solid plug.

It is also possible to compute a figure for the solid bed velocity, V, to compare with W, from a calculation based on the measured mass output rate of the extruder, M_T, assuming the solid bed to be fully compressed and hence have density equal to the density of the solid plastic, ρ_s. Thus,

$$V = M_T / (\rho_s H_o W) \qquad (2.12)$$

where H_o and W have been previously defined as the height and width of the channel in the feed section respectively.

In the calculations above it is assumed that the velocities U, V and W do not

Table 2.4

Results of the Experimental Calculations of Solid Bed Velocity

	Experiment Number					
	5	11	13	15	16	17
Length of solid plug, LS, m	.11	.12	.10	.055	.28	.11
Length of melt plug, LM, m	.22	.17	.065	.11	.14	.09
Periodicity of breaks, T, sec	5.5	15	10	7.5	45	8.5
Solid bed velocity, V, m/s (from flow rate)	0.013	.012	.013	.012	.006	.014
Solid bed velocity calculated at point of break, W, m/s	.02	.008	.01	.007	.006	.013
Maximum solid bed velocity, Um/s	.06	.019	.016	.022	.0094	.024
Velocity component of barrel in z direction, V_{bz}, m/s	.153	.153	.153	.153	.0765	.153

vary in the plane of the channel cross-section. The results of performing these calculations for several of the experiments are shown in Table 2.4.

A comparison between the figures for V and V shows that in most cases reasonable agreement has been achieved which gives confidence to the calculation procedure. Comparison between U and W shows the degree of acceleration that has taken place, in the extreme case quoted here the velocity of the solid bed more than doubles after fracture.

The question must now be asked as to the cause of solid bed break-up. Clearly under certain conditions the boundary stresses on the solid bed must reach a critical state and the bed fractures. The most useful experimental observations concerning the state of the boundry stresses on the solid bed are that screw cooling prevents bed break-up and that bed break-up never occurs without there being a melt film all around the solid bed. The point of significance here is that the screw cooling prevents the formation of a melt film on the screw root. This then would seem to confirm the importance of this lower melt film as regards bed break-up. One further piece of experimental evidence is that the pieces of solid bed that break off undergo significant acceleration. Thus the formation of a melt film on the screw root alters the stresses on the solid bed such as to increase its tendency to accelerate. The implication being that either the solid bed continuously deforms to accomodate these accelerative forces, which one may call a 'ductile' solid bed, or it fractures and the seperated pieces accelerate as a solid body, this one may call a 'brittle' solid bed. Donovan's (10) experimental evidence of solid bed acceleration was based on measurements of an unbroken solid bed in a PVC experiment and in a low density polyethylene experiment. It would seem that taken with the present results PVC can be classified as having a 'ductile' solid bed and low density polyethylene as being 'semi-ductile' in that the occurrence of bed break-up is partially dependent on the particular extrusion conditions. However it seems that most materials in this content have 'brittle' solid beds.

Two important consequences of using screw cooling have already been stated namely the absence of solid bed break-up and surging. In addition to these one notes a marked reduction in output. Observation of the axial pressure profiles

of figures 2.18 (b),2.21 (b) and 2.23 (b) shows that screw cooling reduces the pressure generating capacity of the screw. The source of this loss seems to be the metering zone. The pressure gradients in this region are seen to be low and even to be negative over a short zone. Comparison of Plates 4(b), 7(b) and 9(b) with these pressure profiles indicates that until most of the melting is over no significant pressure generation takes place, unless it occurs during solids flow at the very beginning of the screw. It is possible that the reason for this lack of pressure generation is linked with the absence of solid bed break-up, that is, the accelerative forces on the solid bed are those that are responsible for the pressure build up in it. These thoughts are linked with the fact that without bed break-up the solid bed presumably does not undergo significant acceleration and this also contributes to the reduced output rate in experiments with screw cooling.

This is as far as the discussion on the phenomenon of solid bed break-up can be taken at the moment. It will be returned to in the light of theoretical predictions presented in the following chapters.

Other general points of interest arising from the experimental results will now be described.

Plates 1 and 2 show the cross-sectional samples of plasticised PVC. Two things are apparent from these results; firstly, the long delay before melting starts which is not found with any other material, even rigid PVC. This delay is linked with a lack of pressure build-up as shown in Figures 2.15 and 2.16. The suggestion here is that melting will not start until sufficient pressure has been generated to cause the PVC to 'stick' to the hot barrel surface. In other words the PVC will slip on the barrel surface, even though it is well above its softening temperature, until sufficient pressure has been generated. Clearly no pressure will be generated until the solid bed has been fully compacted. Two things can produce this compaction. One is the reduction in channel cross-sectional area due to the screw taper. The other is the deceleration of the solid bed due to a high down-stream pressure. The term 'feed control' is sometimes used to describe the operation of an extruder if there is no effect on the flow

in the feed section of the later pressure generation and the term 'melt control' is used if the pressure build-up does effect the feed flow. In 'feed control' then, one expects the compaction of the solid bed to be due to channel taper only whereas in 'melt control' part will be due to deceleration of the solid bed caused by pressure build-up.

The results show that the output rate per revolution of the screw is higher when the screw speed is 40 r.p.m. than when it is 80 r.p.m., yet at 80r.p.m. the results suggest that the screw is feed controlled. The reason for this is thought to be the beneficial effect of earlier solid bed compaction which may, in fact, give a higher solids flow rate in that earlier compaction means that there is a greater cross-sectional area for the flow than if this compaction occurred further along the screw. This is assuming that the reduction in solid bed velocity, caused by the pressure initiated compaction, does not fully counteract the benefit of early compaction. In other words the existence of positive pressure right back to the feed hopper may have a beneficial effect on feed flow.

The second observation that can be made from the sectional photographs is that the apparent rate of melting of the PVC is significantly higher at the end of melting compared to that at the beginning. There are two possible explanations for this. One is that due to the zero latent heat of fusion of PVC and the continual heating up of the solid bed as it travels along the screw, there comes a point at which the whole of the remainder of the solid bed reaches its softening point virtually simultaneously and thus will rapidly become mixed and disappear. Secondly it may be that the true rate of melting is not increasing as much as it would appear to. The true rate of melting is measured by the rate of decrease of solid flow rate. As the solid flow rate is a function of its density, cross-sectional area and down-channel velocity, it is not possible to estimate it accurately from the specimens. Thus it is possible here that the solid bed is decelerating and the variation in the true melting rate is small.

A similar effect can be seen in Plate 15 for rigid PVC and similar explanations apply. Also the results of the three water cooling experiments show a

similar seemingly rapid final melting, see Plates 4(b), 7(b) and 9(b). Here however the argument based on zero latent heat is inapplicable and therefore the suggestion that the solid bed is decelerating becomes more likely, the more so in the light of earlier observations on the manner in which screw cooling would seem to prevent solid bed break-up.

The two experiments performed with 'Melinex' produced the most unusual results of all the experiments. The cross-sectional specimens of Plate 12 show that bed break-up occurred, yet the expected pressure traces in such a case were not observed. Figures 2.61 and 2.62 show the slow speed pressure recordings for experiments 23 and 24. Figures 2.63 and 2.64 show higher speed recordings for the same two experiments. As can be seen the surging is most irregular and has a much higher amplitude than that observed with any other experiment. In addition the origin of the surging would seem to be at trace number 1 which is before the initiation of bed break-up. The implication is that effects other than bed break-up are partly or mainly responsible for the surging observed with 'melinex'.

On performing a trial experiment with Melinex it was found that the material was not feeding into the screw. This was due to the size of the granules in relation to the dimensions of the screw channel. To overcome this problem the granules were fed through a granulator which reduced the granular size slightly and also separated the clusters of granules that were partially joined together.

It seems that the cause of the surging with the 'Melinex' in the present experiments could have been due to a feed flow instability, a partial blocking and unblocking of the channel in the feed section. The axial pressure profiles of figures 2.26 show that virtually all the pressure rise in the extruder took place in the feed zone. Also the slow speed pressure traces show that when the pressure of trace 1 increased all the other traces show an immediate increase, albeit of smaller amplitude. These virtually simultaneous pressure rises and falls along the whole length of the screw are again not typical of surging due to bed break-up. In that case there is a deffinite time lapse between the

drop of pressure at the point of the break and a corresponding drop at the point further down-channel, see for example figure 2.51. The reason for this feeding instability in the present experiments is not clear, and further discussion of it is outside the scope of the present work, suffice it to say that its existence has been noted and the results recorded.

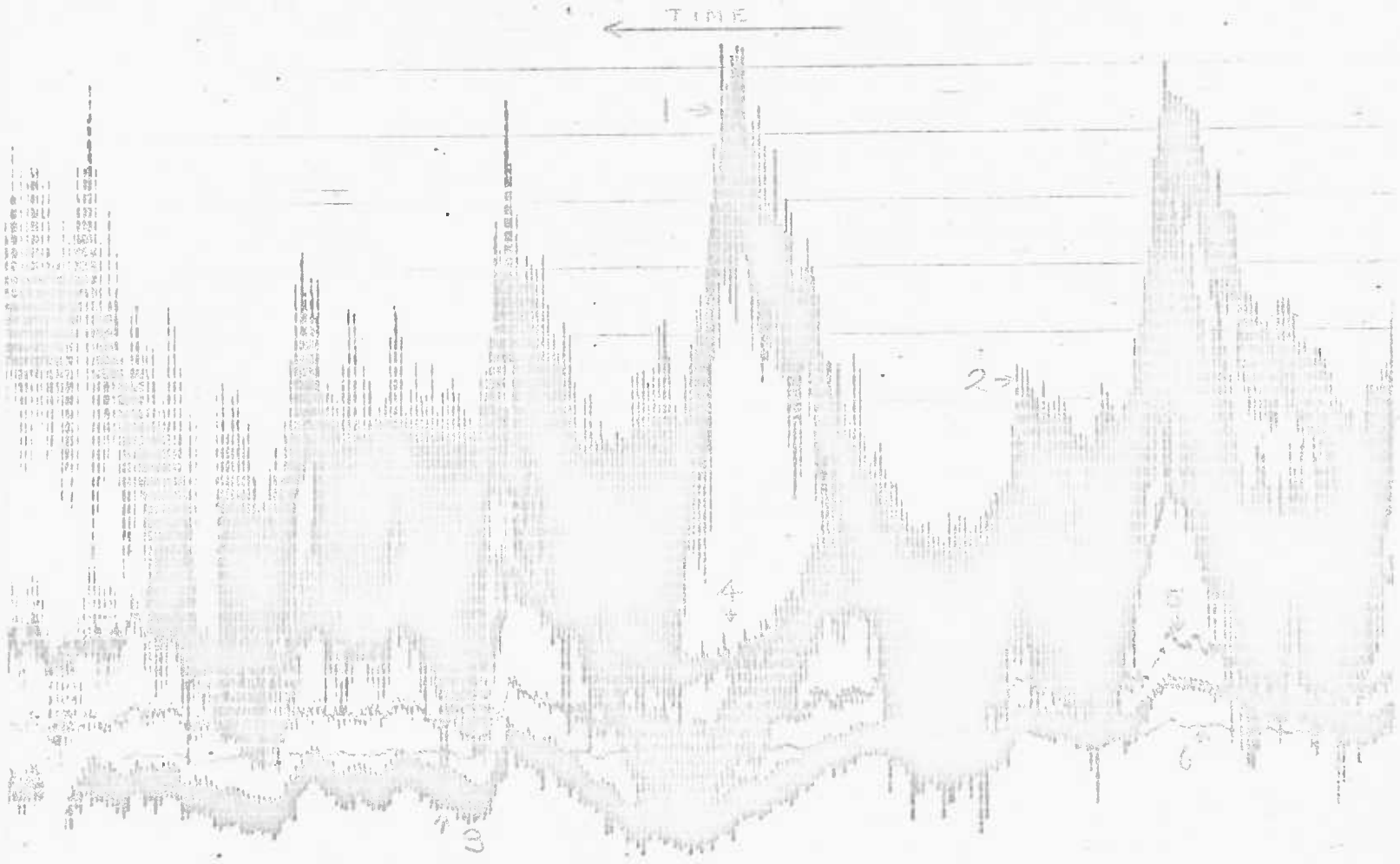


Figure 2.61

Low speed pressure recordings for experiment 23, with Melinex. All six traces shown.

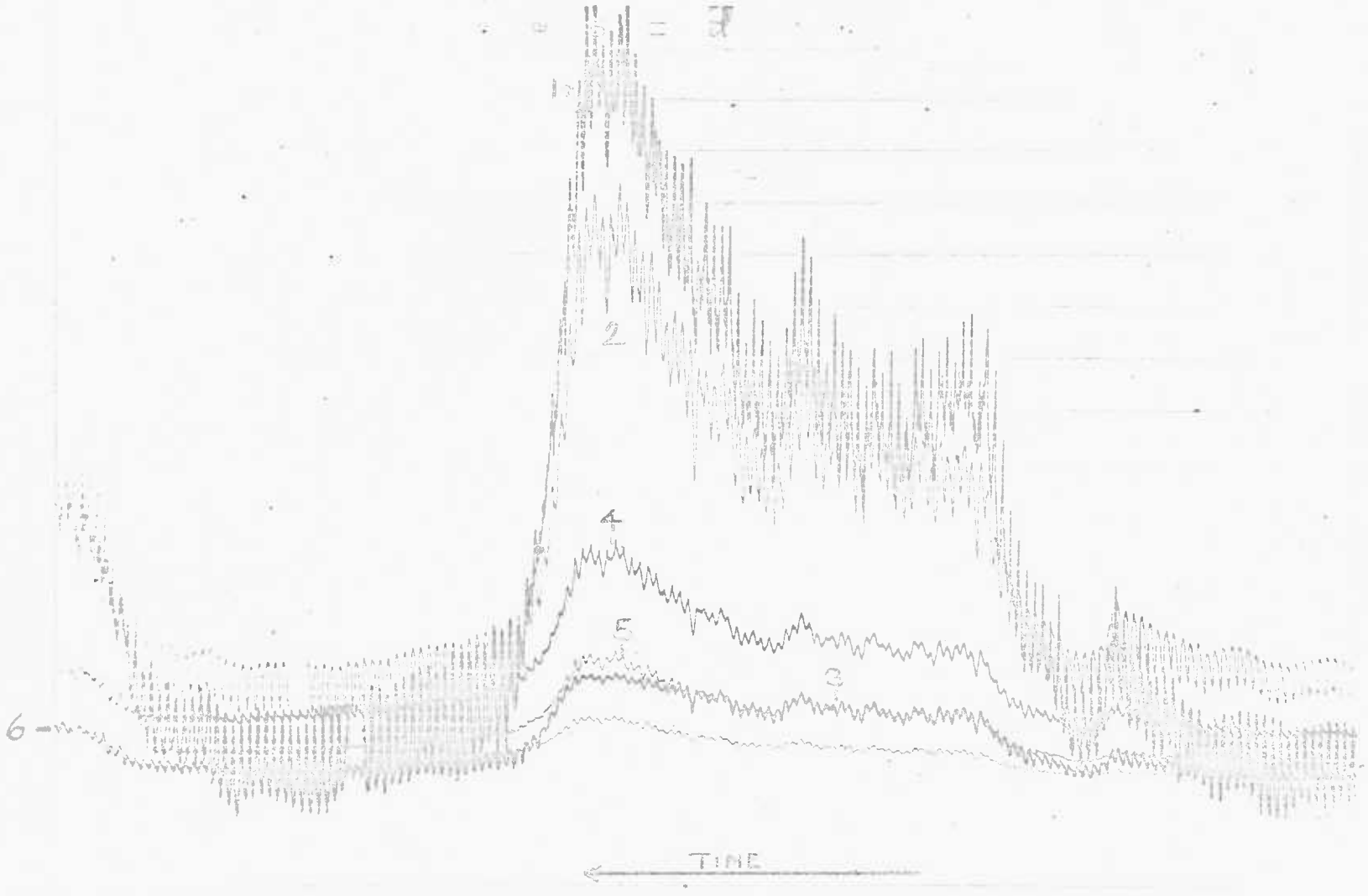


Figure 2.62

Low speed pressure recordings for experiment 24, with Melinex. All six traces shown.

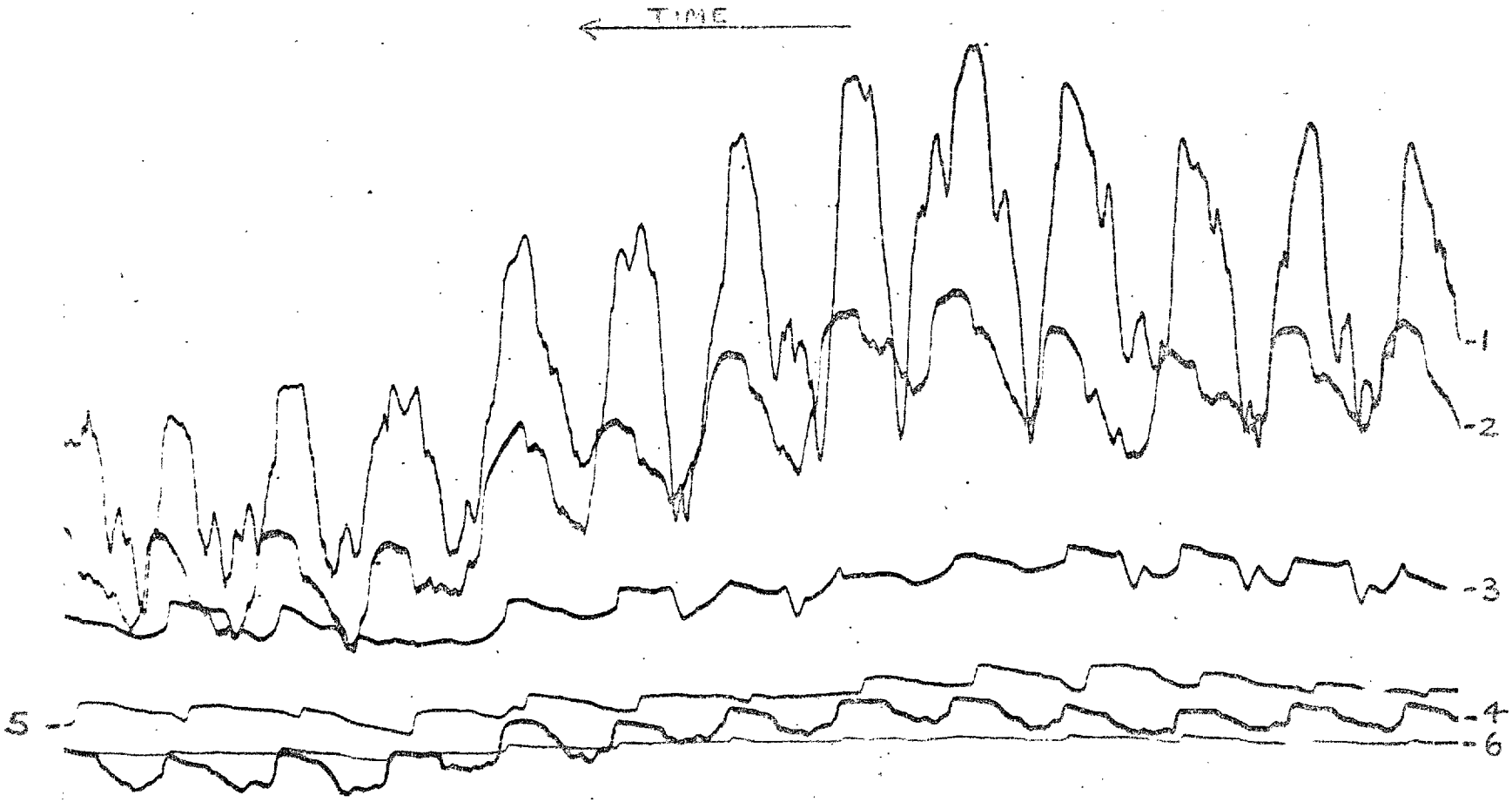


Figure 2.63

High speed pressure recordings for experiment 23, with Melinex. All six traces shown.

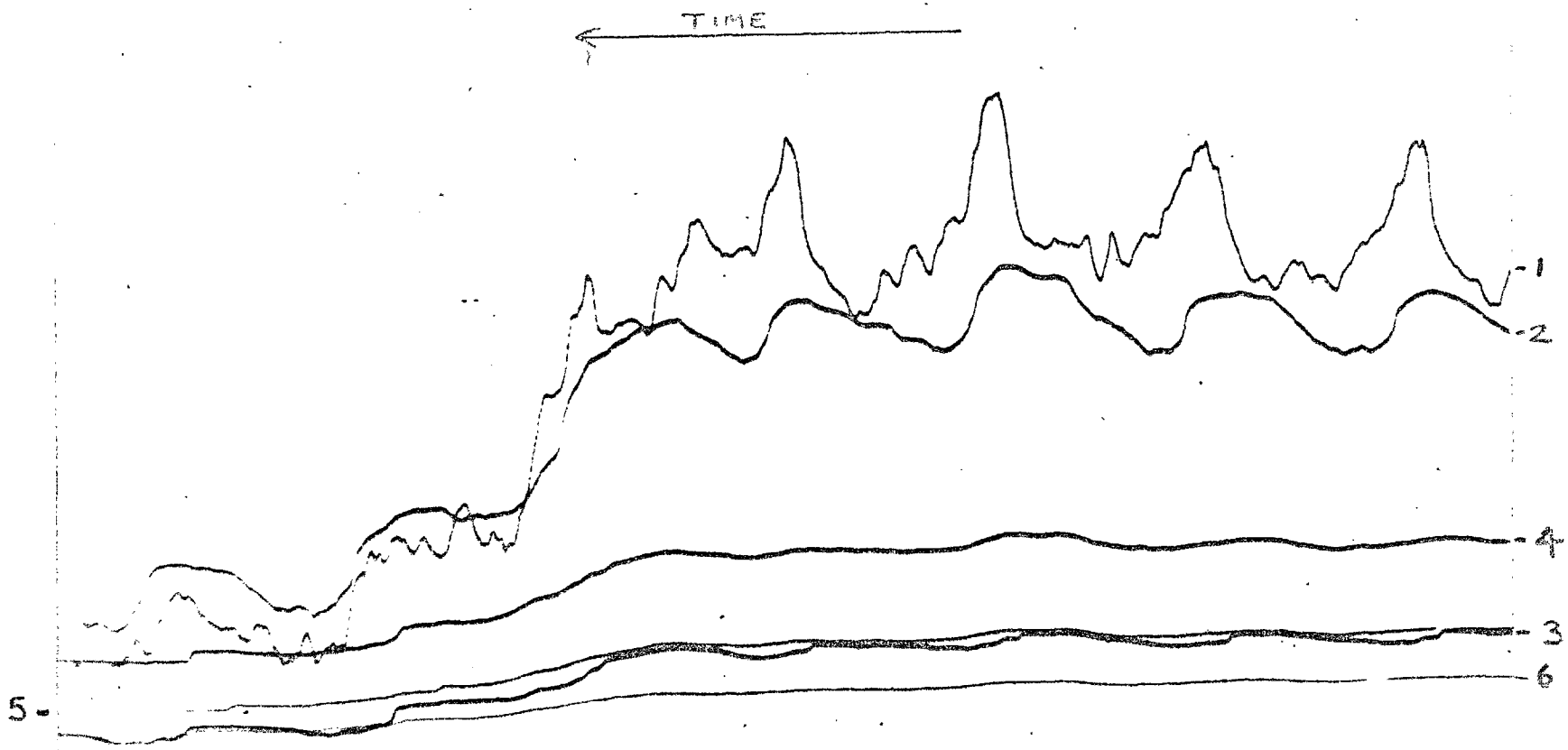


Figure 2.64

High speed pressure recordings for experiment 24, with Melinex. All traces shown.

2.5 Conclusions

The experimental results in the present work in part agree with the melting pattern that has hitherto been reported, initially by Maddock (2).

It has been found that this pattern on a considerable number of occasions is modified in that melt films exist between the solid bed and the screw surface. It has also been found that the melting process can have an inherent instability which manifests itself as solid bed break-up; this in turn produces surging. Examination of the experimental results of cases exhibiting bed break-up and those not doing so leads to the conclusion that in some situations the solid bed may accelerate whilst in others it may decelerate. In those cases when it accelerates it may fracture, in those when it decelerates it does not fracture. The occurrence of solid bed break-up varies between materials and would seem to cause more serious surging problems with the more highly crystalline plastics, not occurring at all for PVC which is essentially amorphous. The most effective way of preventing it is by the use of screw cooling. This however also reduces markedly the flowrate if the other operating conditions are left unaltered. It has been shown how an examination of detailed pressure recordings can lead to a recognition and understanding of the processes occurring within the extruder. In particular the phenomenon of solid bed break-up and the process of melting can be readily identified and followed on such pressure recordings. The following chapters will make use of these observations in the setting up of a mathematical model for the melting process. Initially the predictions of the theory will be compared with the experimental results and then a seperate series of theoretical simulations will be described in an attempt to demonstrate the usefulness of a computer simulation technique in comparison with empirical experimentation.

Chapter 3: Theoretical Analysis of the Melting Process

3.1: Introduction

It has been stated that the eventual aim of the present work is to produce a theoretical simulation of the melting process in single screw extruders. One aim of the previously described experimental work was to provide insight into mechanism involved in this melting process, which can be used to guide the mathematical formulation and to judge the appropriateness of various possible simplifying assumptions concerning the analysis. This is precisely the path followed by the earlier theoreticians of the subject. However because those analyses were the first they made the greatest possible simplifications of the problem in order that a solution could be obtained. Having successfully completed such an initial analysis they then proceeded in refining it. However, one general comment about this refining process is that rarely did it include the re-consideration of the basic interpretation of the observed melting patterns. The present theoretical analysis, is derived from a re-appraisal of the experimental melting patterns of the present and previous experimental work. Of course, the experience gained by previous theoretical analysis has also contributed to the present formulation of the problem.

It is appropriate to proceed by discussing the interpretation of the melting patterns that was used by the first theoreticians and the theories produced by them, pointing out those assumptions which are open to doubt. Having done this the exposition of the present theoretical treatment is given.

3.2: Theoretical Literature Review

The first theoretical analysis of the melting process was performed by Tadmor (4) making use of the experimental observations of Maddock (2). The idealised mechanism he proposed, which formed the basis of his analysis is shown in figure 3.4. The basic assumption of this model and all others is that the thermal and mechanical state of the system at all points in the domain occupied by the melting process is independent of time. In addition, the geometry is simplified as shown in the figure; the material properties are simplified; the solid bed is considered to be homogeneous and continuous; the plastic is considered to have a sharp melting point, and the thermal properties of the material to be constant in each phase. Tadmor's explanation of the thermal state of the domain is based on the occurrence of melting at the solid bed to melt film interface only. The heat for melting supplied to the interface originates partly from the barrel, as conducted heat, and partly from viscous dissipation within the film. Although some heat supplied to the interface is used to heat up the solid from its initial temperature to its melting temperature, the solid bed is assumed not to undergo any bulk increase in temperature as it passes down the channel. This is a consequence of the assumption, made in the thermal analysis of the solid bed, that it is a semi-infinite solid. This means that heat transfer from the melt pool and screw surfaces to the solid bed are neglected. This is reasonable in the case of the melt pool since the height of the solid bed is much less than its width over most of the melting process. One can only reasonably justify the assumption of zero heat transfer from the screw if it is cooled. This point will be discussed in greater detail later. The general assumption that heat conduction and convection down-channel, in the z direction, are neglected applies both to the melt film and the solid bed.

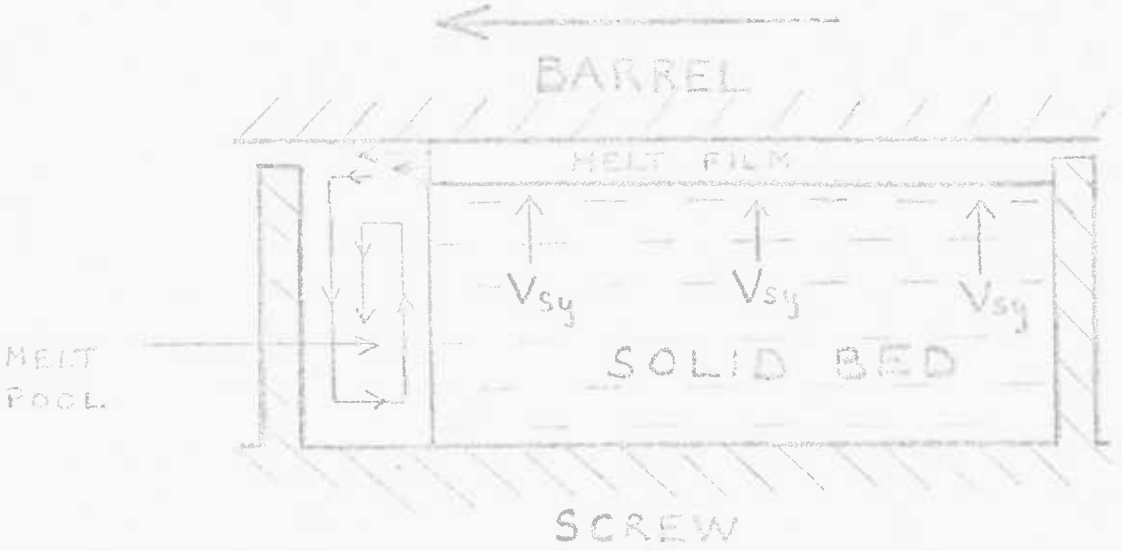
The flow in the melt film is assumed to be fully developed pure drag flow of a Newtonian fluid between parallel plates. This is assuming that the melt film thickness is not a function of x. In addition the flight clearance is assumed to be zero. The flow of the solid bed down-channel is assumed to be plug like and of constant velocity, that is

$$V_{sz} \neq f(x, y, z) \qquad (3.1)$$

In the xy plane the solid bed is assumed to have a velocity V_{sy} at the

Figure 3.1

The melting model used by Tadmor



melting interface. The implications of this are considered later.

The mechanism for maintaining the continuity of the system is this. Newly molten material is continually entering the melt film through the melting interface. At the same time molten material is flowing across the channel and out of the film to collect in the melt pool. The width of the melt pool is thus increasing. At the same time the width of the solid bed is decreasing and there is a steady flow of solid into the melting interface.

The problem thus has two dependent variables, the width of the solid bed, X, and the melt film thickness, δ. X is an explicit function of the independent variable z, while δ is an implicit function of z. The solution essentially requires two basic equations. These are derived from an integral mass balance of the melt film over the xy plane and a different mass balance on the solid bed in the z direction. The former equation relates the melting rate into the melt film with the flow rate into the melt pool. The latter relates the reduction in the solid bed width with the melting rate. One last piece of information required is the melting rate at the interface. This is found by means of an energy balance at the interface. In this fashion the solution, X as a function of z, is derived. The constant value of the solid bed velocity is calculated from the overall mass flow rate, M_T, and the geometry of the channel in the solids feed zone, thus

$$V_{sz} = M_T / (W H_0 \rho_s) \qquad (3.2)$$

The assumptions made in setting up this analysis are of two distinct types. Firstly there are those concerned with interpreting the melting pattern into a mechanism that can be analysed. Secondly are those concerned directly with the ensuing mathematical analysis. The former type of assumption is the most important and will be described in more detail now.

For the mechanism to function as intended the solid bed must undergo a certain form of deformation. That is, the decreasing width of the solid bed and the continual movement of solid into the melting interface imply a continuous re-arrangement of the granules of the solid bed. It is an implicit assumption of this model that the external stresses on the solid bed are sufficient to cause this mode of deformation.

Assuming the solid bed to be continuous and incompressible, the conservation of mass principle may be applied in differential form, instantaneously, as

$$\frac{\partial v_x}{\partial x} + \frac{\partial v_y}{\partial y} + \frac{\partial v_z}{\partial z} = 0 \qquad (3.3)$$

The assumption of constant velocity down-channel simplifies this to,

$$\frac{\partial v_x}{\partial x} + \frac{\partial v_y}{\partial y} = 0 \qquad (3.4)$$

Equation (3.4), together with the relevant boundary conditions, instantaneously describes the deformation pattern of the solid bed as assumed by Tadmor.

The second critical assumption made by Tadmor in his interpretation of the melting pattern concerns the melt film flow. He assumes that the thickness is constant over the width of the bed,

$$\delta \neq f(x) \qquad (3.5)$$

Tadmor also makes the assumption that pressure gradients in the melt film may be ignored in the flow calculations. This assumption together with that of constant film thickness lead to an inconsistency. In reality, due to the successive incremental entrainment of newly molten material across the film, either the film thickness must increase as x increases, or the pressure must decrease as x increases, or a combination of the two must take place so that continuity is satisfied. However it can easily be shown, because of the relatively small film thickness involved, that for the pressure gradient to have any significant effect on the flow rate it must be of such a large magnitude as to be physically unrealistic in the present situation. Additionally the sign of this pressure gradient would need to be negative, whereas all the experimental results show that the pressure gradient in the melt film is positive. Therefore the constant film thickness assumption violates a differential mass balance on the film, although an integral mass balance over the width of the film is not necessarily violated. As it is the integral mass balance that is used in the analysis the assumption may not lead to any significant inaccuracy in this respect However this part of the analysis can be critised on the grounds that the entrainment of newly molten material in the film is implicitly assumed to occur in the x direction only. That is, at any down-channel position all the newly molten material entering the film is assumed to flow into the melt pool at that same down-channel position. Yet clearly the direction of entrainment is more reasonably that of

the relative velocity between the solid bed and barrel. This is at an angle β to the channel wall, as illustrated in figure 2.4.

The last criticism of Tadmor's interpretation of the observed melting patterns is that he chooses to ignore the formation of melt films between the solid bed and the screw surface.

The comparisons between the theoretical predictions of this early model with experiments performed by Maddock (4) showed that the theory predicted too long a melting length. Also the predicted melting rate during approximately the first half of the melting process was too high whilst in the later stages it was too low.

The developement of this model was continued and reported along with new experiments by Tadmor, Duvdevani and Klein (6). They made two improvements to the model. The first and simplest of these was to take account of the effect of thermal convection in the melt film. This they did by adding an extra term into the energy balance at the melting interface accounting for the heat required to raise the temperature of the newly molten material from its melting temperature to the mean temperature of the material flowing from the melt film into the melt pool.

The second improvement was to introduce a Non-Newtonian flow and coupled energy analysis of the melt film. In this the power law constitutive equation with temperature dependence was used. The flow was still assumed to be steady, fully developed drag flow, between parallel plates. The solution to this flow problem was simplified by assuming an initial temperature profile, corresponding to the Newtonian case. An iteration procedure was then adopted to calculate the correct values of the modified coefficients of the equation for the temperature profile corresponding to the Non-Newtonian case.

With these two modifications incorporated into the analysis considerably better predictions were obtained, although the basic interpretation of the melting pattern had not been changed. In this publication (6) another deficiency of the model is apparent. To make the comparison between theory and experiment the start of melting in each should be at the same point along the screw. It was found that the experimental position of this start was at some point after

the barrel temperature had attained the melting temperature of the plastic and that this 'delay' was variable. Because of this it was necessary to measure it from the experiment and to use this as the start point for the theoretical comparison. Some attempt was made to establish an empirical correlation factor to enable this 'delay' to be predicted. It is thought by the author that this 'delay' is partly at least due to the particular interpretation of the melting pattern which forms the basis of this model. Justification for this suggestion will be given later.

Chung (7) reports a further detail improvement to the same basic model. Instead of assuming for the purposes of analysing the temperature distribution in the solid bed that the bed has infinite depth he assumes that the solid is finite and bounded by two parallel plates, and that it is insulated at the screw surface. Chung goes on to define four constants in the equation describing the temperature distribution where only two are strictly necessary, and states that one can assume the screw surface temperature to be constant throughout the melting process and to be equal to the initial temperature of the solid feed. To evaluate these constants four boundary conditions are needed. He specifies the two boundary temperatures and one derivative. For the fourth condition he applies an overall energy balance to the melting process; thus the fourth constant in the temperature profile is calculated so that the energy balance is automatically satisfied. It would seem that the difference between this formulation and that of Tadmor is marginal especially as Chung does not allow temperatures to develope down-channel.

More significant developements of the model were described by Tadmor and Klein (8). Here the model is refined to take account of the effect of a finite flight clearance and curvature of the actual screw channel. The effect of flight clearance on the integral mass balance for the melt film is allowed for by assuming a linear velocity profile through the clearance and calculating the flow rate on that basis. The effect of channel curvature is corrected for by utilising a series of derived correction factors (15).

In addition the scope of the melting analysis is enlarged to include the prediction of pressure in the melting zone. This is done by computing the melt

pool flow rate, which is easily done from a knowledge of the solid bed flow rate, and applying this in a deep channel melt flow analysis of the melt pool. Hence the required pressure gradient is calculated. This procedure is enlarged on somewhat in a later section. In this publication (8) the phenomenon of solid bed breakup is noted and its effect on pressure generation allowed for by computing the pressure gradient from a full channel melt flow analysis after the position of bed break-up. This point of bed break-up is presumably an estimate based on experience and is not predicted by the theory. It therefore must cause some potential inaccuracy in the pressure predictions.

Hinrichs and Lilleleht (11) describe modifications to the Tadmor model to account for flight clearance flow and channel curvature using a cylindrical coordinate system to simplify these corrections. It would seem that the improvements outlined here (11) formed the basis of those described by Tadmor and Klein (15) and mentioned earlier.

All the above mentioned theoretical analysis were based on the original model put forward by Tadmor (4) and therefore if the assumptions made in formulating that model from the observed melting patterns are wrong the subsequent mathematical refinements may not make any significant improvement to the overall accuracy of the simulation of the real melting process. Donovan (10,12) was the first reported worker to re-examine the basic interpretation of the melting patterns. His significant contribution is in the realization that the solid bed can accelerate in a screw compression section. This conclusion was arrived at in the light of experimental results described previously, and inspection of some of the simulations published by Tadmor et al (5). However Donovan does not make the down-channel solid bed velocity a fully dependent variable of the problem. He makes the basic assumption that the solid bed velocity is equal to the average melt pool velocity in the down-channel direction. This assumption together with the inclusion in the mathematical formulation of the problem, of a mass balance across the whole channel enables the solid bed velocity to be computed. It appears that Donovan found that using this formulation of the problem did not always give very accurate predictions. Therefore the basic assumptions that the mean melt pool and solid bed velocities are equal was

relaxed and a Solid Bed Acceleration Parameter (SBAP) defined such that with SBAP = 1 no solid bed acceleration occurs and with SBAP=0 acceleration is a maximum, being the same as that using the assumption described above. Clearly this technique is not altogether satisfactory in that one does not really know what value of SBAP to apply in a particular case. However the computed results when compared with experimental results, show that the value of SBAP for best agreement varies between experiments. This, of course, tends to re-affirm the idea that the solid bed accelerates.

Donovan makes another contribution to the theoretical analysis by considerably refining the thermal analysis of the solid bed. He considers the solid bed to have finite depth and defines the two boundary temperatures as the required boundary conditions. He also includes in the analysis the effect of convection in the z direction, thus allowing for gradual heating up of the solid bed as it moves down-channel. The specification of the problem is completed by defining an initial temperature profile. Further Donovan assumes the melt film is linearly tapered across the channel from the flight clearance to the edge of the solid bed. However for the energy and momentum analysis of the film he reverts for mathematical convenience to the constant film thickness assumption, only using the tapered film to calculate the down-channel solid bed flow rate and the down-channel melt film flow rate. It is possible that the linear variation of film thickness leads to as large errors as the constant thickness assumption in these down-channel flow rate calculations especially if the real cross-channel developement length for the film is a lot less than the solid bed width.

In the melt film energy and momentum analysis Donovan makes the same assumptions as Tadmor et al (5) but his method of solution of the coupled problem is different Donovan uses the exact solution by Martin (33) which has the advantage of simplifying the mathematical and numerical complexity of the overall analysis.

In a later publication (12) Donovan extends his analysis to include pressure predictions in the melting zone. His method would seem to be essentially similar to that of Tadmor and Klein(8,15). Correction factors were employed to account for Non-Newtonian effects in the melt pool flow whilst maintaining

the simple form of a Newtonian flow analysis. That is, the drag and pressure induced components of the flow are separated so that the pressure gradient can be the more easily calculated. Again as with Tadmor and Klein, after the occurrence of bed break-up the pressure gradient is calculated from a melt flow analysis of the whole channel, the presence of the pieces of solid bed being ignored. It should be noted that the predicted pressure profiles were a function of the SBAP. The results showed that the value of SBAP which gave the best agreement with the experimental melting profile did not give the best agreement with the experimental pressure profile. Although the discrepancy was not unacceptable, it was consistent. However the published results, with but one exception, were for compression relief screws with short and rapid tapers. These may have been used so that bed break-up could reasonably have been predicted to occur at the end of the taper. But such a screw design is probably the hardest to successfully simulate because of the rapid variation of screw geometry in the down-channel direction and also because visco-elastic effects may become significant.

One general observation that can be made about the results presented by Donovan is that in a number of cases his model was not able to successfully predict the correct shape of the melting profile, as measured from his experiments, no matter what value of SBAP was used.

Vermeulen, Scargo and Beek (13) developed a model that was different from that of Tadmor and Donovan. The significant difference was that the thickness of the melt film was allowed to vary across the solid bed in the x direction, thus satisfying continuity everywhere in the film. However the other assumptions in this model are such that any improvement in accuracy resulting from a detailed melt film analysis was probably lost. These other assumptions correspond to those made by Tadmor in his earliest formulation (4). The melt is assumed to be Newtonian and the solid bed velocity to be constant. One extra assumption made by Vermeulen et al was that dissipation in the melt film could be neglected. All experimental and other theoretical results have shown that this is far from true and that viscous dissipation can be more significant than conducted heat from the barrel. The justification for making

this assumption is obscure, even on purely mathematical grounds, in that for a Newtonian fluid it is possible to get an analytical solution describing the developement of the film thickness in the x direction including the dissipation term in the energy equation.

The basic model of Vermeulen et al (13) has been considerably improved by Ingen Housz and Gorissen (14). They first of all included the dissipation term in the melt film temperature analysis for the Newtonian case and obtained an analytical solution. They then further extended the model to include Non-Newtonian power law temperature dependent viscosity in the melt film.

This last piece of analysis makes use of Martin's work(33) on analytical solutions for Non-Newtonian shear flow. In this analysis as applied to the melt film flow, although the thickness of the melt film is varying at each point in the film, the velocities and temperatures are assumed to be locally fully developed and the 'lubrication approximation' is applied.

No comparrison between the predictions of this model and experimental work have been published and therefore the effect of the inclusion of the melt film thickness developement in this model is hard to judge.

Those then are the various models that have been published in the literature to date, and it is apparent that most of the effort has gone into refining the mathematical analysis of the details of the models rather than questioning the basic assumptions.

The basic assumptions are essentially interpretations of the observed pattern into a mechanism of flow that is compatible with the observations and the laws of physics. These assumptions fall into three categories; concerning the mode of deformation of the solid bed; concerning the regions where melting takes place, and concerning the flow paths of the newly molten material. These three aspects of any melting model are discussed in the following section leading up to the nature of the basic assumptions made in the present model.

3.3: Discussion of the Basic Assumptions made in the present Melting Model

The solid bed deformation will be discussed first. The experimental results presented in the present work and by other people clearly show that the solid bed does change shape during the melting process. Further this change of shape cannot wholely be accounted for by the continual removal of molten material from its boundaries. The reduction in height of the solid bed may be accounted for in this manner but the usual reduction in the width cannot be, especially as, on occasions the width may increase for a short while. The manner in which this width change is accomplished is critical to the discussion. In the case where, at an intermediate stage in the melting process, the solid bed width increases the cause must be the screw taper. In that case the reduction in height of the solid bed due to the melting is less than the reduction in channel depth due to the screw taper and therefore the metal surfaces cause the bed to deform and increase its width. However in the more normal case where the channel taper is less extreme the bed is observed to deform in the opposite way, its width reducing. In this case the forces producing the deformation are an integral part of the melting process. The sources of the important stresses can be identified as the melt pool pressure, the viscous shear stress on top of the solid bed and the shear stresses on the bottom and the side of the solid bed, either coulomb or viscous depending on the presence of the melt film.

It is possible to identify two extreme modes of deformation of the solid bed, the first corresponds to that assumed by Tadmor, that is, no acceleration of the solid bed. Equation (3.4), previously stated, expresses this condition in terms of the continuity equation, and is re-stated here for convenience

$$\frac{\partial v_x}{\partial x} + \frac{\partial v_y}{\partial y} = 0 \qquad (3.4)$$

This equation is saying that the reduction in the width of the solid bed is manifest as an increase in height of the bed. Of course, due to melting occurring on at least the top surface of the solid bed, in the xy plane, this increase in height is masked in the actual case.

The other possible extreme mode of deformation is given by the following form of the continuity equation

$$\frac{\partial v_x}{\partial x} + \frac{\partial v_z}{\partial z} = 0 \qquad (3.6)$$

This equation corresponds to the case where the reduction in solid bed width is totally accounted for by acceleration of the solid bed and that reduction of the height in the actual melting process is due entirely to the removal of molten material. If this case were an accurate picture of the deformation of the solid bed then one would expect to observe an ever increasing melt film thickness, in the absence of any channel taper. This does not appear to be the case, the results of Tadmor et al (5) are useful in this respect.

The present experimental results together with those of Donovan (10) and the theoretical results of Donovan(10) indicate that solid bed acceleration does take place.

The conclusion must be that the deformation of the solid bed is the general case somewhere between the two extremes, described by the above two equations, and that in terms of the continuity the representation of the deformation, instantaneously is

$$\frac{\partial v_x}{\partial x} + \frac{\partial v_y}{\partial y} + \frac{\partial v_z}{\partial z} = 0 \qquad (3.3)$$

Thus the solid bed should be allowed complete freedom in the formulation of the problem to accelerate. The theoretical work of Donovan (10) was a step in this direction but the indications are that the assumption he made was too restrictive and that the solid bed velocity down-channel should be a fully dependent variable of the problem.

The melt film flow path will now be considered, referring specifically to the upper melt film adjacent to the barrel. An elemental volume of newly molten material at the interface will be dragged in the direction of the relative velocity vector between the barrel and the solid bed. At some point down-channel this element of material will discharge off the edge of the solid bed into the melt pool. The effect on flow rate and velocity profile, in the melt film, of pressure gradient is negligible because the thickness of the film is small as has been mentioned in the last section. The critical point here is that there is a delay between the formation of an element of molten material and the discharge of it in the melt pool. The implicit assumption of all the melting models reported to date is that at any section z the total flow rate into

the melt pool necessarily equals the total melting rate at the same section. At first sight this may seem a question of detail yet the consequences of making this assumption can be significant. In the first place it partly explains the 'delay' in melting that Tadmor comments upon.

This 'delay'may be explained as follows. Melting will begin on top of the solid bed from the point where the barrel temperature exceeds the plastic's melting temperature. Initially the molten material will fill the gaps between the individual granules on the top of the solid bed. Until this has happened no continuous film will exist on top of the bed. Once this continuous film has been formed its thickness will begin to develope in the direction of entrainment as described earlier. It is likely that the thickness of the film is initially less than the flight clearance. Therefore there will be a delay between the formation of the continuous film and its thickness equaling the flight clearance. Once the film thickness exceeds the flight clearance the flight will act as a wiper and the melt pool will begin to develope. The flow into the melt pool will initially grow rapidly as the film thickness at the edge of the solid bed will continue to increase. This increase occurs because the material flowing into the melt pool became molten at an earlier stage. Once the film thickness has become developed and the melt pool formed, the film thickness should gradually decrease as the width of the solid bed decreases and hence the developement length is reduced. The presence of the melt film all around the solid bed can however potentially affect the validity of this last point. Although Vermeulen et al (13) and Ingen Housz and Gorissen (14) allowed for the developement of the film thickness they still assumed that the flow into the melt pool was equal to the melting rate at the section whereas in fact it is a function of the melting rates over the previous sections. The correct flow rate into the pool can be different from one calculated in the manner of Vermeulen and others due to the differences in the solid bed width, or in barrel temperature or in the solid bed velocity that may exist between the relevant down-channel sections over which the melting rate should be calculated.

The general conclusion from the foregoing is that at a section z the flow rate into the melt pool should not be explicitly equated with the melting rate

at that section. This may be avoided by performing an integral mass balance for the melt film over an increment Δz and allowing the film thickness to develope as a function of x and z.

It is now appropriate to consider the importance of other regions within the channel where melting takes place. In other words, it has to be decided if significant melting takes place on the other three sides of the solid bed. One may readily discount the side of solid bed adjacent to the melt pool for two reasons. Firstly the height of the solid bed is small in relation to its width for a good part of the melting process. Also the temperature gradient in the melt pool adjacent to the solid bed is likely to be small in comparison with those in the melt films. Similarly the side of the solid bed adjacent to the flight can be disregarded in terms of significant melting as its height is very small, although the temperature gradient may be fairly high. The bottom of the solid bed in contact with the screw root is a different matter. There have been no published theoretical models which include a melt film in this area though Shapiro (34) is reported to be working on such a model. Clearly with an uncooled screw a point will exist along the screw at which the screw temperature will rise above the melting temperature of the plastic. From this point solid plastic in contact with the screw will melt. The extent to which it does so will depend on the heat transfer coefficient between the plastic and metal, on whether there is any tendency for the plastic to slip at this surface, and on how much heat is transmitted along the screw. Little information is available concerning heat transfer coefficients between plastic and metal. The work of Tharmalingham (45) although not directly applicable to the present situation suggests that perfect thermal contact is likely to exist under the sort of pressures involved here. Certainly unless the material and conditions are such that slip occurs on the screw surface a thin film of melt is likely to form.

Martin (35) performed some relatively simple calculations to investigate the thermal coupling effect of the flow of a viscous material within the metal boundaries. This is the only reported work of this kind on what is a difficult problem and yet would seem to be of great importance. The aims of such

an analysis are to calculate the magnitude of heat flow from the plastic to the screw and when such a heat flux exists, and secondly the occurence and magnitude of the reverse process of heat transfer from the screw to the plastic. The results of Martin's work lead him to suggest that the magnitude of the heat flux back out of the screw is insignificant when compared to the other heat fluxes in the total extruder system. This conclusion, if valid, need not necessarily prevent a significant amount of melting at the screw root. As long as enough heat flows back along the screw to raise the screw temperature above the plastic's melting region, and thus to form an initial thin film, then potentially the dissipation in this film will continue to provide the thermal energy to melt material off the bottom of the solid bed.

With regard to this last point, the effect of solid bed acceleration should be noted. The viscous dissipation in a melt film will be approximately directly proportional to the square of the relative velocity between the two solid boundaries, everything else being constant. Therefore, as the solid bed accelerates, dissipation in the top film adjacent to the barrel will decrease, but this decrease will to some extent be compensated for by an increase in dissipation in the lower film, if the lower film is present.

A last point in favour of including the lower melt film in the melting model concerns directly the acceleration of the solid bed. It has been shown experimentally in the present work that the presence of this melt film is critial both to the acceleration of the solid bed and to the pressure generation in the melting zone. Clearly, therefore, the magnitude of the viscous stress on the bottom of the solid bed should be evaluated in the melting model to allow accurate computation of the solid bed acceleration and the pressure generation. This will become more apparent when the present analysis is outlined and the results of it discussed.

The conclusion of the foregoing is that this lower melt film as it will be called, should be included in the melting model. Ideally the model should allow both conditions, that is, the presence of this film or its absence, according to the screw temperature.

The potential inclusion of such a melt film in the model necessitates that the

thermal analysis of the solid bed should be for a finite solid bed and should specify temperature boundary conditions at each boundary. It should also compute the developement of temperature within the solid bed as a function of z.

It is now useful to consider the flow path of this lower melt film. Clearly, the existence of a continuous film of melt around the solid bed will allow re-circulating flow to occur. However the driving force for any flow in the melt films between the solid bed and the screw must be pressure. Because these films will, for the most part, be thin this cross-channel re-circulation will be negligible. Thus the newly molten material in the lower film will essentially be entrained in the z direction and potentially this film could become 'thick' unlike the top film, due to the absence of a mechanism for removing molten material from it. If this film does become 'thick' then the flow path of material in it will be different, in that the effect of pressure gradients both across and down the channel will be important. However it is not within the scope of the present work to include such pressure gradient effects on the flow in the melt films.

A summary of the conclusions to the foregoing discussion is useful to define the melting model which forms the basis of the analysis to follow.

The solid bed will be allowed to accelerate, its down-channel velocity, V_{sz}, is a dependent variable of the problem. The assumption that the flow of the solid bed is plug like will be made,

$$V_{sz} = V_{sz}(z) \tag{3.7}$$

This does not violate equation (3.3)

The melt film on the bottom of the solid bed will form an integral part of the model, that is, a dependent variable. The thickness of this film, δ_2, is a function of z only.

$$\delta_2 = \delta_2(z) \tag{3.8}$$

The width of the solid bed, X, is the third dependent variable and is also assumed to be a function of z only.

$$X = X(z) \tag{3.9}$$

Ideally the upper melt film should be allowed to develope as a function of x and z. However such a formulation leads to excessive mathematical complexity

in one part of the overall analysis. Indeed, the overall formulation of the problem and the solution to it is facilitated by assuming that the thickness of the upper melt film, δ_1, is a function of z only.

$$\delta_1 = \delta_1(z) \qquad (3.10)$$

This assumption is introduced essentially for mathematical convenience, although the experimental results indicate that over much of the width of the solid bed the percentage variation of the film thickness is small. Thus it is thought to be a reasonably permissible assumption in terms of the effect it has on the accuracy of the model. In addition it enables the problem to be formulated in a way that excludes the criticisms levelled at the assumptions of Fadmor and Vermeulen et al.

The last dependent variable to the problem is the pressure, or more specifically the pressure gradient. Cross-channel pressure gradients will be neglected, therefore

$$\frac{dp}{dz} = f(z) \quad ; \quad p = p(z) \qquad (3.11)$$

Thus the problem is defined in terms in five dependent variables, all functions of the one independent variable z. Clearly five independent equations are needed to solve the problem. These are obtained by application of the laws of conservation of mass and momentum as follows.

1. Differential mass balance in the upper melt film over an increment Δz.
2. Differential mass balance in the lower melt film over an increment Δz.
3. Differential mass balance in the solid bed over an increment Δz.
4. Integral mass balance for the whole channel.
5. Differential force balance on the solid bed over an increment Δz.

This produces a set of five simultaneous ordinary differential equations which are essentially of the first order.

The next section deals with the detailed derivation of these equations and the subsidiary equations required which are derived from various applications of the laws of conservation of energy and momentum.

3.4 The Derivation of the Mathematical Equations Describing the Melting Model

The melting model that is the subject of the present analysis is illustrated in figure 3.2. It may be described as follows.

Melting begins by the formation of a melt film over the solid bed. When the thickness of this film becomes greater than the flight clearance the 'wiping' action of the trailing flight begins and the melt pool starts to form between the solid bed and the trailing flight. To accomodate this melt pool the solid bed deforms. The deformation manifests itself generally in three ways; its width changes; its height changes, though its effect is masked by the continuous melting of material at the melt film interfaces; and it accelerates. At some later point melt films may appear between the solid bed and the screw surface. The film between the side of the solid bed and the flight is treated as if it were an extension of the film between the solid bed and screw root. All the melt film thicknesses are explicit functions of z only. The continuity of the situation is maintained by equating the transfer of material between these three regions; the solid bed; the melt films; and the melt pool.

It was stated at the end of the last section that the required five equations are obtained by application of the laws of conservation of mass and momentum. However if this is done without having performed certain supplementary analysis then those five equations will contain a number of 'secondary' variables and will hence not be in a form from which the required solution can be obtained. In other words these 'secondary' variables must be eliminated from the main five equations. This is done by performing the relevant supplementary analysis which enables these secondary variables to be expressed as functions of the five primary variables. In the exposition of the analysis that follows this supplementary analysis is presented prior to the derivation of the main equations so that the results of it are available to eliminate the secondary variables from the main equations and leave them in a soluble form.

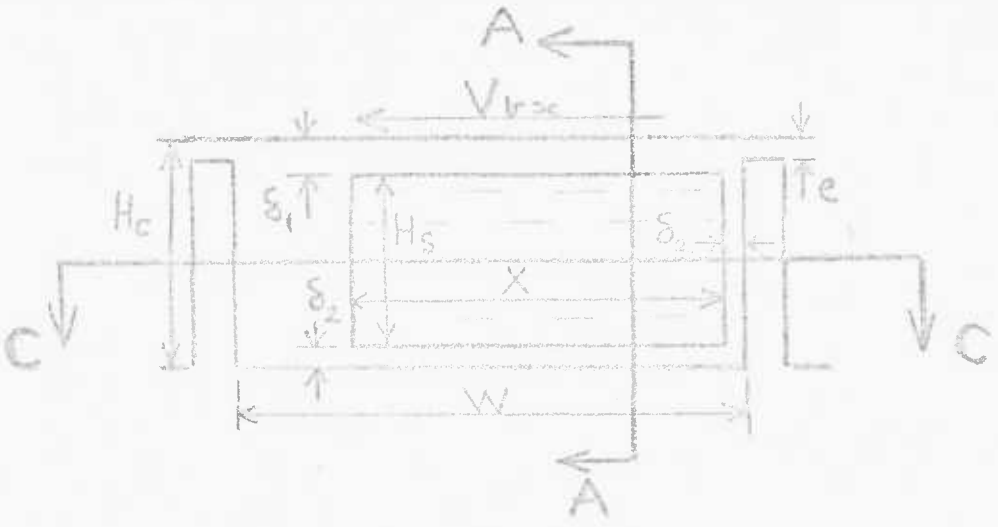
The supplementary analysis consists of four parts. These are; a momentum and energy analysis of the melt films; an energy analysis of the solid bed; a momentum analysis of the melt pool; and an energy analysis at the melting interfaces

between solid bed and melt films. Figure 3.3 shows diagrammatically where the results of these supplementary analysis are used in the derivation of the main equations.

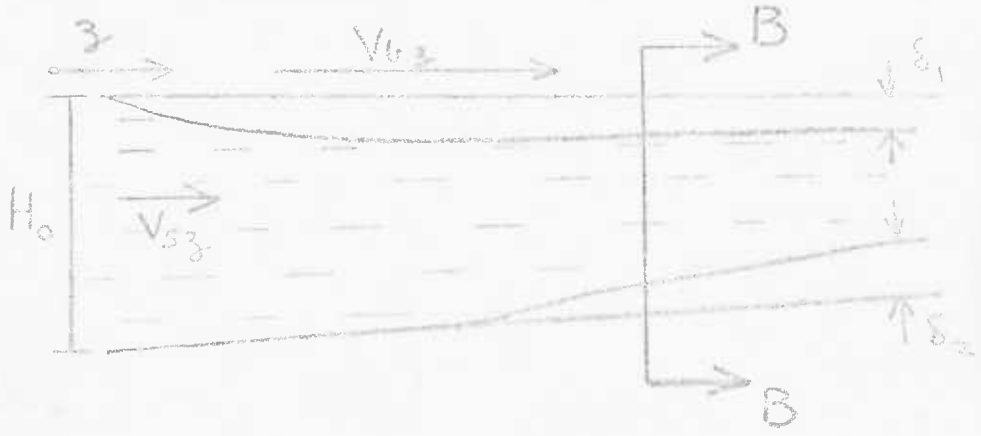
Throughout the following analysis it is assumed that the melting process is steady, that the solid bed is a homogeneous isotropic continuum, that the plastic has constant physical and thermal properties in each phase and that it has an identifiable melting temperature, T_m. Geometrically the screw channel is treated as having been unwound and hence is described by a Cartesian co-ordinate system. The effect of decreasing channel depth is taken account of by assuming the channel to be locally parallel, that is, the lubrication approximation is applied.

Figure 3.2

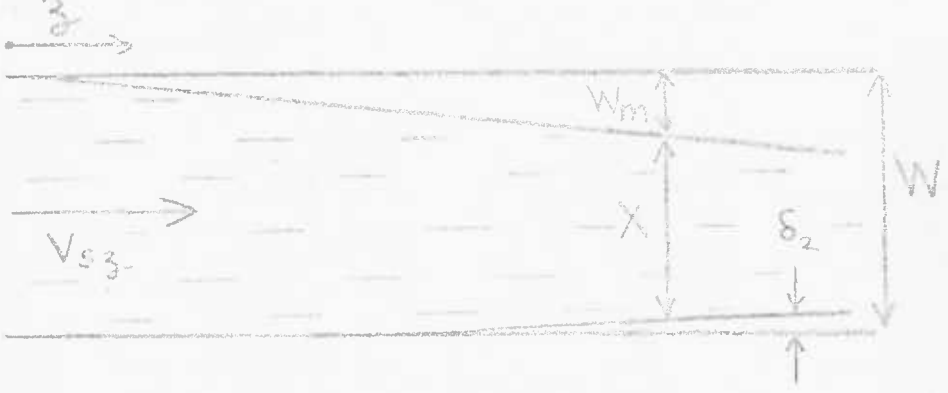
The present melting model



SECTION BB

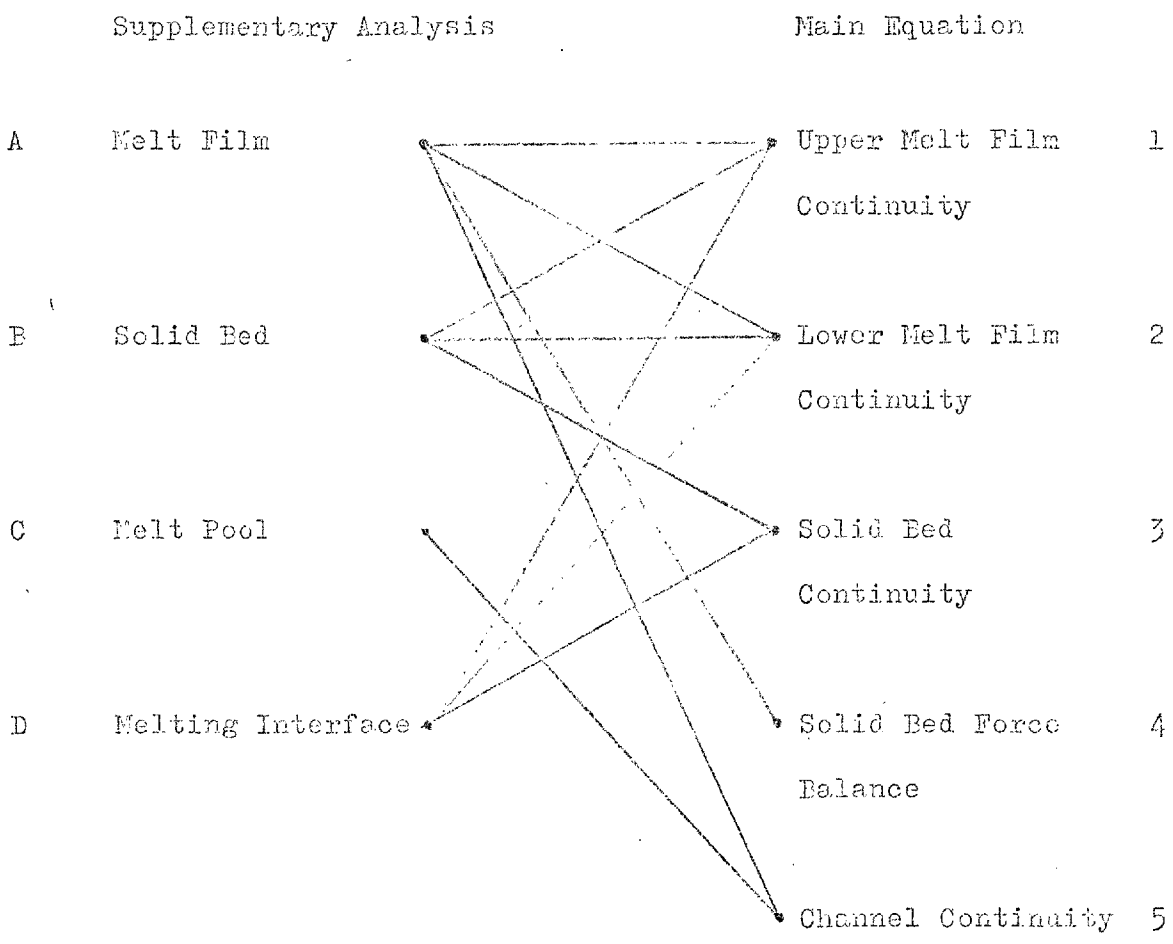


SECTION AA



SECTION CC

Figure 3.3


Supplementary Analysis
Main Equation
A
Melt Film
B
Solid Bed
C
Melt Pool
D
Melting Interface
Upper Melt Film Continuity
1
Lower Melt Film Continuity
2
Solid Bed Continuity
3
Solid Bed Force Balance
4
Channel Continuity
5

Supplementary Analysis.

A: Melt film momentum and Energy analysis

For a Newtonian constant viscosity fluid the mass flow rates in the upper melt film in the x and z directions respectively per unit length, assuming that pressure gradients have negligible effect on the velocity profiles, would be

$$m_{1x} = V_{bx}\, \rho_m\, \delta_1 / 2 \qquad (3.12)$$

and,

$$m_{1z} = (V_{bz} + V_{sz})\, \rho_m\, \delta_1 / 2 \qquad (3.13)$$

where V_{bx} is the component of barrel velocity in the x direction

V_{bz} is the component of barrel velocity in the z direction

V_{sz} is the component of the solid bed velocity in the z direction

ρ_m is the density of the molten plastic

the subscript (1) denoting the upper melt film

The non-Newtonian flow analysis used in the present work is based on the analytical solution developed by Martin (33) and extended by Fenner(39). The detailed analysis is given in Appendix B. It is essentially formulated in non-dimensional terms and the problem it solves is posed as follows, referring to Figure 3.4. The flow is that of fully developed pure drag flow between parallel plates of a power law fluid. Because this analysis is essentially analytical the assumption of fully developed flow must be made. Were that assumption to be relaxed than a different numerical solution procedure would have to be adopted. This would add great complication to the problem of finding a solution technique for the overall analysis. This then is one reason for making the assumption of fully developed flow. Additionally, previous theoretical analyses have used this assumption and it does not seem to have introduced any large errors. With the proviso that at a later stage this assumption could be dropped if it is found to be necessary it will be retained in the present work.

The requirements of the analysis are the boundary temperature gradients, the shear stress which by the nature of the problem is constant across the flow region, and the flow rate. The moving upper boundary in figure 3.4 is the barrel or screw surface according to which melt film the analysis applies, and the solid bed is the lower boundary. The temperature of these boundaries can

Figure 3.4

Sketch of the flow domain used in the melt film analysis

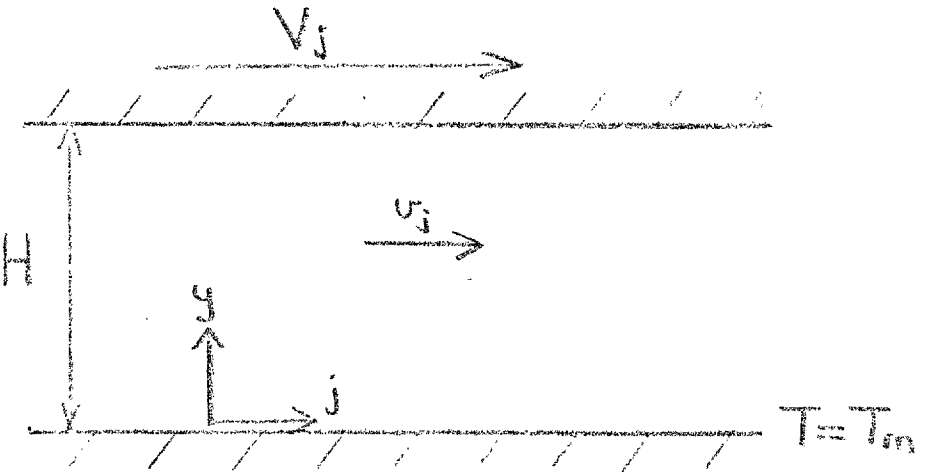
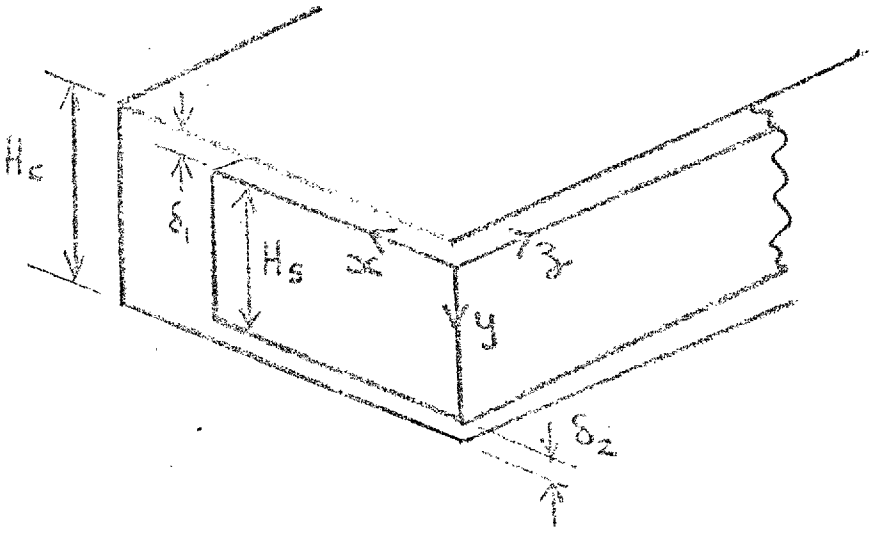


Figure 3.5

The coordinate system for the solid bed energy analysis



in principle be readily specified. The coordinate direction normal to the boundaries is y, whose origin is taken at the solid bed surface. The distance between the plates in this direction is H. The flow occurs in the direction j, with velocity $v_j(y)$, which is the direction of the resultant velocity of the upper surface relative to the lower, V_j. The constitutive equation for the fluid in this analysis is taken to be

$$\eta = \eta_D \left| \frac{1}{\dot{\gamma}_D} \cdot \frac{dv_j}{dy} \right|^{n-1} \cdot \exp\left[-b(T-T_D)\right] \qquad (3.14)$$

where η is the viscosity

T is the temperature

η_D is the datum viscosity as measured at shear rate $\dot{\gamma}_D$, which is usually taken as 1 sec^{-1}; and temperature T_D.

b is the coefficient of temperature sensitivity of viscosity

n is the power law index

η_D, b and n are material properties. The most general form of this constitutive equation, known as the 'power law' model, and its derivation are discussed in detail in Martin(28) and Fenner(29).

When the melt film analysis is applied to the upper melt film, the distance between the boundaries is δ_1, the upper boundary temperature, T_b, and the velocity of this boundary is given as

$$V_{1j} = \left[V_{bx}^2 + (V_{bz} - V_{s3})^2 \right]^{\frac{1}{2}} \qquad (3.15)$$

Thus the results of the analysis is a non-dimensional flow rate, Q^*_{1j}, and a non-dimensional shear stress, τ^*_{1j}, in this j coordinate direction. These qualities are then resolved into x and z directions using the following relationships.

$$Q^*_{1x} = Q^*_{1j} \sin\beta \qquad (3.16)$$

$$Q^*_{1z} = Q^*_{1j} \cos\beta \qquad (3.17)$$

similarly for τ^*_{1x} and τ^*_{1z}

where $$\beta = \tan^{-1}\left[V_{bx} / (V_{bz} - V_{s3}) \right] \qquad (3.18)$$

The corresponding components of the dimensional mass flow rates per unit length, M_j, may be derived from the definition of Q^*_j, which is

$$M_j = \rho_m V_j H Q_j^* \tag{3.19}$$

For the upper melt film these are

$$M_{1x} = V_{bx} \rho_m \delta_1 Q_{1j}^* \tag{3.20}$$

$$M_{1z} = (V_{bz} - V_{sz}) \rho_m \delta_1 Q_{1j}^* + V_{sz} \rho_m \delta_1 \tag{3.21}$$

Comparison of the above two equations with equations (3.12) and (3.13) shows that they are identical if $Q_{1j}^* = 0.5$, as would be expected. The results of the non linear analysis are presented in the form shown above as it explicitly identifies the film thickness, δ_1. This is important for the developement of the complete analysis.

When the non-linear analysis is applied to the lower melt film the distance between the boundaries is δ_2, the temperature of the moving boundary is the screw temperature, T_R, and its velocity is V_{sz}. Thus here the j and z directions are identical. In this case the mass flow rate in the direction per unit length is given as

$$M_{2z} = V_{sz} \rho_m \delta_2 Q_{2j}^* \tag{3.22}$$

where the subscript (2) denotes the lower melt film.

For completeness the relevant expressions for shear stress are now given

$$\tau_{1z} = \bar{\tau}_1 \tau_{1j}^* \cos\beta \tag{3.23}$$

$$\tau_{2z} = \bar{\tau}_2 \tau_{2j}^* \tag{3.24}$$

where, in general, the mean shear stress, $\bar{\tau}$, is given by

$$\bar{\tau} = \eta_D \left| \frac{1}{\dot{\gamma}_D} \cdot \frac{V_j}{H} \right|^{n-1} \cdot \frac{V_j}{H} \cdot \exp\left[-b(T_m - T_D)\right] \tag{3.25}$$

As has been said, later analysis requires a knowledge of the temperature gradients in the melt films. These are

$$\left(\frac{dT_1}{dy_1}\right)_{y_1=0} = \left(\frac{dT_1^*}{dY_1}\right)_{Y_1=0} \cdot \frac{1}{b \cdot \delta_1} \tag{3.26}$$

$$\left(\frac{dT_1}{dy_1}\right)_{y_1=\delta_1} = \left(\frac{dT_1^*}{dY_1}\right)_{Y_1=1} \cdot \frac{1}{b \cdot \delta_1} \tag{3.27}$$

$$\left(\frac{dT_2}{dy_2}\right)_{y_2=0} = \left(\frac{dT_2^*}{dY_2}\right)_{Y_2=0} \cdot \frac{1}{b \cdot \delta_2} \tag{3.28}$$

$$\left(\frac{dT_2}{dy_2}\right)_{y_2=\delta_2} = \left(\frac{dT_2^*}{dY_2}\right)_{Y_2=1} \cdot \frac{1}{b_2 \delta_2} \qquad (3.29)$$

where $\frac{dT^*}{dY}$ is the non dimensional temperature gradient

These then are the relationships derived from the momentum and energy analysis of the melt films which are used in the subsequent analysis.

B: The energy analysis of the solid bed

There are two aspects of this analysis that are of importance in the overall melting analysis. These are the temperature gradients in the solid bed in the y direction at the melt film interfaces and the developement of the temperature of the bulk of the solid bed as it travels in the z direction, downchannel. The coordinate system adopted in this analysis is shown in figure 3.5. It is assumed that the temperature profile is independent of x, to be consistant with the assumption that the melt film thicknesses are independent of x. It is a reasonable approximation during only approximately the first half of the melting process. In addition it is assumed that heat conduction is only important in the y direction.

The effect on the temperature profile in the solid bed of the reducing height of the solid bed due to the tapering of the channel and the developement of the melt films will be accounted for by a similarity approach, where, the continuously reducing height of the solid bed is approximated by a finite series of porallel sections, each successive one being less high than the previous, that is, the solid bed is taken to be locally parallel. The temperature profile at the start of each such section is scaled down from the profile at the end of the previous section according to the ratio of the heights of the two sections. Simplifying the energy equation in the light of the above assumption gives:

$$\alpha_s \cdot \frac{\partial^2 T_s}{\partial y_s^2} = V_{sy} \cdot \frac{\partial T_s}{\partial y_s} + V_{sz} \cdot \frac{\partial T_s}{\partial z} \qquad (3.30)$$

where α_s is the thermal diffusivity of the solid material.

V_{sy} is the velocity of the solid bed in the y direction.

V_{sy} is in general a function of y and z but, in line with the previous assumption, V_{sz} is a function of z only.

The relevant boundary and initial conditions are

$$\begin{aligned} T_s &= T_o \quad \text{at} \quad z = 0 \quad , \text{all} \quad y_s \\ T_s &= T_m \quad \text{at} \quad y_s = 0 \quad , \text{all} \quad z \\ T_s &= T_R \quad \text{at} \quad y_s = H_s \quad , \text{for} \quad z \quad \text{if} \quad T_R < T_m \\ T_s &= T_m \quad \text{at} \quad y_s = H_s \quad , \text{for} \quad z \quad \text{if} \quad T_R \geq T_m \end{aligned} \tag{3.31}$$

where T_o is the initial bulk mean temperature of the solid bed

H_s is the local height of the solid bed, defined in general as

$$H_s = H_o - B.z - \delta_1 - \delta_2 \tag{3.32}$$

and it should be noted that T_R may be a function of z .

The following non dimensional variables are defined

$$\begin{aligned} T_s^* &= T_s / T_o \\ Y_s &= y_s / H_s \\ Z &= z / H_s \\ V_{sy}^* &= H_s V_{sy} / \alpha_s \\ V_{sz}^* &= H_s V_{sz} / \alpha_s \end{aligned} \tag{3.33}$$

Using these definitions equation (3.30) becomes

$$\frac{\partial^2 T_s^*}{\partial Y_s^2} = V_{sy}^* \cdot \frac{\partial T_s^*}{\partial Y_s} + V_{sz}^* \frac{\partial T_s^*}{\partial Z} \tag{3.34}$$

And the boundary and initial conditions become

$$\begin{aligned} T_s^* &= 1 \quad \text{at} \quad Z = 0 \quad , \text{all} \quad Y_s \\ T_s^* &= T_m^* \quad \text{at} \quad Y_s = 0 \quad , \text{all} \quad Z \\ T_s^* &= T_R^* \quad \text{at} \quad Y_s = 1 \quad , \text{for} \quad Z \quad \text{if} \quad T_R^* < T_m^* \\ T_s^* &= T_m^* \quad \text{at} \quad Y_s = 1 \quad , \text{for} \quad Z \quad \text{if} \quad T_R^* \geq T_m^* \end{aligned} \tag{3.35}$$

It is now required to specify the velocity V_{sy}^* . This is done by assuming that it is a linear function of Y_s , thus

$$V_{sy}^*(Y_s) = \left[V_{sy}^*(1) - V_{sy}^*(0) \right] . Y_s + V_{sy}^*(0) \tag{3.36}$$

The values of $V_{sy}^*(1)$ and $V_{sy}^*(0)$ can be calculated from the melting analysis at each interface which is described in detail later. Using the results of that analysis gives

$$V_{sy}^*(0) = - \frac{\omega_1}{\rho_s} \cdot \frac{H_s}{\alpha_s} \tag{3.37}$$

where ω_1 is the mass of the material melting at the upper interface per unit area per unit time.

For the lower surface of the solid bed

$$V^{*}_{sy}(1) \doteq \left[\left(H_s|_{z+\Delta z} - H_s|_{z} \right) \frac{V_{sz}}{\Delta z} + \frac{\omega_2}{\rho_s} \right] \frac{H_s}{\alpha_s} \qquad (3.38)$$

where ω_2 is the mass of material melting at the lower interface per unit area per unit time.

and Δz is the step length in z direction used in the numerical formulation of the problem.

The first term on the RHS of equation (3.38) represents the velocity of the lower interface relative to the upper whilst the second term represents the velocity of the solid relative to the lower interface.

In the actual solution the values of $V^{*}_{sy}(0)$ and $V^{*}_{sy}(1)$ are calculated from a knowledge of the relevant variables at the preceeding two steps. This is therefore an approximation but is justified in that it is a third order one when considered in the context of the overall melting analysis.

Equation (3.34) is solved using a numerical finite difference technique. Because of the importance in the calculations of the temperature gradients at the boundary, and since these, at least initially, will be relatively high, it was thought desirable to construct a variable finite difference grid, such that the grid spacing was smallest in the regions where the temperature was varying most rapidly. The geometry of the grid for a simple five point mesh is shown in figure 3.6.

The grid spacings, $\Delta Y_s(i)$, in the Y_s direction are defined as follows

$$\begin{aligned} \Delta Y_s(i+1) &= \Delta Y_s(i) \cdot \xi \quad \text{for} \quad 1 \leqslant i < (I+1)/2 \\ \Delta Y_s(i+1) &= \Delta Y_s(i) \quad \text{for} \quad i = (I-1)/2 \\ \Delta Y_s(i+1) &= \Delta Y_s(i)/\xi \quad \text{for} \quad (I-1) \geqslant i > (I+1)/2 \end{aligned} \qquad (3.39)$$

where I is the number of grid points in the Y_s direction, which in this case is necessarily an odd number, and ξ is the ratio of adjacent grid spacings and is constant. The above form of variable grid geometry was chosen because the details of it can be easily calculated in the computer program of the solution itself, and readily fit into the format of the finite difference numerical technique. It is also fairly flexible in that by specifying I and ξ the grid is autometically defined and yet variation of these two valves can produce a wide range of grid patterns. For more general usage it has the

Figure 3.6

The finite difference grid used in the solid bed energy analysis

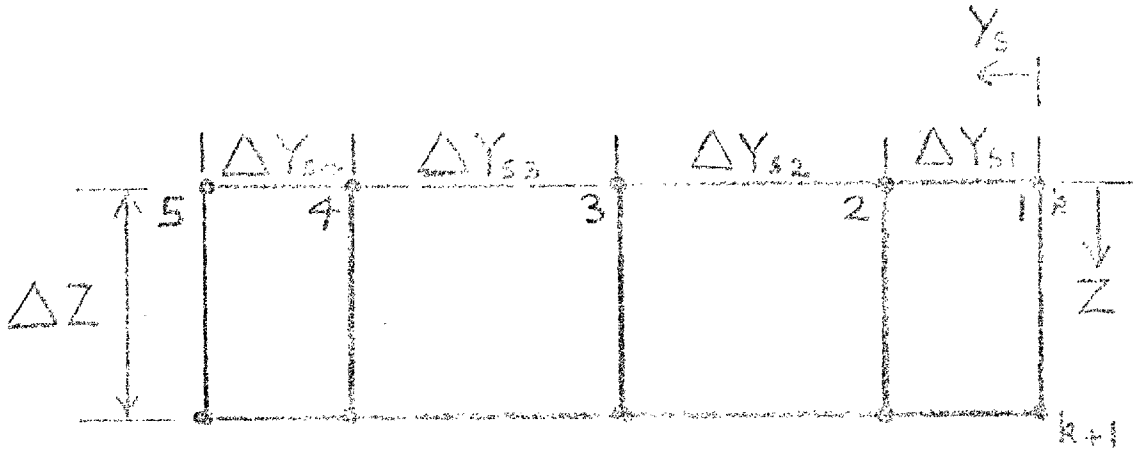
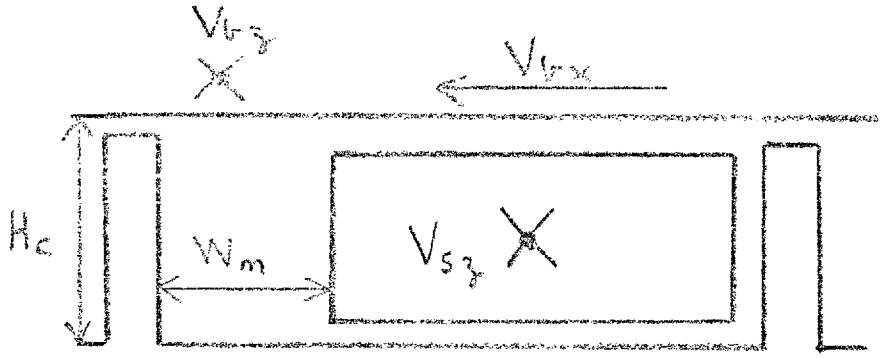


Figure 3.7

The melt pool geometry



limitation that the grid spacings are always closest at the boundaries. In the present case I was taken as 17 and ξ as 1·5. With this grid no problems were encountered in obtaining solutions.

For such a grid the finite difference approximation of the second derivative of temperature with respect to Y_s is

$$\left.\frac{\partial^2 T_s^*}{\partial Y_s^2}\right|_{i,k} = -\frac{2}{\Delta Y_s^2(i)}\left(\frac{T_s^*(i+1,k)}{\xi(1+\xi)} - \frac{T_s^*(i,k)}{\xi} + \frac{T_s^*(i-1,k)}{1+\xi}\right) + O\left[\Delta Y_s^2(i)\right] \qquad (3.40)$$

The derivation of this equation is given in detail in Özişik (37). Because of the convection terms in the present formulation, to avoid stability problems an upward finite difference approximation to the first derivative of temperature with respect to Y_s is used.

$$\left.\frac{\partial T_s^*}{\partial Y_s}\right|_{i,k} = -\left[\frac{T_s^*(i-1,k) - T_s^*(i,k)}{\Delta Y_s(i)}\right] + O\left[\Delta Y_s(i)\right] \qquad (3.41)$$

The temperature derivative in the direction of developement is expressed as

$$\left.\frac{\partial T_s^*}{\partial Z}\right|_{i,k} = \left[\frac{T_s^*(i,k) - T_s^*(i,k-1)}{\Delta Z}\right] + O\left[\Delta Z\right] \qquad (3.42)$$

Using the above finite difference approximations, equation (3.34) at a point in the solution domain defined by

$$Y_s = \sum_{i=1}^{i} \Delta Y_s(i) \quad ; \quad Z = k.\Delta Z \qquad (3.43)$$

is, if a fully implicit type of representation is used,

$$\left[\frac{2}{\Delta Y_s^2(i).(1+\xi)} - \frac{V_{sy}(i,k-1)}{\Delta Y_s(i)}\right].T_s^*(i-1,k) + \left[\frac{V_{sy}^*(i,k-1)}{\Delta Y_s(i)} + \frac{V_{sz}^*(k-1)}{\Delta Z} - \frac{2}{\Delta Y_s^2(i).\xi}\right].T_s^*(i,k) + \frac{2}{\Delta Y_s^2(i).\xi.(1+\xi)}.T_s^*(i+1,k) = \frac{V_{sz}^*(k-1)}{\Delta Z}.T_s^*(i,k-1) \qquad (3.44)$$

Equation (3.44) can be written more simply as

$$a(i+1,k).T_s^*(i+1,k) + a(i,k).T_s^*(i,k) + a(i-1,k).T_s^*(i-1,k) = b(i) \qquad (3.45)$$

The complete system of equations is defined by $1 < i < I$

This system can be written in matrix form as

$$[A]\,[T_s^*] = [B] \qquad (3.46)$$

The matrix of the coefficients, $[A]$, is a tri-diagonal matrix and is

diagonally dominant for $V^{*}_{sy} \leq 0$, which in this particular problem is generally true. Therefore the obvious method of solution of the system defined by equation (3.46) is by a simplified Gaussian Elimination Algorithm applicable to tri-diagonal systems. Such an algorithm is well known and is discussed in Özişik(37) and most texts on numerical techniques, to which the reader is referred for further information.

Thus the temperature profile in the solid bed is obtained step by step downchannel This downchannel stepping is done in time with the stepping of the overall analysis as will be explained in the next section. The dimensional thermal gradients that are calculated by this numerical analysis procedure for use in the derivation of the main equations are stated as follows.

$$\left.\frac{\partial T_s}{\partial y_s}\right|_{y_s=0} = \frac{T_o}{(H_o - B.z - \delta_1 - \delta_2)} \left.\frac{\partial T_s^{*}}{\partial Y_s}\right|_{Y_s=0} \qquad (3.47)$$

$$\left.\frac{\partial T_s}{\partial y_s}\right|_{y_s=H_s} = \frac{T_o}{(H_o - B.z - \delta_1 - \delta_2)} \cdot \left.\frac{\partial T_s^{*}}{\partial Y_s}\right|_{Y_s=1} \qquad (3.48)$$

where, it should be remembered, the dimensionless derivatives are numerically evaluated.

C: Momentum analysis for the melt pool

The melt pool analysis is required to calculate the melt pool mass flow rate in the z direction per unit length, M_{mz}, as a function of the pressure gradient, $\partial p/\partial z$, and the melt pool geometry. For the purposes of this calculation the fluid is assumed to be incompressible and of constant viscosity. The flow is taken to be laminar, steady, isothermal and fully developed. Gravity forces are neglected and no slip boundary conditions are assumed.

The constant viscosity assumption is essentially made for simplicity in the analysis at this stage in the developement of the melting model. It can, however introduce significant errors into the solution as is shown in the results of the present analysis which are presented later and is not therefore necessarily a valid assumption. Figure 3.7 shows the geometry of the situation. It is basically a rectangular flow domain with two moving boundaries. Were the solid bed velocity, V_{sz}, to be zero then the problem would correspond to that of the flow of molten polymer in a screw channel. The solution to that problem with the assumptions stated earlier was the first presented by Rowell and

Finlayson (36) and has been given more recently by Todmor and Klein (115).

The solution is of the form

$$\pi_Q = \frac{F_d}{2} - \frac{\pi_p \cdot F_p}{12} \qquad (3.49)$$

where the dimensionless flow rate, π_Q, is defined as

$$\pi_Q = Q / W H_c V_{b_3} \qquad (3.50)$$

where H_c is defined by equation (2.3) and the dimensionless pressure gradient, π_p, is defined as

$$\pi_p = \frac{\partial p}{\partial z} \cdot \frac{H_c^2}{\eta_w \cdot V_{b_3}} \qquad (3.51)$$

where η_w is the constant viscosity

F_d and F_p in equation (3.49) are known as 'Newtonian Shape Factors' as they are functions of the channel geometry only. They are defined by the following expressions

$$F_d = \frac{16\,W}{\pi^3 H_c} \sum_{i=1,3,5}^{\infty} \frac{1}{i^3} \tanh\left(\frac{i\pi H_c}{2W}\right) \qquad (3.52)$$

$$F_p = 1 - \frac{192\,H_c}{\pi^5 W} \sum_{i=1,3,5}^{\infty} \frac{1}{i^3} \tanh\left(\frac{i\pi H_c}{2W}\right) \qquad (3.53)$$

The first term on the RHS of equation (3.49), that containing F_d, represents the contribution to the total flow rate due to pure drag. The second term, containing F_p, represents that part of the total flow due to pressure. It is because the fluid is of constant viscosity, that is, linear, that these two terms are entirely separate.

It should be noted that when the ratio H_c/W is equal to zero both shape factors equal unity and the flow rate is that of flow between infinite parallel plates. As H_c/W increases the values of the shape factors decrease representing the effect of the stationary sides of the flow channel.

Because of the independence of the drag and pressureinduced components of the flow rate it is possible to take into account the effect of a second moving boundary quite simply. This second moving boundary in the present case is the solid bed. The additional drag flow created by the movement of the solid can be added in as a separate drag flow term. Thus the equation (3.49) becomes

for the melt pool solution

$$\pi_Q = \frac{F_d}{2}\left(\frac{H_s}{W}\right) - \frac{\pi_p F_p\left(\frac{H_s}{W}\right)}{12} + \frac{F_d}{2}\left(\frac{W_m}{H_c}\right)\cdot\frac{V_{s3}}{V_{b3}} \qquad (3.54)$$

Dimensionalizing this gives

$$M_{m3} = \frac{\rho_m (W - X - \delta_2)(H_0 - B_3)}{2X}\left[F_d\left(\frac{H_s}{W_m}\right)\cdot V_{b3} + F_d\left(\frac{W_m}{H_c}\right)V_{s3} - \frac{\partial p}{\partial z}\frac{(H_0 - B_3)^2}{6\eta_N}F_p\left(\frac{H_s}{W_m}\right)\right] \qquad (3.55)$$

The division by X is done for compatibility with the melt film flow rates.

And $$W_m = W - X - \delta_2 \qquad (3.56)$$

η_N is calculated at the mean temperature of the melt leaving the upper melt film and at a mean shear rate which is defined as

$$\bar{\gamma}_m = \left[\left(\frac{V_{b3}}{H_c}\right)^2 + \left(\frac{V_{s3}}{W_m}\right)^2\right]^{\frac{1}{2}} \qquad (3.57)$$

The mean temperature is calculated from the melt film analysis previously outlined by means of the following definition

$$\bar{T} = \frac{\int_0^\delta v_j T\, dy}{\int_0^\delta v_j\, dy} \qquad (3.58)$$

D: Energy conservation at the melting interfaces

Consider the upper film first, let ω_1 be the mass of material melting per unit time. An energy balance over unit area of the interface yields

$$\omega_1 \lambda_1 = k_m \left|\frac{dT_1}{dy_1}\right|_{y_1=0} - k_s \left|\frac{dT_s}{dy_s}\right|_{y_s=0} \qquad (3.59)$$

where k_m is the thermal conductivity of the molten material

where k_s is the thermal conductivity of the solid material

where λ_1 is the effective latent heat of fusion for the upper interface and is defined as

$$\lambda_1 = \lambda + c_m(\bar{T}_1 - T_m) \qquad (3.60)$$

where λ is the latent heat of fusion of the material

c_m is the specific heat of the molten material

$\bar{T}_1$ is the mean temperature of the molten material entering the melt pool from the melt film and as has been said previously is calculated from the melt film analysis applied to the upper film by means of equation (3.58)

The second term on the RHS of equation (3.60) is included as thermal convection

in the y direction in the melt film is ignored in the melt film analysis. The inclusion of this term partly accounts for the omission. However it is an approximation in that it makes the implicit assumption that all the heat required to raise the temperature of an element of molten material from its melting temperature to the mean film temperature is supplied to it at the melting interface whereas it will more realistically be supplied continuously as the element moves into the film away from the interface, prior to being discharged into the melt pool.

The effect of omitting the thermal convection in the y and j directions in the melt film analysis has been investigated by Sundstrom and Young (38). They performed an analysis of the melt film developement for a power law temperature dependent fluid and got good agreement with experiments when thermal convection effects were included in the analysis, but if they were neglected they obtained errors in the predicted melting rate of between 10% and 15%. However they did no computations on the size of error obtained if the latent heat of fusion is modified in the way defined by equation (3.60) and the analysis without thermal convection used. Also the experiments they performed were not typical of extrusion conditions in that the relative velocity of the two surfaces was lower than would be usual in an extruder and hence most of the energy for melting was supplied from the hot metal surface by conduction. However the implications are that at the least the effect of thermal convection in the film should be approximated in some fashion.

The previously derived results of equations (3.26) and(3.47) are substituted into equation (3.59) to give

$$\omega_1 \lambda_1 = \frac{k_m}{6.\delta_1} \left| \frac{dT_1^*}{dY_1} \right|_{Y_1=0} - \frac{k_s T_o}{(H_o - B_3 - \delta_1 - \delta_2)} \left| \frac{dT_s^*}{dY_s} \right|_{Y_s=0} \qquad (3.61)$$

where both non dimensional temperature gradients are implicit functions of δ_1, and V_{s_3}.

For the lower melt film, if ω_2 is the mass melting rate per unit time, then

$$\omega_2 \lambda_2 = k_m \left| \frac{dT_2}{dy_2} \right|_{y=0} - k_s \left| \frac{dT_s}{dy_s} \right|_{y_s=H_s} \qquad (3.62)$$

where $$\lambda_2 = \lambda + c_m (\bar{T}_2 - T_m) \qquad (3.63)$$

Substituting into equation (3.62) from equations (3.28) and (3.48) gives

$$\omega_2 \lambda_2 = \frac{k_m}{\delta_2} \left| \frac{dT_2^*}{dY_2} \right|_{Y_2=0} - \frac{k_s T_c}{(H_0 - B_3 - \delta_1 - \delta_2)} \left| \frac{dT_s^*}{dY_s} \right|_{Y_s=1} \qquad (3.64)$$

In both equations (3.61) and (3.64) the signs of the temperature gradients are included in the equations and thus only the magnitudes are required to be inserted from the previously described analyses. In the analysis of the upper melt film, the lower melt film and the solid bed the origin of the y coordinate and its positive direction were chosen for 'local' mathematical convenience, differently in each case. The inconsistency resulting from combining the results of two analyses in one equation, as is done above, is removed if the signs are explicitly stated in the equation. This can be satisfactorily done in the present case as heat transfer always occurs from the melt film to the solid bed.

That is

$$\omega_i \geq 0 \qquad \text{always} \qquad \text{for} \quad i = 1, 2$$

Finally, it is assumed that the mass melting rate per unit area for the melt film between the solid bed and the screw flight is equal to ω_2.

That concludes the presentation of the supplementary analyses. The derivation of the main equations now follows.

Figure 3.8

An element of the upper melt film

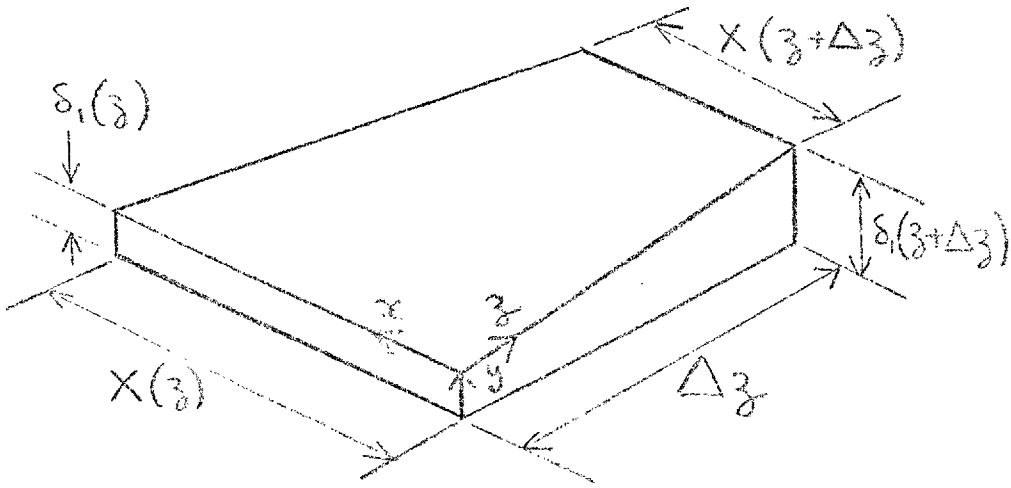
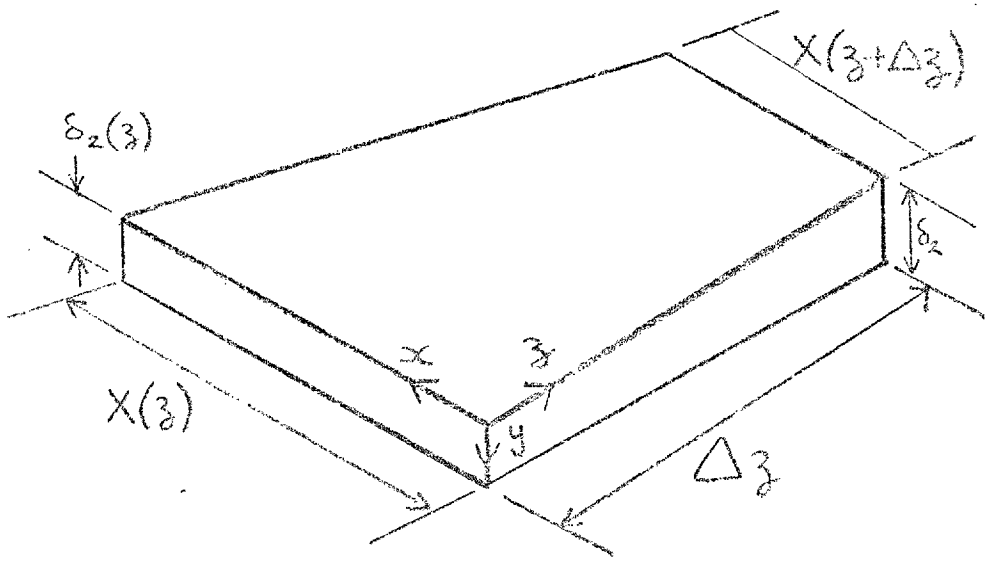


Figure 3.9

An element of the lower melt film



Derivation of Main Equations

1: Conservation of mass in the upper melt film.

The element of melt film considered is shown in figure 3.8. In words the mass balance can be stated as

$$\begin{bmatrix}\text{Change of melt film}\\ \text{flow rate in } z \text{ direction}\end{bmatrix} = \begin{bmatrix}\text{Melting rate over}\\ \text{the interface}\end{bmatrix} - \begin{bmatrix}\text{Net flow rate out of the}\\ \text{film in } x \text{ direction}\end{bmatrix}$$

Mathematically this is

$$\frac{d}{dz}\left(M_{1z}\, X\right) = \omega_1 X - \left(M_{1x} - M_{fx}\right) \qquad (3.65)$$

where M_{fx} is the mass flow rate over the flight in the x direction per unit length and is calculated as if the flow were pure drag flow of a constant viscosity fluid, thus

$$M_{fx} = V_{bx}\, \rho_m\, e / 2 \qquad (3.66)$$

e being the flight clearance

Substituting into equation (3.65) from equations (3.20) (3.21), (3.61) and (3.66) gives

$$\frac{d}{dz}\left\{\delta_1 X\left[\left(V_{bz}-V_{sz}\right) Q^*_{1j} + V_{sz}\right]\right\} = -V_{bx}\left(\delta_1 Q^*_{1j} - \frac{e}{2}\right)$$

$$+\frac{X}{\rho_m \lambda_1}\left[\frac{k_m}{b\,\delta_1}\left|\frac{dT_1^*}{dY_1}\right|_{Y_1=0} - \frac{k_s T_0}{\left(H_0-B.z-\delta_1-\delta_2\right)}\left|\frac{dT_s^*}{dY_s}\right|_{Y_s=0}\right] \qquad (3.67)$$

2: Conservation of mass in lower melt film.

The application of the mass balance to an element of the lower film, shown in figure 3.9 is simplified compared to that for the upper film, in that flow in the x direction is neglected. In words the balance is stated as

$$\begin{bmatrix}\text{Change of melt film flow}\\ \text{rate in } z \text{ direction}\end{bmatrix} = \begin{bmatrix}\text{Melting rate over}\\ \text{the interface}\end{bmatrix}$$

Mathematically,

$$\frac{d}{dz}\left(M_{2z}\, X\right) = \omega_2 X \qquad (3.68)$$

Substituting into this equation from equations (3.22) and (3.64) gives

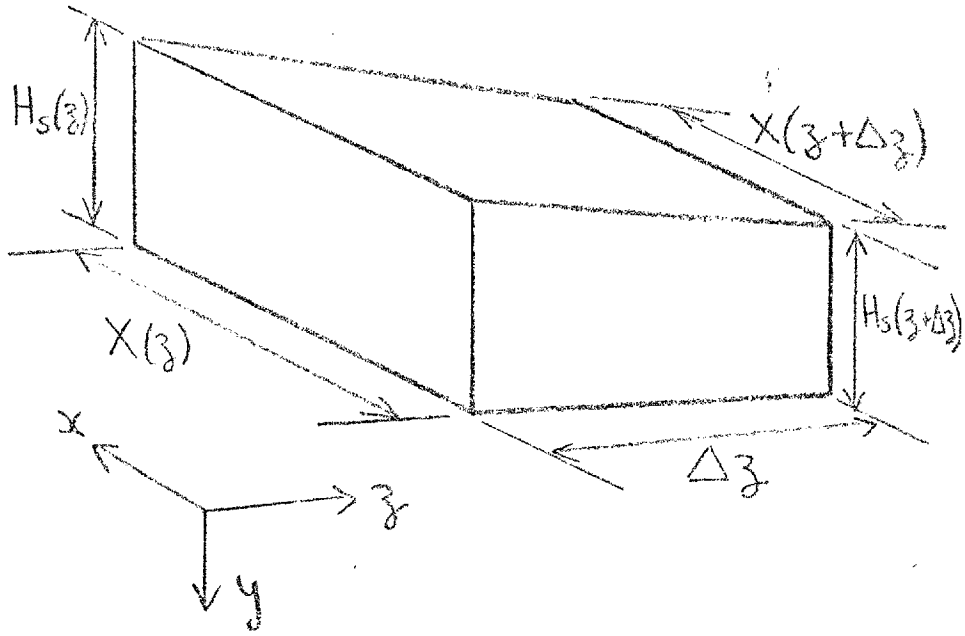
$$\frac{d}{dz}\left(\delta_2 X V_{sz}\, Q^*_{2j}\right) = \frac{X}{\rho_m \lambda_2}\left[\frac{k_m}{b\,\delta_2}\left|\frac{dT_2^*}{dY_2}\right|_{Y_2=0} - \frac{k_s T_0}{\left(H_0-B.z-\delta_1-\delta_2\right)}\left|\frac{dT_s^*}{dY_s}\right|_{Y_s=1}\right] \qquad (3.69)$$

3: Conservation of mass applied to the solid bed.

The element of solid bed considered is shown in figure 3.10.

Figure 3.10

An element of the solid bed



The verbal expression of the mass balance is

[Change of solid bed flow rate in z direction] = - [Melting rate over the upper interface] - [Melting rate over the lower and side interfaces]

Mathematically

$$\frac{d}{dz}\left(V_{sz} \times H_s \rho_s\right) = -\omega_1 X - \omega_2 (X + H_s) \quad (3.70)$$

Substituting into the above equation from equations (3.32), (3.61) and (3.64) gives,

$$\frac{d}{dz}\left[V_{sz} \times (H_o - Bz - \delta_1 - \delta_2)\right] = -\frac{X}{\rho_s \lambda_1}\left[\frac{k_m}{\sigma \delta_1}\left|\frac{dT_1^*}{dY_1}\right|_{Y_1=0} - \frac{k_s T_o}{(H_o - Bz - \delta_1 - \delta_2)}\left|\frac{dT_s^*}{dY_s}\right|_{Y_s=0}\right]$$
$$-\frac{(X + H_o - Bz - \delta_1 - \delta_2)}{\rho_s \lambda_2}\left[\frac{k_m}{\sigma \delta_2}\left|\frac{dT_2^*}{dY_2}\right|_{Y_2=0} - \frac{k_s T_o}{(H_o - Bz - \delta_1 - \delta_2)}\left|\frac{dT_s^*}{dY_s}\right|_{Y_s=1}\right] \quad (3.71)$$

4: Equilibrium of forces on the solid bed

There are two different cases to consider here depending on the nature of the shear stress on the lower surface of the solid bed. The case of coulomb friction stress, arising when no lower melt film is present, is considered first. The case of viscous stress arising when there is a lower melt film is considered later.

It is assumed that in both cases that the pressure in the solid bed is not a function of x or y and that the viscous shear stress exerted on the side of the solid bed by the melt pool can be neglected.

In both cases the verbal expression of the force balance is,

[Change in pressure force over an increment Δz] = [Shear force on top of bed in z direction] + [Shear forces on bottom and side of bed in z direction]

Mathematically for coulomb friction on the bottom and side of the solid bed this is

$$\frac{dp}{dz} H_s X = \tau_{13} X - p\mu (X + H_s) \quad (3.72)$$

where μ is the coefficient of coulomb friction between metal and plastic.

Substituting from equations (3.23) and (3.32) into the above equation gives

$$\frac{dp}{dz} = \frac{\bar{\tau}_1 \tau^*_{1j} \cos\beta}{(H_o - B.z - \delta_1)} - \frac{p\,\mu\,(X + H_o - B.z - \delta_1)}{X(H_o - B.z - \delta_1)} \qquad (3.73)$$

as $\delta_2 = 0$

where it should be noted that $\bar{\tau}_1$ and τ^*_{1j} are implicit functions of δ_1 and V_{sz}, and $\cos\beta$ is an implicit function of V_{sz}.

For the second case with viscous forces on the side and bottom of the solid bed, the force balance mathematically, is

$$\frac{dp}{dz} \cdot H_s \cdot X = \tau_{1z} X - \tau_{2z}(X + H_s) \qquad (3.74)$$

Again substituting into the above equation from equations (3.23), (3.24) and (3.32) gives

$$\frac{dp}{dz} = \frac{\bar{\tau}_1 \tau^*_{1j} \cos\beta}{(H_o - B.z - \delta_1 - \delta_2)} - \frac{\bar{\tau}_2 \tau^*_{2j}(X + H_o - B.z - \delta_1 - \delta_2)}{X(H_o - B.z - \delta_1 - \delta_2)} \qquad (3.75)$$

where $\bar{\tau}_2$ and τ^*_{2j} are implicit functions of δ_2 and V_{sz}.

5: Conservation of mass for the whole channel.

Clearly at every section of the channel the sum of the down channel flow rates in the melt pool, the solid bed and the melt films must equal the throughput rate, M_T, thus

$$M_T = X(M_{1z} + M_{2z} + M_{mz} + M_{sz}) \qquad (3.76)$$

where M_{sz} is the solid bed flow rate in the z direction per unit length, given by

$$M_{sz} = \rho_s V_{sz}(H_o - B.z - \delta_1 - \delta_2) \qquad (3.77)$$

Substituting into equation (3.76) for the various component flow rates as defined by equations (3.21), (3.22), (3.55) and (3.77) gives

$$M_T = X\rho_m \delta_1 Q^*_{1j}(V_{bz} - V_{sz}) + X\rho_m \delta_1 V_{sz} + X\rho_m \delta_2 Q^*_{2j} V_{sz}$$
$$+ \frac{\rho_m(W - X - \delta_2)(H_o - B.z)}{2}\left[F_d\left(\frac{H_c}{W_m}\right)V_{bz} + F_d\left(\frac{W_m}{H_c}\right)V_{sz} - \frac{dp}{dz}\frac{(H_o - B.z)^2}{6\eta_N}F_p\left(\frac{H_c}{W_m}\right)\right]$$
$$+ V_{sz}\rho_s X(H_o - B.z - \delta_1 - \delta_2) \qquad (3.78)$$

The partial derivative of pressure is written as an ordinary derivative as the assumption that pressure is a function of z only, is invoked.

Itis apparent from this equation that the present analysis requires an independent equation relating dp/dz to the primary variables of the problem.

This equation is, of course, obtained from the force balance on the solid bed as previous outlined. It is assumed that the pressure gradient so derived for the solid bed may be applied to the melt pool.

The melting analysis developed by Donovan (12) and Tadmor and Klein (8,15) used the melt pool momentum analysis to calculate the pressure gradient. They were able to do this because a knowledge of the pressure was not required in the melting analysis proper and thus could be calculated separately at each section using the results of the melting analysis at that section. The independence of the melting analysis from the pressure gradient was a consequence of having made sufficient assumptions concerning the solid bed velocity as to render it a dependent variable, thus leaving only the solid bed width and the melt film thickness as independent variables. They hence needed only two main equations which were derived from mass balances on the solid bed and melt film, neither of which contain the pressure gradient. Thus, having at each section calculated the local solid bed width, the geometry of the melt pool was defined. In addition the local melt pool flow rate could be calculated from an equation similar in form to the equation (3.76) and hence the pressure gradient could be calculated.

Such a technique is not possible in the present analysis because the solid bed velocity is an independent variable and the additional equation required is supplied by a mass balance over the whole channel. This equation contains the pressure gradient and in turn this requires that an additional independent equation relating the pressure gradient to the other variables be derived. The resulting set of five equations are simultaneous and as such must be solved for the five variables simultaneously.

This then essentially completes the derivation of the equations describing the present melting model. The formulation results in six equations though only four or five are used at any one time, the sixth being the alternative expression for the pressure gradient should no melt film be present. Thus in the absence of a lower melt film there are four main equations (3.67), (3.71), (3.73) and (3.79). In the presence of the lower melt there are five main equations: (3.67), (3.69), (3.71), (3.75) and(3.78). The solution of these

equations is dealt with in the next section.

The mathematical description of the model is not complete without the relevant boundary and initial conditions. The five general initial conditions are

$$\begin{aligned} \xi_1(0) &= 0 \\ \xi_2(0) &= 0 \\ X(0) &= W \\ p(0) &= p_0 \\ V_{sz}(0) &= M_T/(\rho_s W H_0) \end{aligned} \tag{3.79}$$

where p_0 may be taken as zero or any finite positive value. These are essentially the mathematical initial conditions and it is necessary to modify these slightly to fit in with the numerical nature of the solution technique. These modifications are discussed in the next section.

Additionally the following boundary conditions need to be specified:

The barrel temperature, T_b , as a function of z

The screw temperature, T_R , as a function of z

The barrel velocity relative to the screw, V_b

The melting temperature of the material, T_m

Again further discussion of these conditions is given in the next section.

3.5: The Solution of the Governing Equations of the Model

Before describing the solution scheme it is necessary to make certain changes to the format of the main equations; the indicated differentiations are carried out and the equations re-arranged.

Thus , equation (3.67) becomes

$$c_{11}\frac{d\delta_1}{dz} + c_{12}\frac{dX}{dz} + c_{14}\frac{dV_{s3}}{dz} = d_1 \qquad (3.80)$$

where

$$c_{11} = X\left[(V_{b3} - V_{s3})\,Q^*_{1j} + V_{s3}\right] \qquad (3.81)$$

$$c_{12} = \delta_1\left[(V_{b3} - V_{s3})\,Q^*_{1j} + V_{s3}\right] \qquad (3.82)$$

$$c_{14} = \delta_1 X\,(1 - Q^*_{1j}) \qquad (3.83)$$

$$d_1 = \frac{X}{\rho_m \lambda_1}\left[\frac{k_m}{\nu\delta_1}\left|\frac{dT_1^*}{dY_1}\right|_{Y_1=0} - \frac{k_s T_0}{(H_0 - Bz - \delta_1 - \delta_2)}\left|\frac{dT_s^*}{dY_s}\right|_{Y_s=0}\right]$$
$$- V_{b3}\left(\delta_1 Q^*_{1j} - \frac{\delta}{2}\right) + (V_{s3} - V_{b3})\,\delta_1 X\frac{dQ^*_{1j}}{dz} \qquad (3.84)$$

In a similar fashion equation (3.71) can be written as

$$c_{21}\frac{d\delta_1}{dz} + c_{22}\frac{dX}{dz} + c_{23}\frac{d\delta_2}{dz} + c_{24}\frac{dV_{s3}}{dz} = d_2 \qquad (3.85)$$

where,

$$c_{21} = -X\,V_{s3} \qquad (3.86)$$

$$c_{22} = (H_0 - Bz - \delta_1 - \delta_2)\,V_{s3} \qquad (3.87)$$

$$c_{23} = -X\,V_{s3} \qquad (3.88)$$

$$c_{24} = (H_0 - Bz - \delta_1 - \delta_2)\,X \qquad (3.89)$$

$$d_2 = -\frac{X}{\rho_s \lambda_s}\left[\frac{k_m}{\nu\delta_1}\left|\frac{dT_1^*}{dY_1}\right|_{Y_1=0} - \frac{k_s T_0}{(H_0 - Bz - \delta_1 - \delta_2)}\left|\frac{dT_s^*}{dY_s}\right|_{Y_s=0}\right]$$
$$- \frac{(X + H_0 - Bz - \delta_1 - \delta_2)}{\rho_s\ \lambda_2}\left[\frac{k_m}{\nu\delta_2}\left|\frac{dT_2^*}{dY_2}\right|_{Y_2=0} - \frac{k_s T_0}{(H_0 - Bz - \delta_1 - \delta_2)}\left|\frac{dT_s^*}{dY_s}\right|_{Y_s=1}\right] \qquad (3.90)$$

And equation (3.69) becomes

$$c_{32}\frac{dX}{dz} + c_{33}\frac{d\delta_2}{dz} + c_{34}\frac{dV_{s3}}{dz} = d_3 \qquad (3.91)$$

where,

$$c_{32} = \delta_2\,V_{s3}\,Q^*_{2j} \qquad (3.92)$$

$$c_{33} = X\,V_{s3}\,Q^*_{2j} \qquad (3.93)$$

$$c_{34} = \delta_2 X\,Q^*_{2j} \qquad (3.94)$$

$$d_3 = \frac{X}{\rho_m \lambda_2}\left[\frac{k_m}{\delta_2}\left|\frac{dT_2^*}{dY_2}\right|_{Y_2=0} - \frac{k_s T_0}{(H_0 - \beta_3 - \delta_1 - \delta_2)}\left|\frac{dT_s^*}{dY_s}\right|_{Y_s=1}\right] - \delta_2 X V_{s3}\frac{d\bar{Q}_{2j}^*}{d\beta} \qquad (3.95)$$

The basis of the solution scheme is to solve the above three equations (3.80) (3.85) and (3.91) with the solid bed acceleration locally constant. Thus putting,

$$\frac{dV_{s3}}{d\beta} = \text{constant} = -E \qquad (3.96)$$

enables the three equations to be written as

$$\begin{bmatrix} c_{11} & c_{12} & \\ c_{21} & c_{22} & c_{23} \\ & c_{32} & c_{33} \end{bmatrix}\begin{bmatrix} d\delta_1/d\beta \\ dX/d\beta \\ d\delta_2/d\beta \end{bmatrix} = \begin{bmatrix} Ec_{14} + d_1 \\ Ec_{24} + d_2 \\ Ec_{34} + d_3 \end{bmatrix} \qquad (3.97)$$

or, in matrix form

$$[C][\Psi'] = [D] \qquad (3.98)$$

Assuming the matrices $[C]$ and $[D]$ are locally constant enables the solution of (3.98) for the derivatives of the three main variables, δ_1, X, δ_2, that is the Ψ' field, to be written as

$$[\Psi'] = [C]^{-1}[D] \qquad (3.99)$$

where the functional dependence of the R.H.S. of this equation on the primary or main variables and on the secondary variables of the problem can be shown in the following fashion.

$$[C]^{-1}[D] = [F]\left\{\delta_1, \delta_2, X, V_{s3}, \bar{Q}_{1j}^*, \lambda_1, \left|\frac{dT_1^*}{dY_1}\right|_{Y_1=0}, \left|\frac{dT_s^*}{dY_s}\right|_{Y_s=0}, \frac{d\bar{Q}_{1j}^*}{d\beta}, \lambda_2, \left|\frac{dT_2^*}{dY_2}\right|_{Y_2=0}, \left|\frac{dT_s^*}{dY_s}\right|_{Y_s=1}, \frac{d\bar{Q}_{2j}^*}{d\beta}, \beta\right\} \qquad (3.100)$$

where $[F]\{..\}$ denotes the matrix function.

A direct method is used to solve the system of equations defined by equation (3.98). However, because there are only three equations the necessary manipulation of the coefficients to give three equations of the form shown in equation (3.99) was carried out by hand and written into the overall solution scheme explicitly.

The general solution procedure may be summarised as follows.

At every step in the β direction initial values of the variables are predicted A value for solid bed acceleration is prescribed. Hence the coefficients of

$[C]$ and $[D]$ can be evaluated. The system defined by equation (3.98) is then solved.

Using the new $[\Psi']$ field the values of the variables are corrected and the terms of $[C]$ and $[D]$ re-evaluated. This inner iterative cycle is repeated until a suitable convergence criterion is satisfied. Using these values of the variables the total down-channel flow rate is calculated by use of equation (3.78). This value is compared with the given flow rate. If the discrepancy is outside the prescribed limits then the solid bed acceleration, that is, E, is altered and the whole process repeated. This is the outer iteration. When the flow rate is correct to within reasonable limits the solution proceeds to the next down-channel step.

The different steps of the solution procedure are now dealt with in greater detail. Figure 3.11 shows a simplified flow chart of the calculation procedure. The calculation procedure at each step in the z direction begins with a prediction of the new values of the variables δ_1, δ_2, X, V_{sz}, and p. A simple Euler predictor method is used defined by the following equation for a typical variable ψ_i,

$$\psi_{i,k} = \psi_{i,k-1} + \Delta z . \psi'_{i,k-1} \qquad i = 1,5 \qquad (3.101)$$

which gives the initial value at

$$z = k . \Delta z \qquad k = 1, K \qquad (3.102)$$

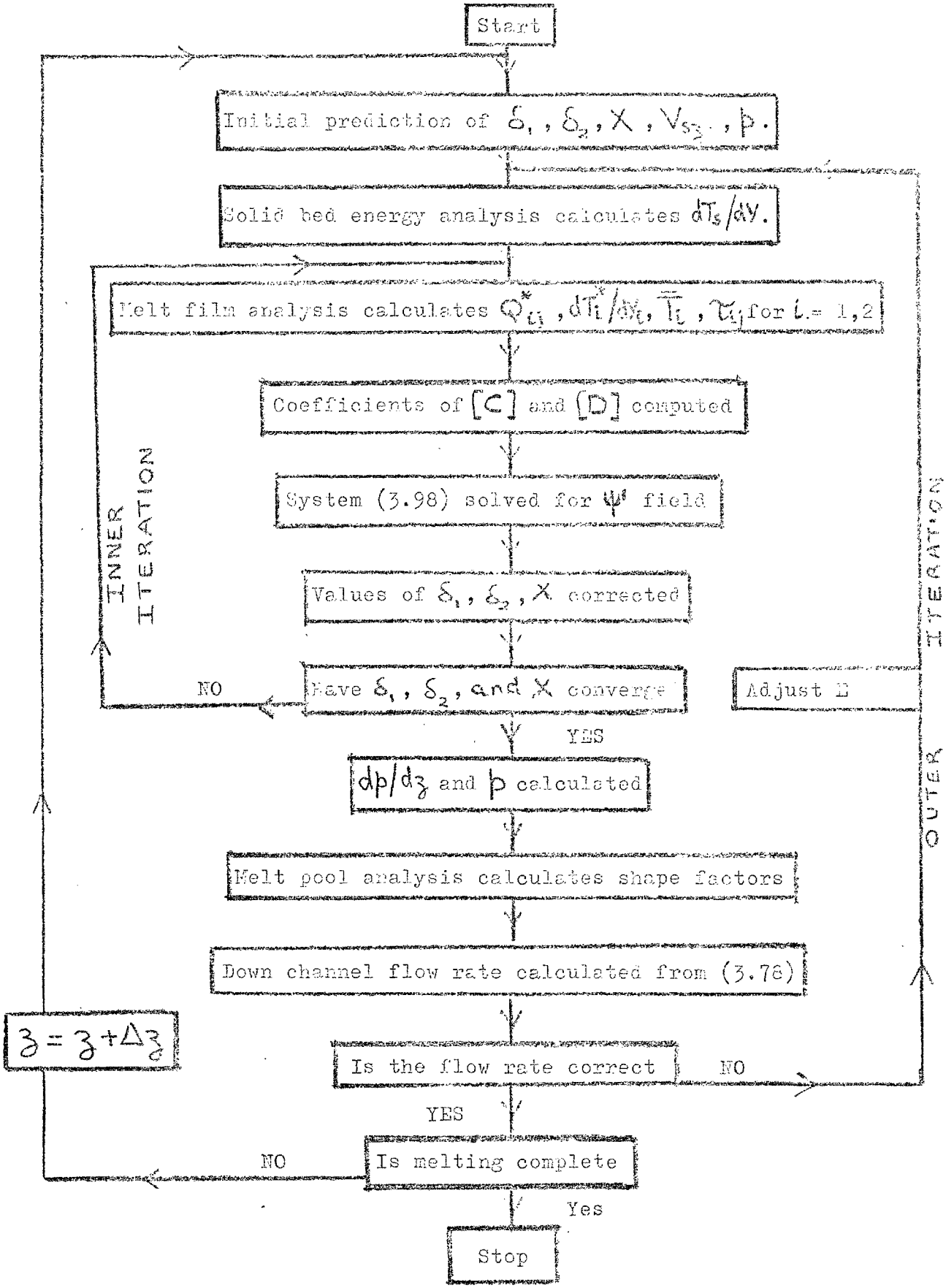
where K is the total number of down-channel steps.

Thus making use of equation (3.101) and the previously calculated values for the variables and derivatives, initial values of the variables are derived, which are approximations to the true mathematical solution. It should be pointed out that at the first step, that is $k = 1$, the previous derivatives are assumed to be zero and the previous values of the variables are their initial values.

These initial approximations are used as input information in the melt film analysis. In this manner the non-dimensional flow rates, mean film temperatures, shear stresses and temperature gradients in the melt films are calculated. Though these at this stage are only initial approximations to the true solution

Figure 3.11

Flow chart of the solution procedure



being derived from approximate data. Similarly the initial values for the non-dimensional temperature gradients in the solid bed are calculated from these initial approximate values of the variables.

In this fashion all the information that is needed to be able to compute the coefficients of the matrices $[C]$ and $[D]$ of equation (3.98) is generated. The value of E that is initially choosen is the final value at the previous step. Thus the stystem defined by equation (3.98) is solved and first approximations to the derivatives of δ_1, δ_2 and X with respect to z for the present step are calculated. These derivatives are used to 'correct' the initial values of variables δ_1, δ_2 and X using the simple Euler type corrector formula

$$\psi_{i,k}^{(n)} = \psi_{i,k-1} + \frac{\Delta z}{2}\left(\psi'_{i,k-1} + \psi'^{(n-1)}_{i,k}\right) \quad i = 1,3 \qquad (3.103)$$

where n here denotes the iteration number of the k^{th} step.

At this stage the value of V_{sz} and its derivative with respect to z are not adjusted and knowledge of the pressure and pressure gradients are not required. Using the correct values of the variables the melt film analysis, but not the solid bed analysis, is invoked again and corrected values of the relevant non-dimensional quantities are calculated. Hence the terms of the matrices $[C]$ and $[D]$ are re-calculated and a new solution of equation (3.98) is obtained. This new solution is then used to re-correct the variables using equation (3.103) again. This 'inner' iteration cycle is repeated until suitable convergence of the values of the variables is obtained. The thermal analysis of the solid bed is not invoked in each cycle of this inner iteration because the information it provides only has a second order effect in the overall solution, and also, this omission is not found to affect significantly the solution stability. Therefore the inclusion of this analysis in each inner iteration cycle is thought not to be worth the extra computation time involved.

What the inner iteration procedure does is to evaluate the values of the variables δ_1, δ_2 and X which satisfy the local boundary conditions of the problem and the particular value of E that has been defined. What is now required is to assertain if this value of E is correct and, if not, then to adjust it until it is. This is the function of the 'outer' iteration cycle.

The essential part of this outer cycle is in invoking equation (3.78). Before

doing this, however, certain preliminary calculations have to be performed. Using the calculated values of the variables δ_1, δ_2 and X, and V_{s3} and p, the pressure gradient in the solid bed is calculated from equation (3.73) if δ_2 is zero or from equation (3.75) if δ_2 is non zero. Having calculated the new value of the pressure gradient the new value of the pressure is calculated using equation (3.103), except that no local iteration is performed. In other words the pressure is updated once per outer iteration only, just as is the temperature field in the solid bed. In addition, the melt pool analysis is invoked and appropriate values of the Newtonian Shape Factors and mean viscosity evaluated. With this information available the total down-channel flow rate is calculated according to equation (3.78). This value is then compared with the known correct flow rate. If there is a discrepancy then the procedure for eliminating this is as follows.

The value of E is altered, and the corresponding value of V_{s3} calculated. The existing values of the other variables are used as new preliminary values for the 'inner' iteration cycle which is now invoked for this new value of E. Before going into the 'inner' iteration cycle, however, the solid bed temperature analysis is invoked to provide new values for the temperature gradients at the boundaries of the solid bed. In this fashion a new set of values of the variables are calculated corresponding to the new value of E. Again the calculation of the 'outer' iteration is performed and the total down-channel flow rate calculated. If it is still in error then E is altered again. The outer iteration continues until this flow rate error is reduced to within any desired level. When this has occurred the solution proceeds to the next down-channel step.

The occurrence of updating the primary variables can be summarised as follows.

δ_1, δ_2, X are updated at every cycle of the 'inner' iteration.

V_{s3}, p are updated at every cycle of the 'outer' iteration.

For the secondary variables of the problem.

$$Q^*_{1j},\ \frac{dQ^*_{1j}}{d\bar{z}},\ Q^*_{2j},\ \frac{dQ^*_{2j}}{d\bar{z}},\ \left|\frac{dT_1^*}{dY_1}\right|_{Y_1=0},\ \left|\frac{dT_2^*}{dY_2}\right|_{Y_2=0},\ \bar{T}_1,\ \bar{T}_2,\ \bar{t}^*_{1j},\ \bar{t}^*_{2j}$$

are updated at every cycle of the 'inner' iteration

$$\left|\frac{dT_s^*}{dY_s}\right|_{Y_s=0},\ \left|\frac{dT_s^*}{dY_s}\right|_{Y_s=1},\ Fd\left(\frac{H_s}{W_m}\right),\ Fd\left(\frac{W_m}{H_s}\right),\ F_p,\ \eta_m$$

are updated at every cycle of the 'outer' iteration

For completeness the channel height, H_c , the screw temperature , T_R , and the independent variable z may be considered to be updated once every down-channel step.

Due to the complexity of the analysis and the need to employ numerical methods to obtain the solution, a computor program was written to perform the calculations That then is the basic scheme of the solution. Certain secondary problems in formulating the solution were encountered. These concerned the specification of the initial and boundary conditions of the problem, which was complicated in some respects by the numerical iterative form of the solution technique. Thus it was not found possible to use as an initial condition, δ_1 equal to zero. Instead this starting value was approximated to by setting δ_1 equal to a small value, typically 0.05 millemetre, that was an order of magnitude below the thickness of the developed film. The effect of varying this starting value on the overall solution was negligible but care had to be taken with this value to ensure the initial steps of the solution were stable.

In general the lower melt film does not appear until some time after the upper one. The point of formation of this lower film will be the point at which the screw temperature reaches the melting temperature of the plastic. Upto this point the thickness of this film is effectively zero. However, it is not possible to obtain a finite solution by simply putting δ_2 equal to zero. It requires a modified formulation to avoid the appearance of zero's in the denominators of the various equations. These modifications are built into the computor program. At the point of formation of the lower melt film an initial value must be taken that is non zero, again because of the numerical formulation. However the choice of this value is much more critical than that for the upper film. This is because the equation that calculates the pressure gradient across the solid bed changes with the appearance of the lower film. If an unsuitable initial value of lower film thickness is taken then this can lead to a serious discontinuity in the pressure gradient and possible instability of the solution. In reality this lower melt film gradually spreads across the width of the solid bed from the corners inwards, taking typically about half a 'turn' of the screw to do so. Therefore the effect of the appearance of the lower melt film in reality is more gradual than in the theory, though it is

thought possible that there is in practice a physical instability caused by the appearance of the lower melt film linked with the occurrence of solid bed break-up. This is discussed again in a later section. It is because this gradual appearance of the lower melt film cannot be handled in the present theory that extra care has to be taken at the point of appearance of this film in the theory. To minimise the unstable influence of the appearance of the lower melt film the initial value of it is calculated on the basis that the pressure gradient remains constant around the region of the film formation. Experimental evidence suggests this to be reasonable. Thus, if at step k in the z direction, the screw temperature is just below melting temperature then there is no lower melt film, and the pressure gradient is calculated (3.73). If, then, at step $k+1$ the screw temperature is greater than or equal to the melting temperature then it is required to calculate an initial value of . This is done by re-writing equation (3.75) explicitly for δ_2. Using the value of the pressure gradient calculated at step k, a value for δ_2 is obtained. In general the value of δ_2 so calculated is larger than it could reasonably be in that its maximum developement length is only one down-channel step length, Δz. Because of this, this calculated initial value of δ_2 is compared with a value obtained from a simple, approximate, analytical solution that calculates the thickness of film as a function of developement length. This analysis is given in Appendix C. As it is an analytical solution it starts with zero film thickness. If the thickness computed in the analytical solution, say δ_A, is less than δ_2 as calculated from the continuity of pressure gradient principle then it is assumed that δ_2 is still zero at step $k+1$ and the solution proceeds on this basis. At step $k+2$ the procedure is repeated. In the calculation of δ_A the boundary temperature, that is, the screw temperature, is generally greater at each successive step as is the potential developement length for the lower melt film. This means that at each successive step the value of δ_A will be greater and therefore nearer to as calculated from the pressure gradient equation, as this is only marginally influenced by the increasing screw temperature. If δ_A is still less than δ_2, then δ_2 is once again set equal to zero. Eventually δ_A will be greater than or equal to the initial value of δ_2. When this happens the solution proceeds

with δ_2 as a working variable.

This procedure proved to be very stable in use but had one drawback. In some cases it was found that at the first step at which δ_2 was taken to be non zero a discontinuity in the flow rate of unmelted material was observed. This was due to the sudden appearance of the lower melt film and the molten material in it. If this discontinuity was unacceptably large then an alternative procedure was adopted to calculate the initial value of δ_2. The initial value was set at some suitable small thickness and then to avoid an instability in the solution due to a large pressure gradient discontinuity it was assumed that the solid bed velocity remained constant for the following three steps. The solution to the analysis corresponding to the assumption of zero solid bed acceleration, that is $E = 0$, is easily obtained. Only one 'outer' iteration has to be performed at each step, and thus the solution of the 'inner' iteration cycle is the solution to the constant solid bed velocity model. By doing this, the value of the pressure gradient became redundant information as far as the 'inner' iterative solution for δ_1, δ_2 and X was concerned. This second scheme was not in fact as stable as the first but did remove the discontinuity in the calculating melting rates, this being the only justification for its use in that there are no experimental grounds for holding the solid bed velocity constant, even locally.

The initial temperature of the material is set equal to ambient temperature. In general the melting mechanism does not start to function until some point down the screw and there is thus an initial period corresponding to the solids conveying zone during which the solid material recieves an amount of 'pre-heating'. The nature of the present thermal analysis of the solid bed allows the effect of this 'pre-heating' to be calculated. Doing this means that the computor program begins to operate at the start of the screw and that the main melting calculation commences at some point after this. It is therefore necessary to specify the point at which the main calculation begins. In general this can be taken at the point at which the barrel temperature becomes equal to the melting temperature and thus allowing the program to automatically calculate the so called 'melting delay'. It is comparatively straight forward to provide a barrel temperature profile as input data for the program.

The initial value of solid velocity is calculated by equation (3.79). If the channel begins to taper during the 'pre-heating' stage then the solid bed velocity is up dated at each step in the following manner

$$V_{s\zeta}(\zeta) = M_T / \rho_s W (H_o - B\zeta) \qquad (3.104)$$

The value of solid bed velocity which is used in the first step of the main melting calculation is calculated so that the effect of the initial upper melt film is accounted for, thus

$$V_{s\zeta} = \left(M_T - M_{f\zeta}.W\right) / \left(\rho_s W \left(H_o - B.\zeta - \delta_1\right)\right) \qquad (3.105)$$

where $M_{f\zeta}$ is given by equation (3.21)

It now remains to discuss the screw and barrel temperature boundary conditions. In the present application of this analysis the barrel temperature was taken to be independent of ζ in line with the experimental barrel temperatures which were constant during the melting region. This meant that the barrel temperature was unrealistically high at the very beginning of the channel, that is, during the pre-heating of the solid bed. However the effect of this is marginal in terms of the overall analysis. More important, perhaps is the fact, that the point of beginning of melting was not automatically specified. The specification of this initiation point in the present work is discussed in the next section.

In the absence both of any suitable theoretical means of predicting the screw temperature profile and of any experimentally measured profiles it was found necessary to use an empirical formula for the screw temperature, thus

$$T_R = T_b\left(1 - \exp(g.\zeta)\right) + T_o \exp(g\zeta) \qquad (3.106)$$

where,

$$g = \ln\left(\frac{T_m - T_b}{T_o - T_b}\right) / \zeta_m \qquad (3.107)$$

where ζ_m is the ζ coordinate at which the screw temperature equals the melting temperature.

Thus the screw temperature, as defined by (3.106), is equal to ambient temperature, T_o, at $\zeta = 0$, and is asymptotic to the barrel temperature as ζ increases.

To compute the coefficient g requires a knowledge of ζ_m, the value of which thus becomes an additional boundary condition. The choice of ζ_m is discussed

in the next section.

The following section presents the results of the theoretical simulations of the experiments which were described in chapter 2. These theoretical and experimental results are then compared and discussed.

3.6 : Experimental and Theoretical Correlations.

3.6.1: Introduction

Chapter 2 of the present work described the experimentation that has been performed and discussed the results of those experiments. One aim of the experiments was to obtain insight into the mechanisms that function within the extruder in the melting region so that a mathematical model of the melting behaviour could be the more accurately formulated. The previous sections of this chapter dealt with the ensuing formulation of the model and with the mathematical techniques used in obtaining solutions to the mathematical system.

Having performed such a theoretical melting analysis it is then necessary to check the results of the analysis. Because of the nature of the mathematical formulation it is not possible to perform simple checks on the system. By this it is meant that it is never possible to obtain an analytical solution to the problem with which the numerical solution can be compared. In addition the problem is such that no matter what simplifying mathematical assumptions are made, it neverthe less remains a complex one. The reason for this is that the formulation of the problem begins by making fundamental assumptions as to the physical behaviour of the overall system, and only after this has been done are the mathematical assumptions made. Thus even if the mathematical analysis is totally comprehensive there is no certainty of accurately analysing the overall system unless the basic physical interpretation is totally comprehensive and correct, that is, no real significant effect is ignored. Clearly one does not expect, at this stage, the physical interpretation of what is observed to happen in the melting region to be totally comprehensive and correct, rather that it is adequate and amenable to mathematical analysis. Given the present basic assumptions that are made to define the present melting model it has not been found possible to solve the problem in any other way than that discussed in the previous chapter, no matter what simplifying assumptions are made. Also there is no great value in using the results of other melting analyses as a check on the accuracy of the present analysis since all other reported analyses make different basic interpreations of

the real melting process.

The general conclusion that is made is that the best way to perform useful checks on the accuracy of the solution is by comparison with experiments. Of course, the present set of experiments were performed with this function in mind. It is the purpose of this section to present the results of the comparisons between the present theoretical results and the present experimental results, and to discuss them.

Clearly to perform theoretical simulations of real experiments it is necessary to have a certain amount of data. An outline of the data that is required is given in the following sub-section.

3.6.2: The Data Requirements of the Melting Analysis

The input data required by the computer program used to generate the theoretical solutions falls into three categories; geometric data which defines the extruder; the material properties; and the particular operating conditions.

The geometric data required is listed in Table 3.1, together with the actual values for the two screws used in the present experimental work. All quantities are in S.I. units.

The feed and taper section lengths are the mean helical lengths of the channel in these sections and as such are calculated from mean values of channel depth and helix angle using the various geometric relationships quoted in chapter 2.1. It is also necessary to specify the down-channel step length to be used in the program. This is normally done by allowing a total of 300 steps and sub-dividing the total helical length of the screw by this number. It was found by experience of running the program that 300 steps was about the optimum number. Any fewer number tended to increase the likelyhood of instability in the program to an unacceptably high level, whilst any greater number simply increased computation time without giving any real advantages in terms of accuracy or stability.

A fairly comprehensive knowledge of the material properties is needed by the program. The relevant properties are listed in Table 3.2 together with the values used in the theoretical program for each experimental material and the source of the information.

Table 3.1

The Geometric Data required by the computer program for each screw used in the experiments.

	Screw A	Screw B
Channel width, W , m.	0.02994	0.02994
Feed section channel depth, H_o , m.	.008127	0.005715
Coefficient of channel taper, B , m/m.	.005516	0.002821
Flight clearance, e , m.	.00016	.00016
Helix angle, Θ .	17.65	17.65
Screw diameter, D , m.	.03827	.03827
Feed zone length m.	.508	.5434
Taper zone length m.	1.105	1.126

Property	Material						
	LDPE1	HDPE1	PP1	Plasticised PVC	LDPE powder	Melinex	Rigid PVC
Density of solid, ρ_s , kg/m^3	882.5	990	875	1490	882.5	I.C.I. RESTRICTED INFORMATION	1387
Density of melt, ρ_m , kg/m^3	775.0	856	760	1346	775.0		1340
Specific heat of solid, c_s , J/kg°C	3087	2329	2325	1260	2240		810
Specific heat of melt, c_m , J/kg°C	2537	2691	2800	1550	1900		1075
Latent heat of fusion, λ , J/kg	53,980	219,300	54,500	8000	53,600		32,000
Melting Point, T_m ,°C	111	134	160	120	110		120
Thermal conductivity of melt, k_m, J/m°Cs	.24	.224	.11	.18	.24		.161
Thermal conductivity of solid, k_s J/m°Cs	.308	.41	.215	.17	.308		.165
Datum viscosity, η_D , Ns/m^2	30,765	9,172	5,864	34,986	7,887		40,000
Power law index n	0.337	.422	.364	.267	.44		.315
Temperature sensitivity of viscosity, b ,°C^{-1}	.0137	.008	.0123	.0159	.0124		.015
Datum temperature of viscosity, T_D , °C	140	170	220	150	140		150
Source of Information	RAPRA +I.C.	RAPRA + I.C.	RAPRA +I.C.	I.C.I. +I.C.	I.C.I. +I.C.	I.C.I	I.C.I. +I.C.

Table 3.2

Material Properties required by the Computor Program for each Experimental Material.

The thermal properties that are functions of temperature, e.g. specific heat, and for which data was available showing this variation with temperature, were averaged in each phase over the relevant temperature ranges. For the solid phase this temperature range was from the initial feed temperature of the material, i.e. T_o , to the melting temperature, T_m . For the fluid phase the range was from T_m to the barrel set temperature, T_b .

The materials were assumed to have a distinct melting point, corresponding to a discontinuity in the enthalpy – temperature curve. In the case of thermoplastic materials this is an assumption and therefore the actual data measured for the material was used as a basis for producing an idealised set of data. Thus the real enthalpy – temperature curve was replaced by a stylised scheme, shown in figure 3.12, which has the following features; constant specific heat for the solid phase; constant specific heat for the fluid phase; a distinct melting point; a finite latent heat of fusion.

These ideal enthalpy curves were constructed in the following fashion. The melting point was taken as the point of maximum specific heat as ascertained from the measured data. The mean specific heats calculated from the data over the previously defined temperature ranges. The latent heat of fusion was calculated by first calculating the actual enthalpy change from the initial temperature of the material, T_o , to the barrel set temperature, T_b , and the equating this with the enthalpy change as calculated over the same temperature range from the mean specific heats and the latent heat; the latent heat being the only unknown quantity in the equation.

The viscosity measurements for each material were performed on an Instron testing machine fitted with a capillary rheometer attatchment; the usual two capillary technique to eliminate end errors was employed (44). The measurements were made, in general, over a shear rate range of 2.914 to 2914^{-1} and usually at three different appropriate temperatures. The results were fed into a computer program which calculated the parameters characterising the materials viscosity variation acc ording to the 'power law' constitutive equation; that is, the power law index n , the temperature sensitivity b, and the datum viscosity η_D at shear rate $\dot{\gamma}_D = 1$ sec^{-1}, and at temperature T_D which was chosen according to the particular range of measurement. The program

Figure 3.12

The idealised relationship between enthalpy and temperature

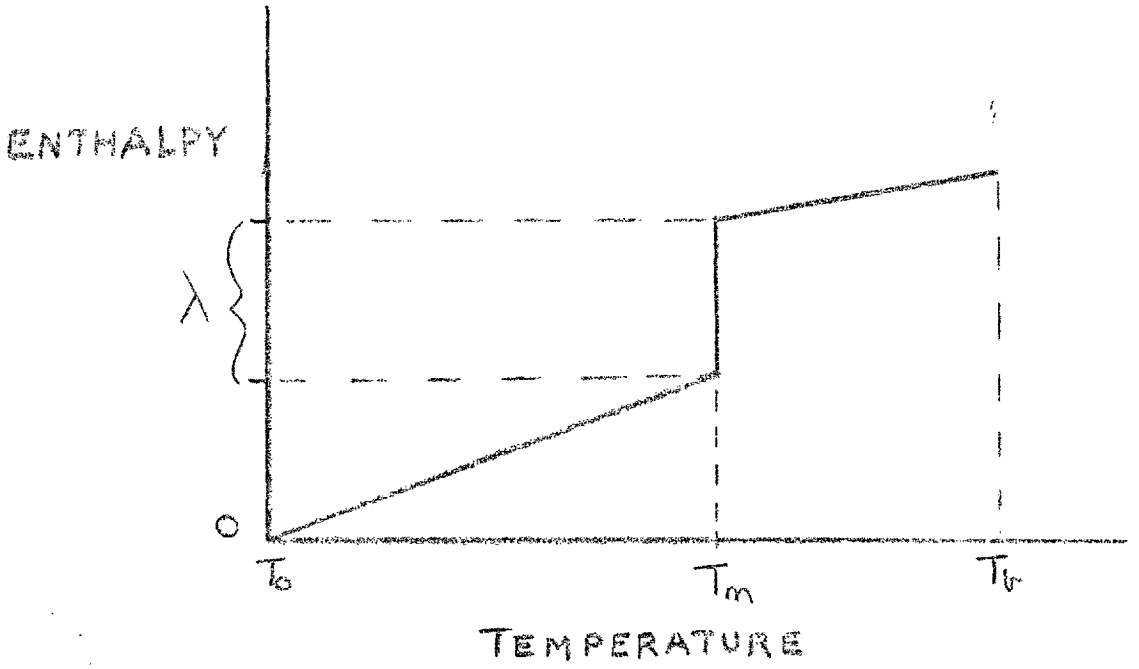


Table 3.3

The operating conditions required by the computer program for each experiment.

Expt. No.	Screw Speed r.p.m.	Flow rate kg/s	Barrel Temp °C	Initial Temp °C	Screw melt point m
1	80	.006	160	20	1.35
2	40	.00334	160	20	.901
3	80	.00613	160	20	1.35
4	40	.00335	160	20	.8
5	80	.00319	150	20	.54
6	40	.00162	150	20	.54
7	80	.00359	150	20	.56
8	80	.00233	150	20	1.85
9	40	.00138	150	20	.515
10	40	.00133	250	20	.5
11	80	.00299	250	20	.55
12	40	.00155	250	20	.52
13	80	.00315	250	20	.55
14	80	.00238	250	20	1.85
15	80	.00312	170	20	.9
16	40	.00157	170	20	.85
17	80	.00344	170	20	.9
18	80	.00229	170	20	1.85
19	40	.00136	170	20	.78
23	80	.00532	300	20	1.25
24	40	.00273	300	20	.9
25	80	.00338	150	20	.5
26	40	.00192	150	20	.5
27	80	.00368	150	20	.5
28	40	.00130	150	20	.5
30	40	.00309	160	20	.9

calculated sets of values of these three parameters, each set corresponding to one decade of shear rates. The values corresponding to the most appropriate range of shear rates were then used in the melting program.

The operating conditions that need to be specified in the program are listed in Table 3.3 with the values used for each simulation.

The initial pressure was always taken as zero. Although this is not necessarily realistic due to pressure generation in the feed section, it can be justified in that the initial predicted pressure rise was usually found to be large such that the program adjusted the zero initial pressure rapidly to one compatible with the other variables of the analysis. Also it would be difficult to know what alternative initial value of pressure to specify unless an analysis of the solid feed section of the extruder were to be coupled with the melting analysis. This point is returned to later.

As was stated in the previous section, for the present application of the analysis, the barrel temperature was assumed to be constant over the entire length of the screw. This therefore meant that the point along the channel at which melting started needed to be specified. This start point was in fact defined on the basis of the experimentally observed start point. Similarly the point along the channel at which the screw temperature becomes equal to the melting point was defined by inspection of the experimental samples for evidence of melting on the screw root.

Thus with the data outlined above the computer program was used to perform simulations of the experiments, the results of which are now given.

3.6.3: Presentation of the Results

The main basis of the comparison between the theory and the experiments is the melting rate which is represented as a solid bed profile.

Experimentally these were measured by projecting the photograph prints of the experimental cross-sections, that are shown in the Plates, and tracing round the enlarged images onto plain paper. A planimeter was then used to measure the area of solid and melt from these tracings. The ratio of the area of solid to the total cross-sectional area of the specimen was then plotted

against the helical down-channel distance to form the experimental solid bed profile. Although this is nominally the area ratio it was compared with the solid bed width ratio predicted by the theory. This was done because of the difficulty of measuring accurately the cross-sectional area of the melt films from the specimens. This meant that the measured ratio was, in fact, more of an indication of the ratio of mean solid bed width to channel width.

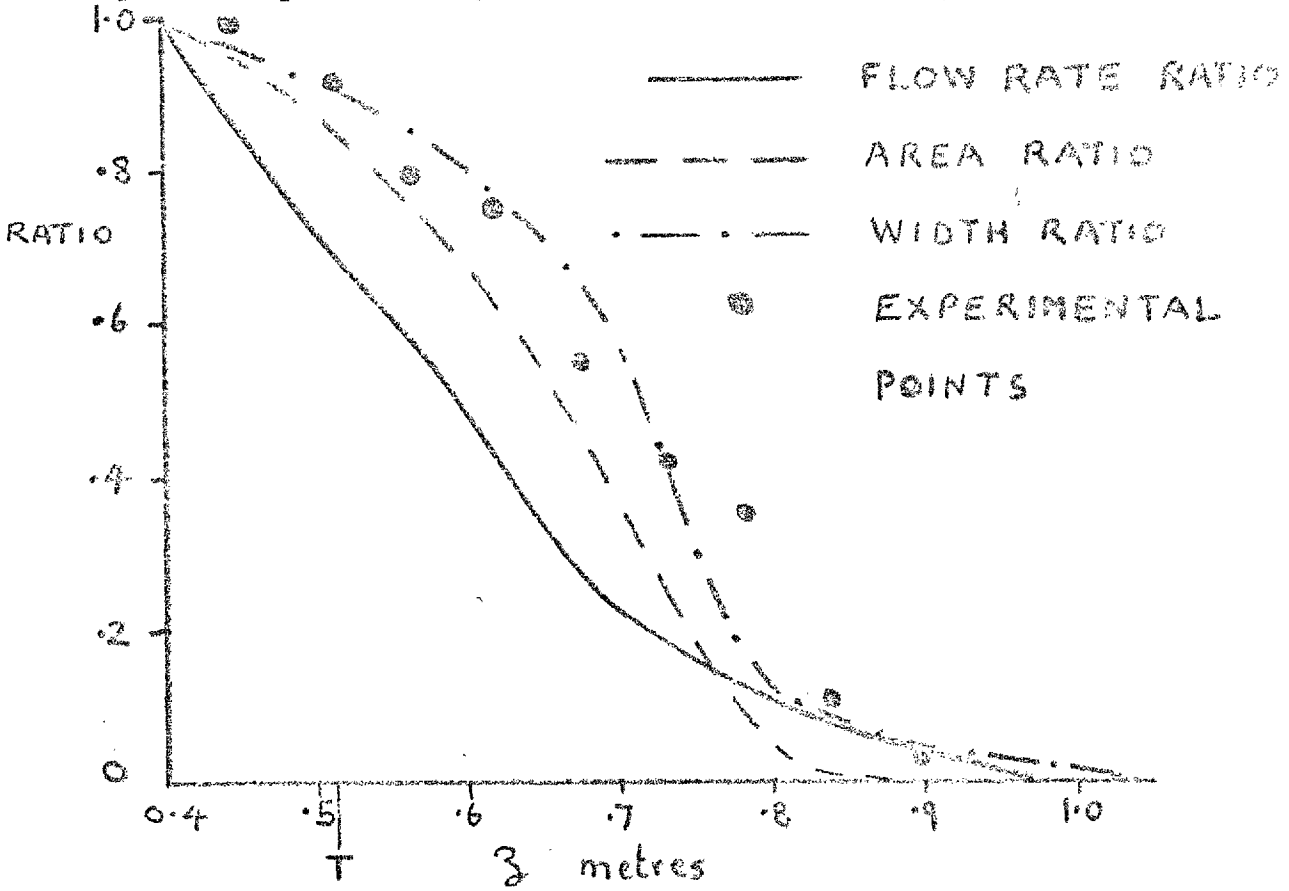
Figure 3.13 shows the different profiles one gets by plotting the different ratios for two experiments. Three theoretically predicted ratios are shown in each case. Curves A, B, and C represent the solid bed to channel width ratio variation, the solid bed to channel area ratio variation and the solid bed to total down-channel flow rate variation respectively. This last ratio gives an exact indication of the predicted melting rate, but of course, it is not possible to use it in a meaningful comparison with the experimental results. This is because of the impossibility of measuring the true experimental melting rate, due to the different unknown down-channel velocities in the melt flow and solid flow regions.

In this figure and others the positions of the beginning and end of the tapered section of screw are marked on the z axis by T's, and the point at which the screw temperature reaches the melting point of the plastic is marked by an M. In figure 3.13 it is clear that the theoretical area ratio, curve B, gives virtually as good a prediction as the width ratio, curve A. This proved to be the case in a lot of the experimental comparisons. Indeed in some cases this area ratio gave a significantly better prediction. However as has been said the experimental measurements correspond to width ratios and therefore must be compared with the theoretical width ratios. It is likely that the reason for the sometimes better agreement of the predicted area ratio is a co-incidental combination of factors peculiar to particular experiments. The area ratio at any point is lower than the width ratio by an amount equal to the area of the melt films. With the present screw geometry, in particular the small channel depth, the effect of the areas of the melt films is quite large.

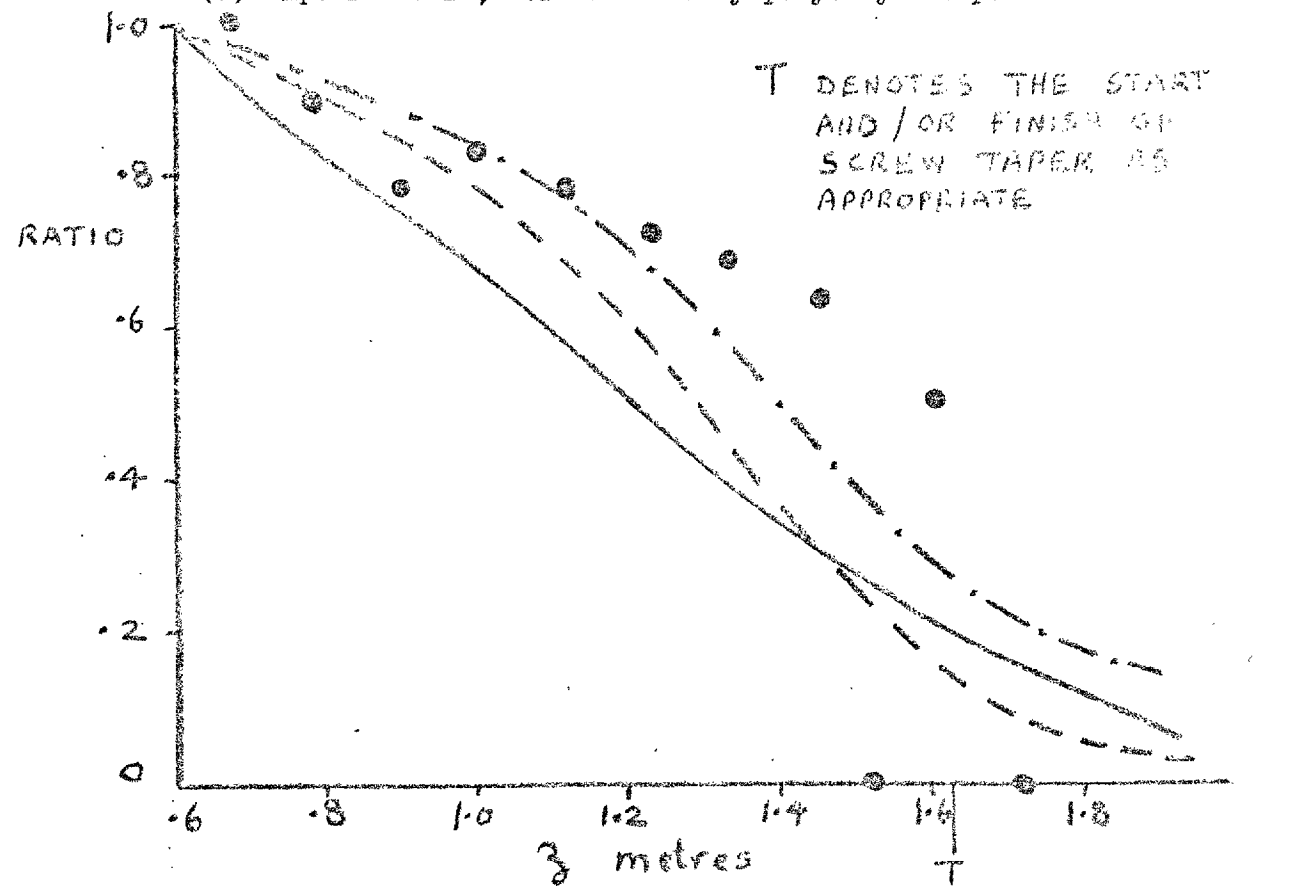
Results of simulations performed with larger screw sizes which are presented in the next chapter confirm this. For all the other experimental comparisons

Figure 3.13

The theoretical melting profile expressed in three ways for two of the present experiments together with the experimental profile



(a) Experiment 28, for low density polyethylene powder



(b) Experiment 17, for high density polyethylene

presented in the present work only the theoretical width ratio is plotted. The solid bed profiles for plasticised PVC, experiments 1 to 4, are shown in figures 3.14 and 3.17 to 3.19. Figure 3.14 also shows the variation of the other four main variables from the theoretical analysis. The general agreement is good though the theory consistently predicts too large a solid bed width during the later stages of melting, without there being a large error in the predicted completion of melting. Figure 3.14 also shows theoretical predictions calculated making the restrictive assumptions of constant solid bed velocity and no lower melt film. The predictions are derived from the present theory with the solid bed acceleration set equal to zero, that is $E = 0$, throughout. The results are not necessarily identical to results obtained from the one Tadmor derived (4,15) as the present formulation of the analysis is different. It can be seen from the figure that the constant solid bed velocity solution does not give as good a fit as the more general analysis. The effect of having no lower melt film is a secondary one for two reasons. Firstly, in general, the melting rate at the lower interface is an order of magnitude less than that at the upper. Secondly with the constant solid bed velocity assumption the effect of the lower melt film on the pressure gradient is of no consequence since the pressure gradient is not needed in the melting calculations. Therefore the resulting poorer fit is most likely to be a consequence of the assumption of constant solid bed velocity.

The corresponding results for low density polyethylene granules are shown in figures 3.15 and 3.20 to 3.23. Again figure 3.15 also shows the variation of the other main variables of the theory. The general agreement between theory and experiments is good. With the screw cooling experiment, no.8, depicted in figure 3.23, the theory predicts too high a solid bed width ratio though the end of melting is in excellent agreement with the experimental findings. Figures 3.20 and 3.21, also show constant solid bed velocity solutions and again these are less accurate than the more general solution. In the case of the screw cooling experiment, figure 3.23, the solid bed width predictions assuming constant solid bed velocity are more accurate but the predicted finish of melting is much less accurate.

Figure 3.14

The theoretical variations of the melt film thickness, solid bed velocity, pressure and solid bed width ratio with channel position in the z direction for experiment 3 with plasticised PVC. The experimental pressure and melting profiles are also shown. N(80); Q(367); D(5/32)

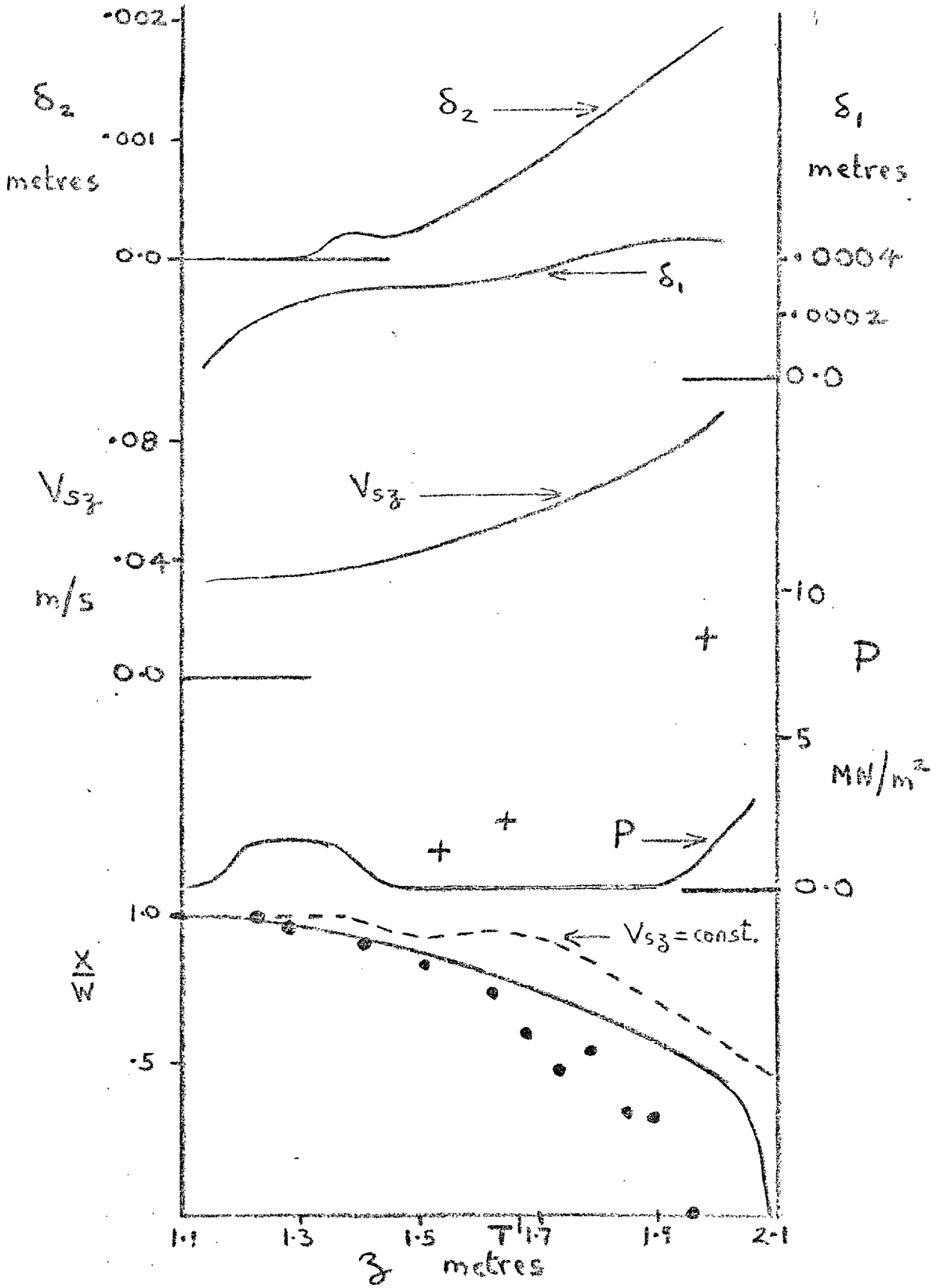


Figure 3.15

The theoretical variations of the melt film thickness, solid bed velocity, pressure and solid bed width ratio with channel position in the z direction for experiment 9 with low density polyethylene. The experimental pressure and melting profiles are also shown. N(40); Q(83); D(1/16).

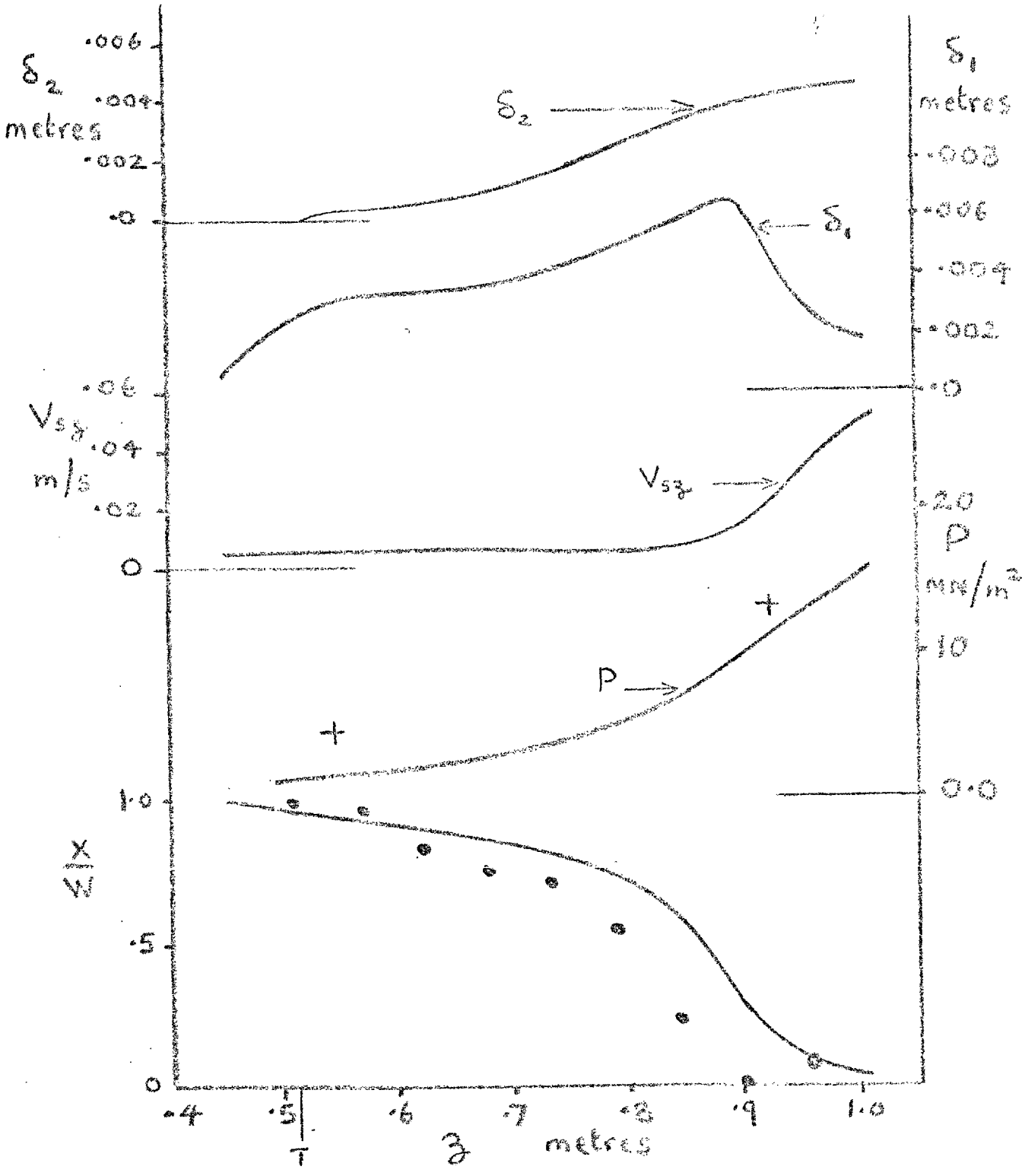


Figure 3.16

The theoretical variations of the melt film thickness, solid bed velocity, pressure and solid bed width ratio with channel position in the z direction for experiment 27 with low density polyethylene powder. The experimental pressure and melting profiles are also shown. N(80); Q(221); D(5/32)

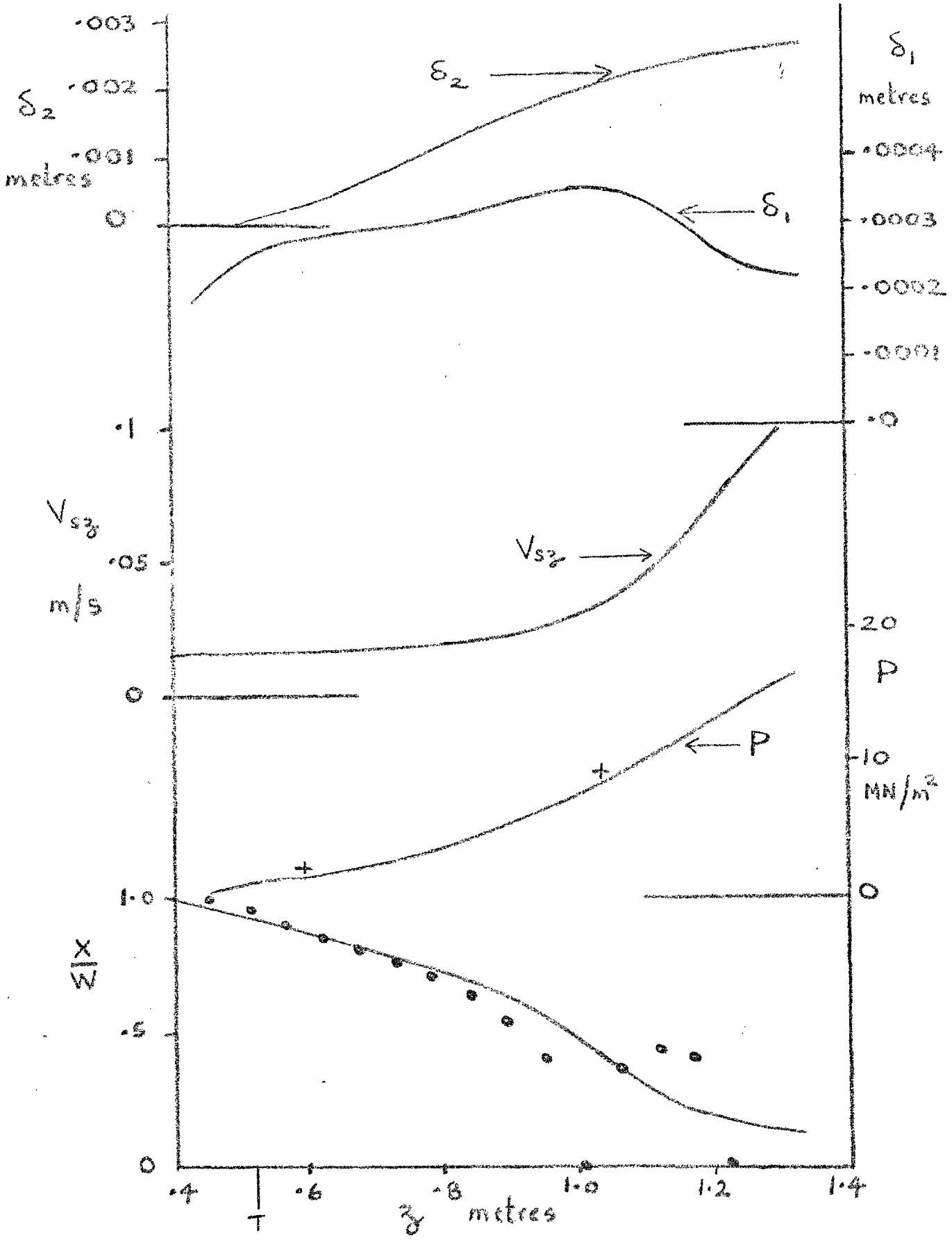
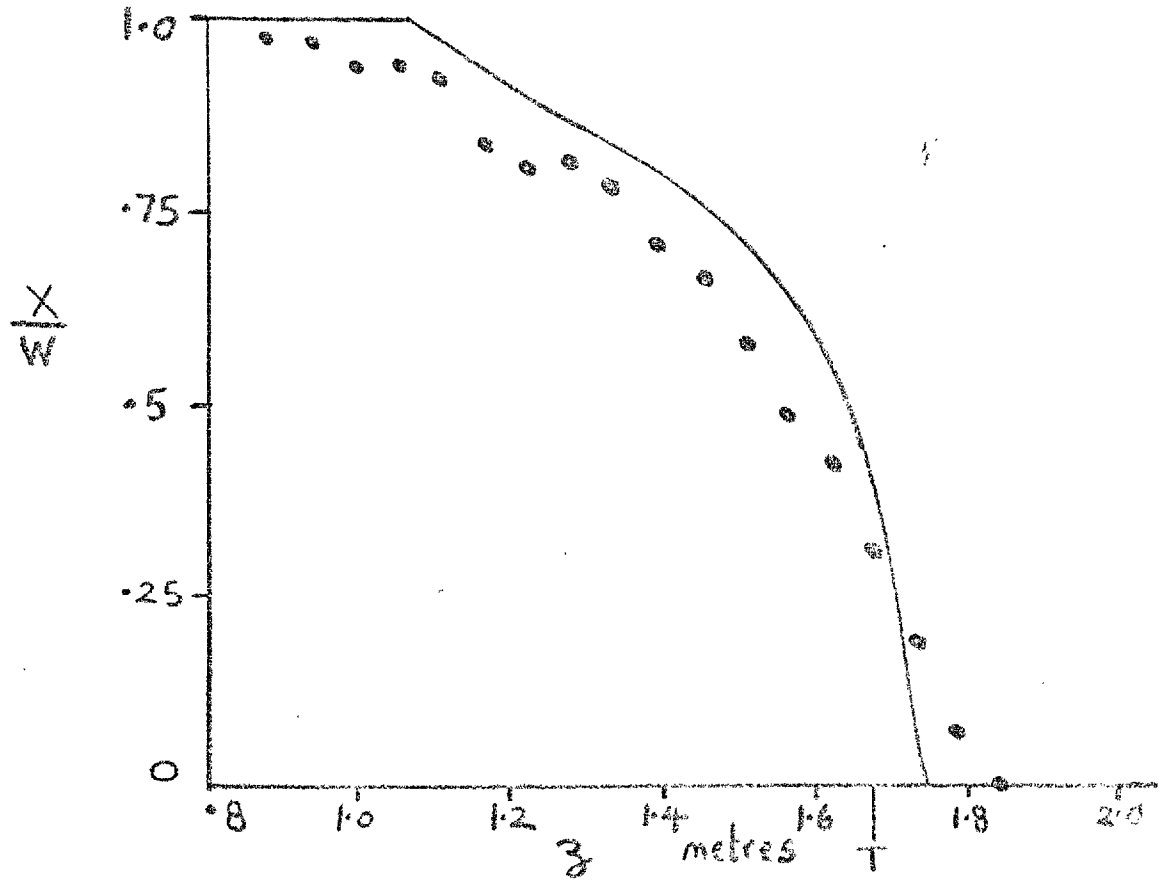


Figure 3.17

The experimental and theoretical solid bed profiles for experiment 1 with plasticised PVC. N(80); Q(360); D(3/32)



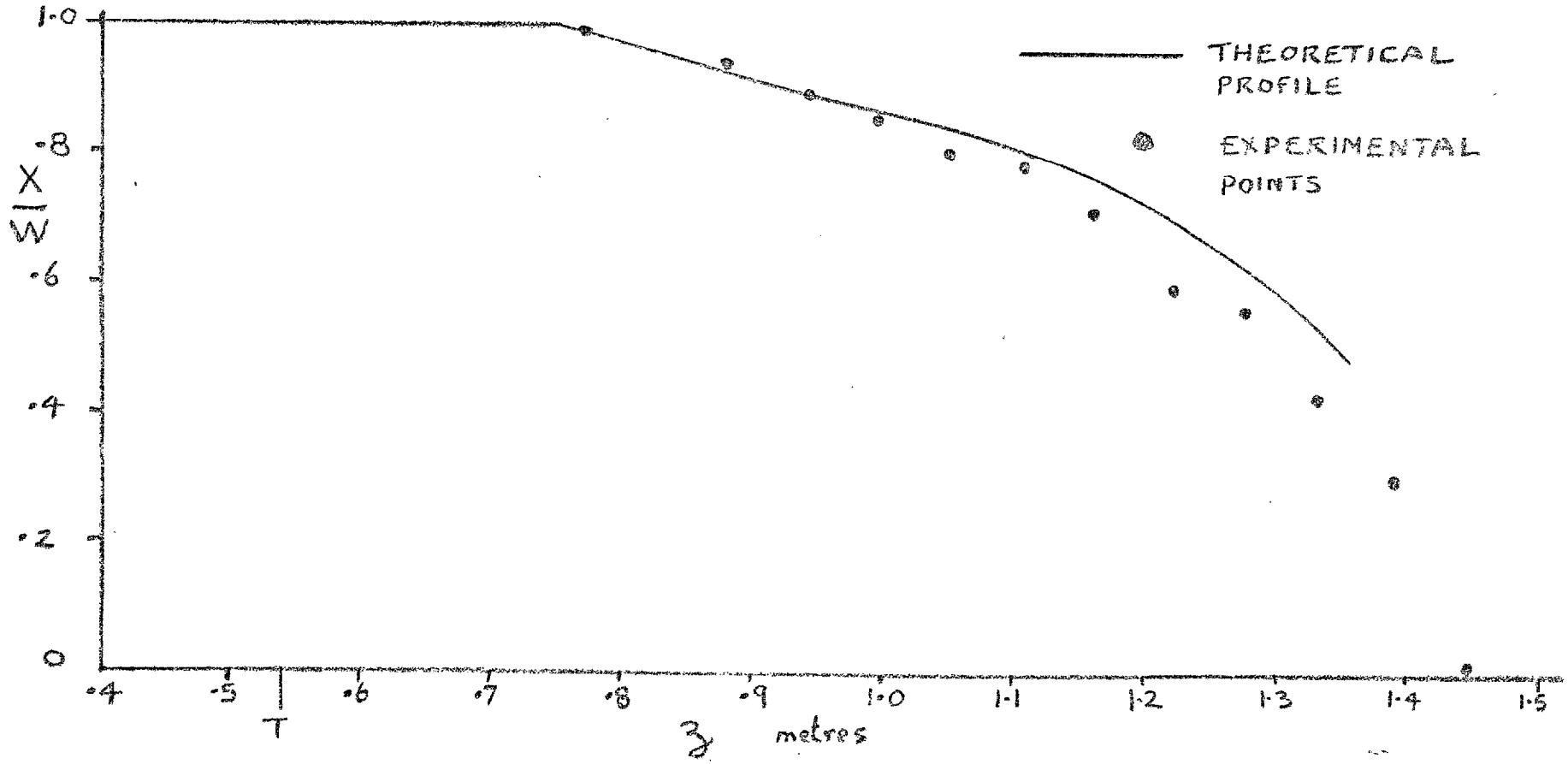


Figure 3.18

The experimental and theoretical solid bed profiles for experiment 2 with plasticised PVC. N(40); Q(200); D(3/32)

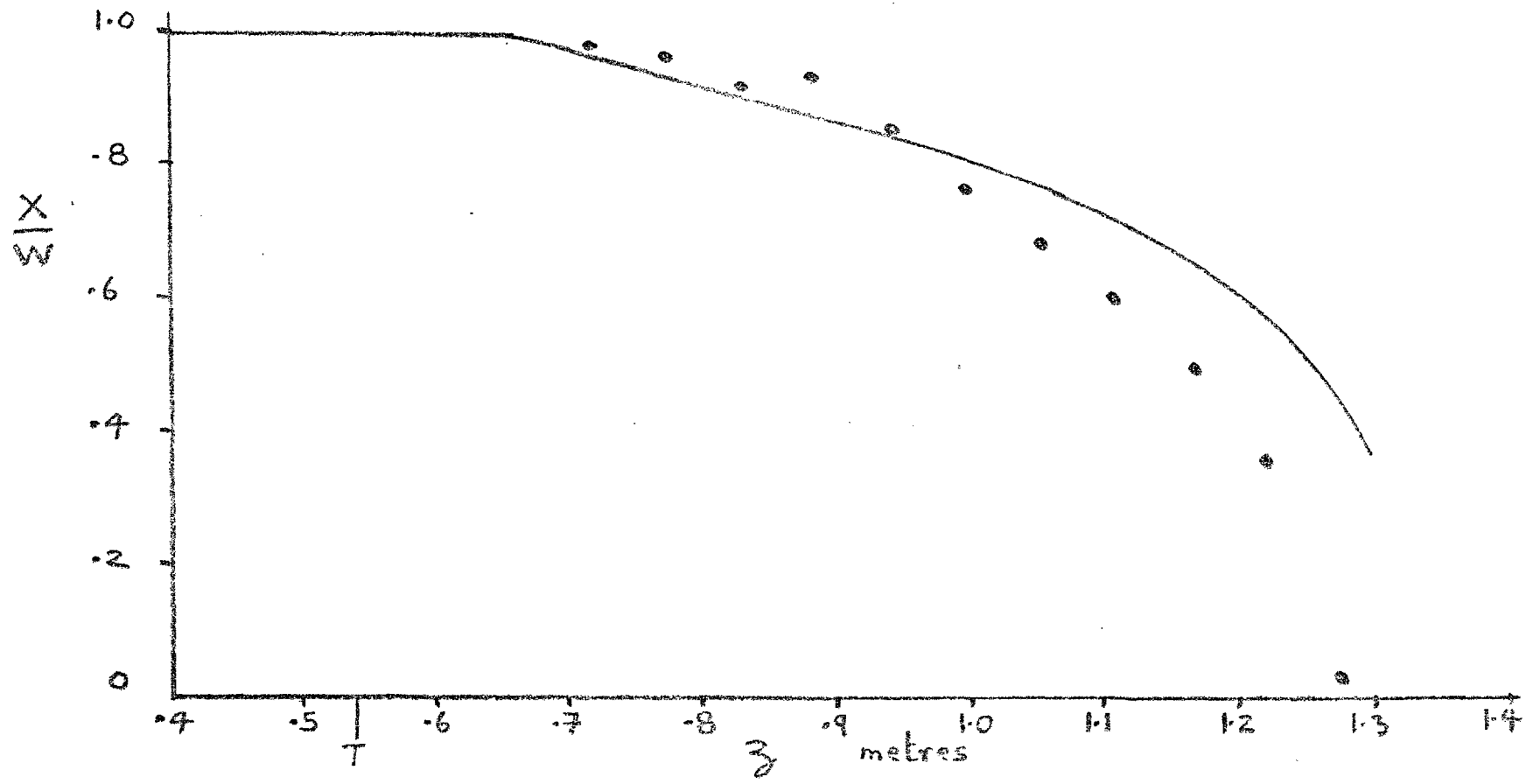


Figure 3.19

The experimental and theoretical solid bed profiles for experiment 4 with plasticised PVC. N(40); Q(201); Q(1/16)

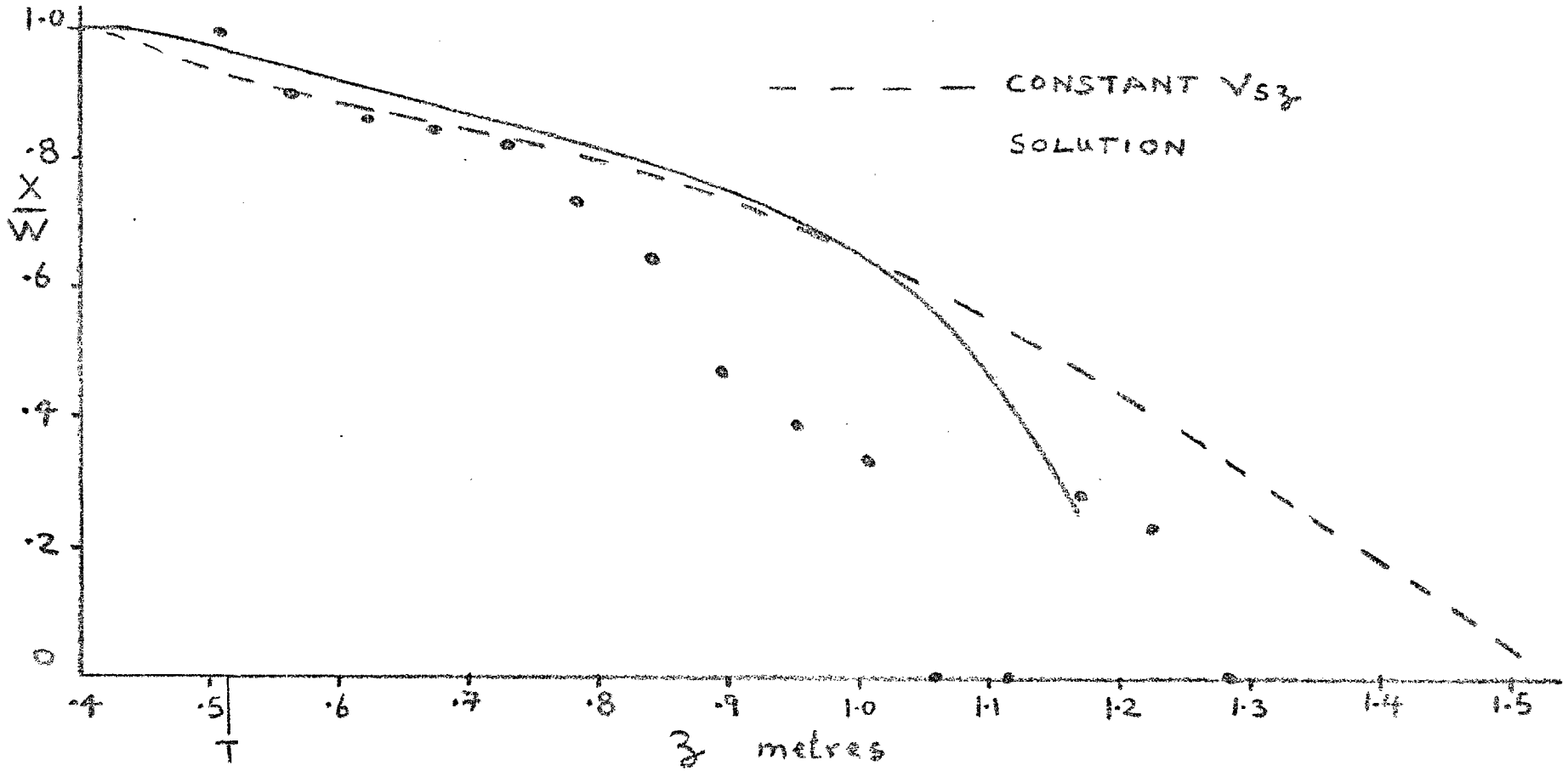


Figure 3.20

The experimental and theoretical solid bed profiles for experiment 5 with low density polyethylene granules. N(80); Q(191); D(3/32)

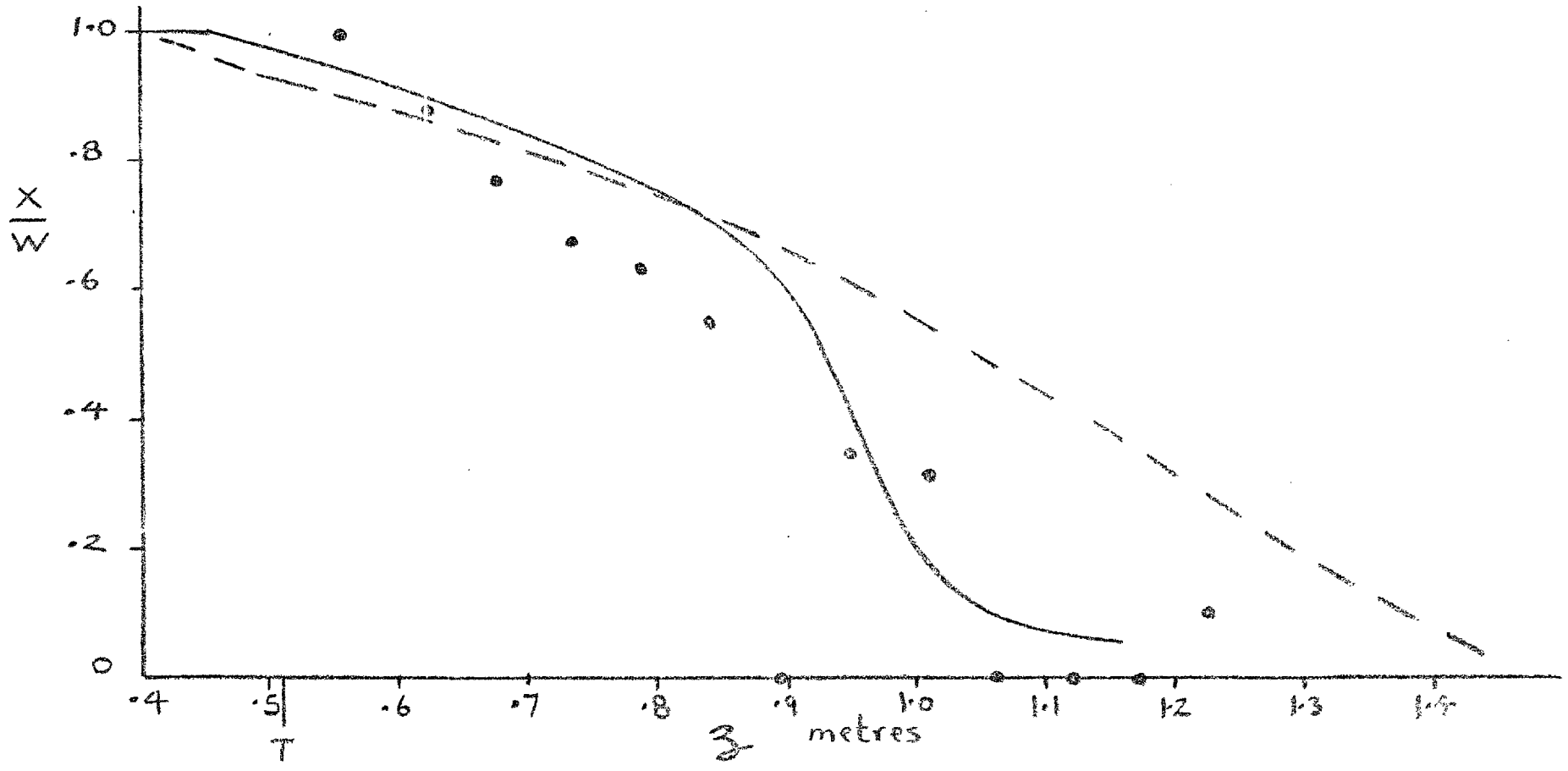


Figure 3.21

The experimental and theoretical solid bed profiles for experiment 6 with low density polyethylene granules. N(40); Q(97); D(3/32)

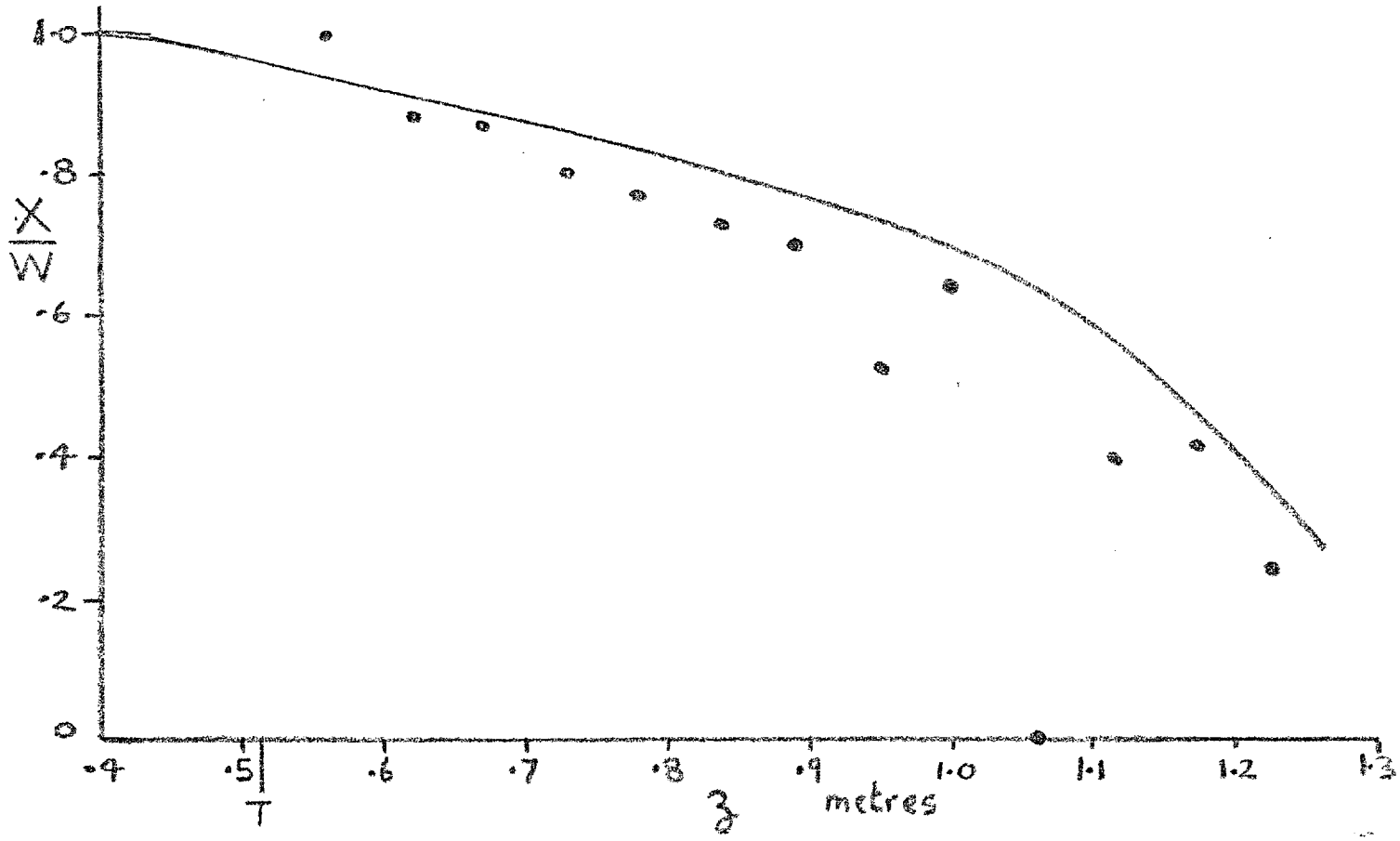


Figure 3.22

The experimental and theoretical solid bed profiles for experiment 7 with low density polyethylene granules. N(80); Q(215); D(5/32)

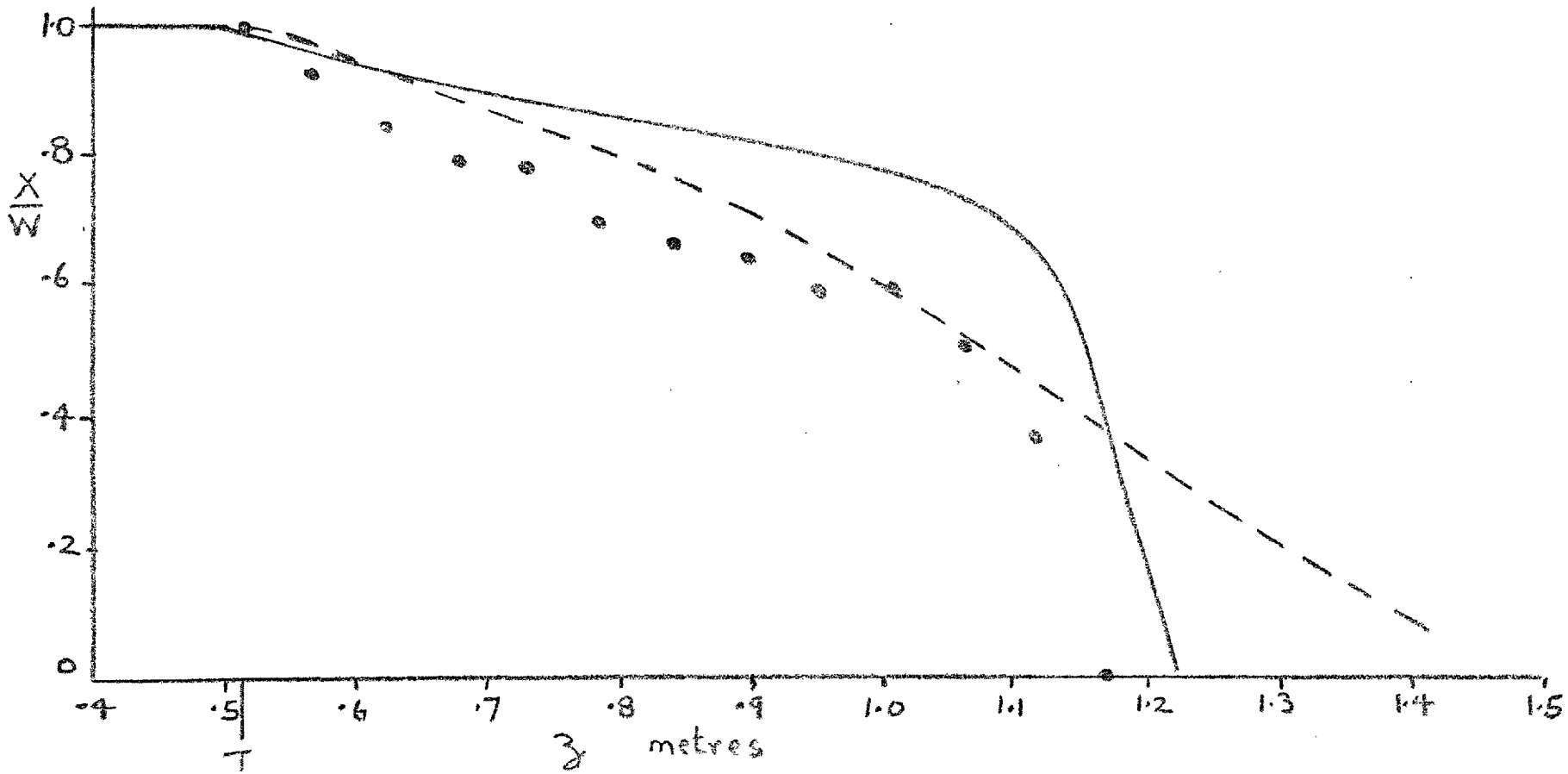


Figure 3.23

The experimental and theoretical solid bed profiles for experiment 8 with low density polyethylene granules. N(80); Q(140); D(3/32)

The theoretical and experimental solid bed width profiles for polypropylene are shown in figures 3.24 to 3.28. The level of agreement here is not as good as for plasticised PVC and low density polyethylene. It would seem that although the shape of the theoretical curves is similar to the experimental ones the predicted end of melting is consistently well after the observed end. It is possible that this error may be due to inaccurate data. This point is discussed in the next chapter in the light of further theoretical simulations on the effect on the predictions of varying the input data.

Figures 3.13(b) and 3.29 to 3.32 show the results for high density polyethylene. The degree of agreement is generally good. Again, as with the low density polyethylene results of figure 3.23 for the screw cooling experiment, the theoretical predictions for the screw cooling experiment of figure 3.31 show too high a solid bed width ratio, yet accurately predict the finish of melting. Figures 3.29 to 3.31 include theoretical results for the constant solid bed velocity case, showing less satisfactory agreement than the general analysis, except for the screw cooled case of experiment 18.

The results for Melinex are shown in figures 3.33 and 3.34. It is immediately apparent that although agreement with the experimental results is good during the initial stages of melting, the theory is unable to make reasonable predictions much after the appearance of the lower melt film. The theory is predicting a rapid reduction in solid bed width which then remains fairly constant but small, and hence giving a low melting rate. In practice the solid bed breaks so that the broken pieces of the bed are still comparatively wide and melting continues at a similar rate. It would seem that the Newtonian nature of molten Melinex is responsible for the theoretical prediction of a rapid solid bed width reduction and corresponding high solid bed acceleration. as soon as the lower melt film forms. This point is discussed in the next chapter. The constant solid bed velocity solution shown in figure 3.33 shows poor agreement in terms of the shape of the profile but predicts the end of melting perhaps more realistically than the general model.

Figures 3.13(a), 3.16, 3.35 and 3.36 show the solid bed width profiles for the low density polyethylene powder experiments. Figure 3.16 also shows the

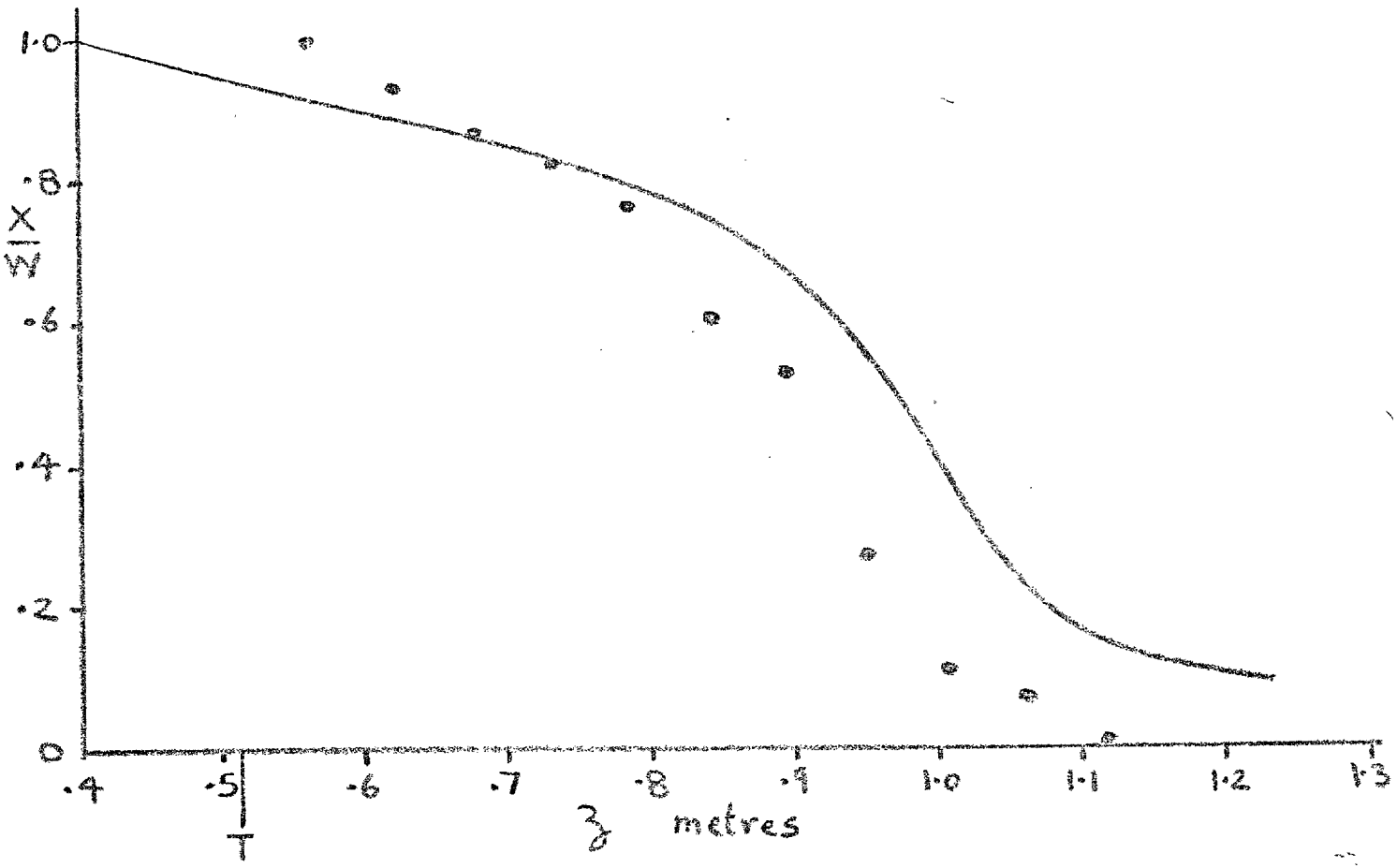


Figure 3.24

The experimental and theoretical solid bed profiles for experiment 10 with polypropylene. N(40); Q(80); D(1/16)

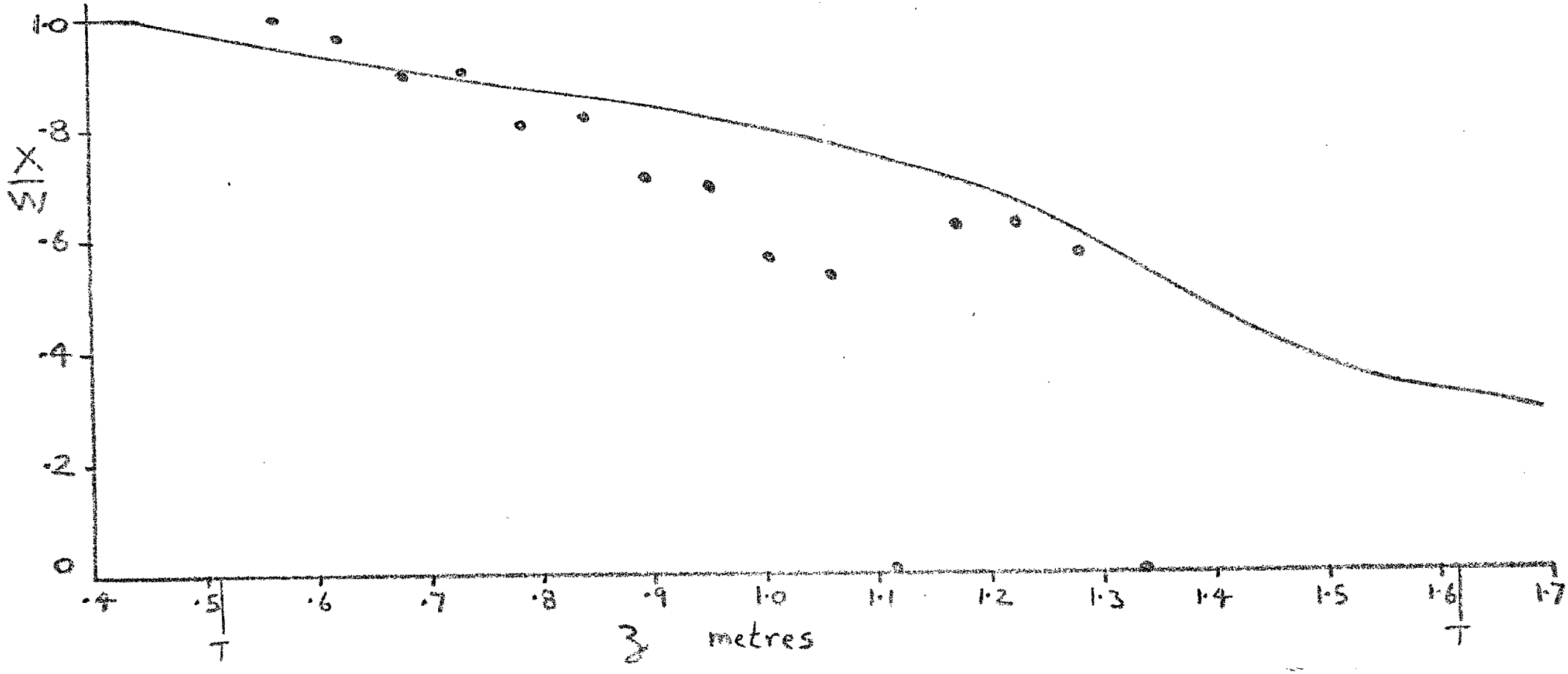


Figure 3.25

The experimental and theoretical solid bed profiles for experiment 11 with polypropylene. N(80); Q(179); D(3/32)

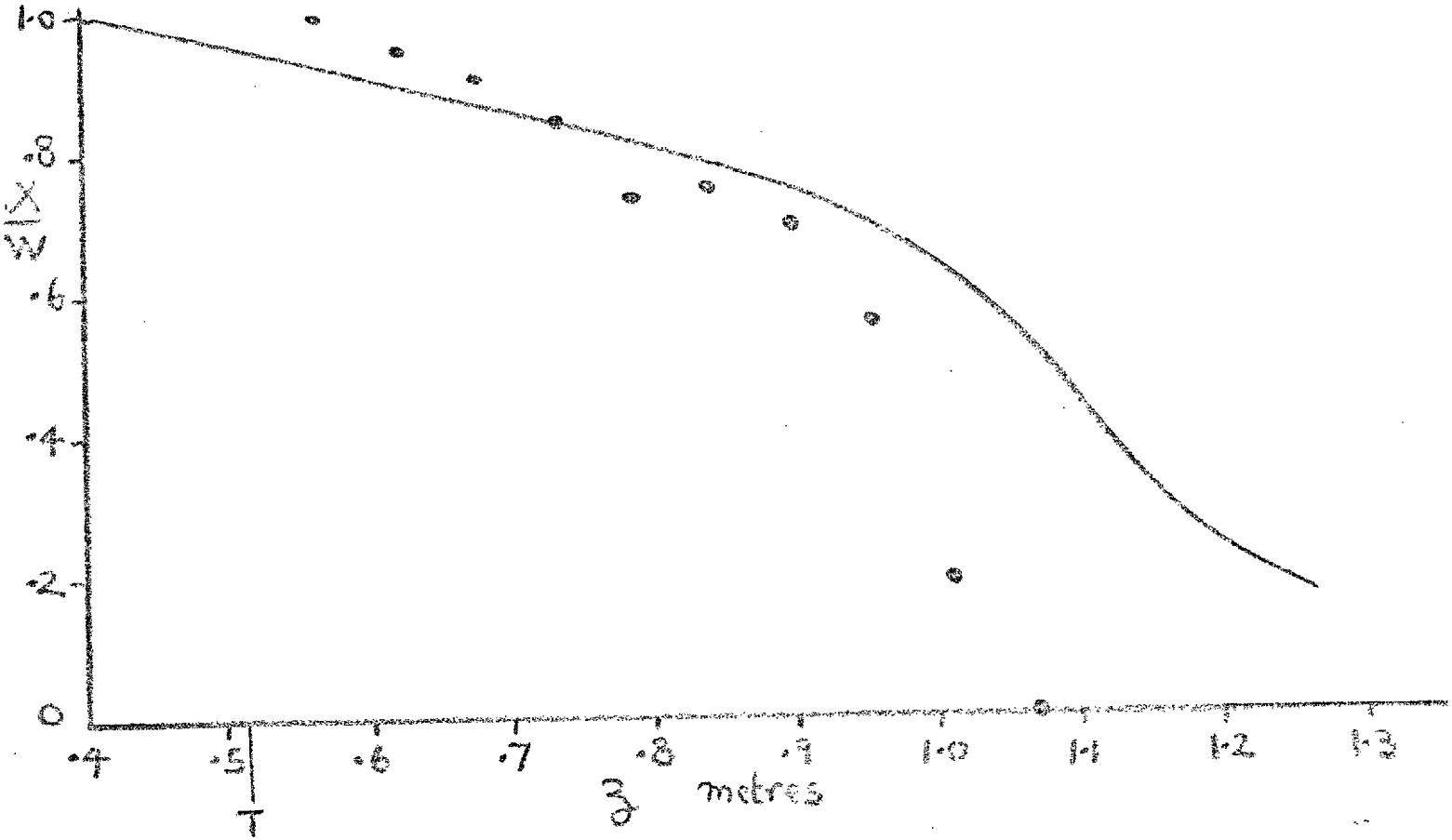


Figure 3.26

The experimental and theoretical solid bed profiles for experiment 12 with polypropylene. N(40); Q(93); D(3/32)

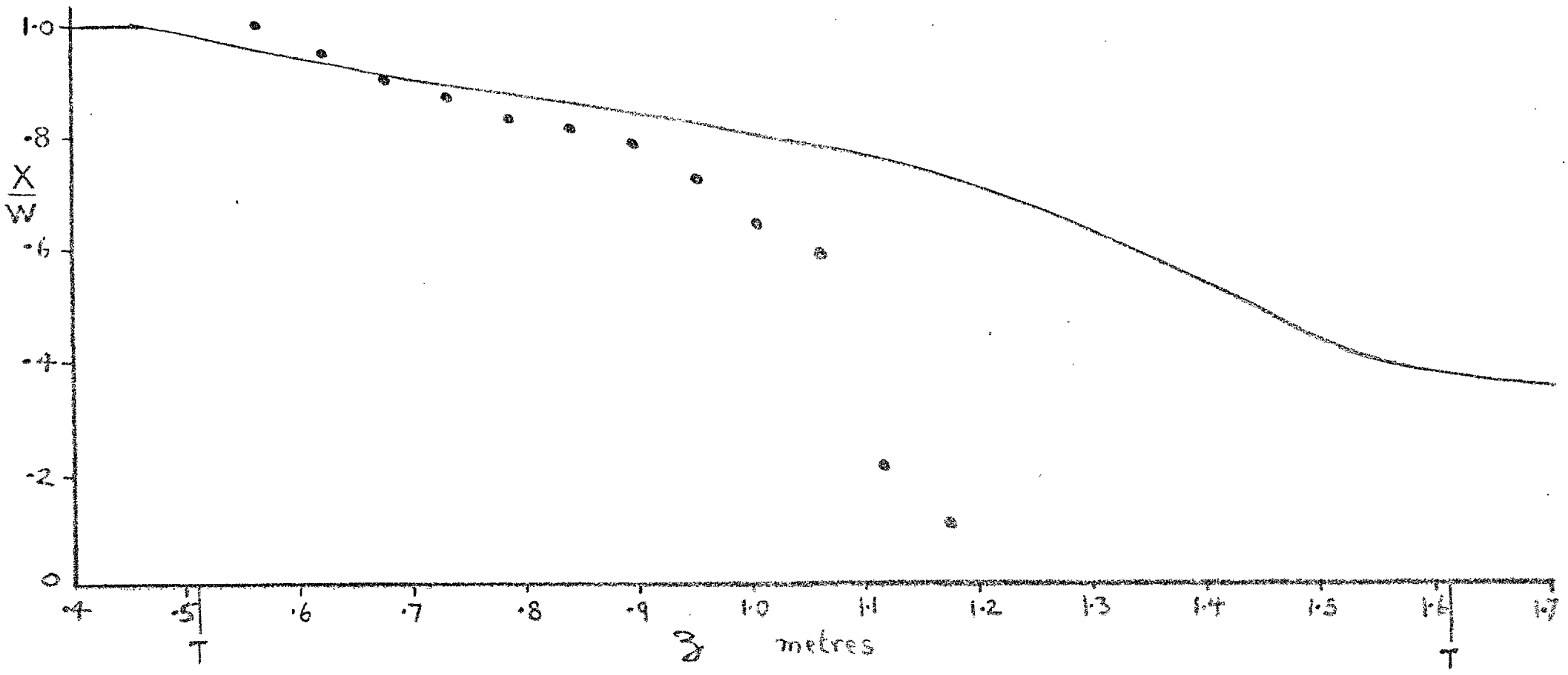


Figure 3.27

The experimental and theoretical solid bed profiles for experiment 13 with polypropylene. N(80); Q(189); D(5/32)

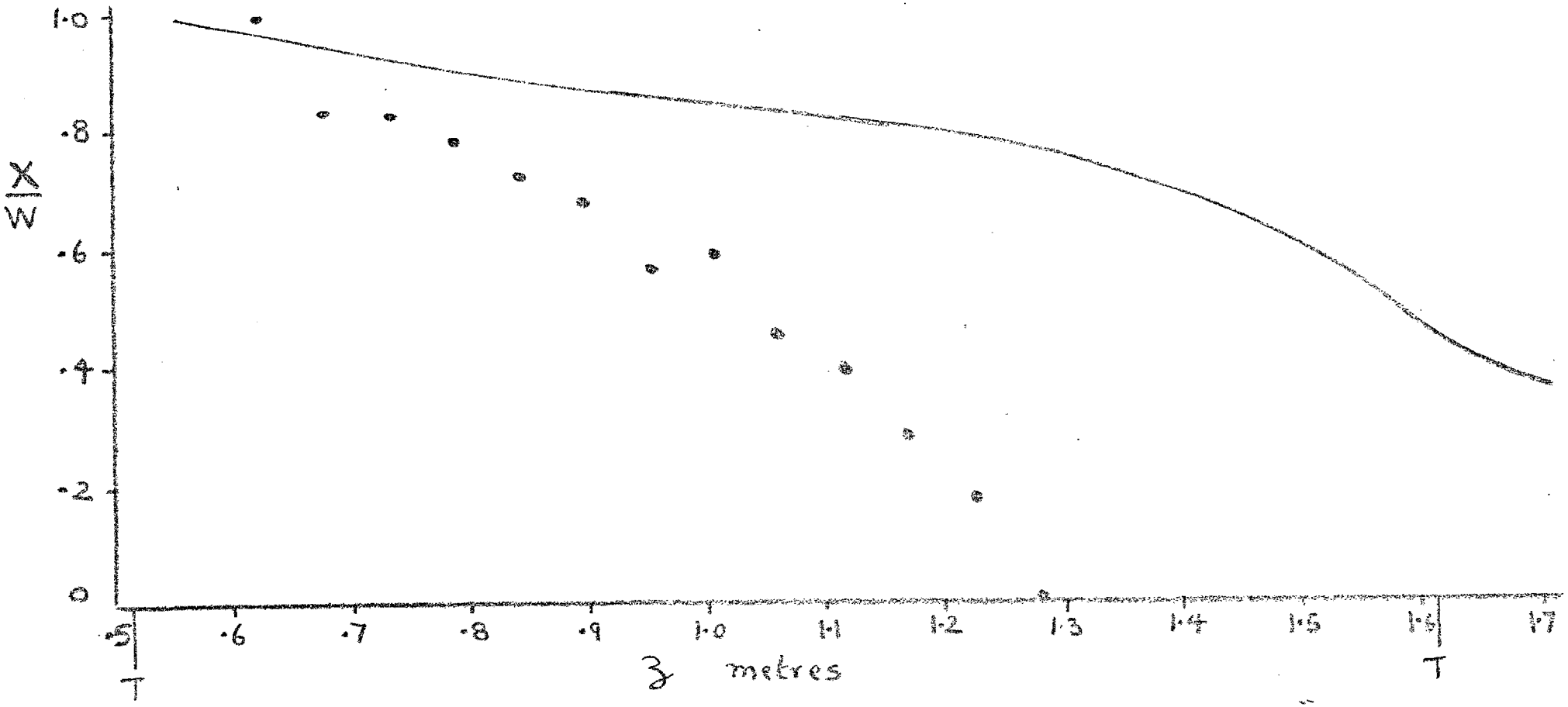


Figure 3.28

The experimental and theoretical solid bed profiles for experiment 14 with polypropylene. N(80); Q(143); D(5/32) Screw cooling used

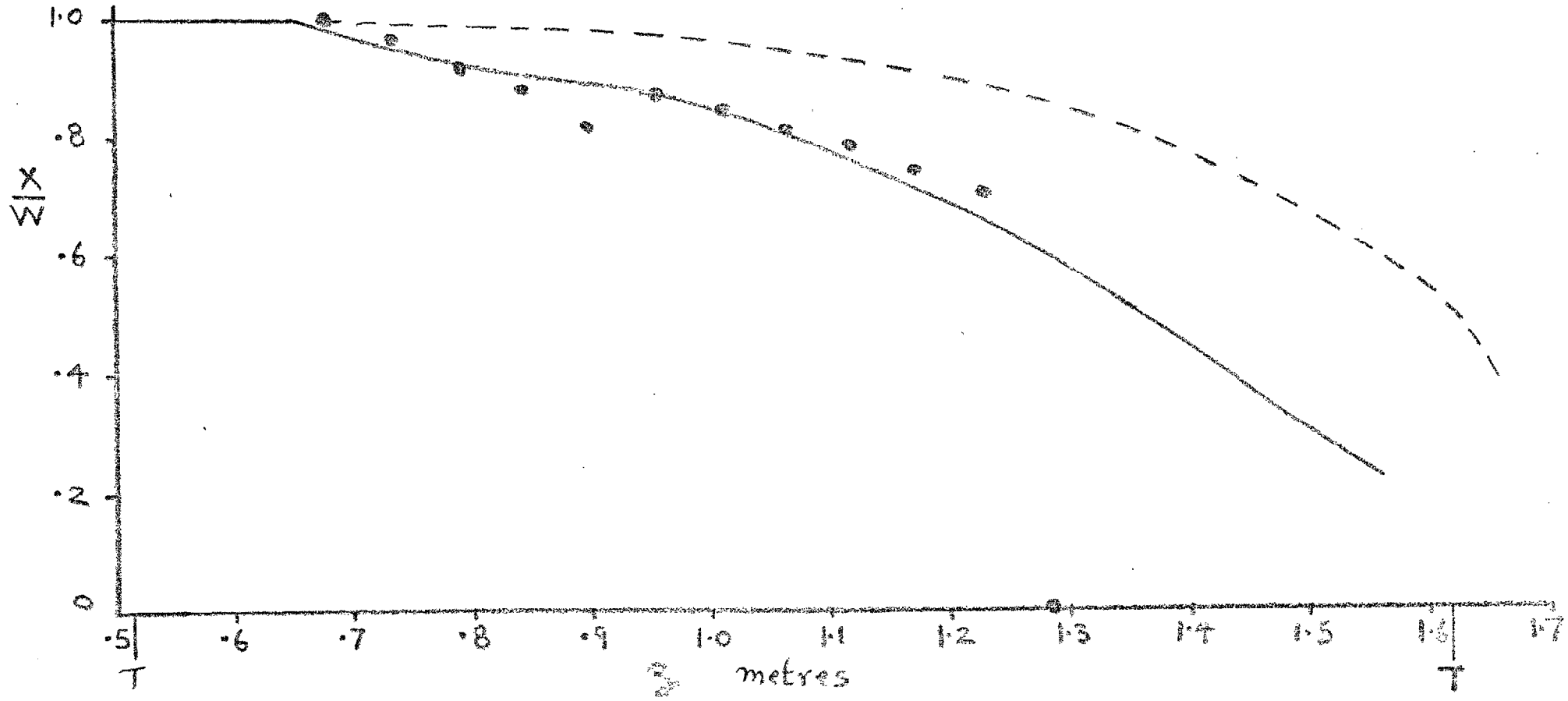


Figure 3.29

The experimental and theoretical solid bed profiles for experiment 15 with high density polyethylene. N(80); Q(187); D(3/32)

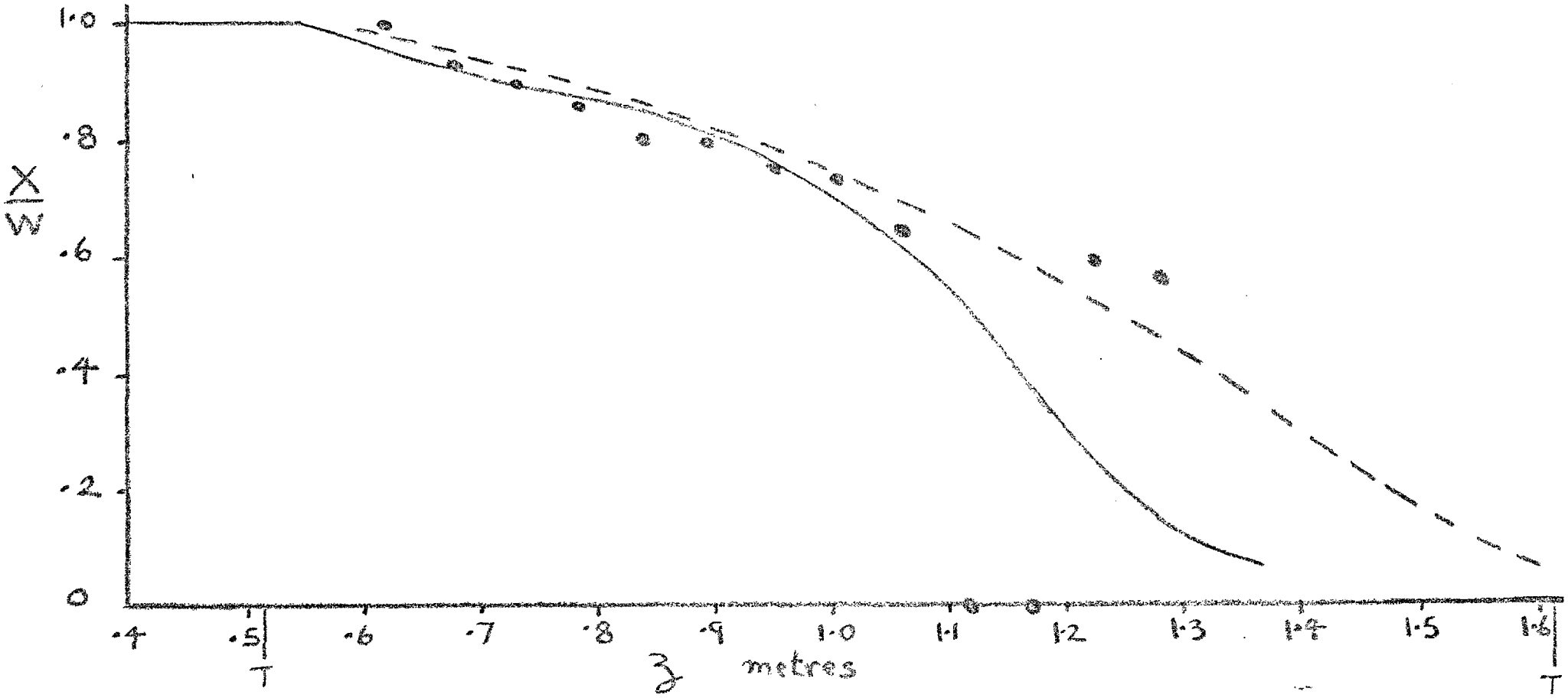


Figure 3.30

The experimental and theoretical solid bed profiles for experiment 16 with high density polyethylene. N(40); Q(94); D(3/32)

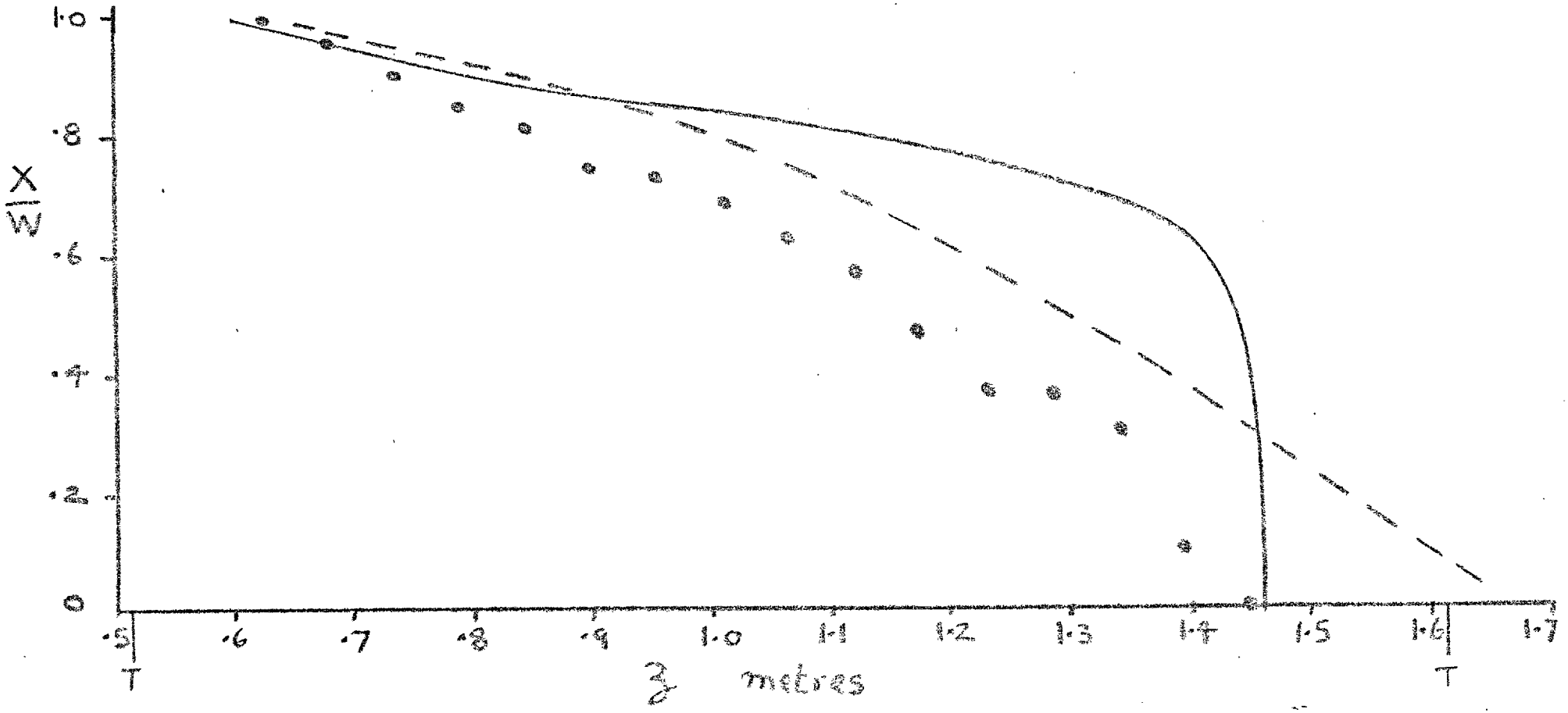


Figure 3.31

The experimental and theoretical solid bed profiles for experiment 18 with high density polyethylene N(80); Q(137); D(3/32). Screw cooling used.

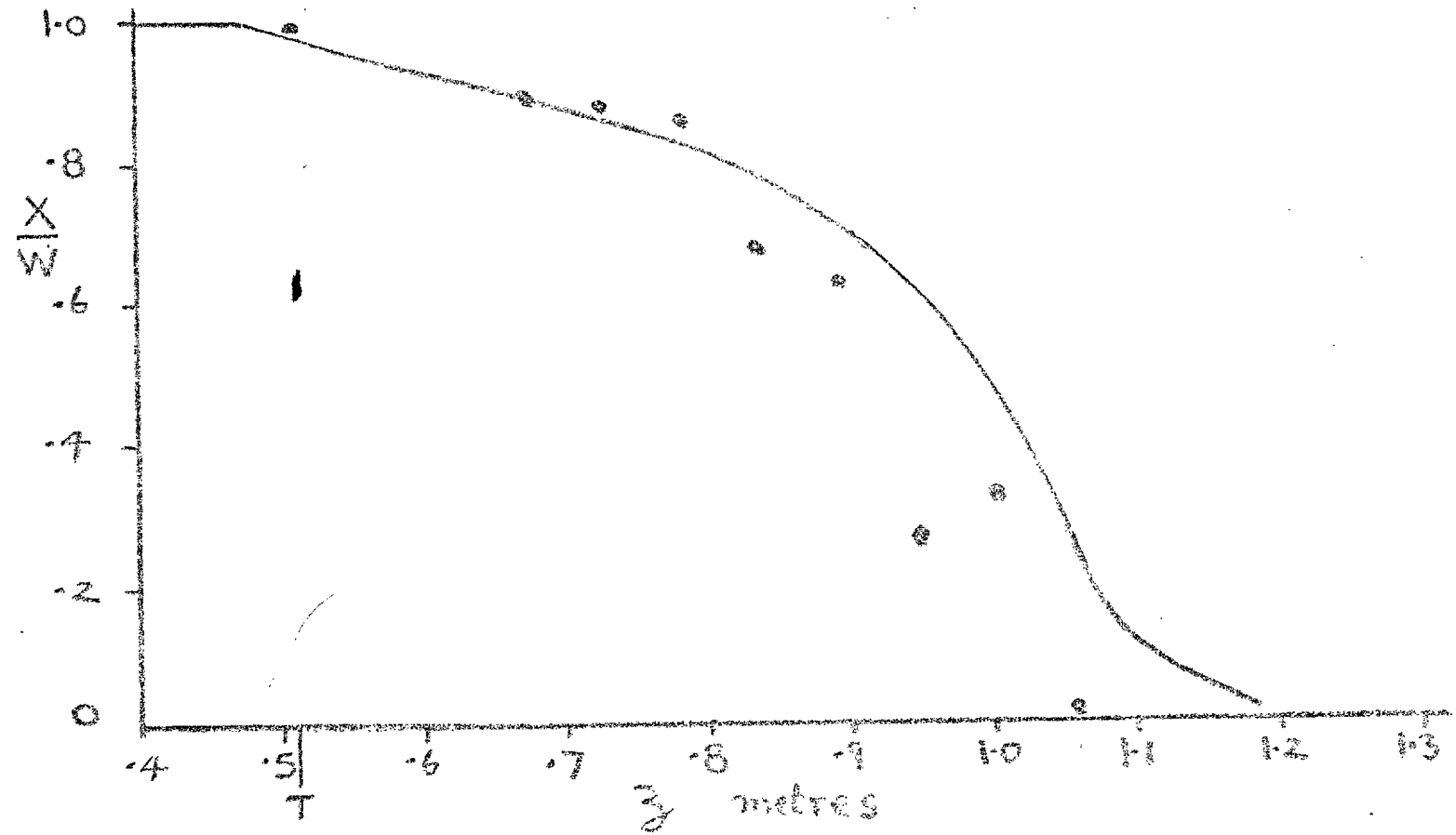


Figure 3.32

The experimental and theoretical solid bed profiles for experiment 19 with high density polyethylene. N(40); Q(81); D(1/16)

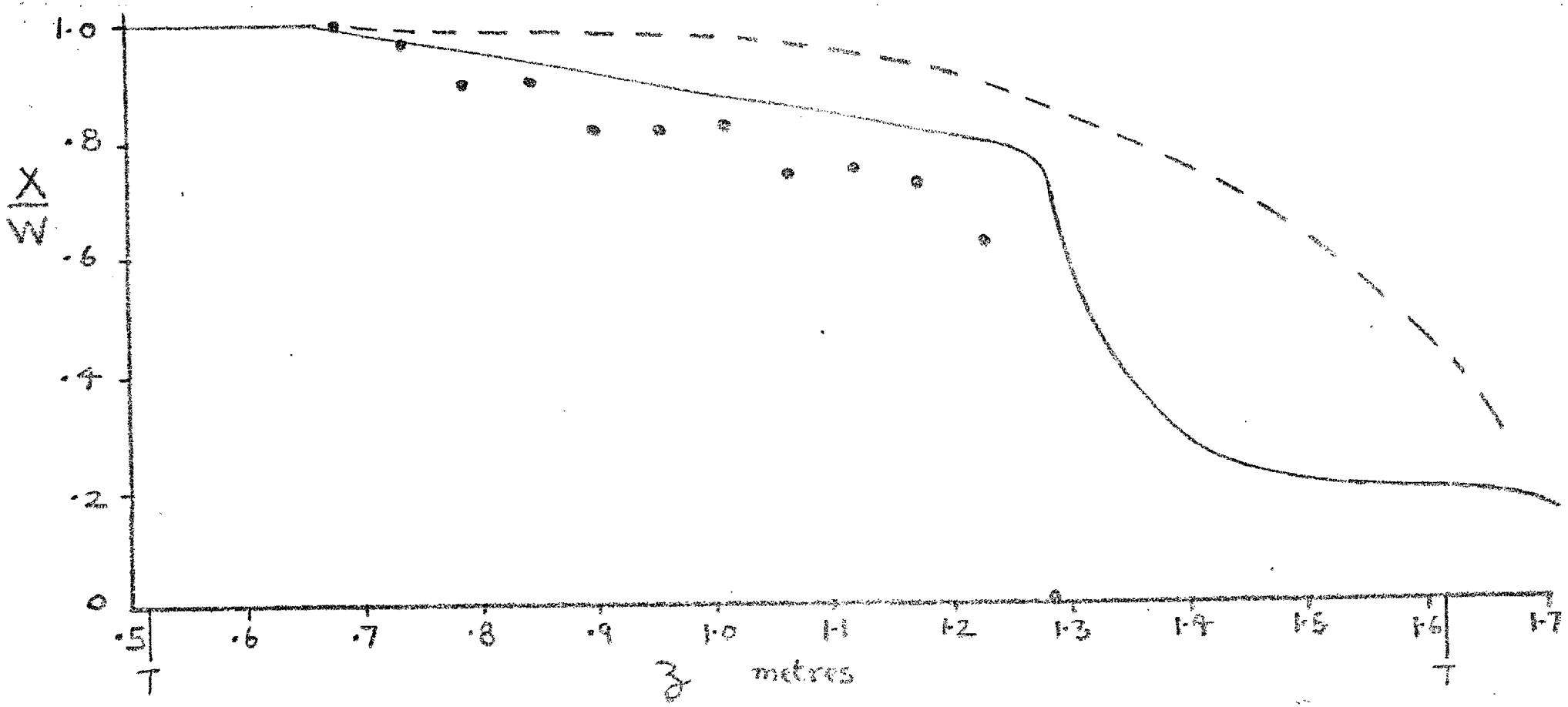


Figure 3.33

The experimental and theoretical solid bed profiles for experiment 23 with Melinex, N(80); Q(319); D(3/32)

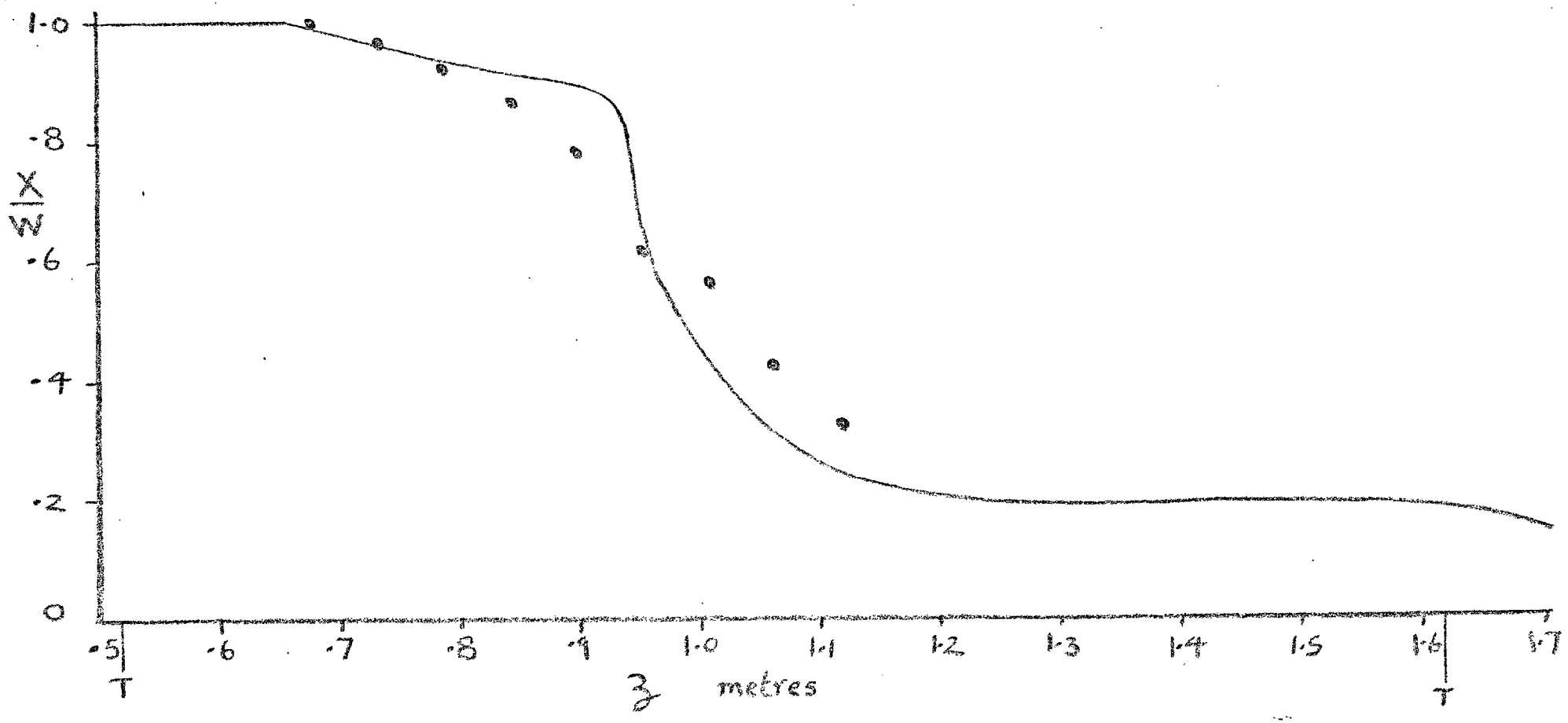


Figure 3.34

The experimental and theoretical solid bed profiles for experiment 24 with Melinex. N(40); Q(164); D(3/32)

variation of the other four variables of the problem. Much the same comments apply to these results as were applied to the other results; generally good agreement and generally better agreement with the full analysis than the constant solid bed velocity analysis.

Figure 3.37 shows the results for experiment 30 with rigid PVC; again the fit is good. The results for experiment 29 with rigid PVC were not obtained due to instabilities in the melt film analysis caused by the very high viscosity of the material coupled with its high temperature sensitivity. However, it is thought that this problem can be overcome by applying better starting conditions in the Newton Raphson iterative technique, that is used to obtain the solution to the melt film analysis, see Appendix B.

Results are not shown for the polystyrene experiments because insufficient data was available to run the program. However in the light of the other results this omission is not thought to be too serious.

That concludes the presentation of the melting profile comparisons. Before discussing the implications of them it is advantageous to present some comparisons between the experimental pressure profiles and the theoretical predictions. The theoretical and experimental pressure profiles for plasticised PVC in experiment 3 are shown in figure 3.14. It is obvious that agreement is poor. This may be partly due to an inaccurate specification of the point of formation of the lower melt film, coupled with the fact that at this point, in the case of PVC, the constant solid bed velocity change over condition was used as opposed to the continuity of pressure gradient condition. This meant that some discontinuity in the pressure gradient occurred and it could have been sufficient to cause the inaccurate pressure predictions.

Figures 3.15 and 3.38 show the pressure curves for two low density polyethylene experiments. There is much better agreement here than for the PVC, noting that the continuity of pressure gradient condition was used at the formation of the lower melt film. It can be seen, however, that during the later stages of melting the theoretical pressure is rising increasingly higher than the actual pressure. The same comments apply to the pressure results in figure 3.39 for polypropylene and to these of figures 3.40 and 3.41 for high density polyethylene.

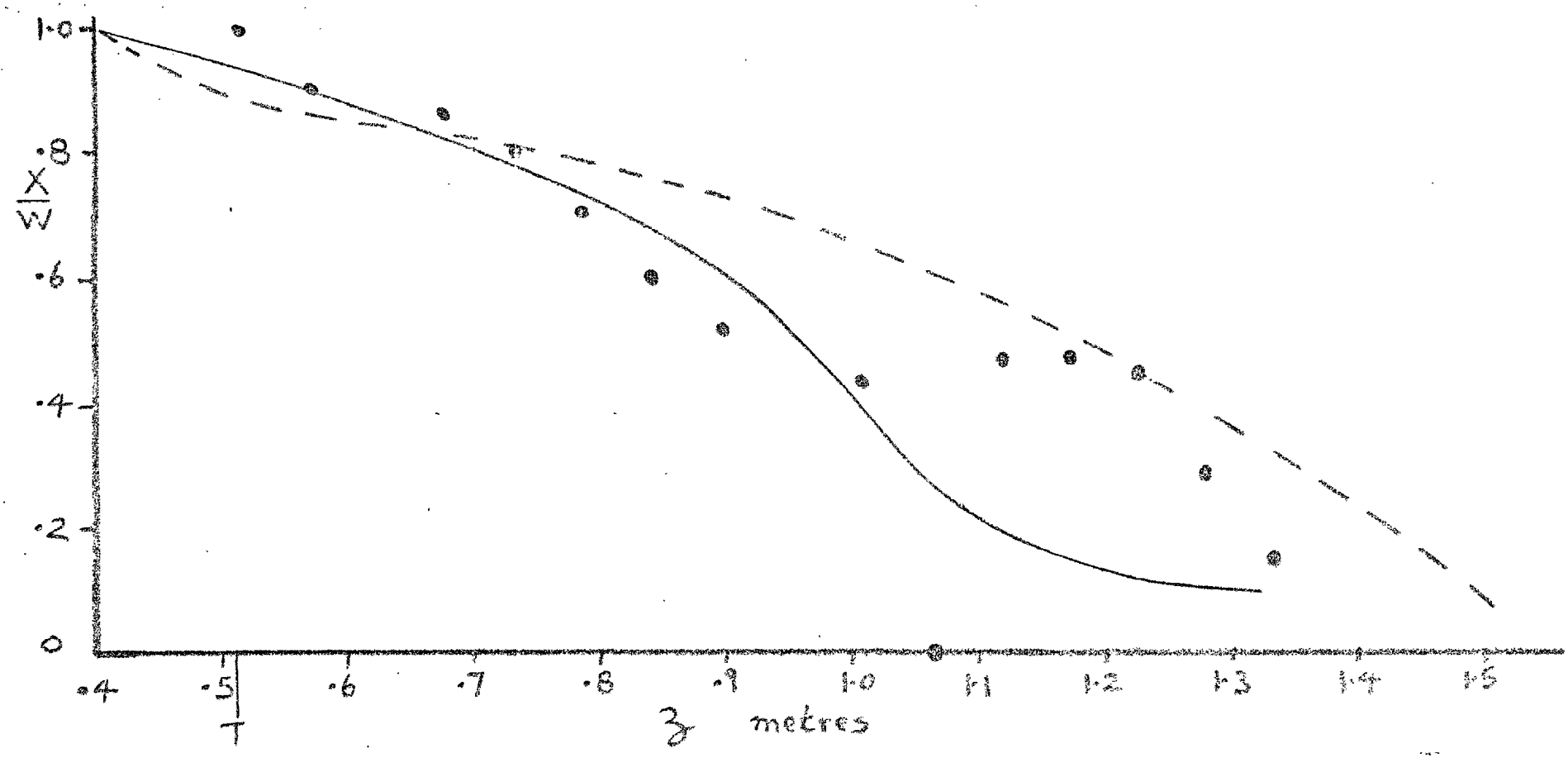


Figure 3.35

The experimental and theoretical solid bed profiles for experiment 25 with low density polyethylene powder. N(80); Q(203); D(3/32)

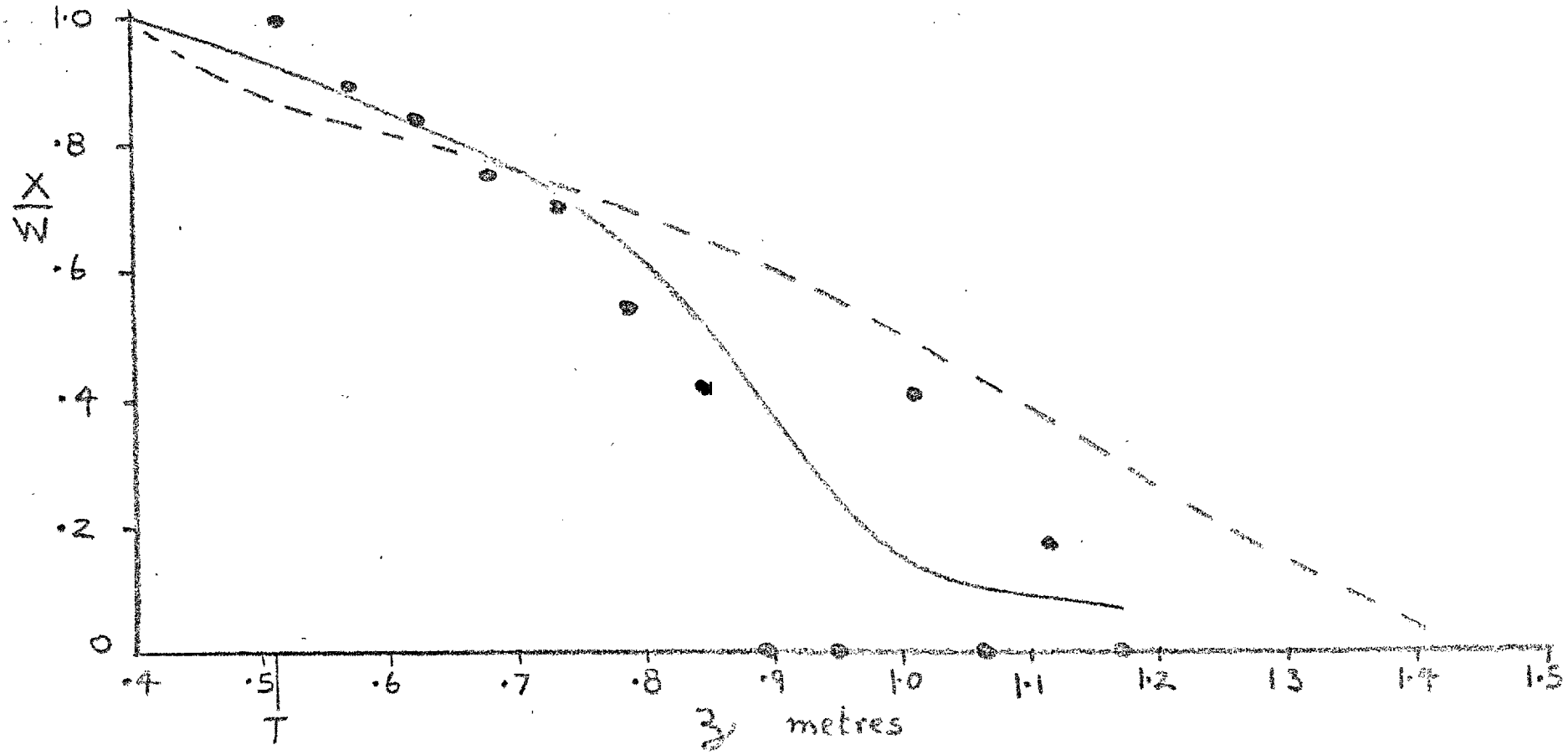


Figure 3.36

The experimental and theoretical solid bed profiles for experiment 26 with low density polyethylene powder N(40); Q(115); D(3/32)

Figure 3.37

The experimental and theoretical solid bed profiles for experiment 30 with rigid PVC powder. N(40); Q(185); D(3/32)

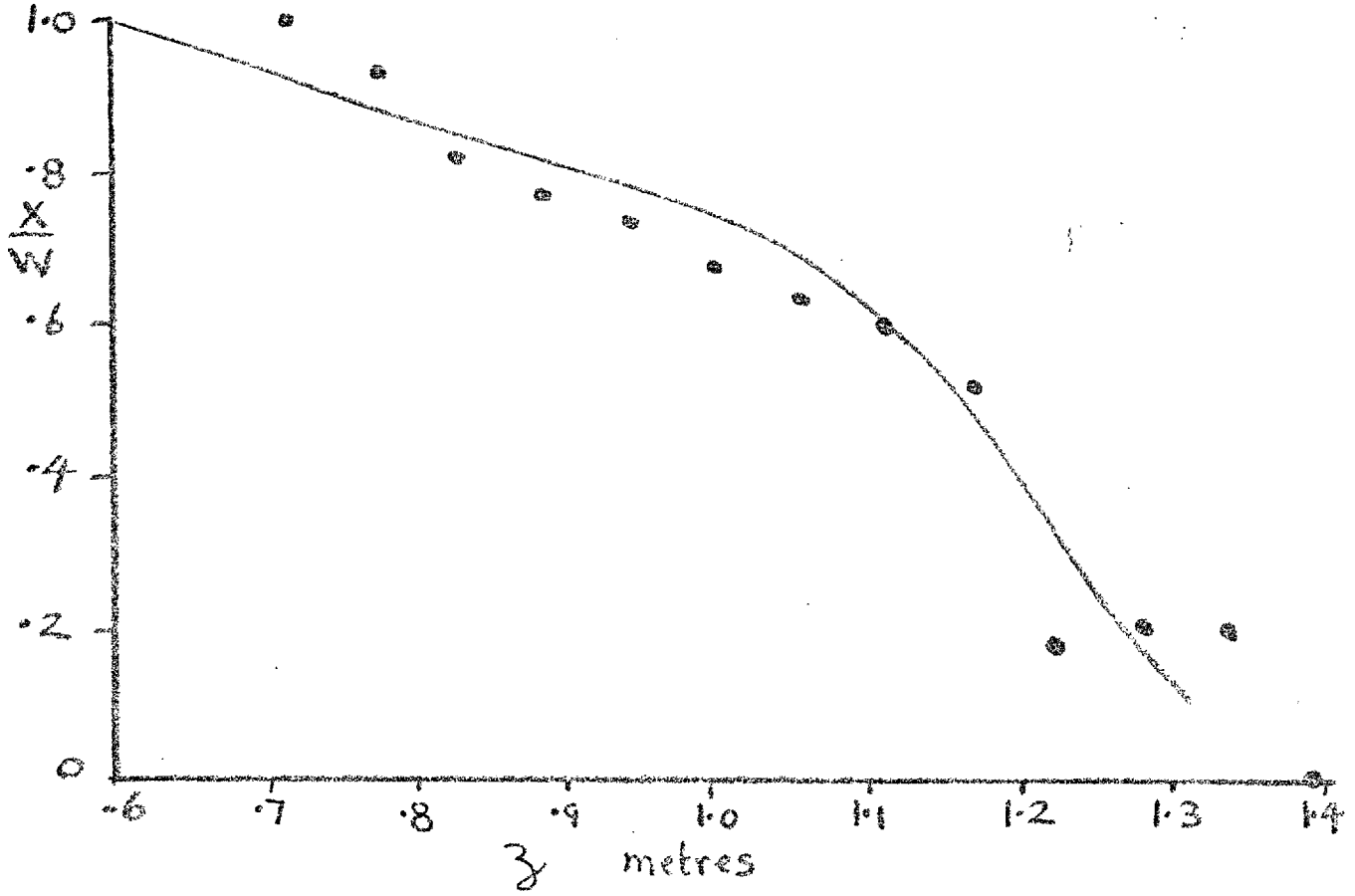


Figure 3.38

The experimental and theoretical pressure profiles for experiment 5 with low density polyethylene granules. N(80); Q(191); D(3/32)

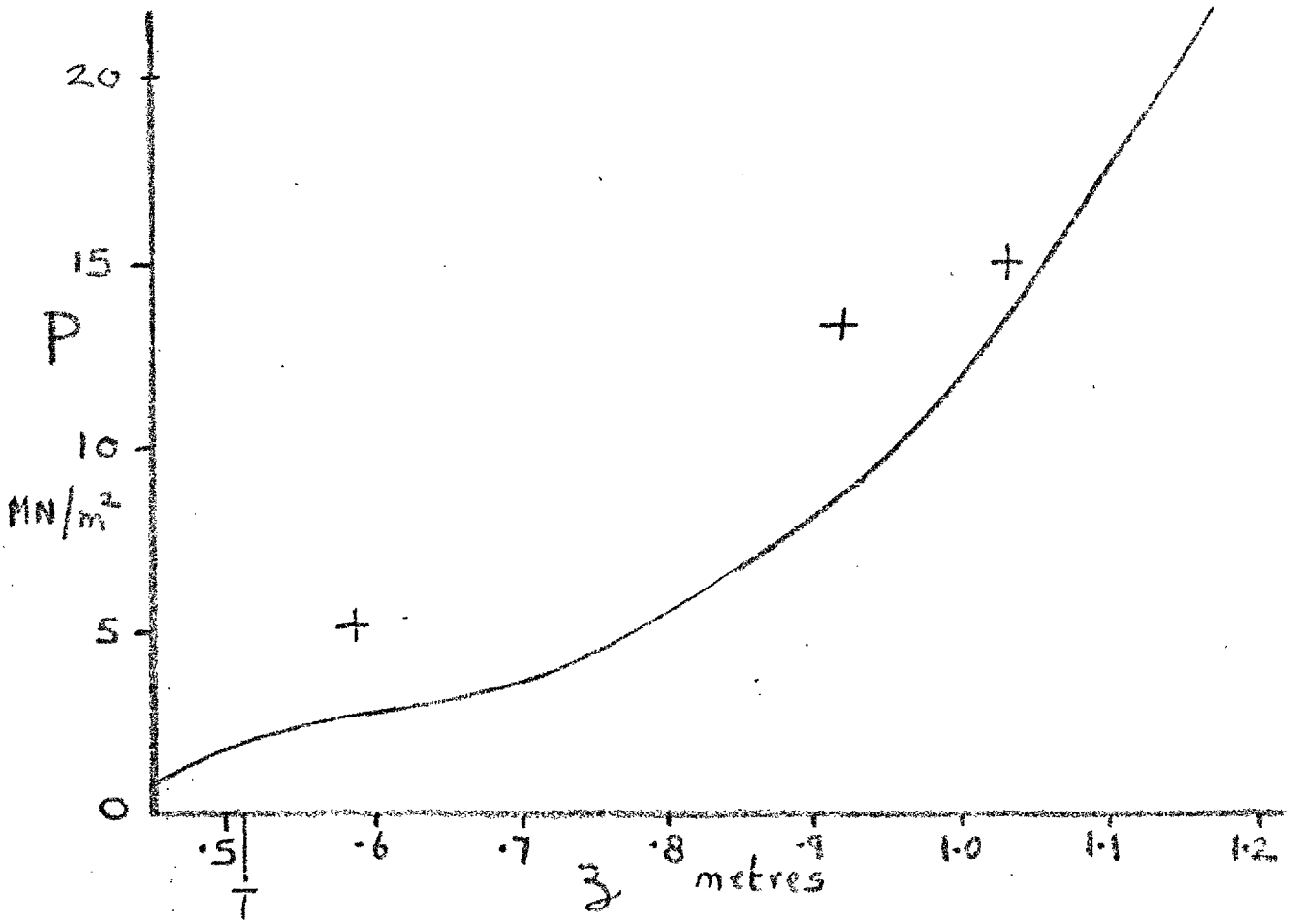


Figure 3.39

The experimental and theoretical pressure profiles for experiment 11 with polypropylene. N(80); Q(179); D(3/32)

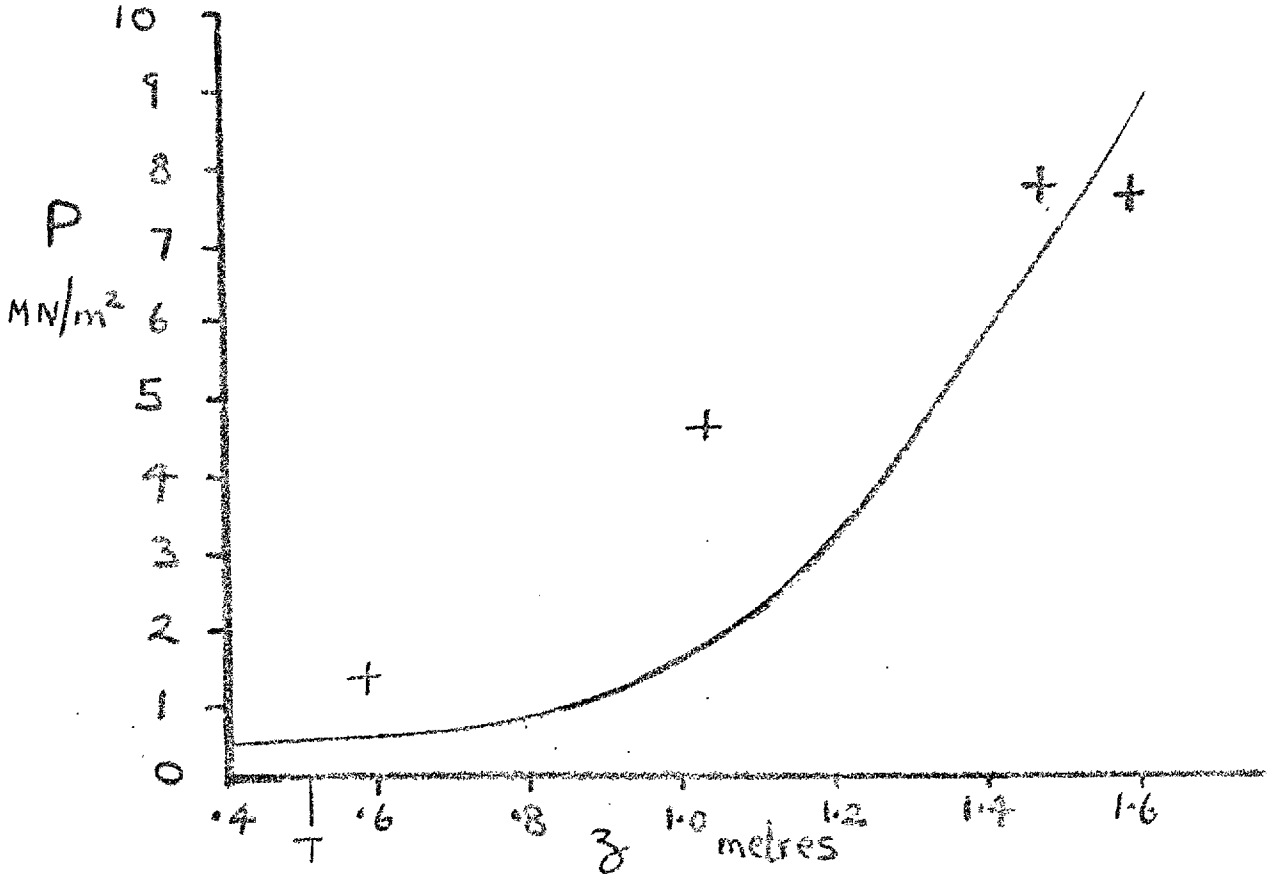


Figure 3.40

The experimental and theoretical pressure profiles for experiment 16 with high density polyethylene. N(40); Q(94); D(3/32)

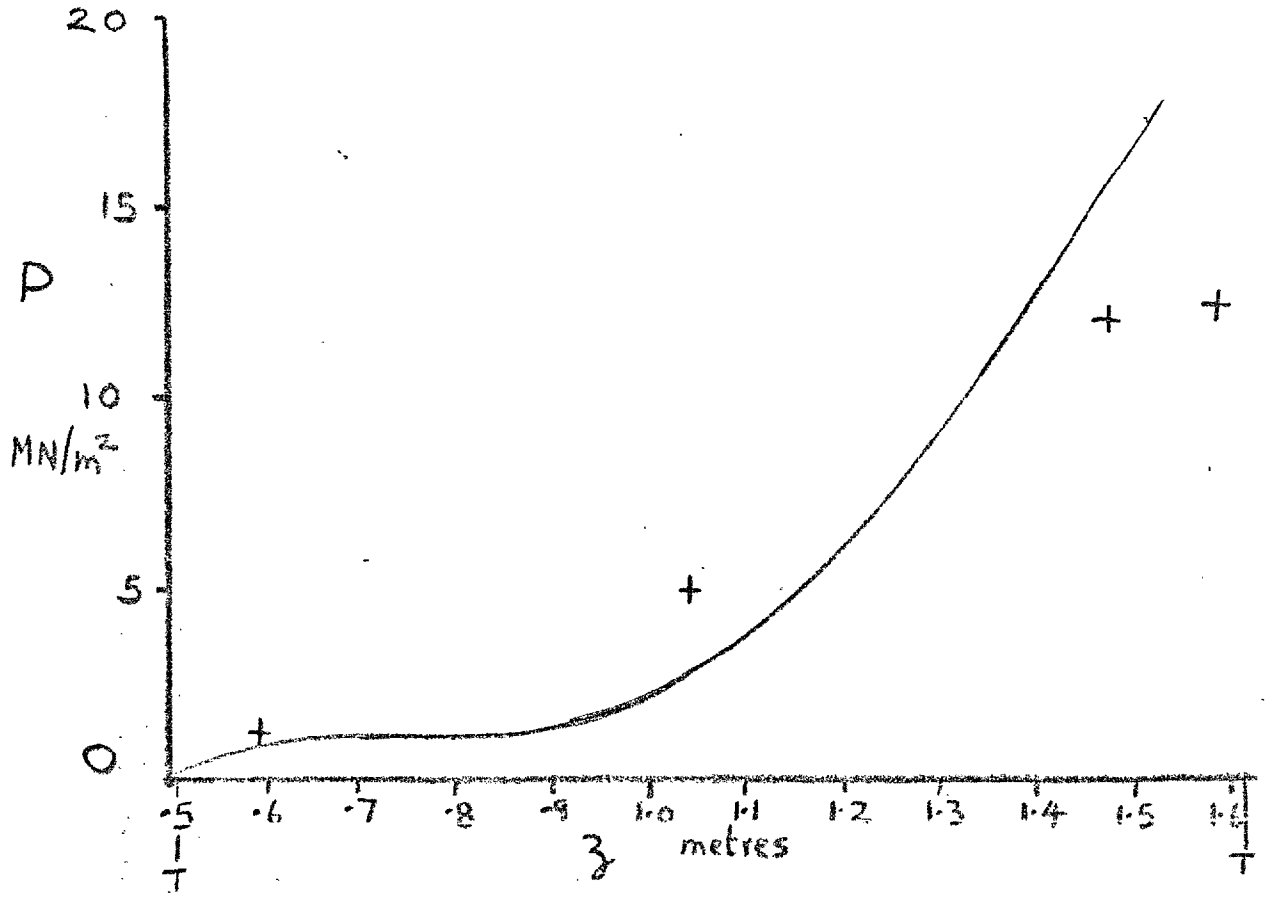


Figure 3.41

The experimental and theoretical pressure profiles for experiment 15 with high density polyethylene. N(80); Q(187); D(3/32)

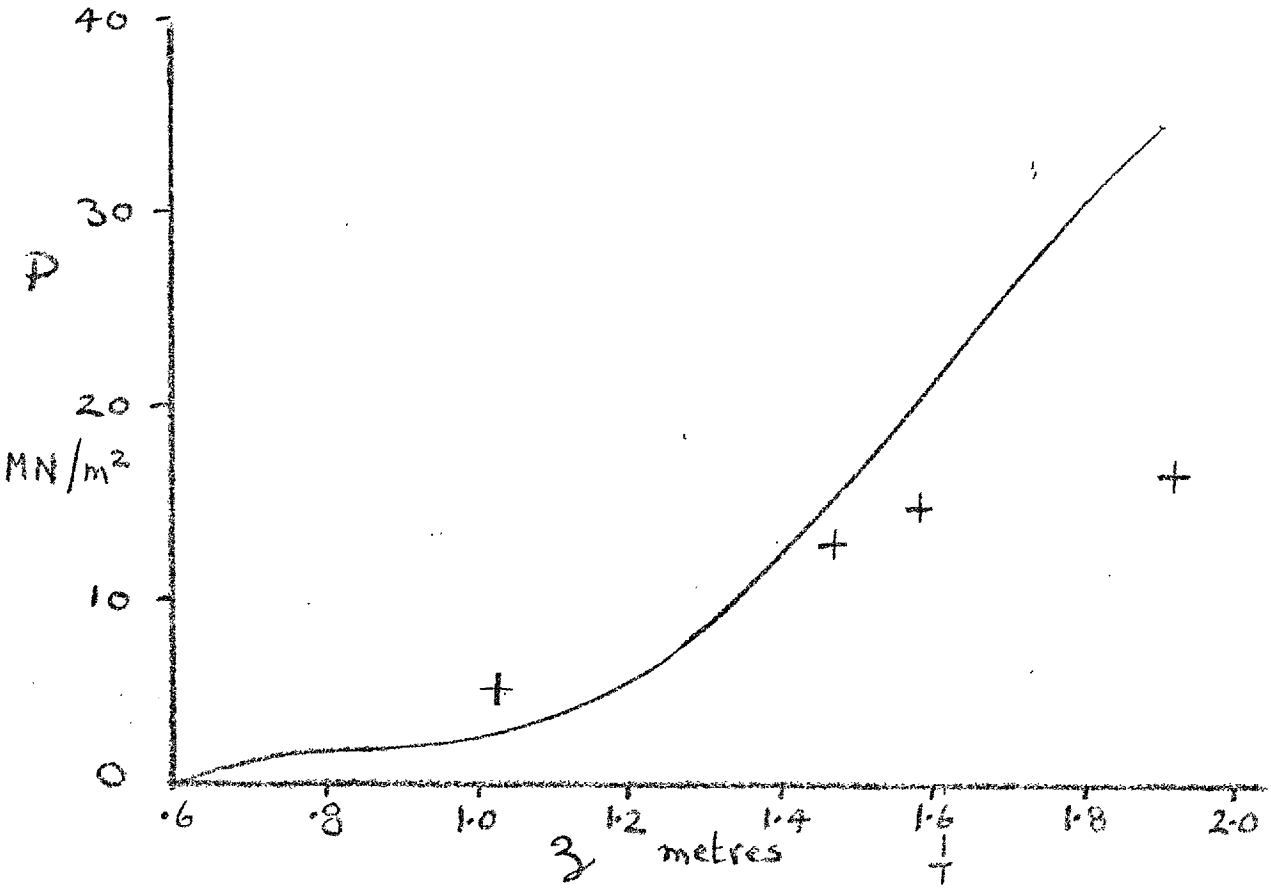


Figure 3.42

The experimental and theoretical pressure profiles for experiment 8 with low density polyethylene granules. N(80); Q(140); D(3/32). Screw cooling used.

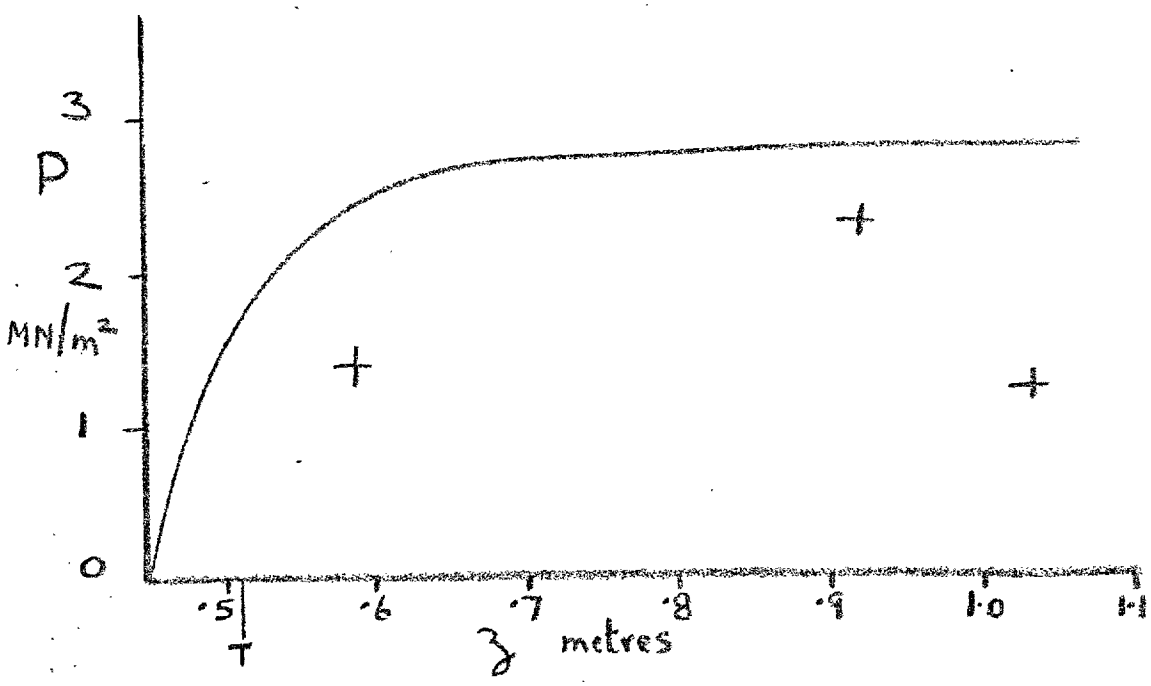


Figure 3.43

The experimental and theoretical pressure profiles for experiment 18 with high density polyethylene. N(80); Q(137); D(3/32). Screw cooling used.

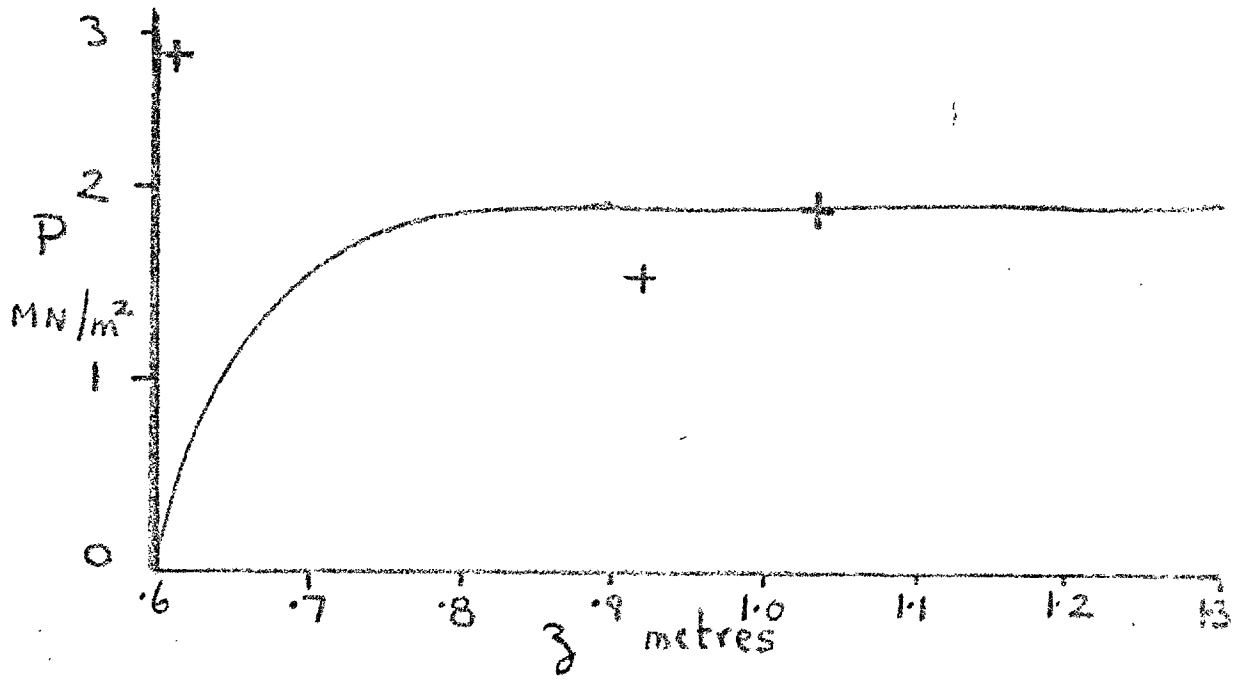
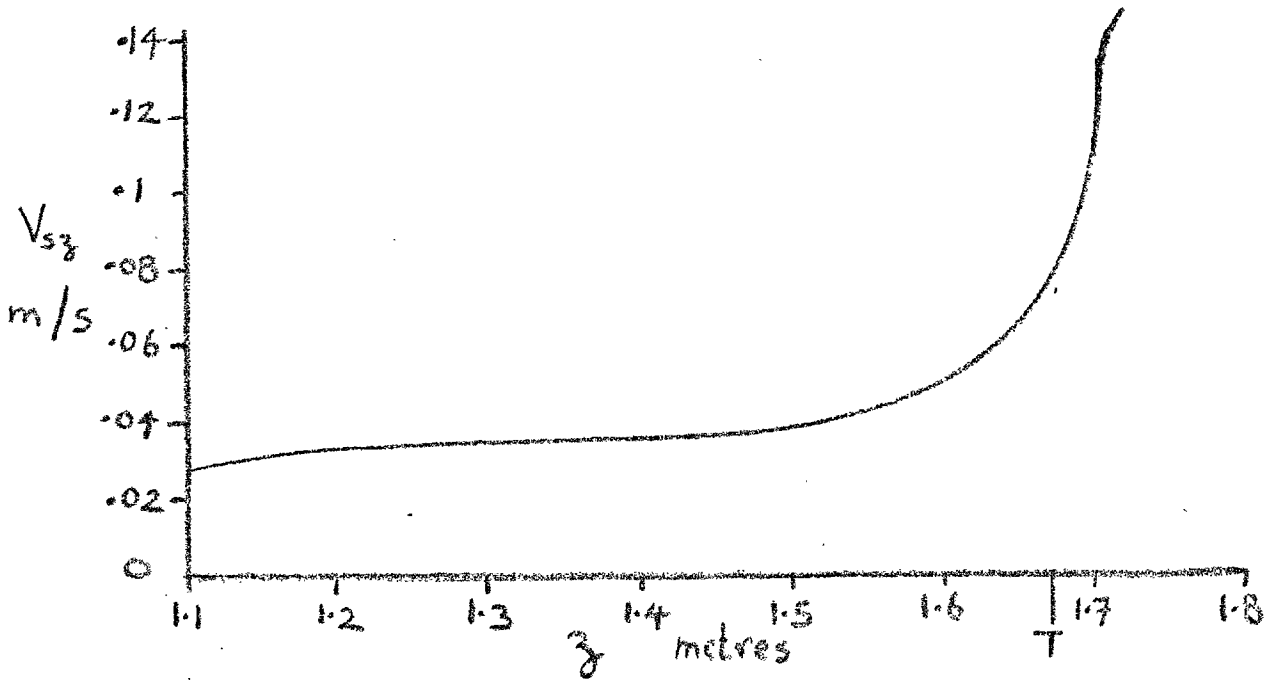


Figure 3.44

The theoretical solid bed velocity profile, experiment 1 for plasticised PVC. N(80); Q(360); D(3/32)



The pressure results for two of the experiments with screw cooling are shown in figures 3.42 and 3.43 for low and high density polyethylene respectively. Here the present analysis does not successfully predict the change in sign of the pressure gradient that is experimentally observed.

It would appear then that the present analysis gives generally good predictions of the melting profile but not of the pressure profile. Clearly if this is so, then the effect of the pressure gradient on the melting rate is a secondary one, though its effect on the solid bed acceleration and hence shape of the solid bed width profile may be more significant. This effect is discussed later.

There are several reasons why the analysis does not give accurate pressure predictions. Firstly, during the early stages of melting before the formation of the lower melt film, the pressure gradient is highly dependent on the coefficient of friction between the plastic and the screw root. Unfortunately data concerning such coefficients of friction is scarce and the variation of the coefficient with temperature is even less well documented. It is therefore difficult to know with any degree of certainty if a reasonably correct value is being used. Secondly the effect of the lower melt film, when it is present, on the pressure gradient calculation must be considered. It can be seen from the previously described figures showing the pressure profiles that, generally, when the lower melt film is present the predicted pressure gradient is higher than the actual one. Inspection of the equation (3.75) shows that one possible explanation for this is that the shear stress on the lower surface of the solid bed, τ^*_{zj}, is too small. The most obvious reason for this would be that the thickness of the lower film was too great. Observation of the experimental cross-sectional specimens in the Plates and inspection of the theoretical results shows that in general the predicted thickness of the lower melt film is larger than the actual thickness. The theoretical variation of the lower film thickness may be seen in figures 3.14 to 3.16 and compared with the corresponding experimental cross-sections shown in Plates 2(a), 5(a) and 14(a), bearing in mind that the width of the experimental specimens is approximately 3 centimetres. Thus it would seem that it is very

possible that the inaccuracy of the pressure gradient is due to an inaccuracy in the lower film thickness.

There is an obvious explanation for such an inaccuracy in the lower film thickness. Essentially the thickness will depend on the melting rate at the lower interface, in that all the material melting at that interface is retained in the lower melt film. The melting rate at the interface depends on the heat flux into the interface which has two main sources; viscous dissipation in the film; and heat conducted from the screw into the film. Now the thermal boundary condition used at the screw surface is the temperature and thus the heat flux from the screw to the film will essentially depend on the amount of viscous dissipation and the temperature difference between the screw and the melting point of the plastic. This heat flux in the theoretical model will not depend on the availability of heat in the screw itself. It has been stated by Martin (35) that heat flux back along the screw is likely to be insignificant in comparison with other heat fluxes in the extruder system. This may be interpreted as meaning the heat flux from the screw to the lower melt film will be an order of magnitude less than that from the barrel to the upper melt film. Inspection of these heat fluxes in the theoretical analysis shows that using the screw temperature as the relevant thermal boundary condition in the lower melt film analysis produces heat fluxes from the screw of the same order of magnitude as those across the barrel surface. Thus here is a potential source of error. It would seem that a more realistic thermal boundary condition at the screw surface would be zero temperature gradient. From the present evidence this would reduce the heat flux to the lower interface which in turn would reduce the melting rate there and this would lead to a generally thinner lower melt film. The reduction in thickness of this melt film would then give a lower pressure gradient and thereby potentially a more accurate one.

It is now appropriate to discuss the tolerable but consistent error in the melting profiles, namely the generally high predictions of solid bed width, especially with the screw cooling experiments. To do this one needs to look at the interaction of the acceleration of the solid bed on the melt pool flow

rate and the effect of the pressure gradient on the melt pool flow rate. In general the higher is the acceleration, the greater is the rate of reduction of the solid bed width. This, of course, means that the higher the acceleration is the wider is the melt pool, though the flow area of the melt pool also depends on the channel taper. Concentrating on one cross-section of the channel such that the channel depth is fixed, enables the effect of the change in solid bed width on the down-channel flow rate to be studied. Basically, once the melting rate is calculated the new solid's flow rate is determined and it only remains to manipulate the velocity and width of the solid bed to suit overall continuity. The higher the solid bed velocity, the smaller will the width need to be. In turn this means that the melt pool is wider. The combination of increasing melt pool width and increasing solid bed velocity will produce an increasing flow rate in the melt pool, since the width of the solid bed does not significantly affect the pressure gradient.

From the foregoing it can be seen that as the true solid bed width is often less than the predicted solid bed width, and as the melt pool flow rate would be larger if the predicted solid bed width were reduced, that is if it were predicted more accurately, then it follows that to retain the same melt pool flow rate and yet reduce the solid bed width, by predicting it more accurately, the pressure gradient would have to be increased. However it has already been seen that the pressure gradient predictions are too high! In other words the implication is that if the predictions of solid bed width were more accurate the pressure predictions would be less accurate.

This inconsistency is thought to be due to the error introduced into the melt pool flow rate calculation by the assumption that the fluid has a constant viscosity. Comparison between non-dimensional pressure gradient, π_p, and non-dimensional flow rate, π_q, for Newtonian and non-Newtonian fluids are given in several publications, see for example Fenner(29). Such comparisons show that for a given π_q the more non-Newtonian the fluid is, the lower is the corresponding π_p. Or for a given value of π_p the more non-Newtonian the fluid is, the lower is the flow rate π_q. Thus in the present case for the given pressure gradient and melt pool geometry the melt pool flow rate as

calculated is unrealistically high. Therefore the width of the melt pool is calculated to be smaller than it realistically is. In other words if the melt pool analysis were for a non-Newtonian fluid the general predictions of bed width would be lower, and therefore, potentially more accurate, since the melt pool would need to be wider to accomodate the required flow rate. In this way more accurate predictions of solid bed width should result without causing less accurate pressure predictions.

If in addition the correction to the lower melt film analysis was made, as discussed previously, then potentially improved pressure predictions would result as well. Such a reduction in pressure gradient would tend to oppose the reduction in solid bed width caused by the introduction of a non-Newtonian melt pool analysis. Without obtaining comparative solutions it is not possible to say how significant this interaction would be.

It is now useful to study the theoretical predictions of solid bed velocity. Figures 3.14,3.44 and 3.45 show the results for three plasticised PVC experiments. It is easy to see from figure 3.14 that the acceleration of the solid bed whilst it is of significant size is moderate and uniform. In experiments 1 and 4 the acceleration of the solid bed increased rapidly but not until approximately 80% of the plastic had melted. In which case the more rapid acceleration is of little significance.

Figure 3.15 shows the results of experiment 9 for low density polyethylene granules. Here it can be seen that the solid bed has a region of high acceleration. The beginning of which corresponds approximately to the observed bed break-up point. It can also be seen in this figure how the region of high acceleration produces a rapid reduction in solid bed width. This reduction in solid bed width produces in turn a reduction in the upper film thickness. Also,the increasing solid bed velocity reduces the rate of increase of the lower melt film thickness.

Figure 3.16 shows similar results for low density polyethylene powder. Notice again how the start of the region of high acceleration corresponds to the position of solid bed break-up.

Figures 3.46 and 3.47 show the solid bed velocity variation for the two Melinex

Figure 3.45

The theoretical solid bed velocity profile, experiment 4, for plasticised PVC. N(40); Q(201); D(1/16)

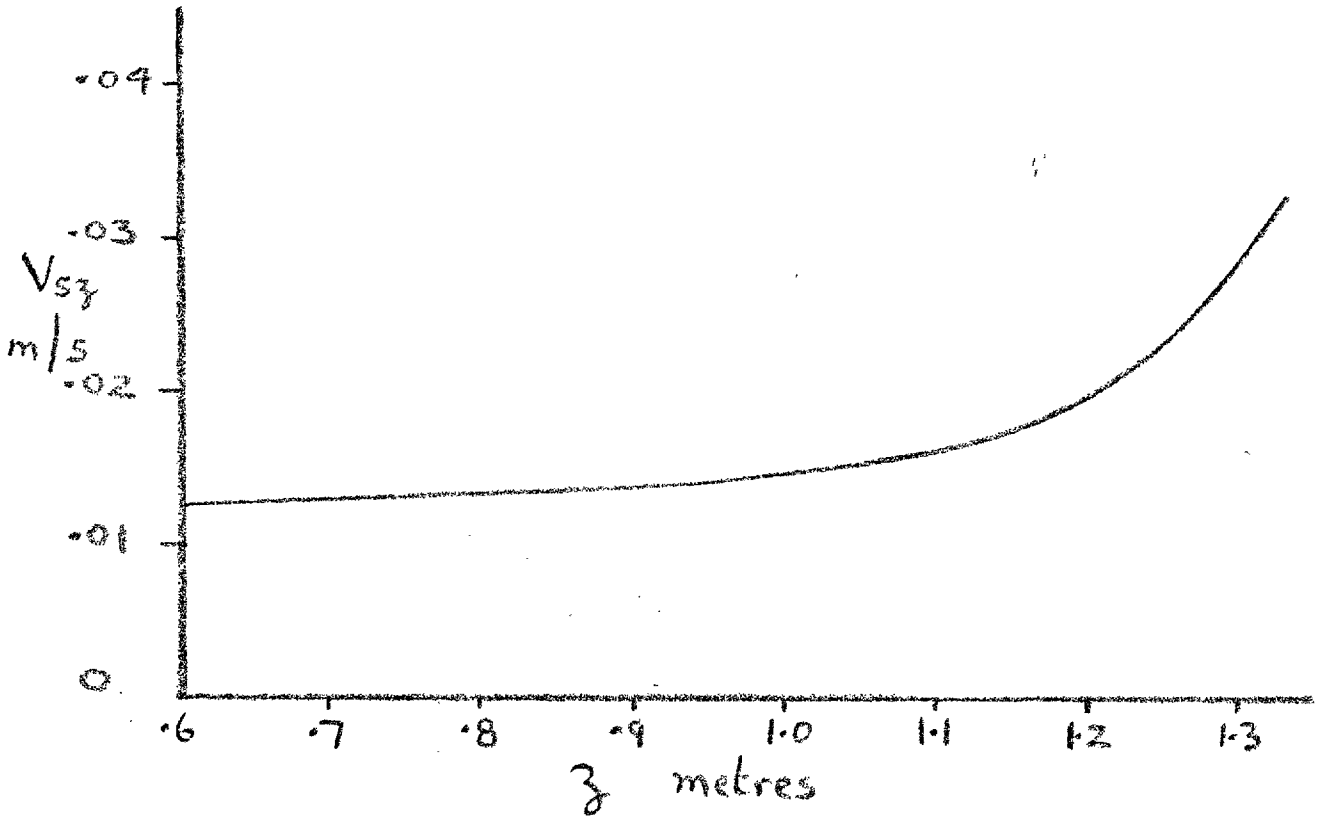


Figure 3.46

The theoretical solid bed velocity profile, experiment 23, for Melinex. N(80); Q(319); D(3/32)

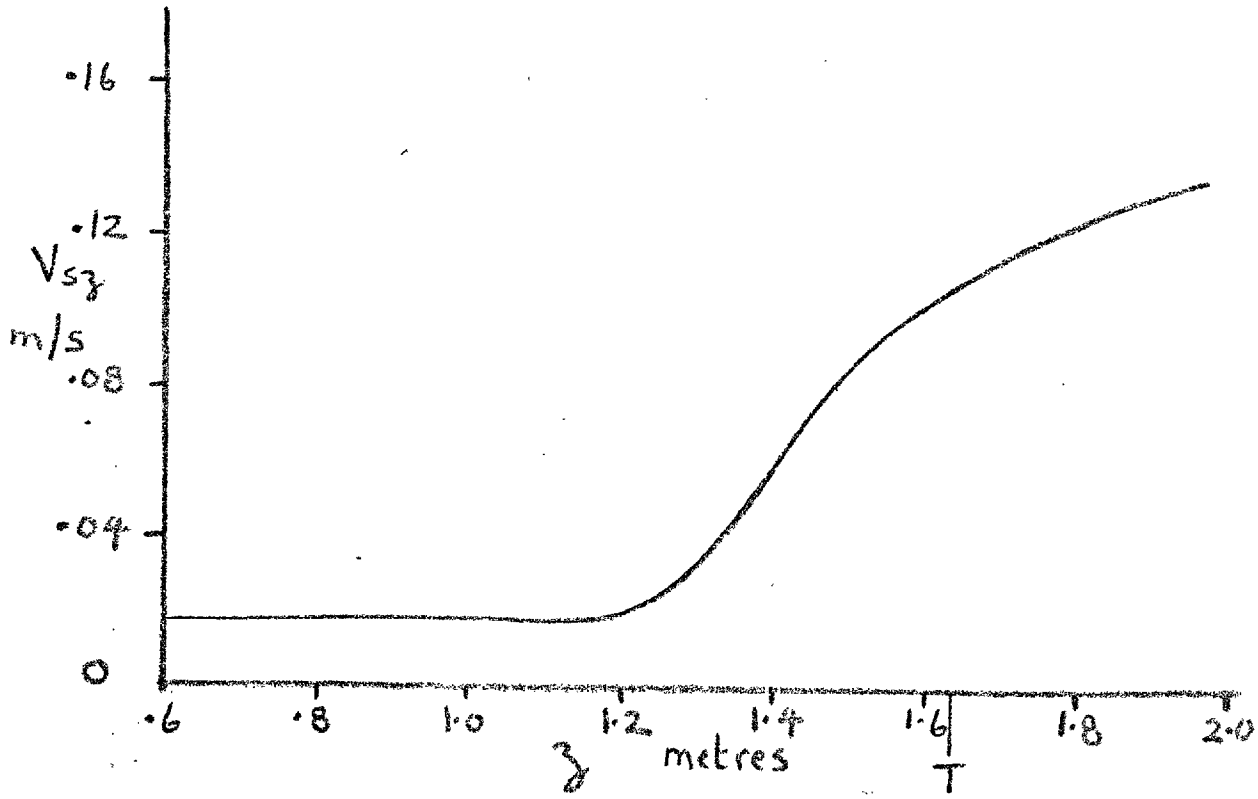


Figure 3.47

The theoretical solid bed velocity profile, experiment 24, for Melinex. N(40); Q(164); D(3/32)

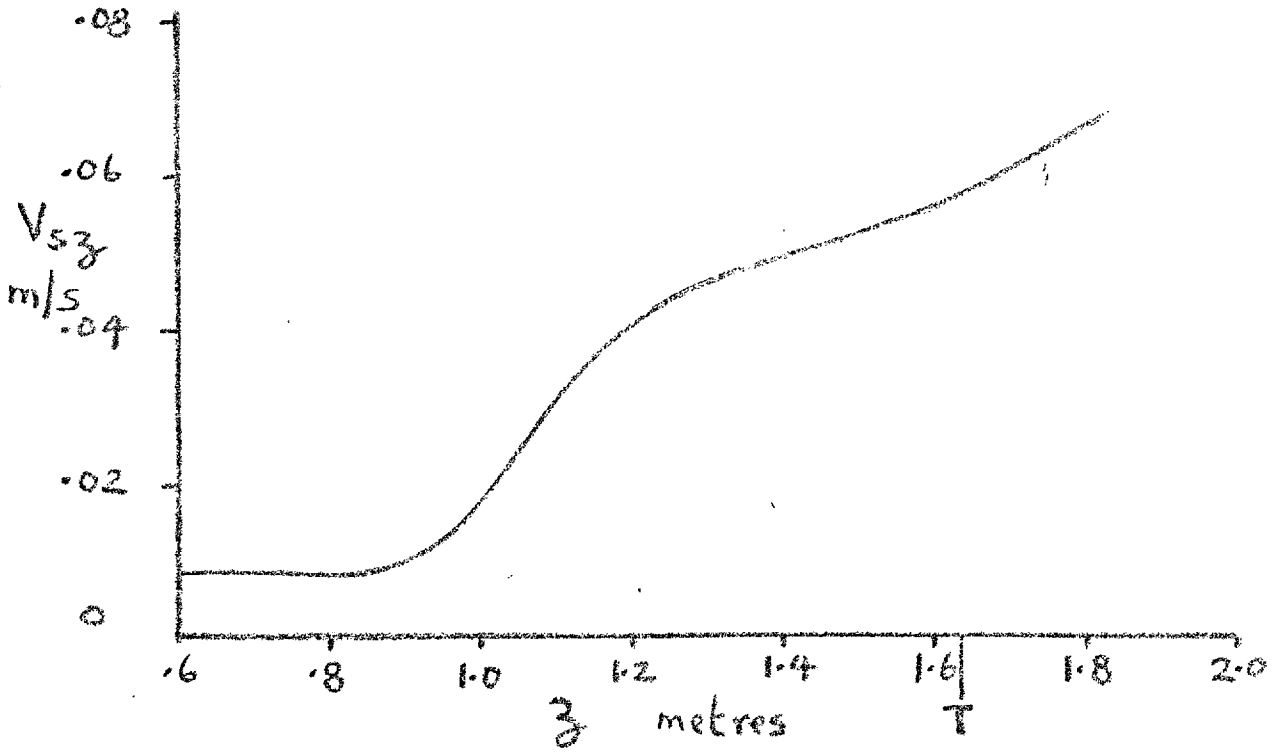
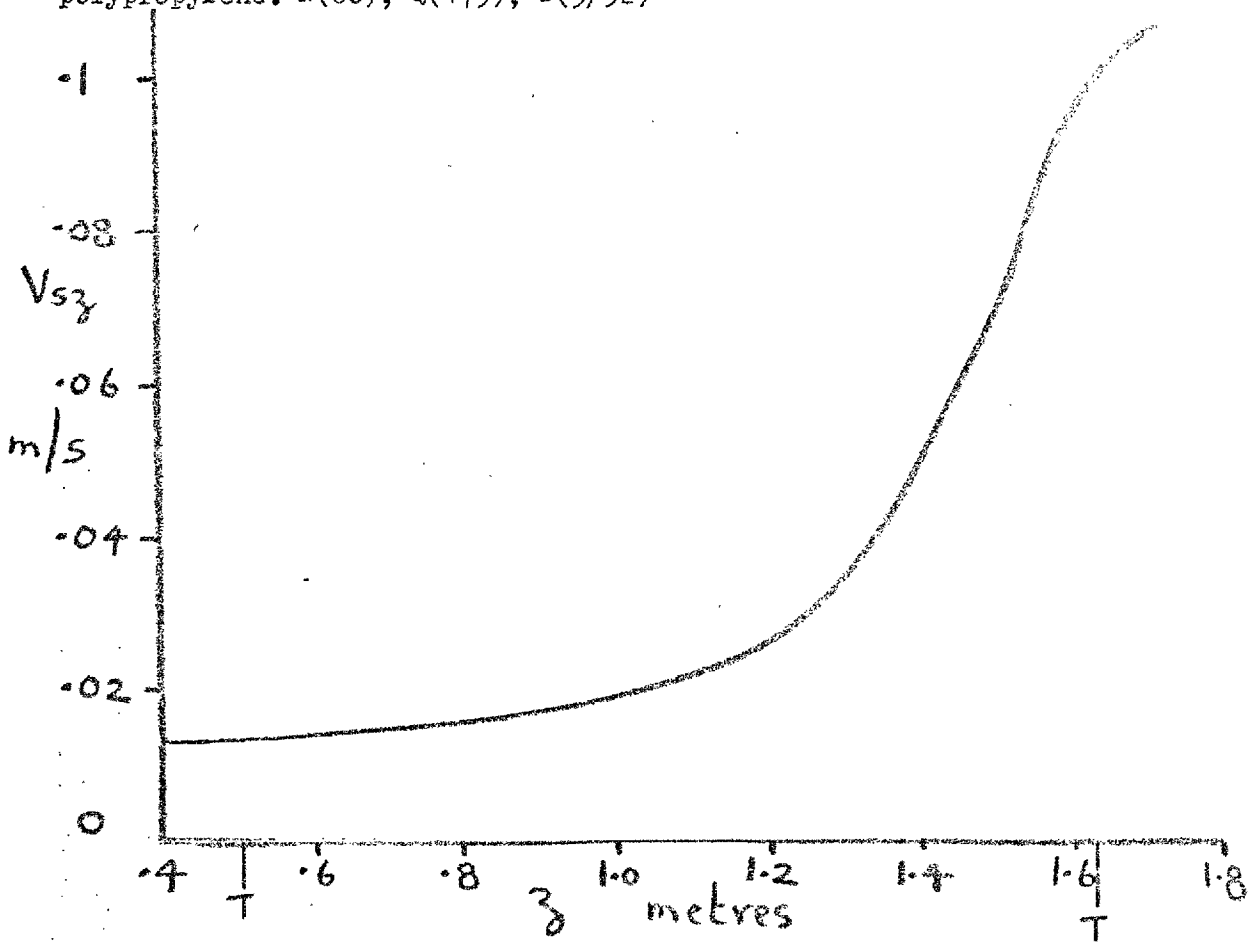


Figure 3.48

The theoretical solid bed velocity profile, experiment 11 for polypropylene. N(80); Q(179); D(3/32)



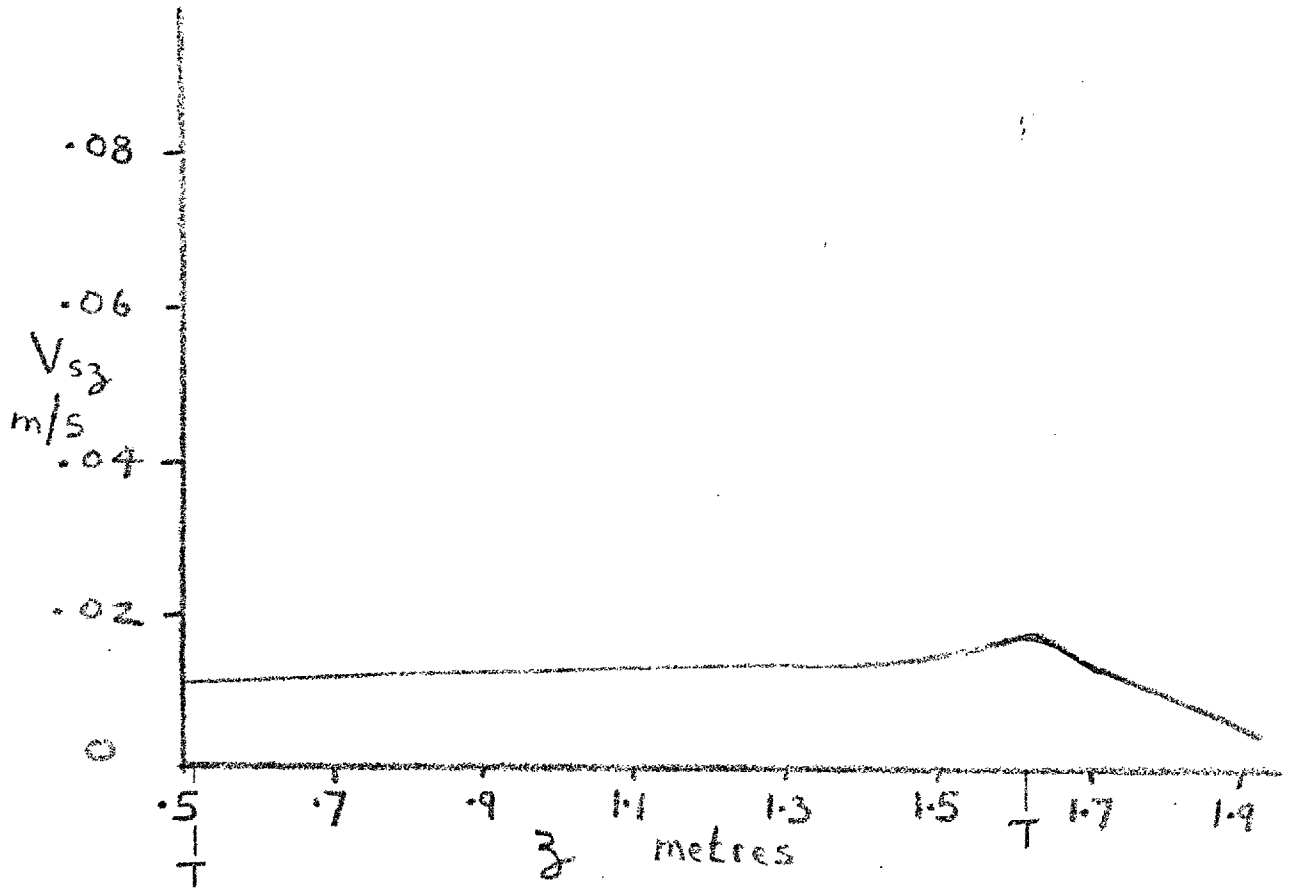
experiments. Here the initial point of high acceleration corresponds to the point of bed break and also the point of formation of the lower melt film. For the other materials the point of formation of the lower melt film preceeded the experimental bed break-up point and the theoretical high acceleration region by up to several 'turns' of the screw, depending on conditions. Figure 3.48 shows results for polypropylene simulating experiment 11. Again the point of bed break-up corresponds to the beginning of the region of high acceleration. Figure 3.49 shows the simulated results for the corresponding experiment performed with screw cooling. It is immediately noticeable that the analysis predicts that no violent solid bed acceleration takes place in the absence of a lower melt film.

The conclusions to be drawn from the foregoing theoretical and experimental results in that the theoretical analysis agrees with the experiments in that if solid bed break-up occurs then the corresponding simulation predicts a region of high solid bed acceleration, the beginning of which occurs whilst there is still a significant amount of unmolten material. If experimentally there is no bed break-up and no screw cooling then the theory predicts no high acceleration before most of the material has become molten. If, experimentally, there is screw cooling and therefore no bed break-up then the theory predicts no region of high acceleration at all.

These are conclusions based on essentially qualitative comparisons. The final solid bed velocities, in the cases where high accelerations occur, are predicted to be anything up to an order of magnitude larger than the initial solid bed velocities. The experimental indications suggest that the actual velocity change is probably much less than this. The results tabulated in Table 2.4 suggest that a tripling of the velocity is as much as is likely to happen. It is thought possible that the magnitude and extent of the solid bed acceleration in the theoretical predictions is greater that it realistically is, partly because of the incorrect and high pressure gradient. Of course, in practice the solid bed breaks because it cannot withstand the stresses on it that tend to produce rapid accelerations, so that the bed does not actually undergo rapid acceleration. The theory does not take account of any break in the solid

Figure 3.49

The theoretical solid bed velocity profile, experiment 14, for polypropylene N(80); Q(143); D(5/32). Screw cooling used.



bed and perhaps therefore it necessarily predicts these very high final bed velocities. A concluding discussion of solid bed break-up, its causes and occurrence, will be given in the next chapter after the presentation of some more relevant theoretical results.

3.6.4: Conclusions

It has been shown in this section that the present melting analysis described in the earlier sections of this chapter can make adequate predictions of the melting behaviour of a wide range of plastics and over a fair range of operating conditions. It can also make useful predictions of solid bed acceleration which can be used to predict the occurrence of solid bed break-up in practice. In its present form the model does not give particularly good predictions of pressure.

It is thought that if two modifications were to be made to the detailed analysis of the problem then significant improvements in the accuracy of the predictions of pressure and solid bed width would be obtained. The first of these modifications is to specify zero temperature gradient at the interface between the lower melt film and the screw surface. The second is to replace the Newtonian melt pool flow analysis by a non-Newtonian one.

The next chapter attempts to show amongst other things how the theory in its present form can be made use of in simulating extrusion trials from several different points of view.

Chapter 4 : Theoretical Simulations and Conclusions

4.1 : Introduction

Having developed a theoretical analysis of the melting region in single screw extruders and shown that the results obtained from it are, for the most part, in good agreement with experimental results, it is now proposed to present some results obtained from the analysis for a variety of simulated extrusion trials.

It was stated in the introduction to the present work that there are three main uses to which a theoretical analysis can be put; to aid in extruder design; to aid in developing plastics having better processing performance; and to optimise extruder operating conditions in particular applications. There is not scope in the present work to comprehensively and completely demonstrate the use of the analysis in each of these three areas. Rather than concentrate on one particular application it was thought better to present as wide a range of results as possible to indicate areas where more extensive and detailed use of the analysis could yield practically useful results and hence reduce the need for potentially costly experimentation.

In the field of extruder design results are given which show the effect of varying the overall 'compression ratio' of the screw, that is, the ratio of the channel cross-sectional area in the feed zone to that in the metering zone, on the melting behaviour. Other results are given showing the effect of the rapidity of taper with a constant compression ratio and the effect of extruder size on its melting performance is illustrated. With regard to the latter effect two 'scale-up' laws are investigated.

As regards the processing behaviour of materials, some results are presented which show the effect on the melting performance of varying various thermal and flow properties of the material.

In the area of optimising operating conditions the effect of varying degrees of screw cooling is investigated and the effect of flight clearance on the melting performance demonstrated.

In the concluding section to this chapter various aspects of the theoretical results presented in this and the preceding chapter are used to discuss the

phenomenon of solid bed break-up. Lastly the manner in which the present melting analysis may be combined with analyses of the other parts of the extrusion process is indicated.

4.2 : Theoretical Simulations concerning Extruder Design

Figures 4.1 and 4.2 show the effect on the solid bed width profile and down-channel solid bed velocity, respectively, of varying the screw 'compression ratio the taper length remaining constant. The properties of the material used in all the extruder design simulations are given in Table 4.1. The geometric data and operating conditions for the compression ratio simulations are given in Table 4.2. Basically everything was held constant except the compression ratio and hence the metering section channel depth.

It is apparent from the results that as the compression ratio is increased so the acceleration of the solid bed begins earlier, has a higher maximum value and ultimately achieves a higher velocity. It should be noted that the length of the compression section corresponds to just under nine turns of the 2.5 inch (63.5 millemetre) diameter screw which is used as the basis of the simulation. In the figures the helical positions of the start and finish of the tapered zone are indicated on the Z co-ordinate axis by T's.

It should be pointed out that on the basis of these results it cannot be inferred nor be suggested that with,say, a two turn compression section that similar trends would be observed. A study of the full computer output showed that varying the compression ratio does not significantly affect the true melting rate in the various cases. The results of the predictions for the 4 : 1 and 8 : 1 compression ratio's show that at a certain point in the compression section the pressure reaches a maximum, and thereafter the pressure gradient continues negative until zero pressure is predicted and the program stops. These points of peak pressure are indicated in the figures by a P. It would thus seem that for the given data both an 8 :1 and a 4 : 1 compression ratio are too high.

Figures 4.3 and 4.4 show the effect on the solid bed width profile and down-channel solid bed velocity profile respectively, of varying the length of the

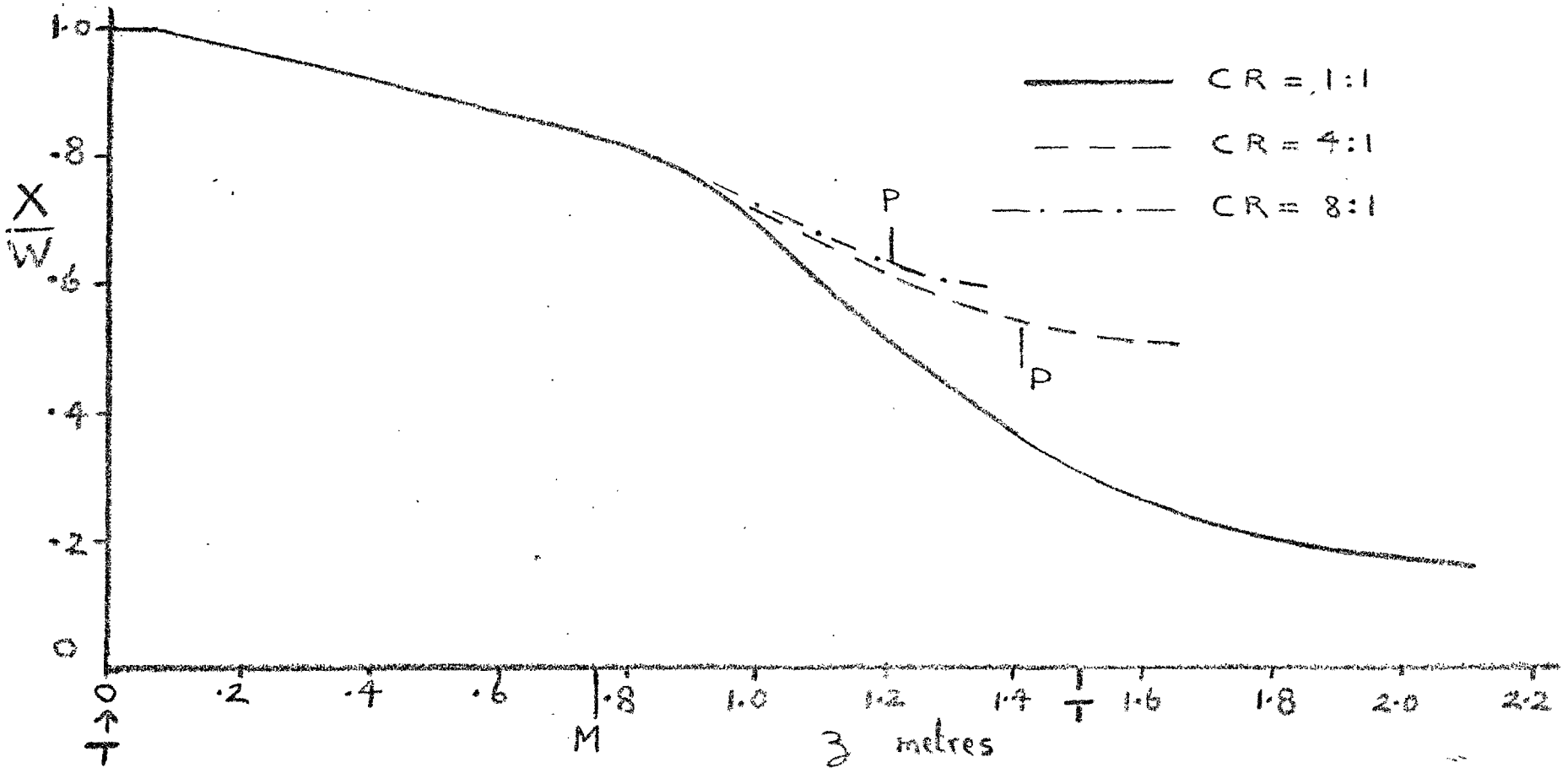


Figure 4.1

Theoretical predictions of the effect of varying the screw compression ratio on the solid bed profile

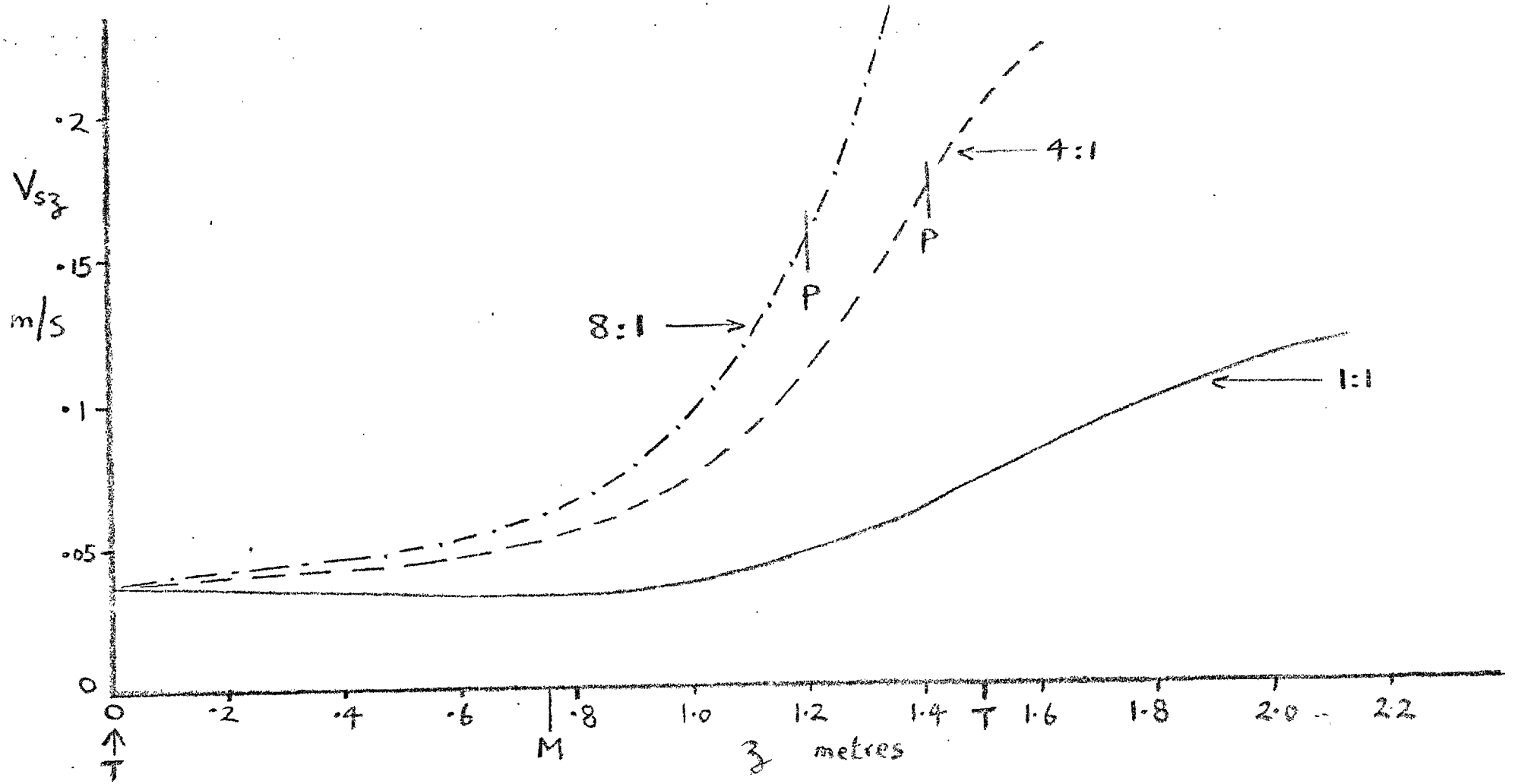


Figure 4.2

Theoretical predictions of the effect of varying the screw compression ratio on the solid bed velocity profile

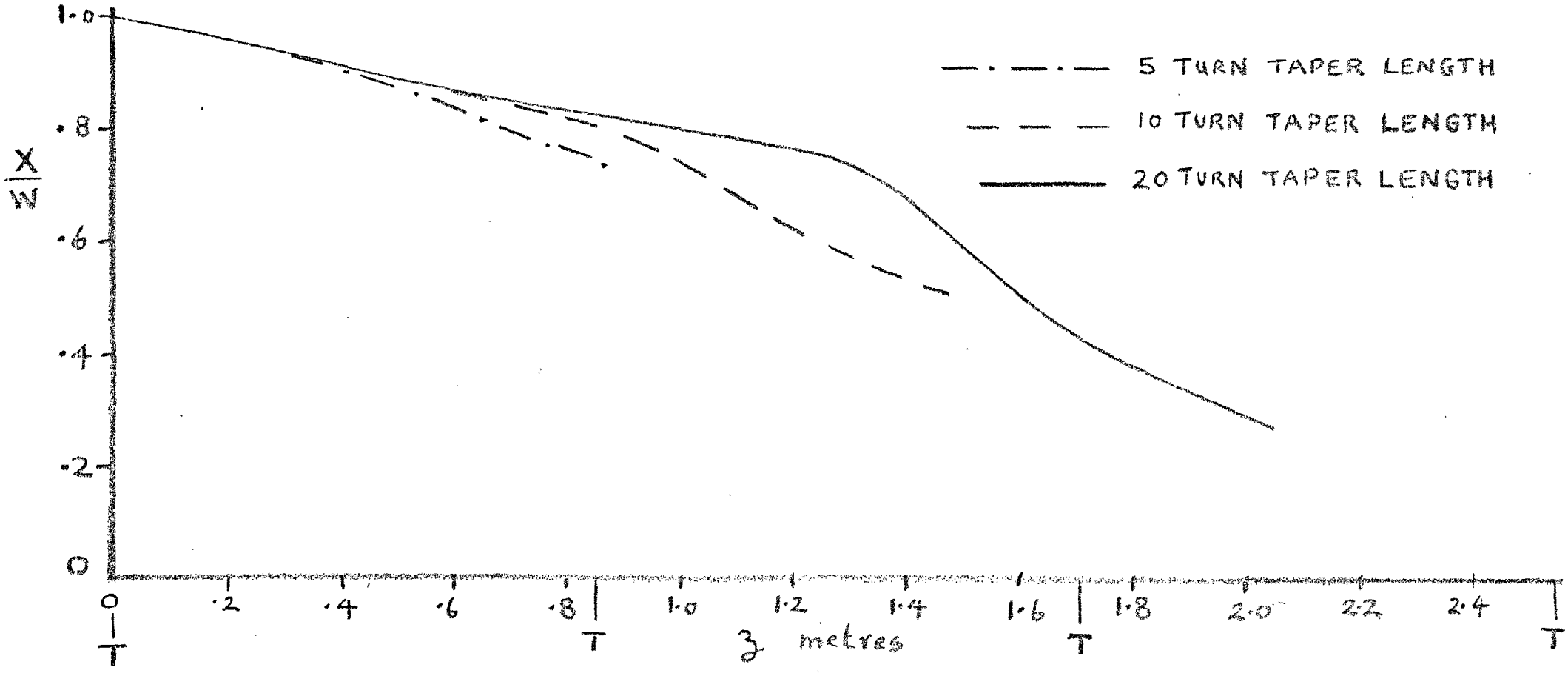


Figure 4.3

Theoretical predictions of the effect of varying the length of the tapered section of the screw on the solid bed profile

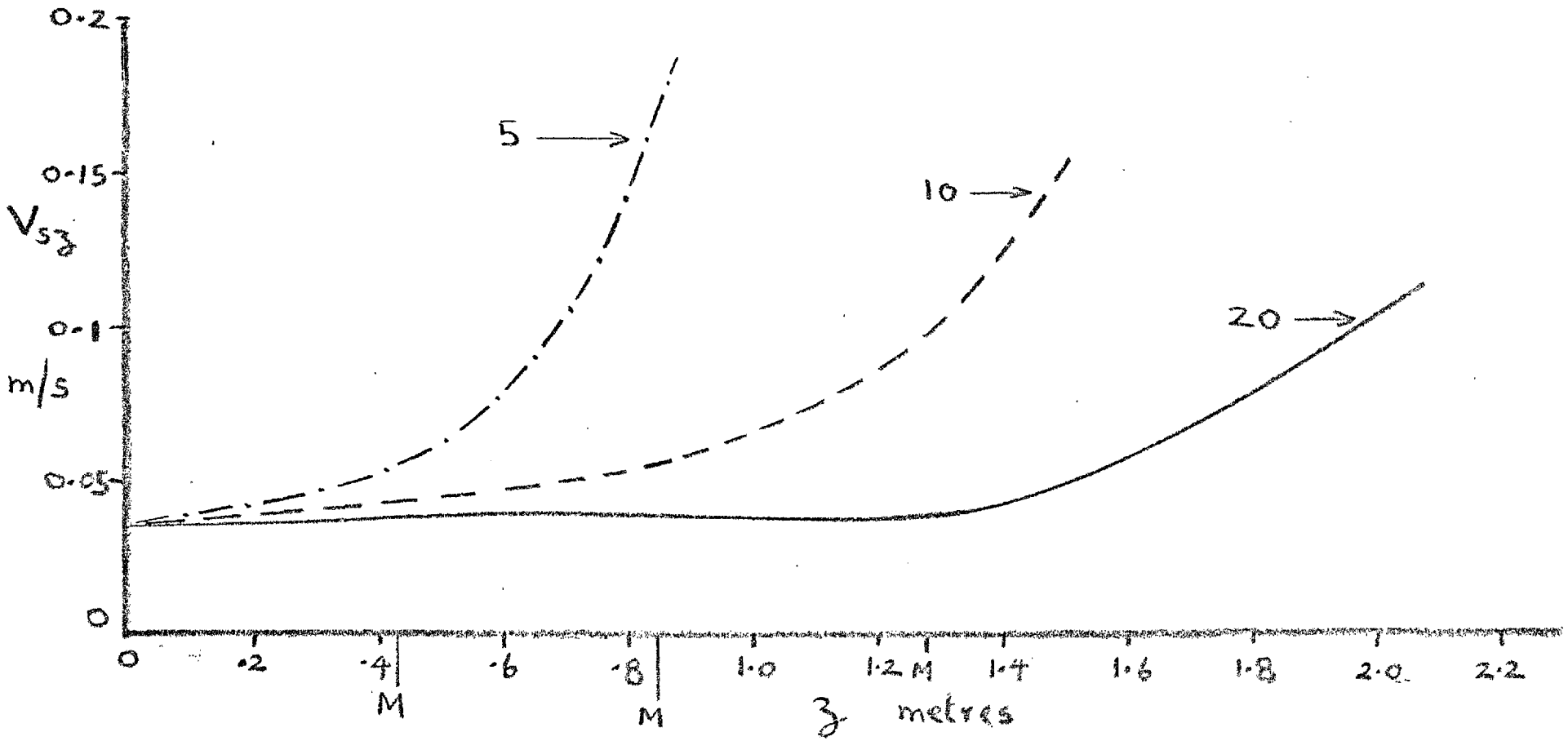


Figure 4.4

Theoretical predictions of the effect of varying the length of the tapered section of the screw on the solid bed velocity profile

Table 4.1

The properties of the material (low density polyethylene) used in the extruder design simulations.

Property	Value
Density of solid, ρ_s , kg/m^3	880
Density of melt, ρ_m , kg/m^3	750
Specific heat of solid, C_s , J/kg^oC	3000
Specific heat of melt, C_m , J/kg^oC	2100
Latent heat of fusion, λ , J/kg	50000
Melting point, T_m , ^oC	110
Thermal conductivity of melt, k_m , J/m^oCs	0.346
Thermal conductivity of solid, k_s , J/m^oCs	0.3075
Datum viscosity, η_D , Ns/m^2	6895
Power law index, n .	0.5
Temperature sensitivity of viscosity, b , $^oC^{-1}$	0.01
Datum temperature of viscosity, T_D , ^oC	140

	Compression Ratio Variation				Taper length Variation		
	1	2	3	4	1	2	3
Channel width, ,m	.0541	.0541	.0541	.0541	.0541	.0541	.0541
Feed section channel depth, ,m	.0105	.0105	.0105	.0105	.0105	.0105	.0105
Coefficient of channel taper, , m/m	0.0	.0035	.005215	.00613	.00921	.004605	.0023025
Flight clearance, , m	.0001	.0001	.0001	.0001	.0001	.0001	.0001
Helix angle	17.65	17.65	17.65	17.65	17.65	17.65	17.65
Screw diameter, ,m	.0635	.0635	.0635	.0635	.0635	.0635	.0635
Feed zone length, m	0.0	0.0	0.0	0.0	0.0	0.0	0.0
Taper zone length, m	1.5	1.5	1.5	1.5	.8525	1.705	2.5575
Screw Speed, , r.p.m.	80	80	80	80	80	80	80
Flow rate, , kg/s	.0189	.0189	.0189	.0189	.0189	.0189	.0189
Barrel temperature, , C	150	150	150	150	150	150	150
Initial temperature, , C	20	20	20	20	20	20	20
Screw melt point	.75	.75	.75	.75	.427	.852	1.278

Table 4.2

The Geometric Data and Operating conditions used in the Compression Ratio and Screw Taper Simulations

compression section assuming a constant ratio of 4 :1. The details of the different screw geometries are given in Table 4.2. It can be seen how the solid bed acceleration and velocity increases as the length of the compression section is reduced. This is similar to the results of figures 4.1 and 4.2 in that as the coefficient of channel taper increases so does the solid bed velocity. It should be noted that the point of formation of the lower melt film was taken to be half way along the tapered section so that the results of figures 4.1 and 4.2 are not strictly comparable with those of figures 4.3 and 4.4 even though the other data is similar. The point of formation of the lower melt film is indicated by an M in the figures.

Notwithstanding the foregoing comments it is interesting to compare the results for the 10 turn taper section in figure 4.4 with those for the 4.1 compression ratio screw in figure 4.2 since the data for these two is very similar. For the 10 turn taper section no pressure peak was observed in the results indicating that it therefore constituted a workable screw design whilst the slightly shorter taper length would not. It would seem that for this particular flow rate, material, and geometry a 10 turn compression zone with a 4 : 1 compression ratio represents some form of limit to possible screw designs.

It would be easy to conclude from the above results that the best screw design is one with zero taper. This however is not necessarily the correct interpretation of the results. The effect of beginning melting in a non-tapered section but continuing in a tapered section has not been investigated, neither has the behaviour with very short compression sections. Further the model assumes that at the beginning of melting the solid bed is fully compacted and that its density equals that of the solid material. In practice such compaction may not satisfactorily occur without some degree of channel taper. Thus what may be concluded from figures 4.1 to 4.4 is that for the particular data of those simulations and assuming the solid bed to be fully compacted at the start of the melting region, then no channel taper after the start of melting will give the most stable melting behaviour.

Some results concerning scale-up of extruder design are now presented. The data which forms the basis of these simulations is taken from a paper entitled

'Some Melt Flow and Mechanical Design Aspects of Large Extruders'. by R.T Fenner and J.G. Williams (40). Two different scale-up rules are investigated from melting performance aspects. By scale-up is meant making predictions of the performance of essentially large diameter extruders from a knowledge of the performance of smaller machines.

It was suggested (40) that an ideal method of scale-up, from the melt flow point of view would involve holding two critical non-dimensional quantities constant. These two quantities are the Peclet number, P_e , where

$$P_e = \rho_m V_{bz} H_c c_m / k_m \qquad (4.1)$$

and a viscous heating parameter, π_H , where

$$\pi_H = 1 - \exp(-b \Delta T) \qquad (4.2)$$

where b is the normal temperature sensitivity of viscosity in the power law constitutive equation; and

$$\Delta T = \bar{\tau} \bar{\gamma} H_c / 2 k_m \qquad (4.3)$$

The Peclet number expresses the ratio between thermal convection effects in the melt flow. It is normally high in polymer melt flows, 10^3 - 10^5 typically, indicating the importance of thermal convection.

The non-dimensional group π_H is a measure of the effect of the temperature variation through the melt caused by the conduction of heat generated by viscous dissipation. If the value of π_H is zero then this indicates that any temperature rise due to dissipation has negligible effect on the viscosity. If the value of π_H approaches unity the practical effect is that the material is likely to overheat if it reaches the fully developed state.

It is shown (40) that it is not practical to hold both P_e and π_H constant during scale-up because to do so would involve very low output rates for the larger size machines.

The first practical rule of scale-up to be investigated is one proposed by Maddock. Basically the metering section channel depth, H , is defined as

$$H = H_A \sqrt{\frac{D}{D_A}} \qquad (4.4)$$

where D_A =6 inch ; $H_A = 0.05 . D_A$

and the screw speed is defined as

$$N = N_A \sqrt{\frac{D_A}{D}} \qquad (4.5)$$

where N_A = 60 r.p.m. and is the speed of the 6 inch size machine.

Using these relationships and the results for output rates quoted in (40), three different size screw geometres were formulated based on 2,6, and 10 inch diameter extruders (50.8, 152.4 and 254 millemetre respectively). To enable complete specification of the geometry for the melting region it was assumed that the overall compression ratio was 3:1 and the length of taper section was 15 turns, for all screw diameters. The details of the screw geometries and the operating conditions are given in Table 4.3 under scale-up 'A'. The material properties are given in Table 4.1.

Using this scale up law it was shown (40) that both P_e and π_H rise substantially as the diameter rises. An alternative procedure was suggested. This involved using the same variation of channel depth, equation (4.4), but to maintain π_H constant. Results were presented for $\pi_H = 0.99$. It was shown that this method gave a much more nearly constant Peclet number. Using the results presented in (40) for this alternative scale-up law three more screw geometries were formulated, these are detailed together with the operating conditions in Table 4.3 under scale-up 'B'.

The results of the melting analysis for scale-up 'A' are given in figure 4.5, those for scale-up 'B' are given in figure 4.6. The results are presented in non-dimensional form to enable the effect of the scale-up rules to be observed. The melting rate, is the true melting, that is, the ratio of solids flow rate to total flow rate. The solid bed velocity is plotted as the ratio of bed velocity to down-channel barrel velocity. Both these variables are plotted against the axial screw position in'turns'.

It can be seen that both scale-up rules work well in terms of melting rate, in that the non-dimensional melting profiles are very nearly co-incident. Of the two, scale-up 'B' is slightly the better. However, inspection of the solid bed velocity profile shows that as screw diameter is increased so the solid bed acceleration increases. Again scale-up 'B' is slightly the better in this respect, in that the variation of solid bed acceleration with screw diameter is less than that given by the predictions of scale-up 'A'. However

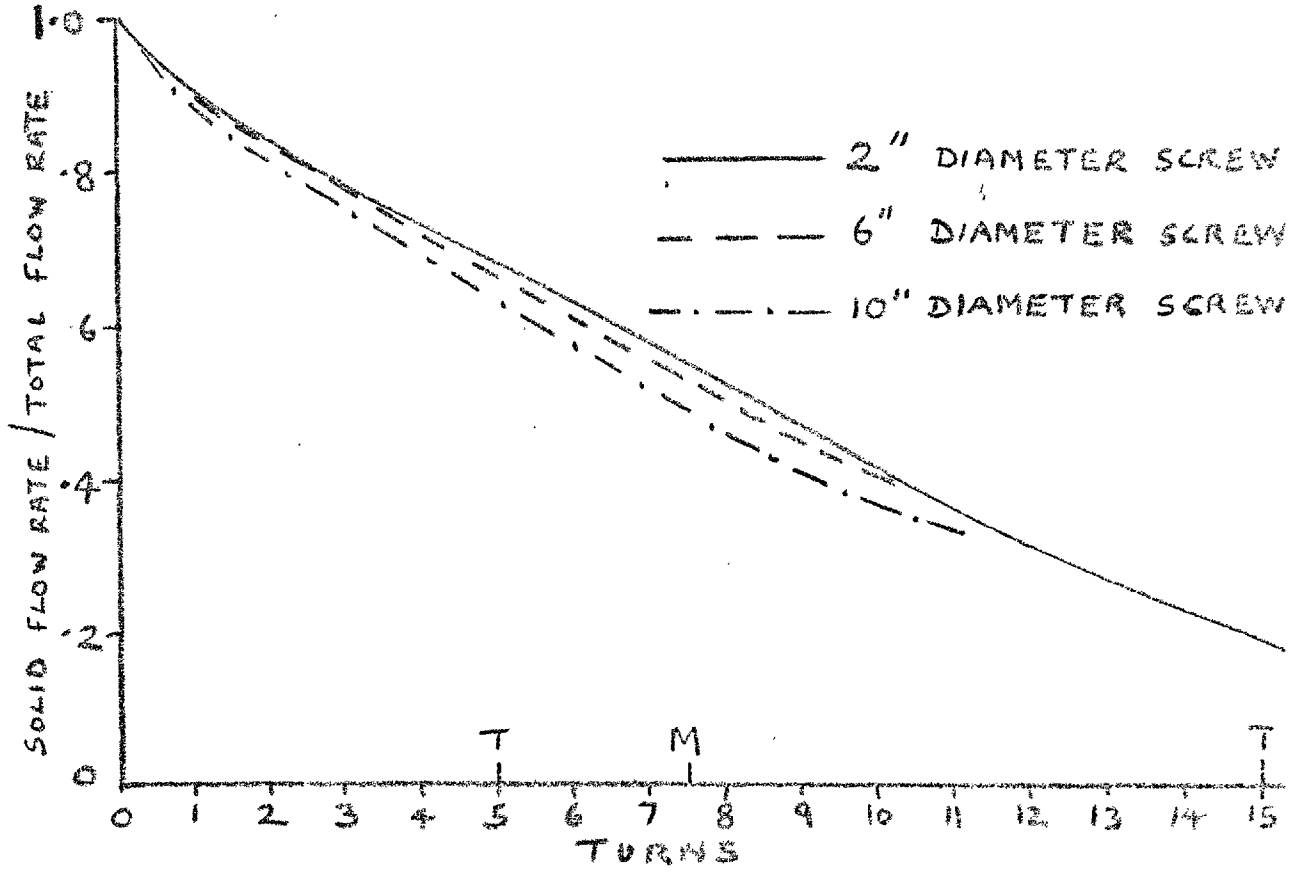
	Scale-up A			Scale-up B		
	1	2	3	1	2	3
Channel width, W, m	.0436	.1307	.2179	.0436	.1307	.2179
Feed section channel depth, H_0, m	.0132	.0229	.0295	.0132	.0229	.0295
Coefficient of channel taper, B, m/m	.004135	.002214	.00168	.004135	.002214	.00168
Flight clearance, e, m	.0001	.0001	.0001	.0001	.0001	.0001
Helix angle, Θ	17.65	17.65	17.65	17.65	17.65	17.65
Screw diameter, D, m	.0508	.1524	.254	.0508	.1524	.254
Feed zone length, m	0.0	0.0	0.0	0.0	0.0	0.0
Taper zone length, m	2.127	6.876	11.71	2.127	6.876	11.71
Screw Speed, N, r.p.m.	104	60	46	320	86	46
flow rate, M_T, kg/s	.0148	.141	.3854	.0377	.193	.3854
Barrel temperature, T_b, C	150	150	150	150	150	150
Initial temperature, T_0, C	20	20	20	20	20	20
Screw melt point, m	1.0635	3.438	5.855	1.0635	3.438	5.855

Table 4.3

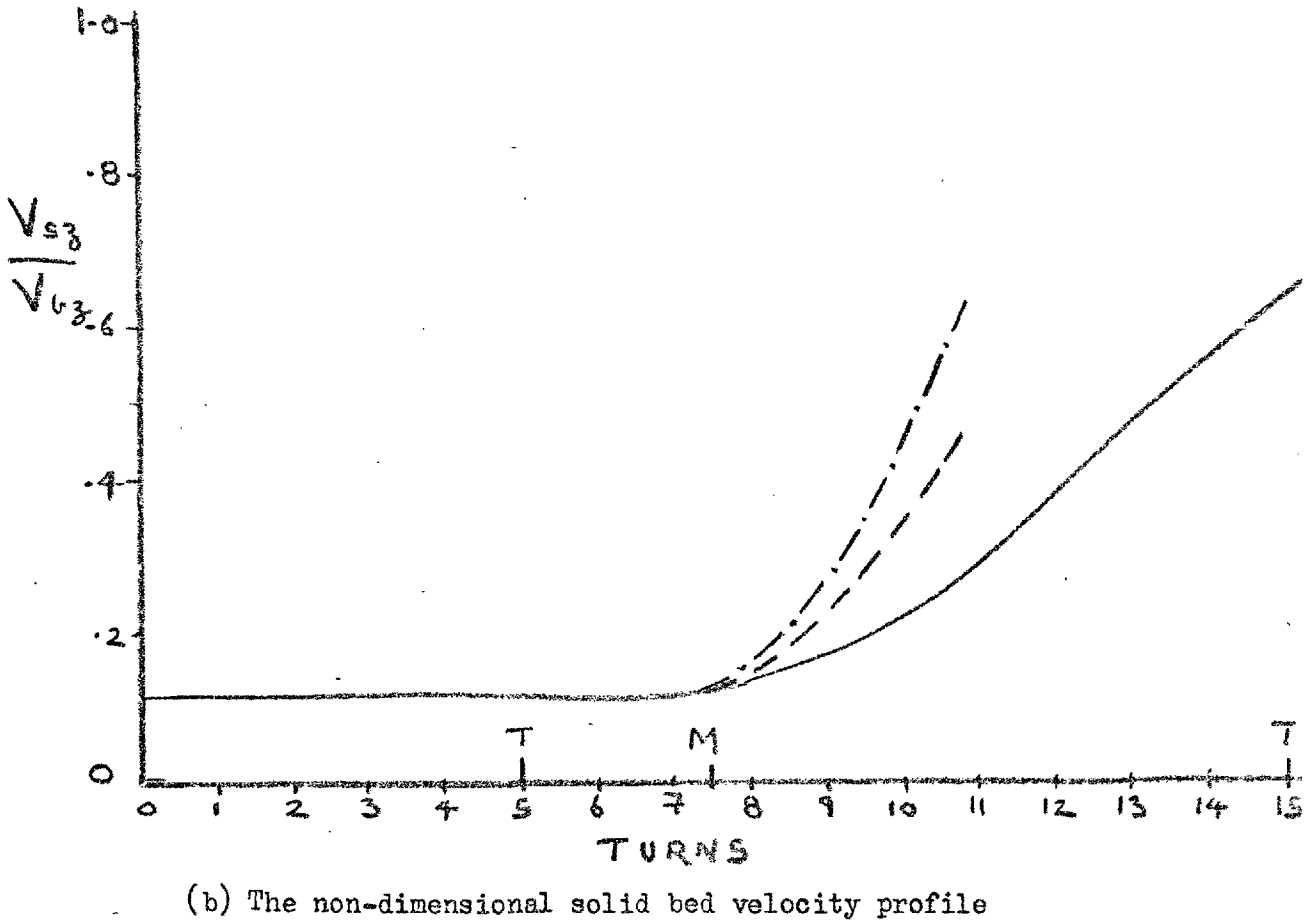
The Geometric Data and Operating Conditions used in the Scale-Up Simulations

Figure 4.5

Theoretical predictions resulting from the application of scale-up law A.



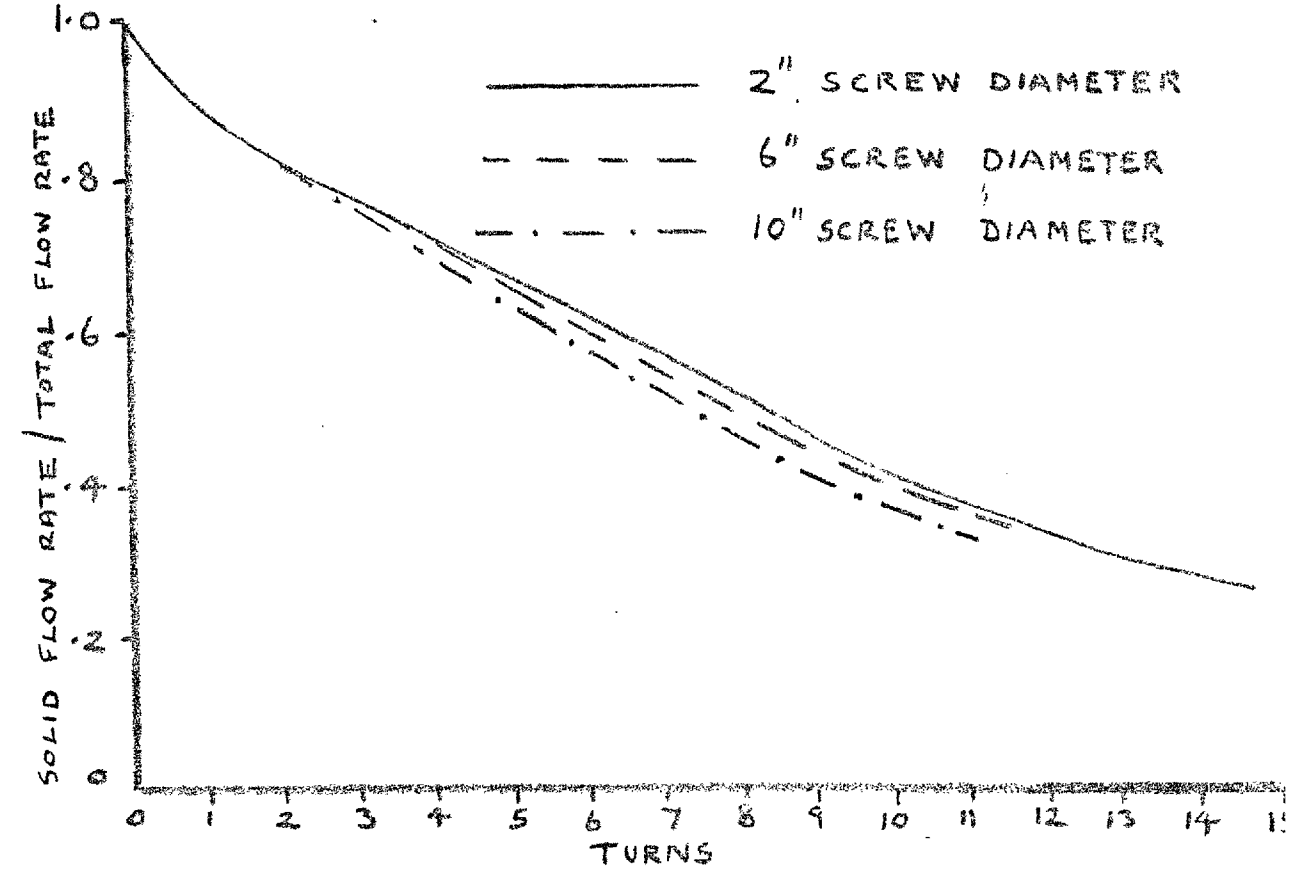
(a) The non-dimensional solid flow rate profile



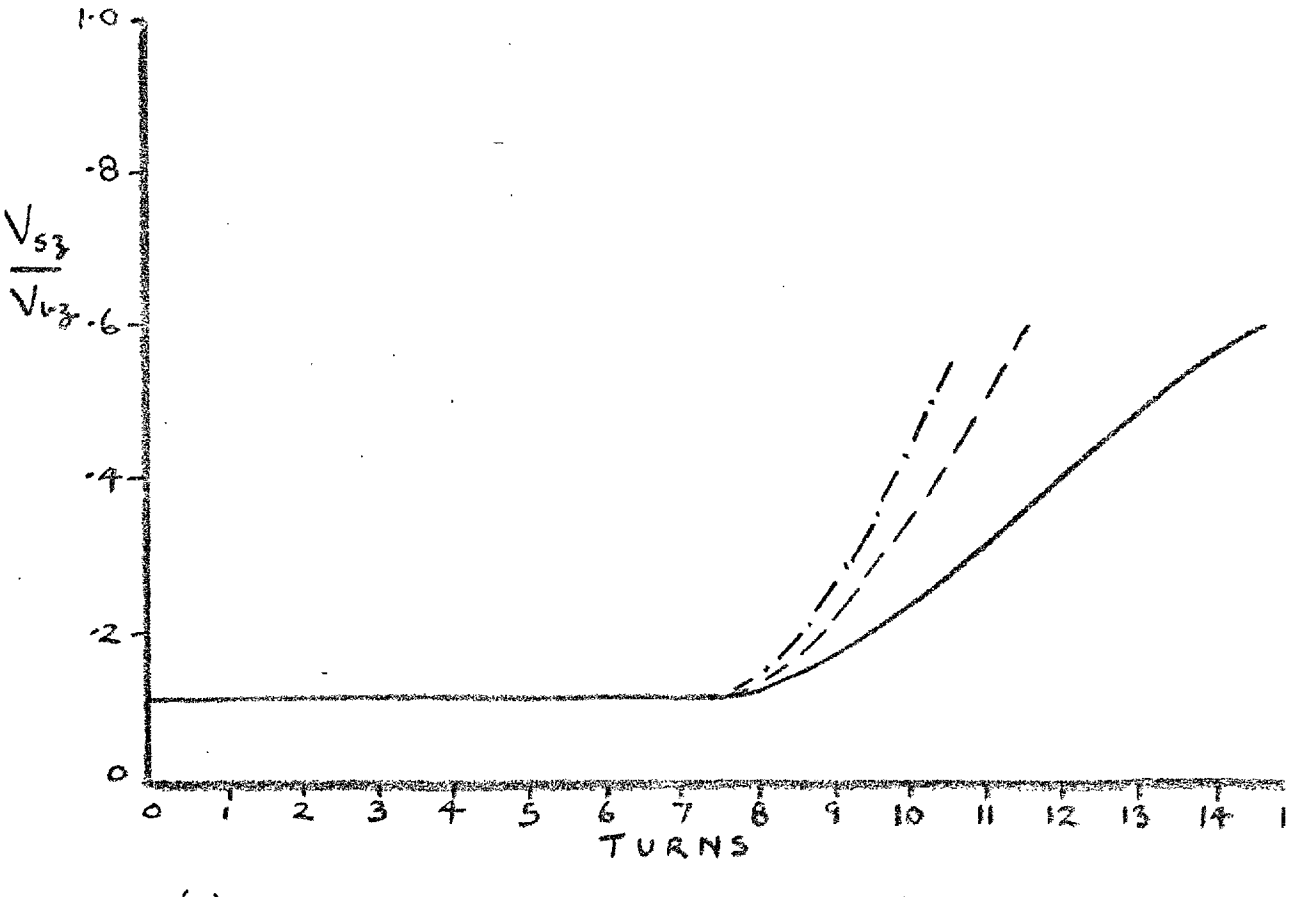
(b) The non-dimensional solid bed velocity profile

Figure 4.6

Theoretical predictions resulting from the application of scale-up law B.



(a) The non-dimensional solid flow rate profile



(b) The non-dimensional solid bed velocity profile

neither can be considered adequate in this respect. The implication is that using either of these scale-up rules to design a 10inch(254 millemetre) diameter screw, based on the results of trials on a 2 inch (50.8 millemetre) diameter screw is likely to give no trouble with melting capacity but that surging is likely to be more pronounced. Of course, this is not always an important consideration especially for large diameter machines.

This concludes the limited simulations concerning screw design applications of the present theory. It is hoped that they serve to indicate the potential usefulness of the analysis.

4.3 Theoretical Simulations of the effect of material Properties on melting performance.

Figure 4.7 shows the effect of varying the proportion of the total enthalpy increase imparted to the material, that is taken up by the latent heat of fusion of the material. The basic data for this simulation is taken from experiment 15 of the present work. It can be seen how an increase in the latent heat tends to flatten out the solid bed width profile although the effect is not particularly marked.

Figure 4.8 shows the effect of varying the thermal conductivity of the material, again based on data from experiment 15. The effect here is most marked. Not unexpectedly the greater the conductivity the higher is the melting rate. The sensitivity of the melting rate to the value of the thermal conductivity means that it is of great importance to obtain accurate values of it if accurate theoretical simulations are to be performed. It is possible in the present work that the bad fit between the theoretical and experimental results for the polypropylene experiments was caused by inaccurate values for the thermal conductivity.

Further interesting results are obtained by investigating the effect of varying the parameters of the power law constitutive equation. Figure 4.9 shows the effect of varying the datum viscosity, η_D, based on the data for experiment 11, on the solid bed width profile. Clearly the increase in viscous dissipation increases the melting rate, and also the higher viscosity material,

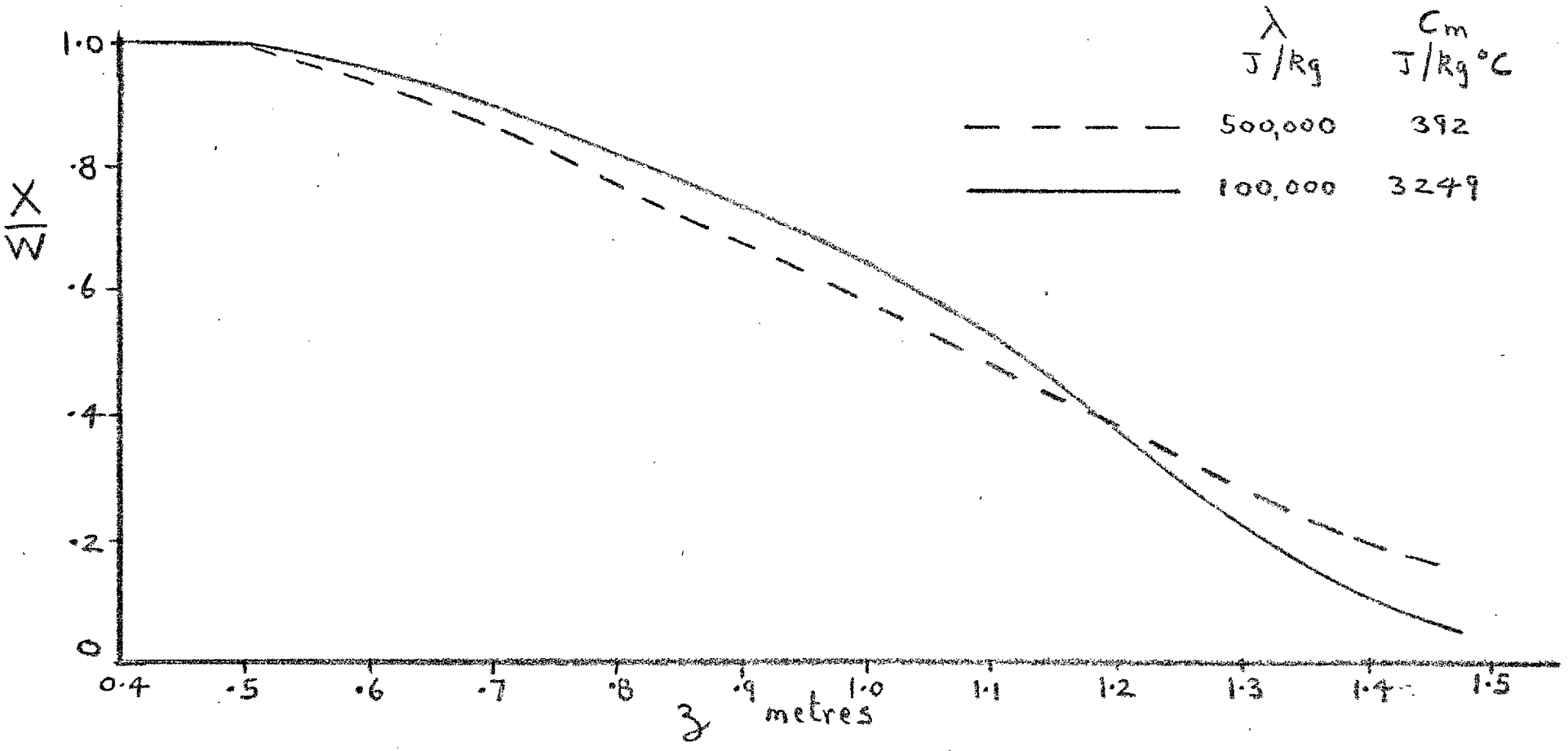


Figure 4.7

Theoretical predictions showing the effect of varying the ratio of latent heat of fusion to specific heat on the solid bed profile

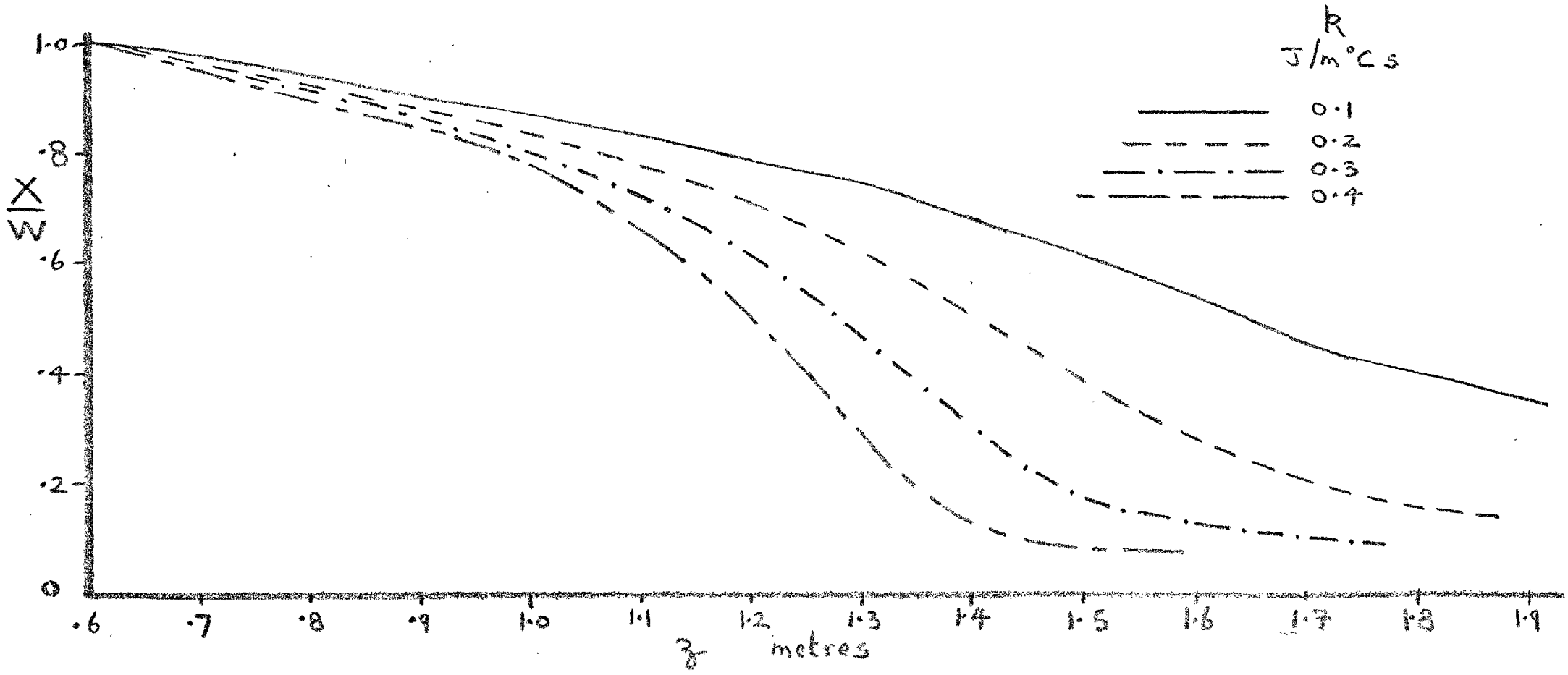


Figure 4.8

Theoretical predictions showing the effect of varying the thermal conductivity on the solid bed profile

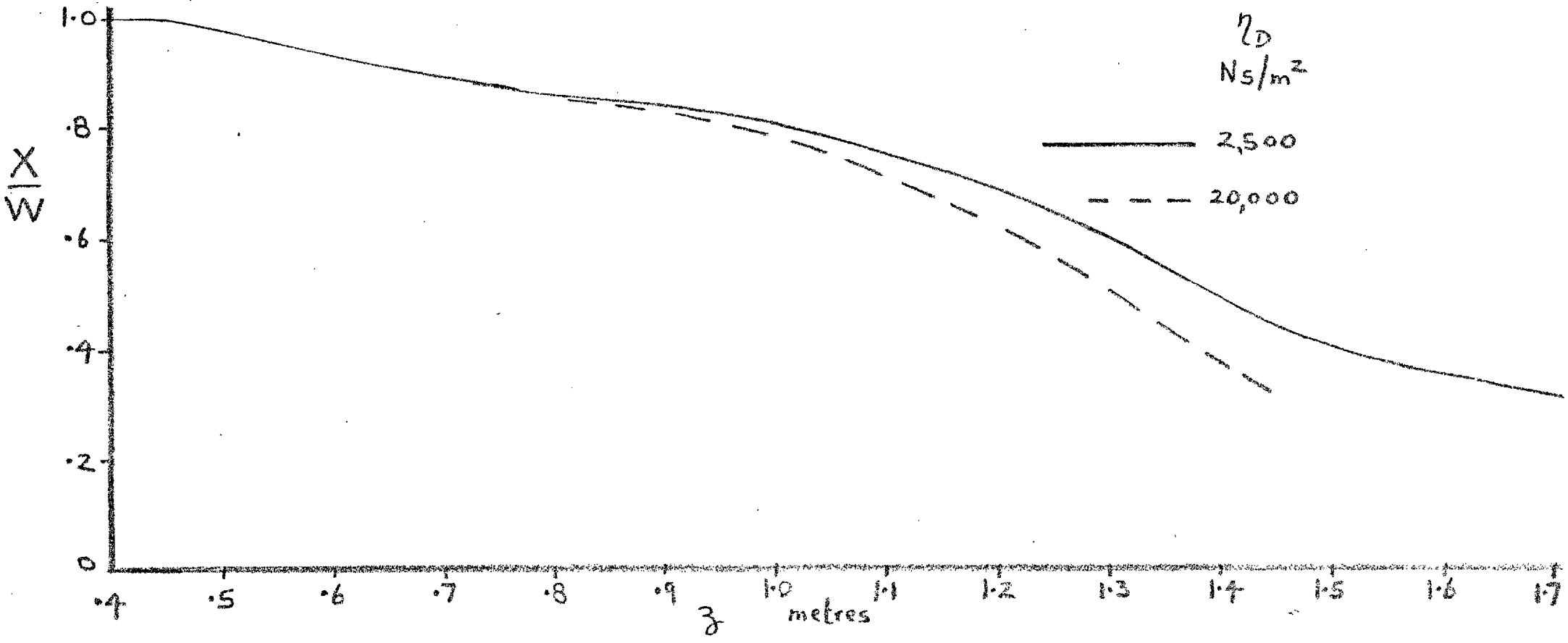


Figure 4.9

Theoretical predictions showing the effect of varying the base viscosity on the solid bed profile

of necessity, generates higher pressures.

Figure 4.10 shows the effect of varying the coefficient of temperature sensitivity of viscosity, b , on the solid bed width profile. Increasing the temperature sensitivity is effectively increasing the mean level of viscosity since much of the melt in the melt films is at a temperature lower than the datum temperature of the viscosity measurement. Thus the melting rate is increased as the temperature sensitivity is increased. The primary effect of varying both the datum value of viscosity and its temperature sensitivity is to alter the melting rate, the effect on solid bed acceleration is secondary, and is probably a consequence of the different melting rates rather than these viscosity parameters.

The same, however, cannot be said of the effect of varying the power law index on the melting behaviour, which is shown in figure 4.11, again based on experiment 11. Of course the more Newtonian the fluid is the higher will be the viscous dissipation as long as the datum viscosity and temperature sensitivity remain constant and as long as the datum shear rate is below the shear rates that occur in the analysis. Thus one expects an increase in melting rate as the power law index decreases towards the Newtonian value of zero. This is in fact the case up to the point of formation of the lower melt film, as can be seen in the figure. There after, however, a more complex situation arises. The results show that the more Newtonian the fluid is the earlier does significant solid bed acceleration occur and the higher is the maximum solid bed velocity. This behaviour will affect the melting rate since the melting rate is directly proportional to the solid bed width. Thus for the extreme Newtonian case the dissipation in the melt film is the highest melting rate per unit solid bed width, yet the solid bed width averaged over the melting region is least. These two effects tend to counteract one another such that the finish of melting does not vary significantly with the variation in power law index. Of course this is, in a sense, co-incidental because of the particular data used in this simulation. The significance of these results is in the effect on the point at which significant solid bed acceleration begins, relative to the point of formation of the lower melt film.

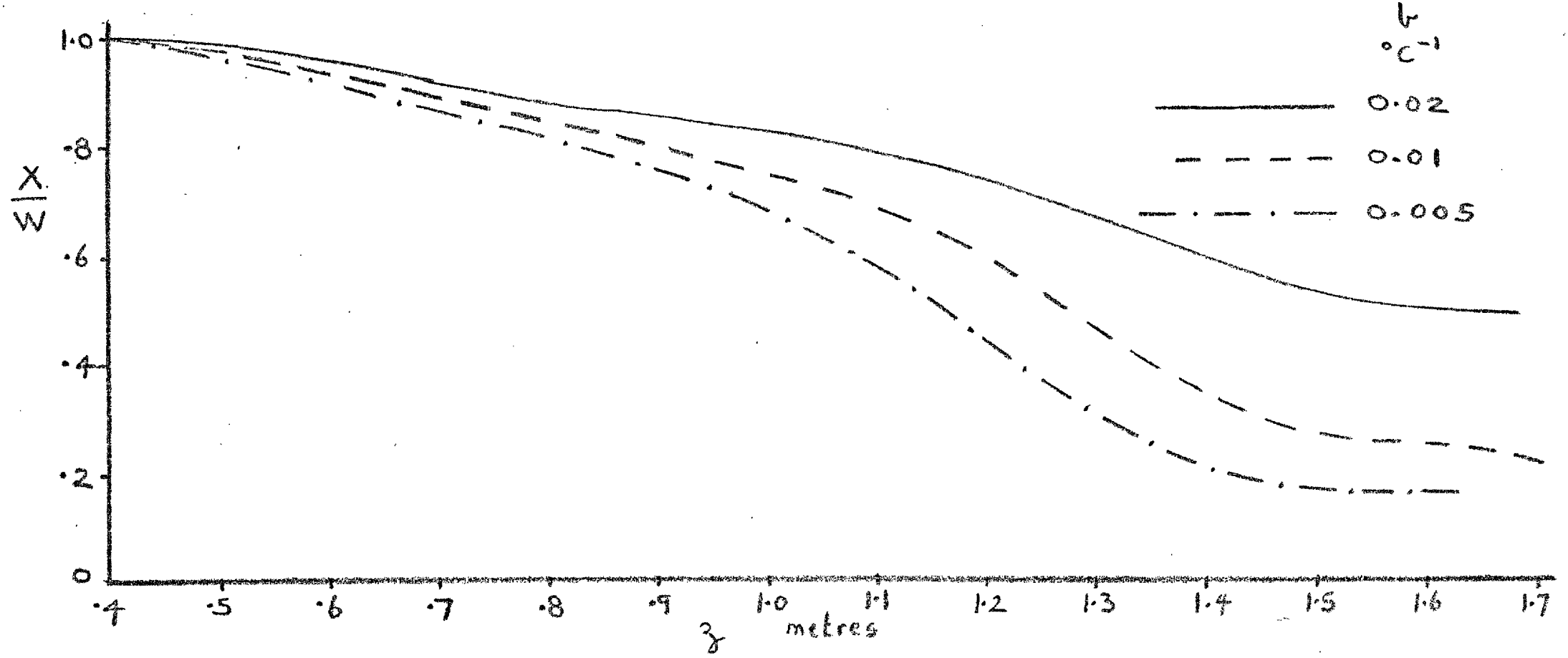


Figure 4.10

Theoretical predictions showing the effect of the coefficient of temperature sensitivity of viscosity on the solid bed profile

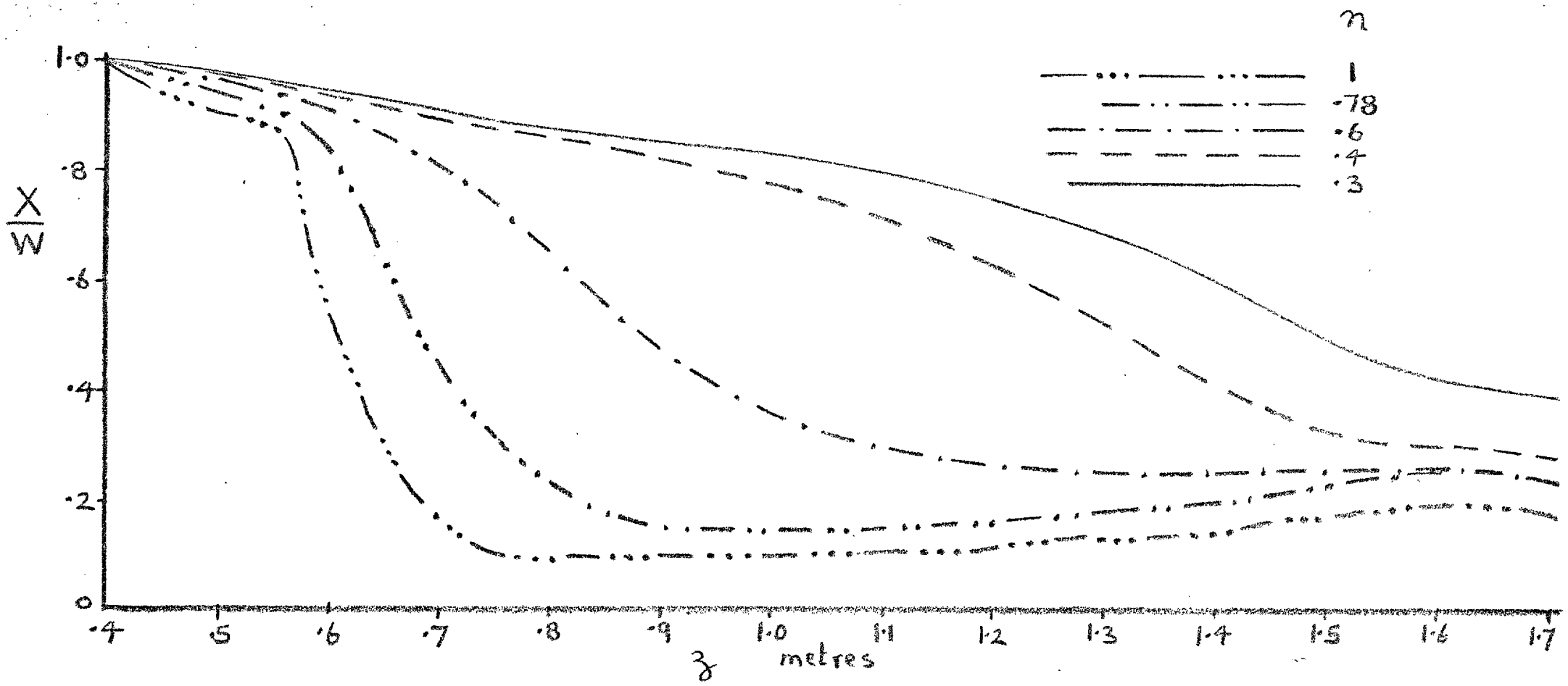


Figure 4.11

Theoretical predictions showing the effect of varying the power law index on the solid bed profile

In practice the melting profiles predicted for nearly Newtonian materials, such as Melinex, do not exhibit this long region where the solid bed width is small compared to the channel width. This is because the solid bed does not remain continuous as the theory assumes it to do, rather it periodically breaks and one sees a series of separate pieces with regions of channel completely full of molten material between regions of solid and melt. The present steady state theory cannot predict such behaviour and therefore the predictions of the melting profile for such materials cannot be accurate. However it is possible that the theory may be useful in such cases as a tool in designing screws to minimise such solid bed accelerations.

4.4 Theoretical Simulations of factors affecting the performance of Extruders in operation.

Figure 4.12 shows the effect of varying the flight clearance based on the data of experiment 5. Compared with the predictions of the effect of flight clearance on melting performance published by Tadmor and Klein (15), the present results show much less sensitivity to increases in flight clearance. Without good experimental data with which to make comparisons it is difficult to pass comment on the accuracy of such predictions. It is interesting to note that the present predictions suggest, if accurate, that the greater the flight clearance is, the less will be the effect on the melting performance of an increase in the flight clearance.

Figure 4.13, which is based on data from experiment 7, shows the effect of varying the point of formation of the lower melt film on the melting behaviour, thus simulating varying degrees of screw cooling. The detailed results for these simulations show that the presence of the lower melt film is important as regards the overall melting rate, in other words, there is a significant energy input to the material from the dissipation in the lower film and from the screw. It has already been commented that the heat flux from the screw may be over-estimated in the present model but the dissipation is certainly a real and significant effect. Therefore one expects a higher melting rate, all other things being equal, when the lower melt film is present. The

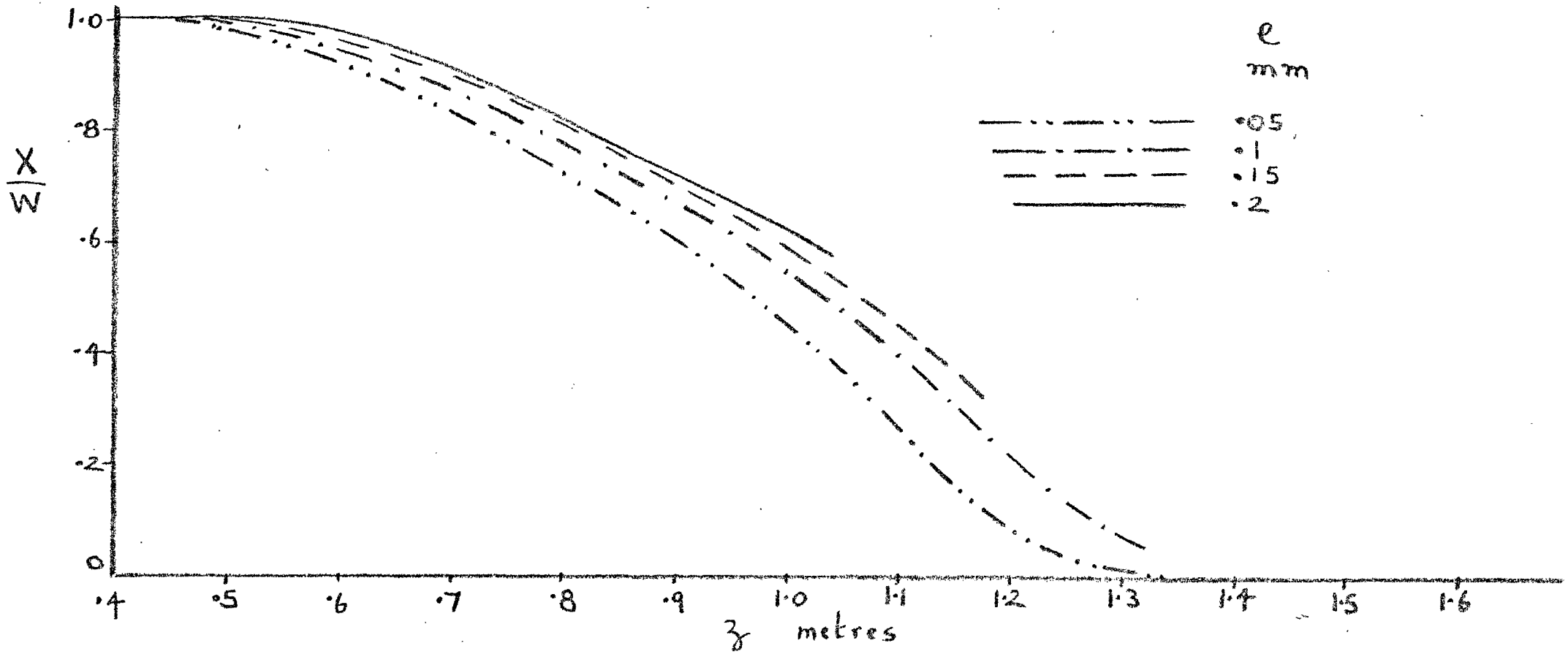


Figure 4.12

Theoretical predictions showing the effect of varying the flight clearance on the solid bed profile

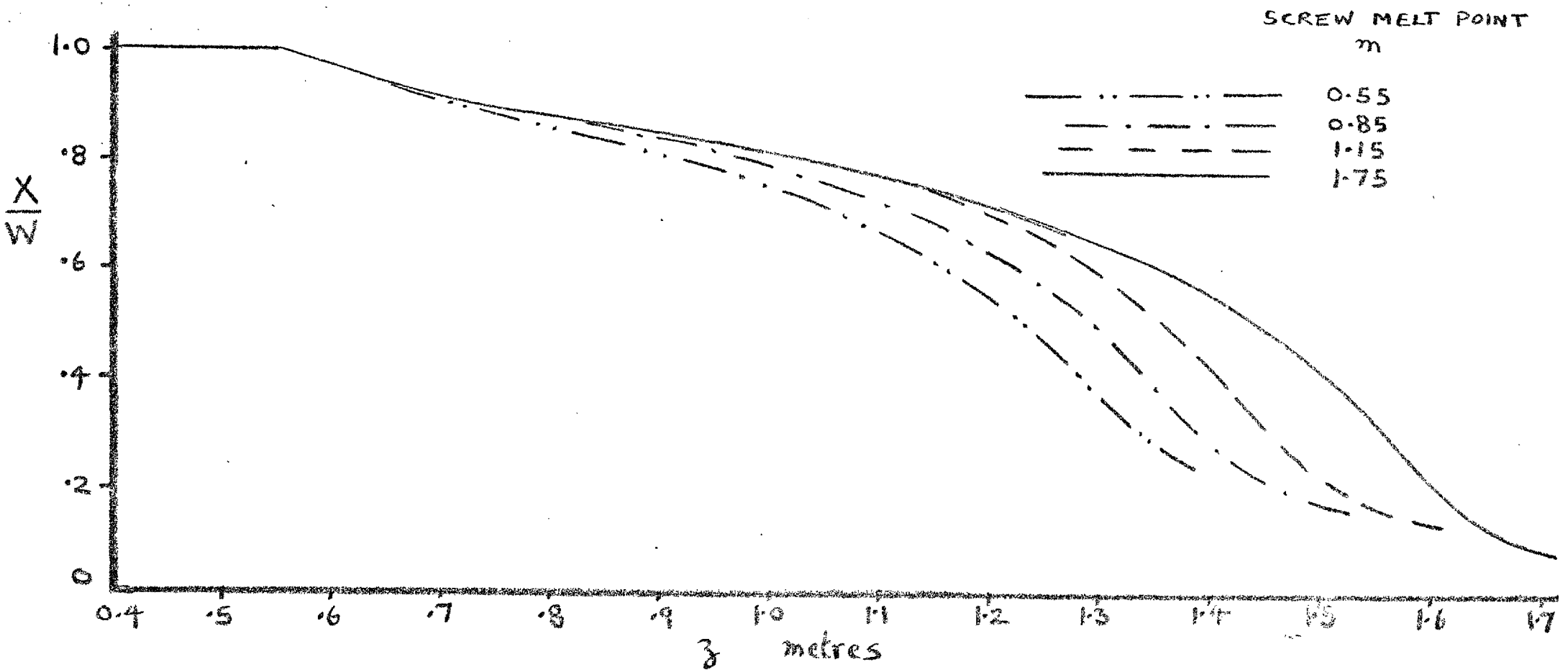


Figure 4.13

Theoretical predictions showing the effect of varying the point of formation of the lower melt film on the solid bed profile

results also indicate another effect of the lower melt film, that is, its effect on the onset of significant solid bed acceleration. It would seem that the earlier the lower melt film forms, the earlier does significant solid bed acceleration occur.

This concludes the presentation of the results of the theoretical simulations of extrusion trials. The next section presents a concluding discussion of the various experimental and theoretical results, with special regard to the phenomenon of solid bed break-up.

4.5 : Concluding Discussion.

It is now appropriate to discuss the correlation between theory and experiments concerning solid bed break-up. The experiments showed that a lower melt film was necessary if bed break-up was to occur. The theoretical predictions show agreement with this, in that in the absence of the lower melt film no significant acceleration of the solid bed was predicted. Additionally the theoretical predictions for PVC showed no significant solid bed acceleration until the very end of melting where its effect is of little importance, which agrees with the absence of solid bed break-up in the PVC experiments. Further, theoretically, the more Newtonian the plastic, which generally means the more crystalline the plastic, the earlier after the formation of the lower melt film did significant acceleration take place. In a general way this agrees with the experimental results which tended to suggest that the more crystalline the polymer the more severe was the surging due to bed break-up, although this is difficult to quantify, especially as the 'Melinex' results were inconclusive due to feed section surging which completely masked the pressure variations due to solid bed break-up. In the absence of any means of measuring screw temperatures in the experiments it was not possible to compare the point of bed break-up with the point of formation of the lower melt film in the experiments and hence it was not possible to confirm the theoretical predictions.

It must be remembered that in the present theory no constitutive equation for the solid bed has been specified, merely its deformation; and therefore one cannot necessarily expect to be able to predict the point of actual bed break-up. If trends of the present theoretical predictions concerning the

point of formation of the lower melt film and the onset of significant solid bed acceleration together with their dependence on the nature of the flow properties of the material, are an accurate reflection of the actual behaviour, then one implication of it would be that the inherent strength of the solid bed is not necessarily the overriding factor in any criterion of solid bed fracture.

It is useful to look at the ratio of the shear stresses acting on the solid bed in z direction. Restricting attention to the upper and lower surfaces only, the ratio of these stresses for the Newtonian constant viscosity case, making usual assumptions about the melt film flow behaviour, is

$$\frac{\tau_{1z}}{\tau_{2z}} = \frac{(V_{bz} - V_{sz})}{\delta_1} \cdot \frac{\delta_2}{V_{sz}} \qquad (4.6)$$

which is independent of viscosity

In the theory the initial value of δ_2 is computed on the basis that the pressure gradient is locally constant, and of course the pressure gradient is calculated essentially from the difference between the above two shear stresses. Normally the initial value of δ_2 so calculated is of the same order of magnitude as δ_1 though usually smaller. Because all the material melting off the bottom of the solid bed is necessarily retained in the lower film, the thickness of this film will increase steadily and therefore so does the ratio δ_2/δ_1. In the absence of any solid bed acceleration this means that the shear stress ratio in equation (4.6) will increase and as a consequence the pressure gradient will increase. In theoretical terms such an increase in pressure gradient in the absence of solid bed acceleration would so restrict the melt pool flow rate that the overall continuity of the down channel flow rate would be impossible to maintain. However, acceleration of the solid bed allows continuity to be maintained on two counts. By allowing a reduction in width of the solid bed it increases the flow area of the melt pool, and secondly the increased velocity of the solid bed will reduce the shear stress ratio in equation (4.6).

This then is the mechanism that operates in the theoretical model as applied to a Newtonian constant viscosity fluid. In the case of non-Newtonian, temperature dependent viscosity fluid the situation is more complex in that the shear

stress ratio, τ_{1z}/τ_{2z} is a function of the shear rate and temperature profiles in both films. The viscosity in the lower film will in general be higher than that in the upper film for two reasons. The mean temperature of the lower film is generally lower than the upper and the mean shear rate will also be lower, both of which tend to increase the viscosity in the lower film compared to the upper. Thus this effect will reduce the ratio of the shear stresses acting against the effect due to the film thickness ratio. The more non-Newtonian the material the greater will be this counter effect. All of which means that the acceleration required of the solid bed to maintain continuity is reduced in the case of a non-Newtonian material compared with a Newtonian one.

Of course, even with non-Newtonian fluids significant solid bed acceleration is predicted by the theory but always at a finite measurable distance after the formation of the lower melt film. As the lower melt film developes several significant effects take place, all of which tend to increase the shear stress ratio and hence the likelyhood of significant acceleration. Obviously the ratio of the film thickness is working to this end. In addition some acceleration of the solid bed is taking place which on the one hand tends to reduce the acceleration of the solid bed, see equation (4.6) and on the other hand tends to increase it in that it increases the shear rate in the lower film and hence reduces its viscosity and hence shear stress. Thirdly the screw temperature is increasing which will tend to increase the mean temperature of the lower melt film with a consequent reduction in viscosity and hence shear stress. It is not therefore surprising that at some stage these effects combine so that significant acceleration of the solid bed begins.

It is also possible to identify in the theory a positive feedback cycle that causes an instability and means that once the solid bed acceleration reaches a certain critical point it increases rapidly until conditions have become adjusted and the acceleration levels out. This feedback cycle may be described as follows. It can be followed more easily by reference to figures 3.15 and 3.16.

Acceleration of the solid bed causes a reduction in the solid bed width. A reduction in the solid bed width tends to reduce the thickness of the upper

melt film at a subsequent section since the effective developement length of the film is reduced. A reduction in the upper melt film thickness without a corresponding change in the lower melt film thickness causes an increase in the shear stress ratio in the solid bed. This in turn requires greater acceleration of the solid bed to maintain continuity. Hence if the dominant factor in determining the upper melt film thickness is the solid bed width then the unstable feedback mechanism described above is likely to occur.

The above discourse refers essentially to the postulated melting model and therefore only if the model is an accurate representation of the actual melting mechanism can it be applied as an explanation of solid bed break-up. Present experimental evidence does not conclusively demonstrate that it is accurate, and as it does not allow for the possibility of bed break-up it is necessarily inaccurate to some extent. Yet the results do suggest that up to and including the fracture of the solid bed the model is reasonably accurate.

The conclusion of the discussion of the theoretical analysis as regards the onset of bed break-up is that the point at which significant solid bed acceleration occurs corresponds to a certain stress state of the solid bed. This state is one in which there is a comparatively high shear stress gradient across the solid bed and a comparatively high pressure gradient in the solid bed, and by implication according to an assumption of the model, a comparatively high pressure gradient in the melt pool. The comparison being made with conditions that apply when the solid bed acceleration is low. Further, this state that brings about significant solid bed acceleration, because of the assumptions of the model is independent of the properties of the solid bed, in that it is only the properties of the fluid that affect the stresses on the solid bed.

Turning to the real situation it has been stated that the size of the granules did not noticeably affect the occurrence of bed break-up. This observation goes a little way to support the theoretical conclusion that solid properties are not necessarily of paramount importance in controlling solid bed break-up. If one were seeking the simplest possible constitutive equation for a solid bed in the present context it might well be that the solid bed has infinite strength

in compression and zero strength in tension. In other words the criterion for fracture of the solid bed would be that fracture occurs when any principal stress becomes zero. This may well be an excellent first approximation to the real situation. Of course, if it is, the idea that the criterion of fracture is independent of material could be applied.

The obvious next step in formulating a theory to accurately predict the point of bed break-up is to undertake a detailed stress analysis of the solid bed. This is outside the scope of the present work, but it is hoped that the foregoing may be of use to other workers in formulating such an analysis.

To re-cap then the theoretical explanation of the occurrence of significant solid bed acceleration is that a certain critical stress state is reached that consists of a high shear stress gradient across the solid bed in the z direction and a high pressure gradient in the melt pool and potentially a high melt pressure. This stress state is brought about by a combination of factors but is essentially due to conditions in the lower melt film being such that the shear stress on the bottom of the solid bed in the z direction becomes smaller and smaller compared to that on the top of solid bed. The reason for this reduction in this shear stress is the increasing thickness and increasing temperature of the lower melt film. Once conditions have reached a certain stage an instability occurs due to the interrelationships between the different variables of the problem. This instability causes a short period of high solid bed acceleration. It should be noted that this instability, due to the previously described positive feedback mechanism is not a mathematical instability but a physical one in the postulated melting model.

Qualitatively the trends and predictions of the analysis correlate favourably with the experimental results although the evidence is by no means conclusive. However there is no reason why one should not apply the above explanation to the real situation. In which case, of course, the unstable region of high acceleration in the theoretical model becomes synonymous with the region in which the solid bed fractures in the real case. This region of high acceleration in the theoretical model is highly qualitative and can only be identified

by inspection of a graph of the solid bed velocity against channel position such as have been shown earlier.

Having postulated an explanation of solid bed break-up on the basis of the theoretical treatment some implications of it are of relevance. Firstly, does the explanation suggest means by which solid bed break-up may be avoided? It has been shown experimentally that one way, and perhaps the easiest way, to avoid solid bed break-up is to prevent the formation of the lower melt film by the use of screw cooling. Of course, the stabilizing effect of screw cooling has long been appreciated and used. Though this is, in principle, a simple method it is by no means ideal in that it would seem to inevitably involve a loss in output rate. Looking at the various experimental and theoretical results concerning screw cooling experiments suggests that the reason for this is the reduction in pressure generating capacity in the melting region. In the light of the previous discussion it would seem that this loss is inevitable if the shear stress on the lower surface of the solid bed is due to dry friction. If this is so then to achieve higher output rates the pressure of the lower melt film is necessary. Therefore, ways of preventing solid bed break-up whilst allowing the presence of the lower melt film must be sought.

Essentially what is needed to fulfill this requirement is a thin film of low temperature that does not get thicker nor hotter as it developes downchannel. Of course the thinner and the cooler the film is so the higher will be the dissipation which will then tend to increase the temperature of the film and its thickness due to the increasing melting rate. However, one could perhaps visualize some form of temperature control system for the screw which would attempt to maintain the screw temperature in the melting region, some few degrees above the melting point of the plastic. Whether such a system would be economicably viable were it to be effective is uncertain. It is certainly technically possible and undoubtably would give a very sensitive extra control of the extruders performance.

An alternative method perhaps could involve a screw design having a reducing channel depth and increasing channel width, that is, a tapered variable pitch screw.

The idea behind this being that the solid bed width should remain virtually constant and that the increasing amount of molten material collects in the increasingly wide channel, so that as the pressure gradient increases the solid bed width does not need to reduce to accommodate the melt flow in the melt pool. Thus the unstable feedback mechanism is less likely to function since the upper melt film is less likely to reduce in thickness due to a reduction in the solid bed width. As the overall melting rate is directly proportional to the solid bed width this form of screw design will not have such a high potential melting capacity as a conventional design would have. However, if surging caused by solid bed fracture were sufficiently troublesome that it needed to be eliminated then this might give a better solution then screw cooling, say. Further the results presented previously illustrating the effects of scale-up showed that for larger machines the melting capacity is likely to be more than adequate but that surging becomes more severe.. Therefore a reduction in the potential melting capacity of the machine by adopting such a form of screw design may not in fact reduce the actual output required of the machine.

It now remains to discuss briefly how the present melting analysis may most effectively be combined with analyses of the other two regions of the extruder; the solids feed region and the melt flow region.

Ideally a non-isothermal feed flow theory should precede the melting analysis. This could then provide the initial pressure for the melting analysis, the initial solid bed temperature distribution and most importantly the actual starting point for the melting analysis. The theory recently published by Tadmor and Brayer (41) would seem ideal in this respect. Because of the way the present theory has been formulated such a non-isothermal feed flow analysis would automatically match up with the present analysis and would not require an intermediate analysis as the Tadmor melting analysis does, that of the so called 'delay zone' (42).

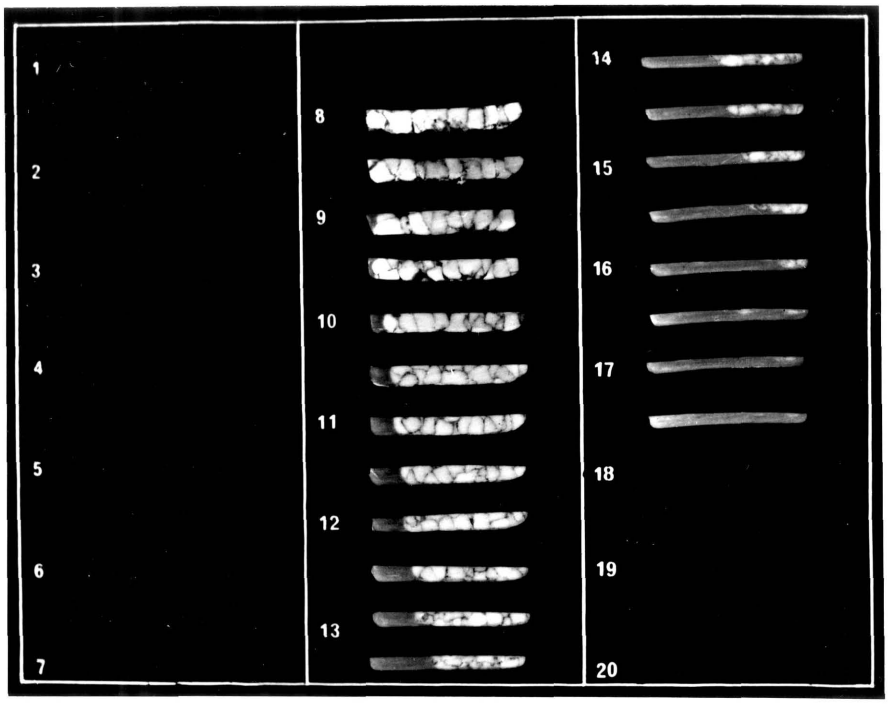
As regards the melt flow analysis, it would again be fairly straightforward to link the melting analysis to the melt flow analysis if the melt pool flow analysis were to be for non-Newtonian fluids. In its present form the analysis

of the melt pool flow is for Newtonian constant viscosity fluids. The information the present analysis provides is a mean melt pool temperature, melt pressure and the finish of melting. This is sufficient to initiate a melt flow analysis though it is a long way from being ideal. Perhaps the ideal case would be to have a thermally developing non-Newtonian flow analysis for the melt pool. Of course when the width of the solid bed becomes zero the melt pool occupies the whole of the channel and the analysis would proceed as the melt flow analysis.

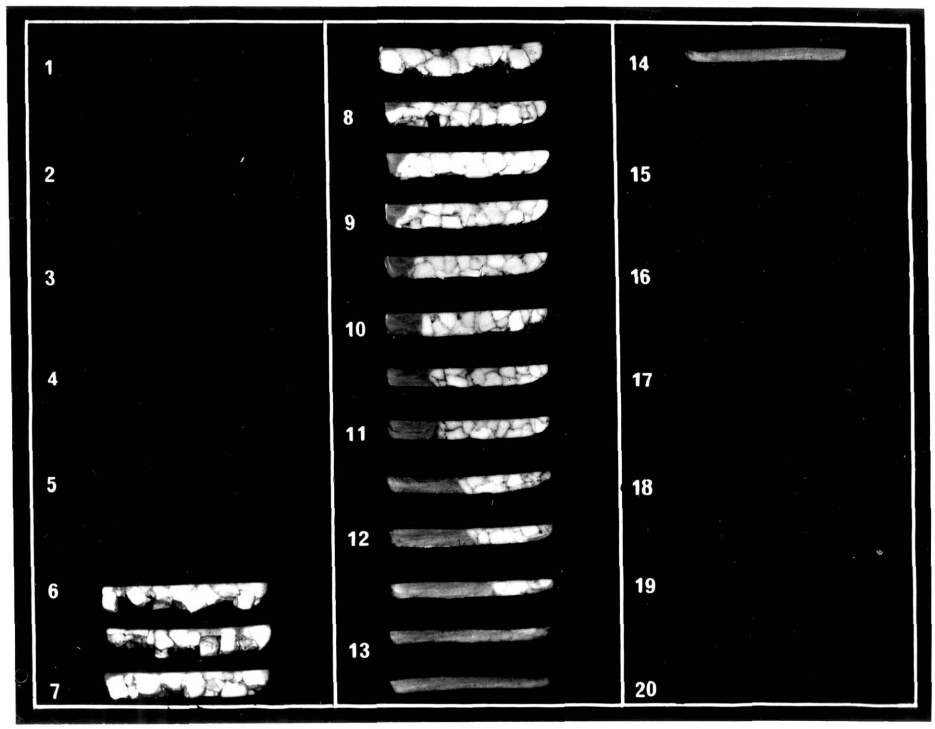
The Plates Showing the Experimentally

Obtained Cross-Sectional Specimens

PLATE 1

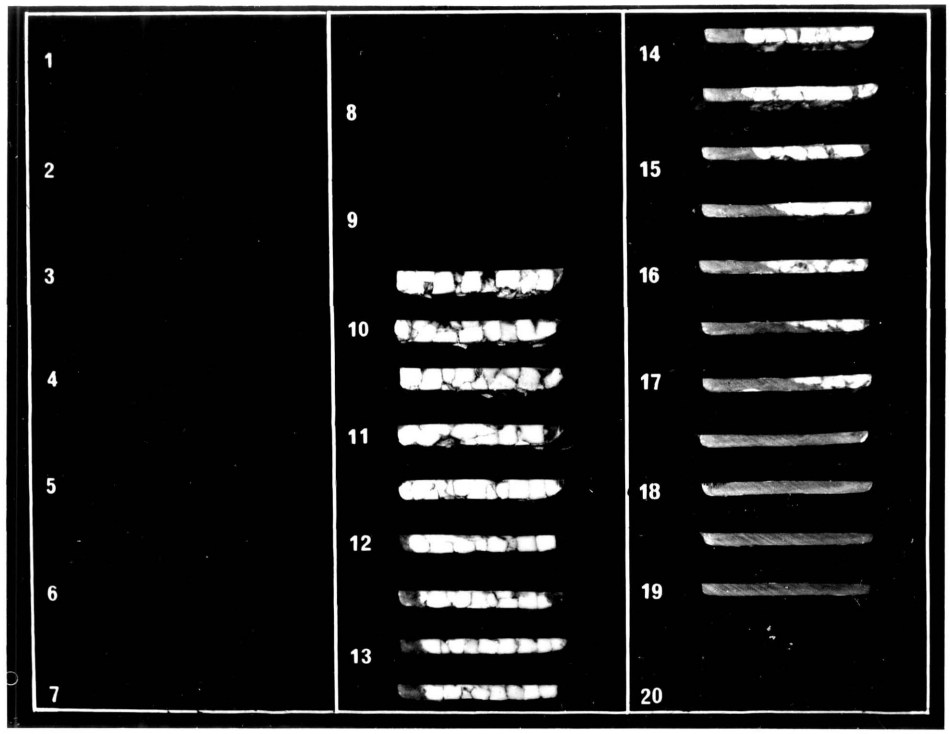


(a) Experiment 1: Plasticised Polyvinyl Chloride Granules N(80); Q(360); D(3/32)

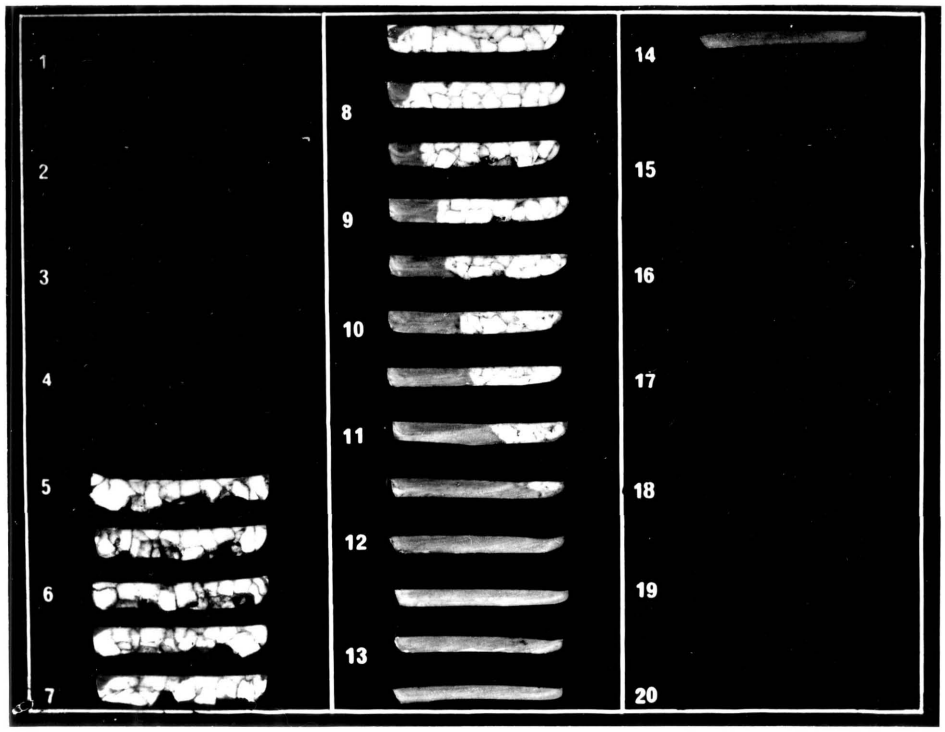


(b) Experiment 2: Plasticised Polyvinyl Chloride Granules N(40); Q(200); D(3/32)

PLATE 2

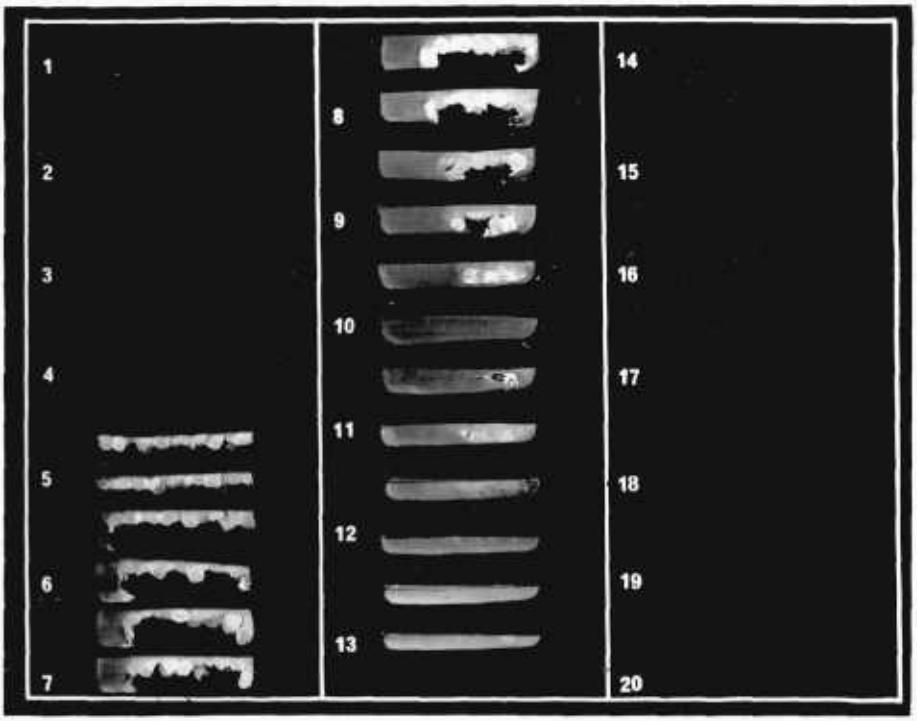


(a) Experiment 3: Plasticised Polyvinyl Chloride Granules
N(80); Q(367); D(5/32)

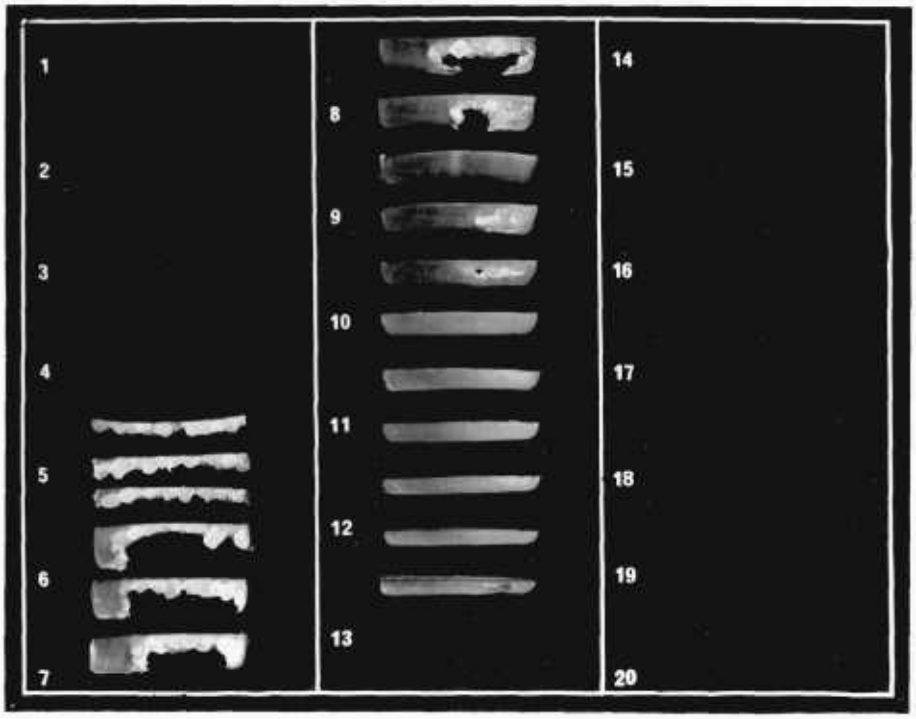


(b) Experiment 4: Plasticised Polyvinyl Chloride Granules
N(40); Q(201); D(1/16)

PLATE 3

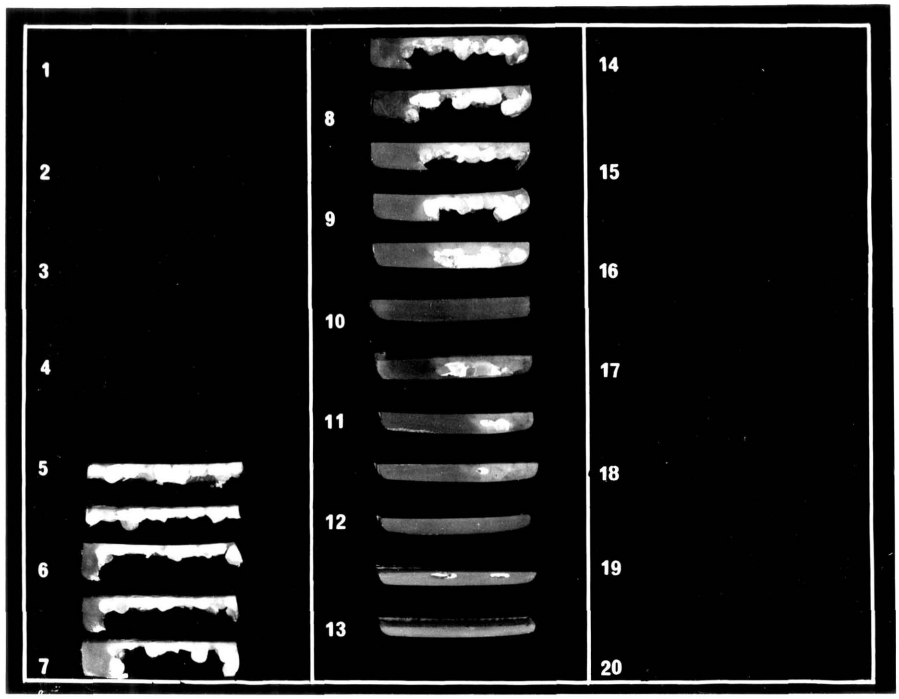


(a) Experiment 5: Low Density Polyethylene Granules
N(80); Q(191); D(3/32)

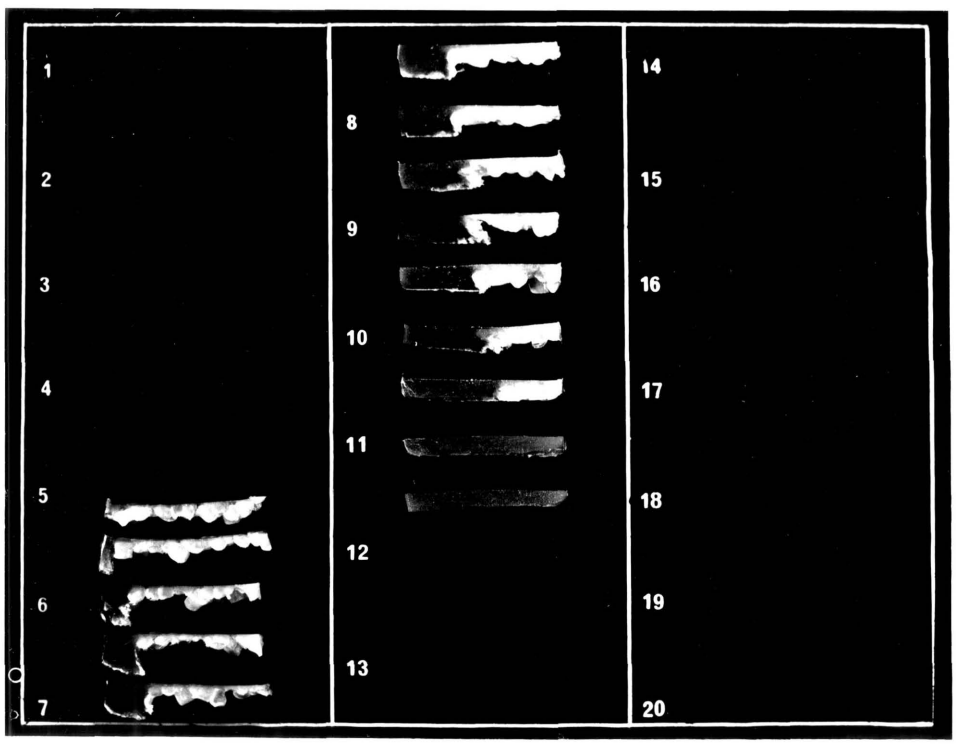


(b) Experiment 6: Low Density Polyethylene Granules
N(40); Q(97); D(3/32)

PLATE 4

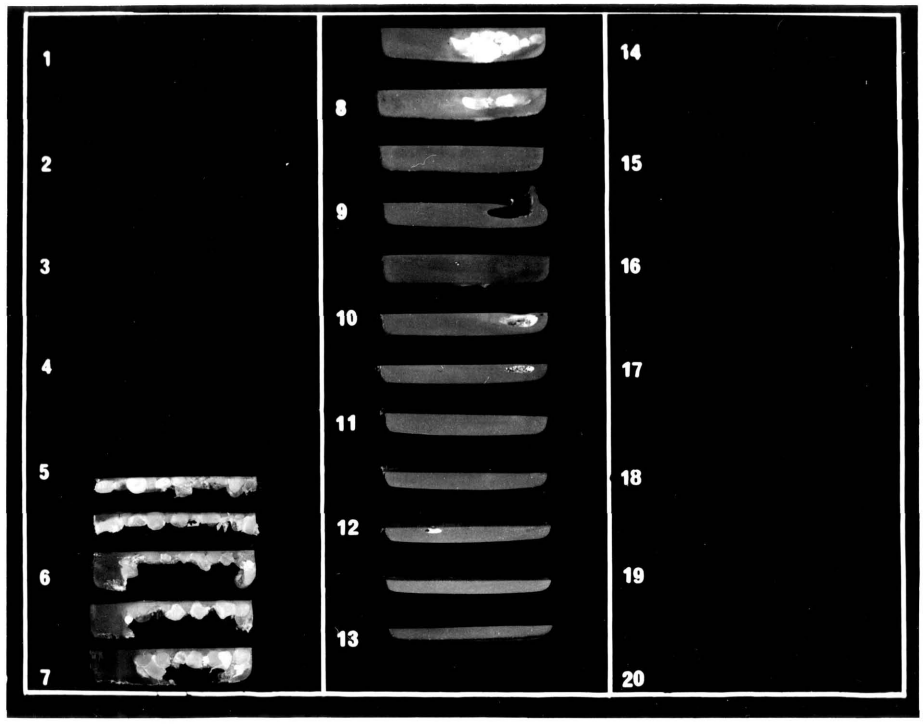


(a) Experiment 7: Low Density Polyethylene Granules
N(80); Q(215); D(5/32)

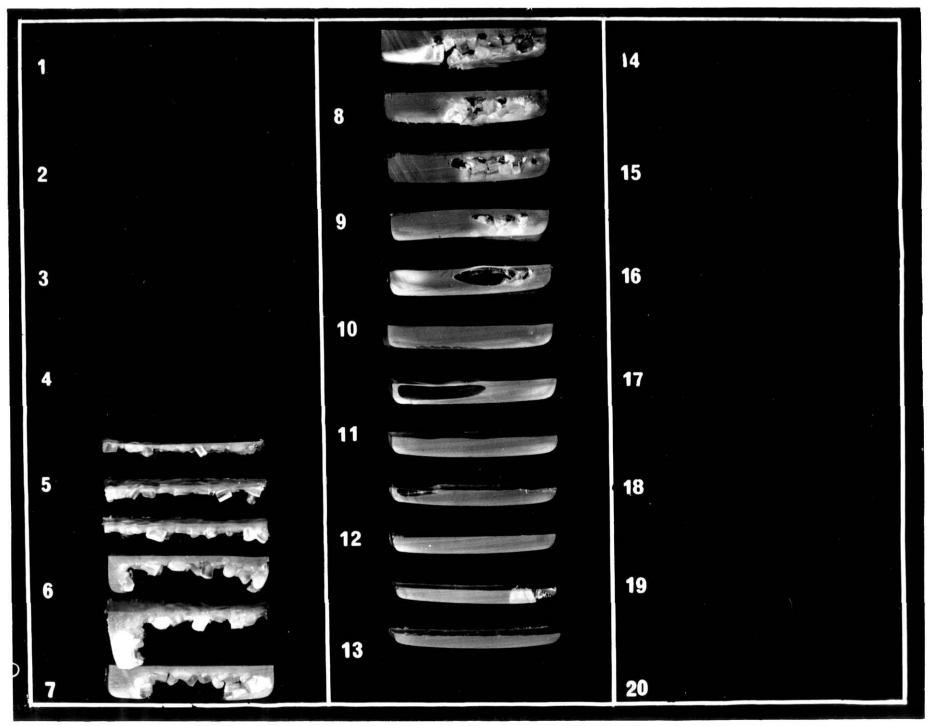


(b) Experiment 8: Low Density Polyethylene Granules,
with Screw Cooling
N(80); Q(140); D(3/32)

PLATE 5

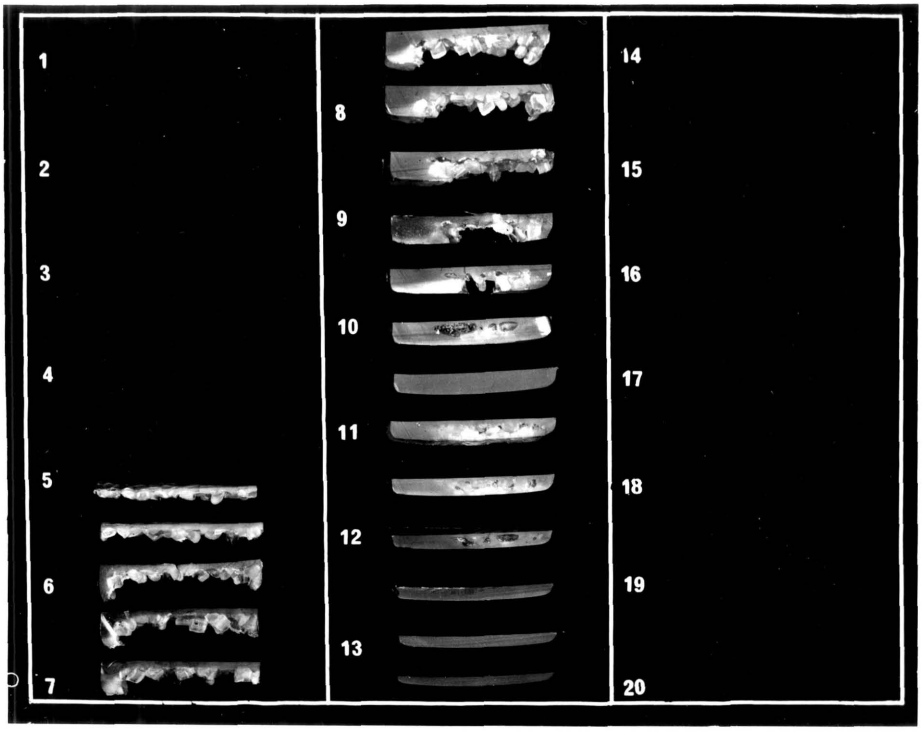


(a) Experiment 9: Low Density Polyethylene Granules
N(40); Q(83); D(1/16)

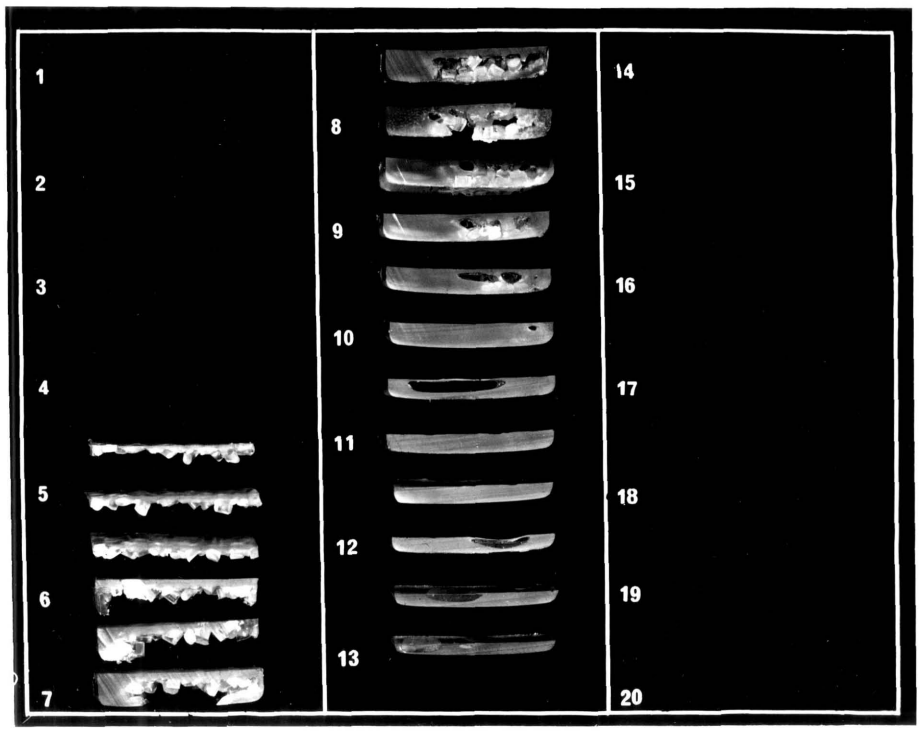


(b) Experiment 10: Polypropylene Granules
N(40); Q(80); D(1/16)

PLATE 6

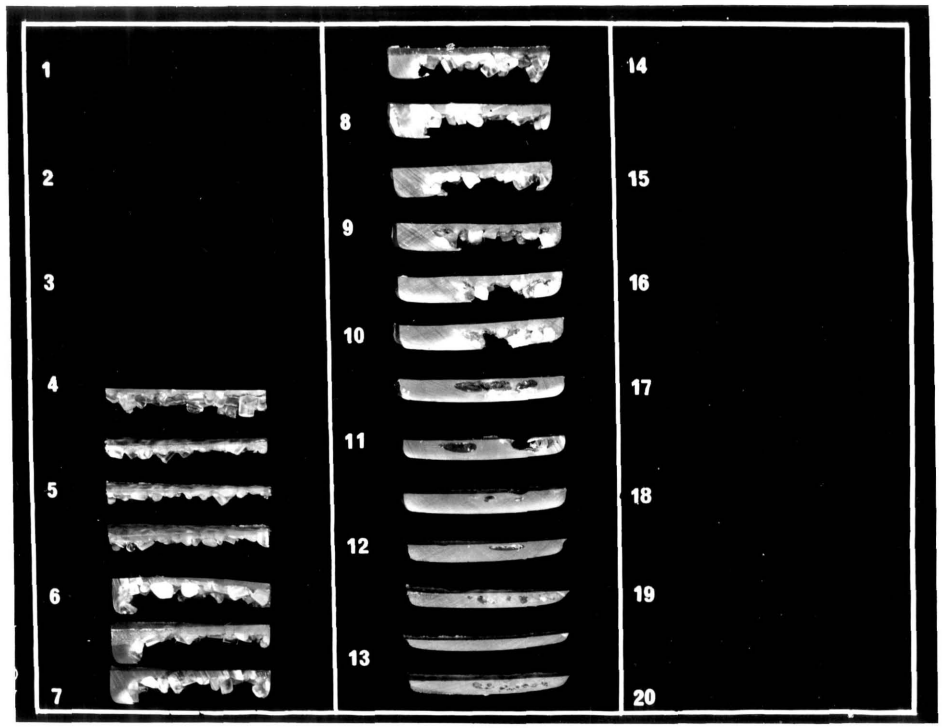


(a) Experiment 11: Polypropylene Granules
N(80); Q(179); D(3/32)

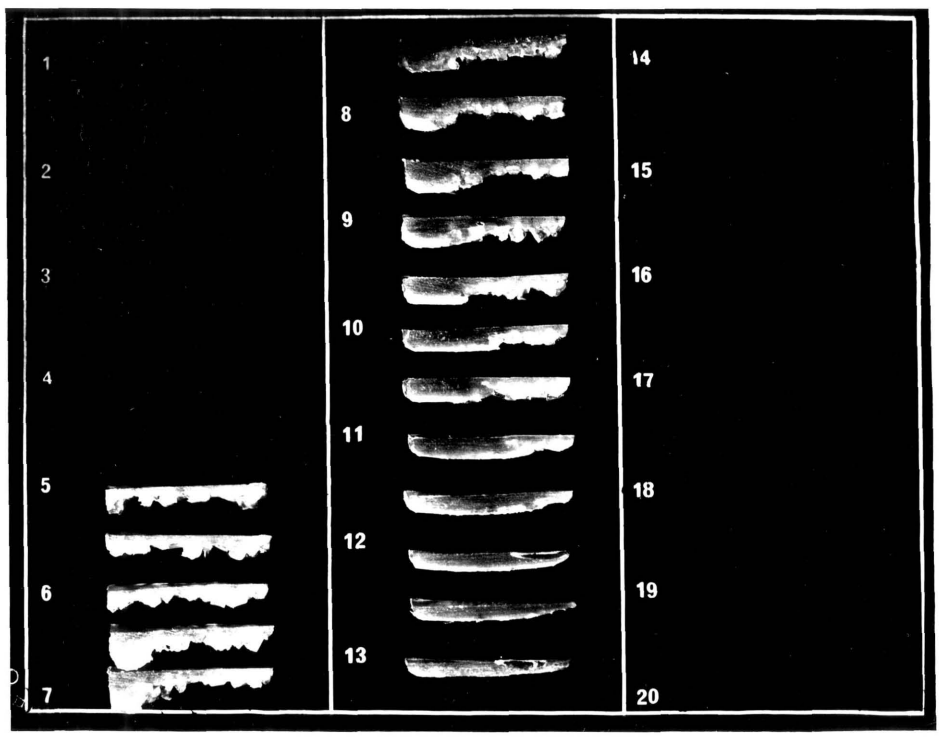


(b) Experiment 12: Polypropylene Granules
N(40); Q(93); D(3/32)

PLATE 7

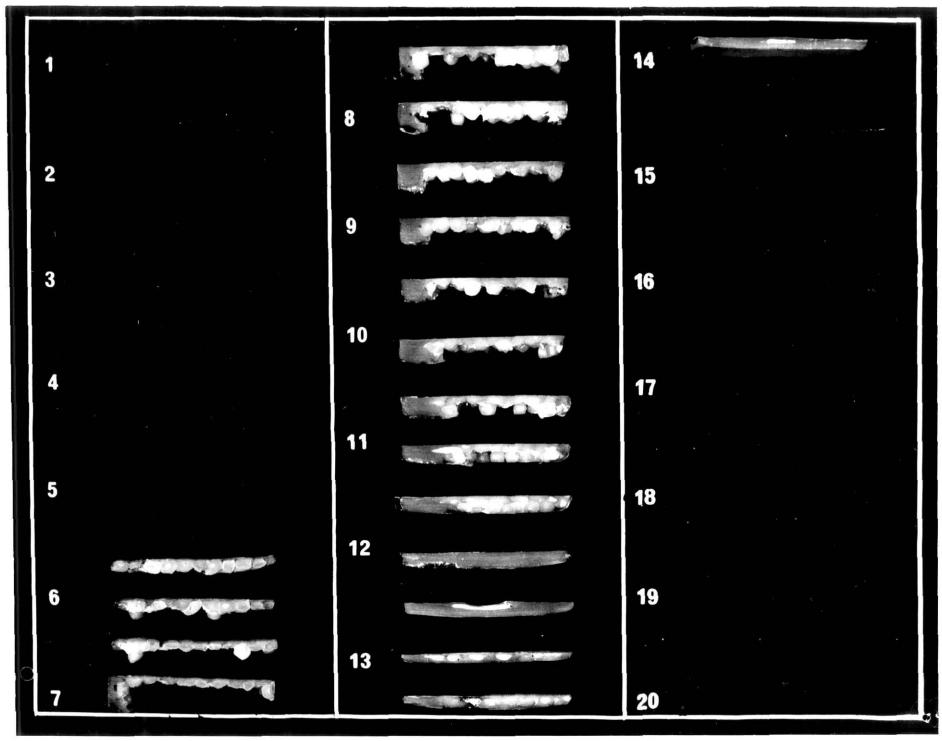


(a) Experiment 13: Polypropylene Granules
N(80); Q(189); D(5/32)

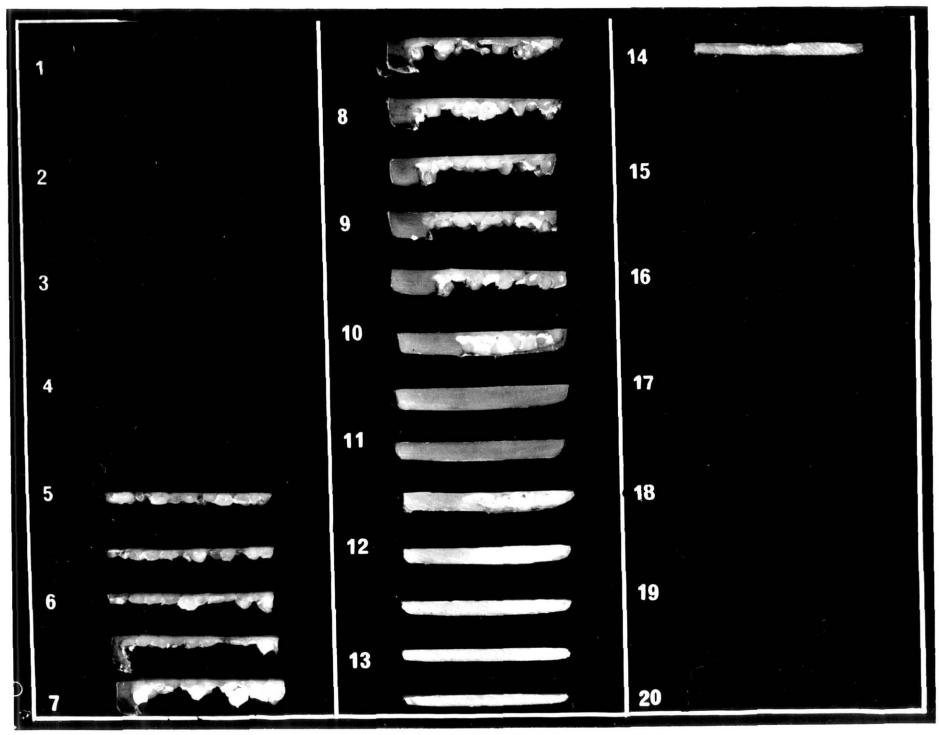


(b) Experiment 14: Polypropylene Granules,
with Screw Cooling
N(80); Q(143); D(5/32)

PLATE 8

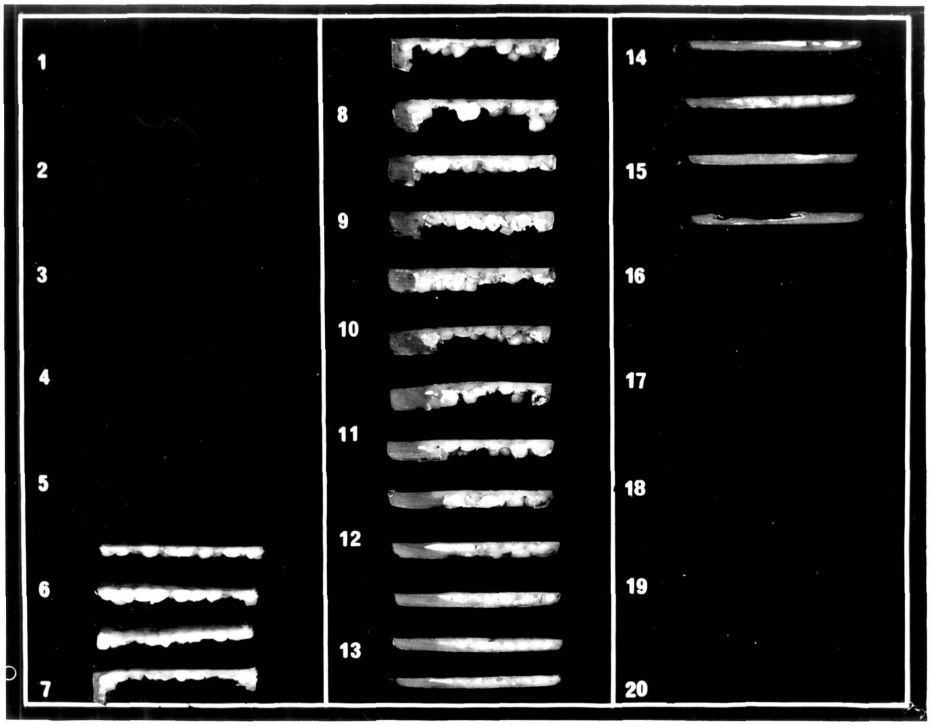


(a) Experiment 15: High Density Polyehthylene Granules
N(80); Q(187); D(3/32)

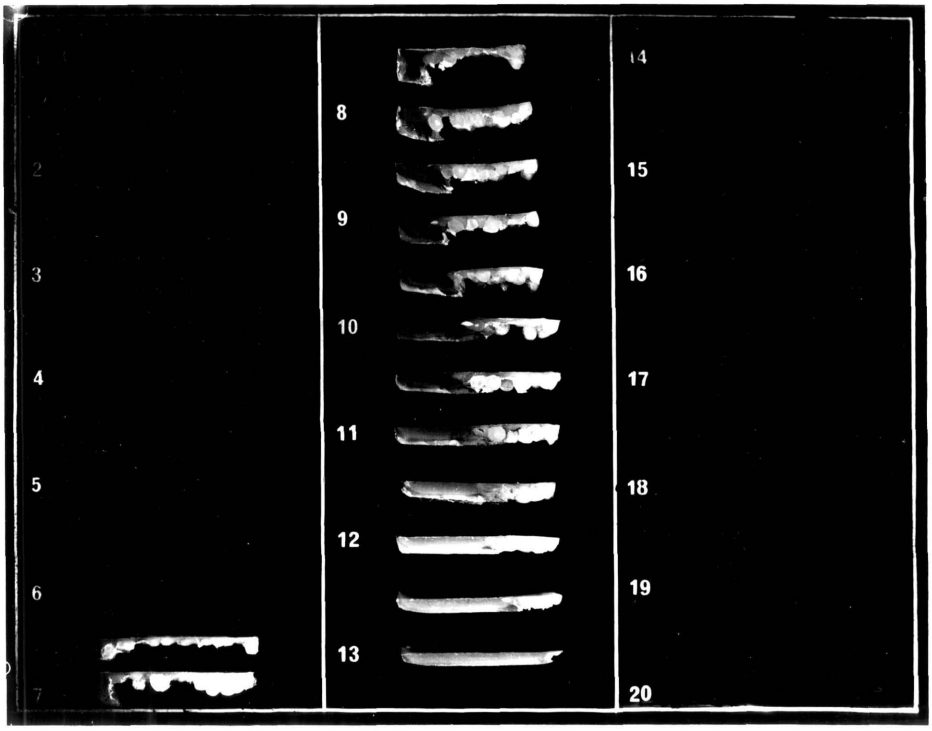


(b) Experiment 16: High Density Polyethylene Granules
N(40); Q(94); D(3/32)

PLATE 9

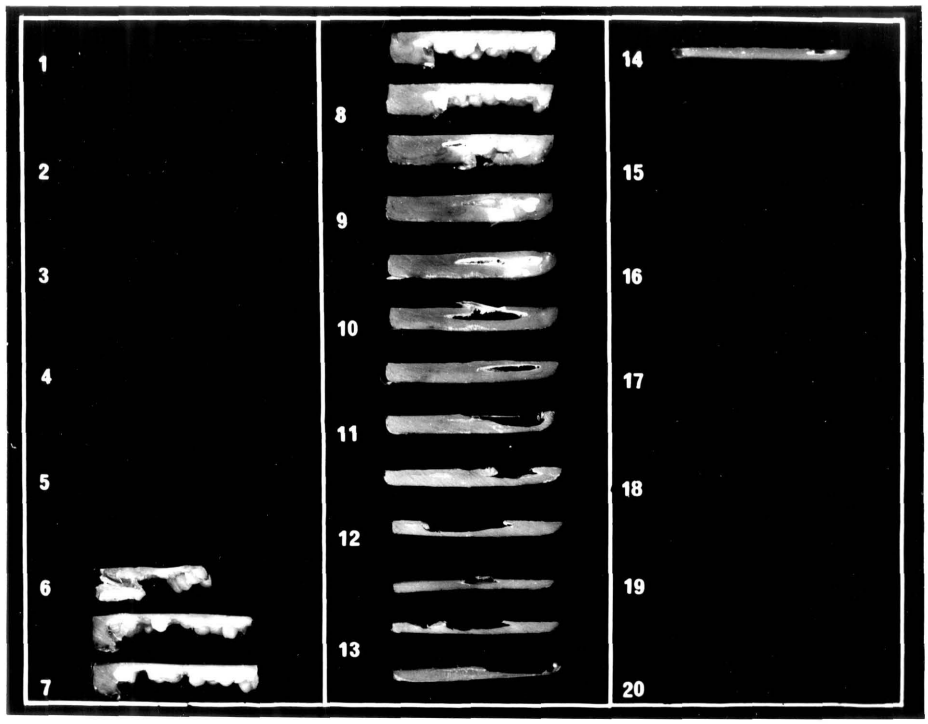


(a) Experiment 17: High Density Polyethylene Granules
N(80); Q(206); D(5/32)

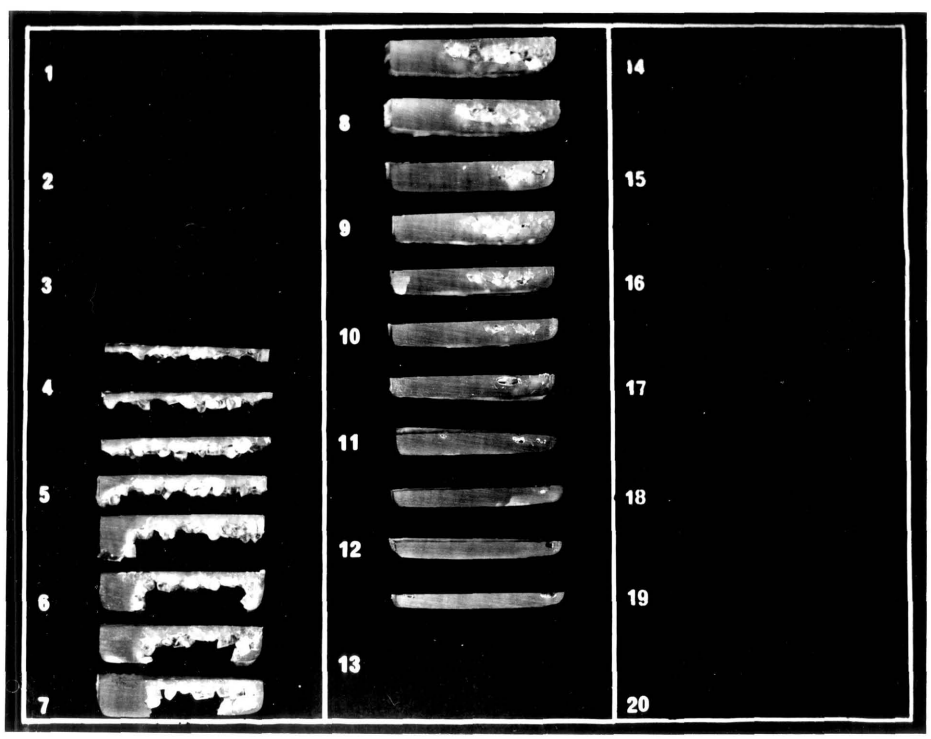


(b) Experiment 18: High Density Polyethylene Granules, with Screw Cooling
N(80); Q(137); D(3/32)

PLATE 10

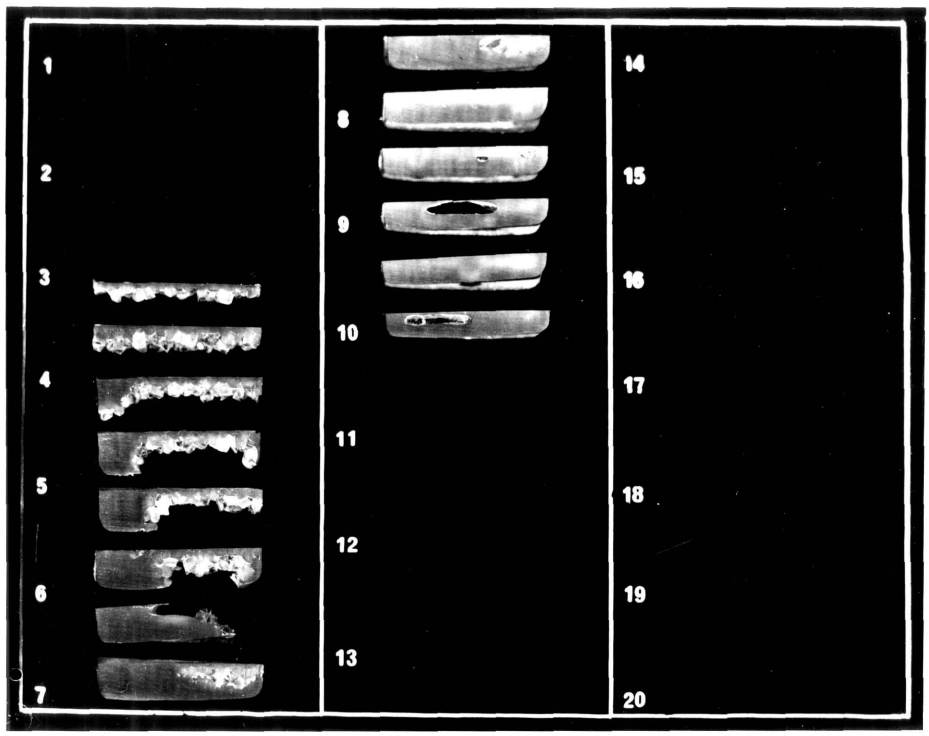


(a) Experiment 19: High Density Polyethylene Granules
N(40); Q(81); D(1/16)

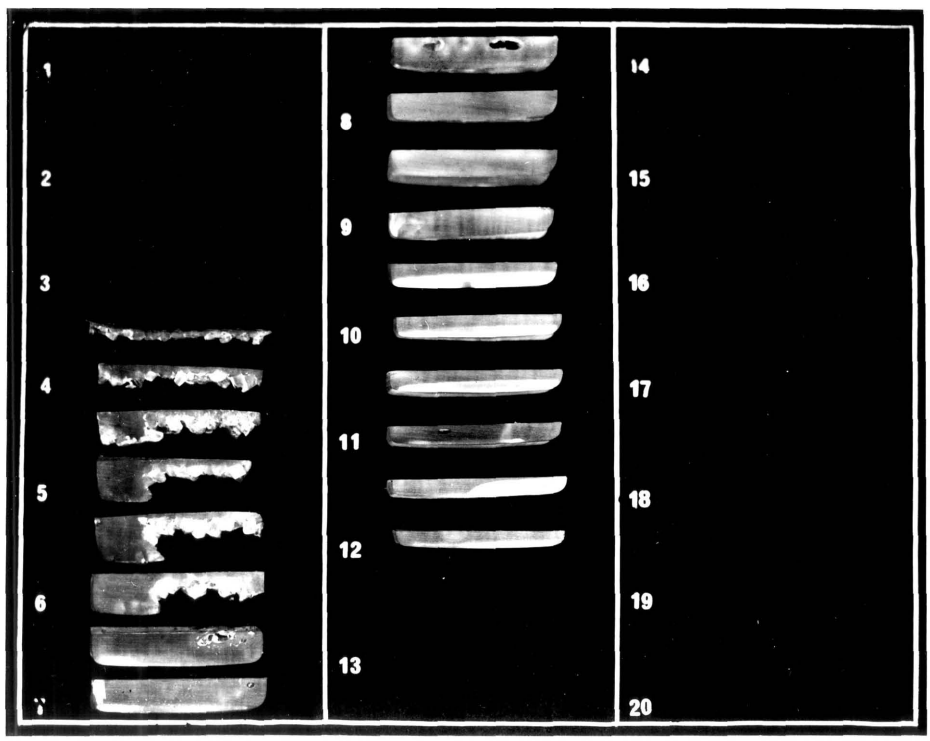


(b) Experiment 20: Polystyrene Granules
N(80); Q(266); D(5/32)

PLATE 11

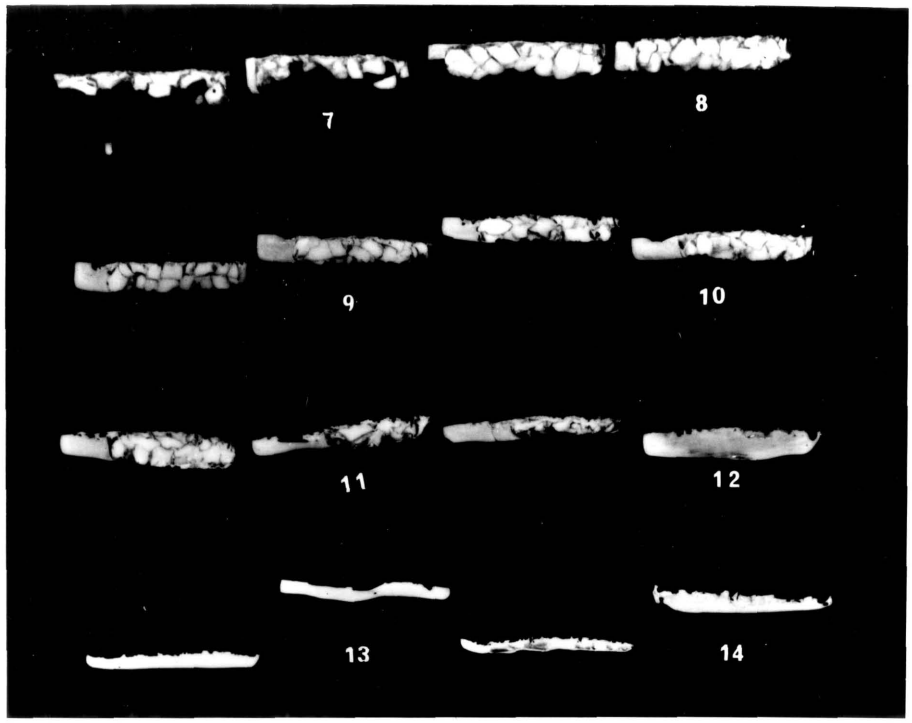


(a) Experiment 21: Polystyrene Granules
N(40); Q(110); D(3/32)

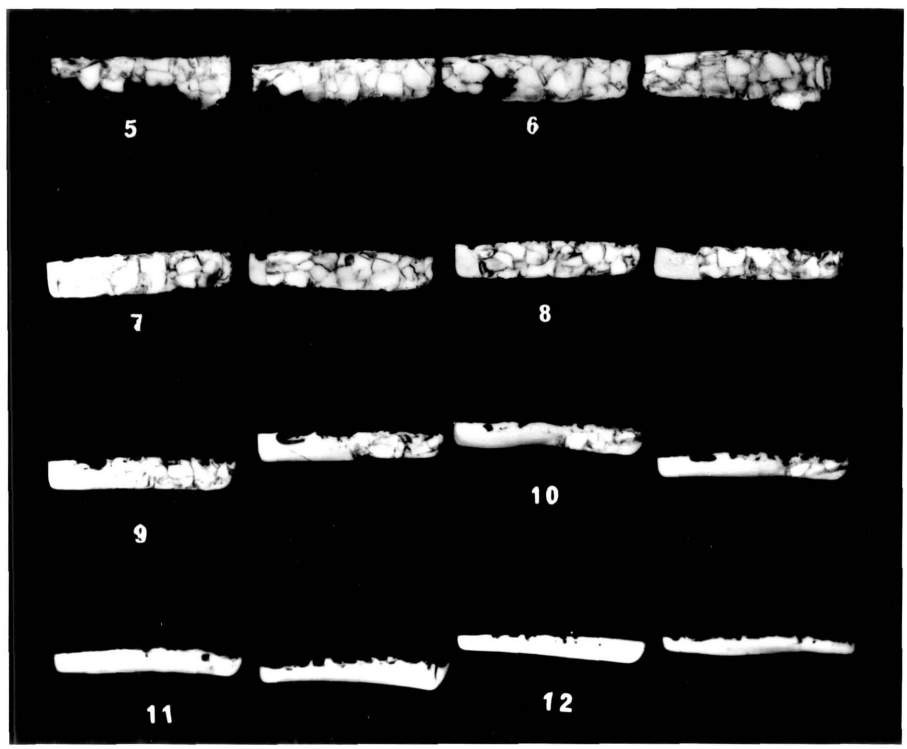


(b) Experiment 22: Polystyrene Granules
N(40); Q(128); D(1/16)

PLATE 12



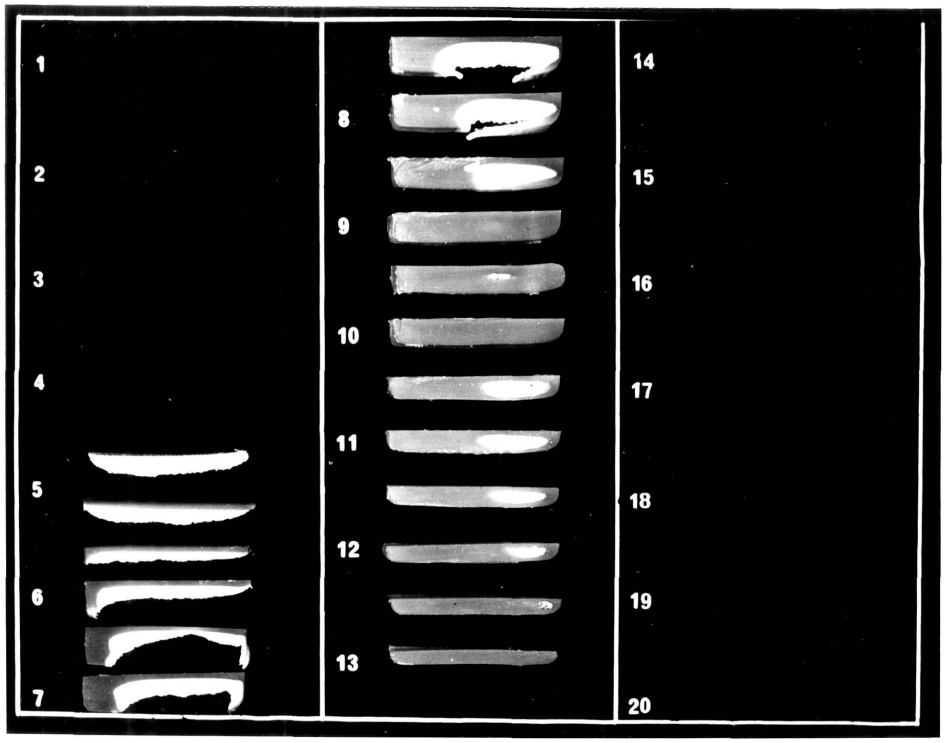
(a) Experiment 23: Polyethylene Terephthalate Granules
N(80); Q(319); D(3/32)



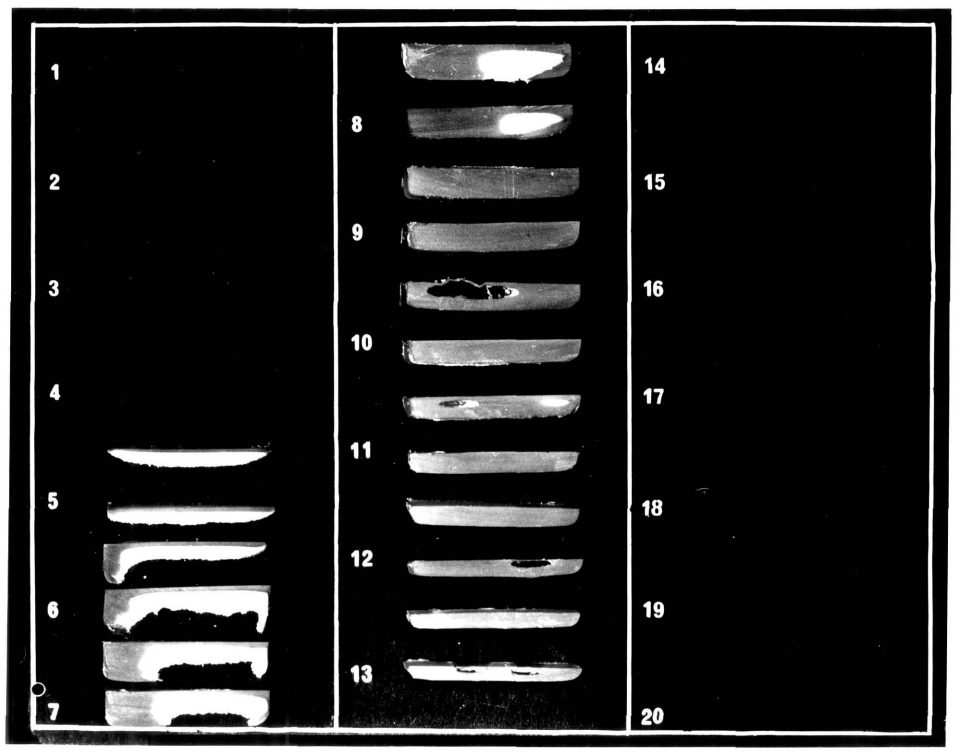
(b) Experiment 24: Polyethylene Terephthalate Granules
N(40); Q(164); D(3/32)

N.B. The above specimens are arranged in Rows not Columns

PLATE 13

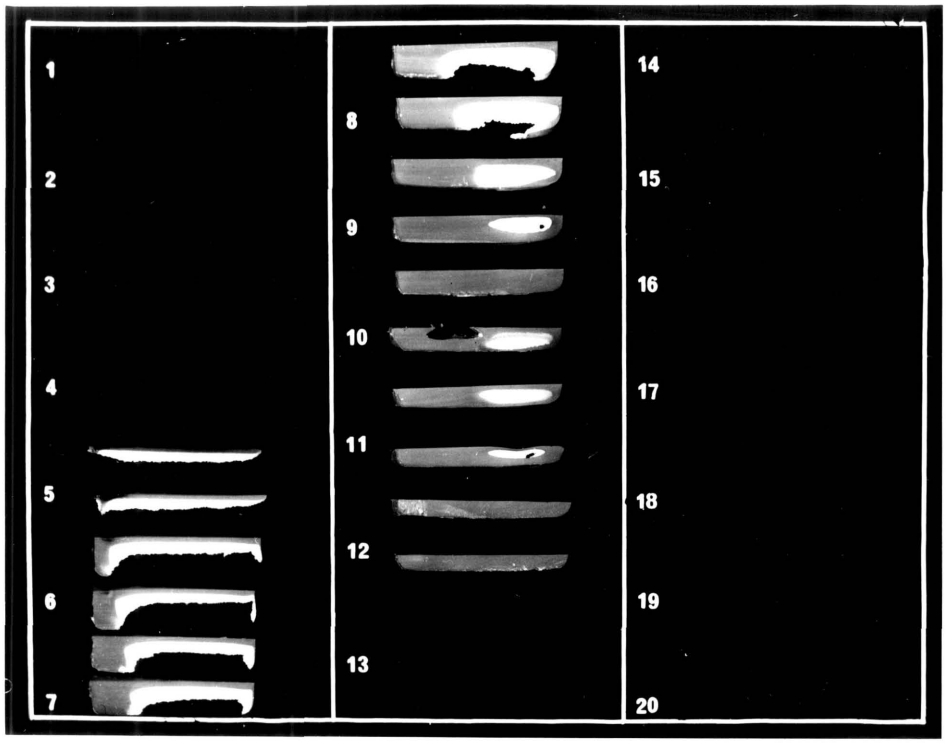


(a) Experiment 25: Low Density Polyethylene Powder
N(80); Q(203); D(3/32)

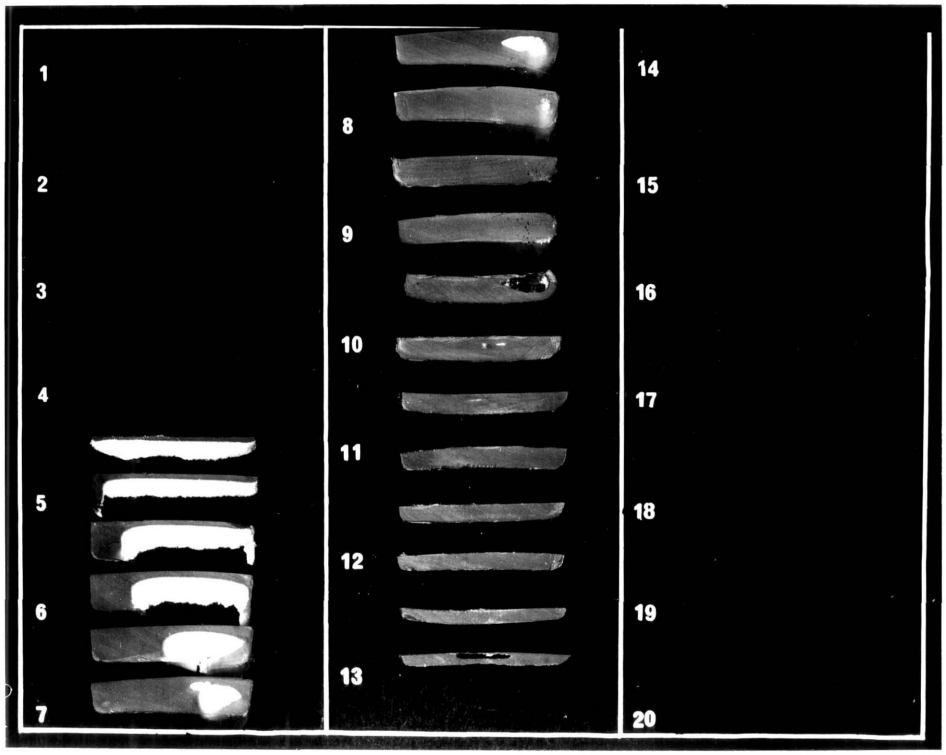


(b) Experiment 26: Low Density Polyethylene Powder
N(40); Q(115); D(3/32)

PLATE 14

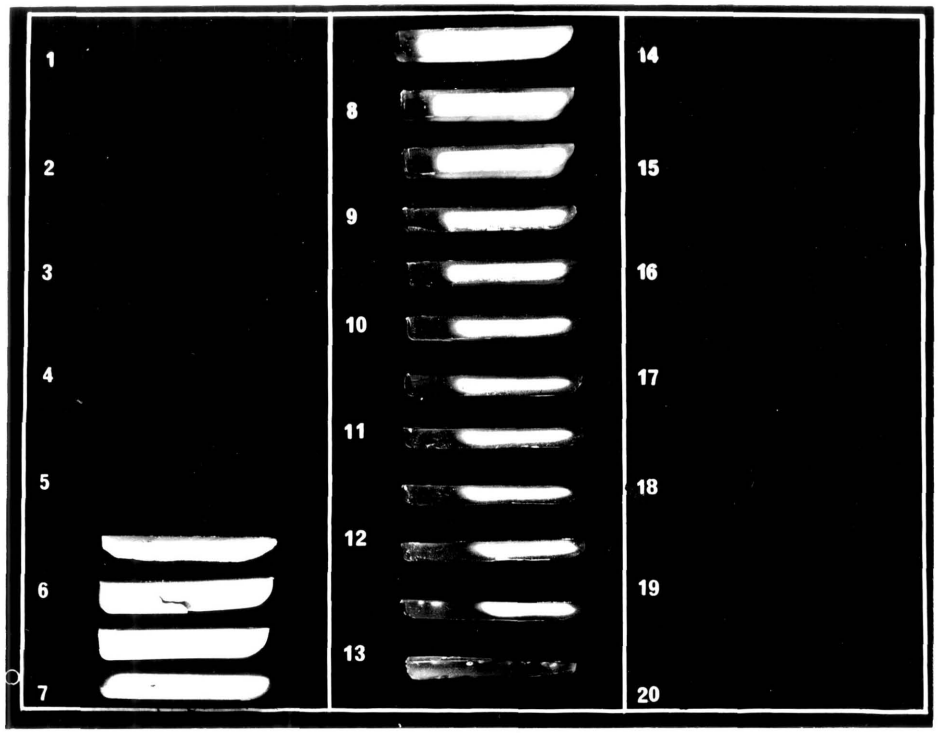


(a) Experiment 27: Low Density Polyethylene Powder
N(80); Q(221); D(5/32)

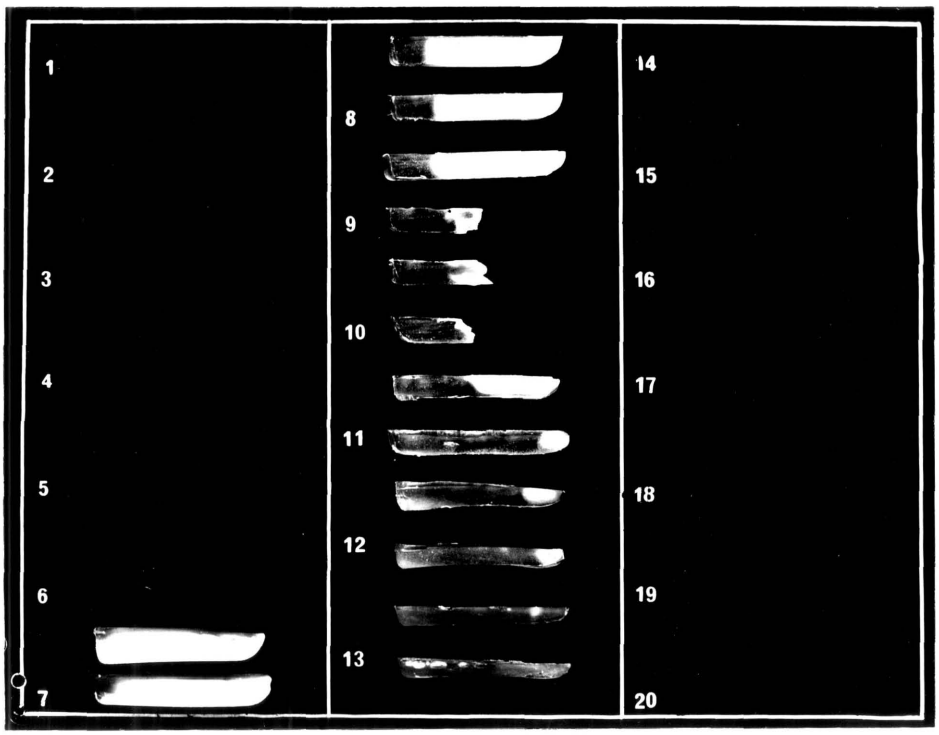


(b) Experiment 28: Low Density Polyethylene Powder
N(40); Q(78); D(1/16)

PLATE 15



(a) Experiment 29: Rigid Polyvinyl Chloride Powder
N(80); Q(419); D(3/32)



(b) Experiment 30: Rigid Polyvinyl Chloride Powder
N(40); Q(185); D(3/32)

Notation

Note: Greek symbols, sub-scripts and super-scripts are listed after the main list of symbols.

Symbol	Description	Units
A	coefficient of channel taper per unit axial length .	m/m
$[A]$	matrix of the coefficients of the variables, used in the energy analysis of the solid bed .	
$a(i,k)$	general term of matrix $[A]$.	
B	coefficient of channel taper per unit helical length .	m/m
$[B]$	matrix of the constants, used in the energy analysis of the solid bed .	
$b(i)$	general term of matrix $[B]$.	
b	flight land width or,	m
	coefficient of the temperature sensitivity of viscosity in the 'power law' constitutive equation.	deg C^{-1}
$[C]$	Matrix of the coefficients of the variables in the governing equations of the melting model .	
C_{ij}	general term of matrix $[C]$.	
C_m	specific heat at constant pressure of the molten material .	J/kg°C
C_s	specific heat at constant pressure of the solid material .	J/kg°C
D	screw diameter .	m
D_A	screw diameter used as a datum in the scale-up simulations .	m
$[D]$	matrix of the constants in the governing equations of the melting model .	
d_i	general term of matrix $[D]$.	
E	local constant value of the solid bed acceleration .	m/s^2
e	flight clearance .	m
F_d	Newtonian drag flow shape factor	

F_p	Newtonian pressure flow shape factor.	
G	pressure gradient, or	N/m^3
	Griffith number in Appendix B.	
H	metering section channel depth, or	m
	distance between the parallel boundaries of the melt film analysis, see Appendix B.	m
H_A	channel depth used as a datum in the scale-up simulations.	m
H_c	channel depth.	m
H_o	feed section channel depth.	m
H_s	solid bed depth.	m
I	number of nodal points of the finite difference grid used in the energy analysis of the solid bed in the y direction.	
i	nodal point index in finite difference grid, in the y direction.	
j	coordinate direction, variously defined.	
K	number of grid points in the z direction.	
k	nodal point index in finite difference grid, in the z direction.	
k_m	thermal conductivity of the molten material.	J/ms °C
k_s	thermal conductivity of the solid material.	J/ms °C
L	overall axial length of the screw.	m
L_S	mean length of broken pieces of solid bed.	m
L_M	maximum length of melt between pieces of solid bed.	m
l	axial coordinate.	
M	mass flow rate per unit length.	kg/ms
M_j	mass flow rate per unit length in the j direction	kg/ms
M_{lz}	mass flow rate per unit length in the z direction in the upper melt film.	kg/ms
M_{lx}	mass flow rate per unit length in the x direction in the upper melt film.	kg/ms

M_{2z}	mass flow rate per unit length in the z direction in the lower melt film.	kg/ms
M_{sz}	mass flow rate per unit length in the z direction for the solid bed.	kg/ms
M_{mz}	mass flow rate per unit length in the z direction for the melt pool.	kg/ms
M_{fx}	mass flow rate per unit length in the x direction through the flight clearance.	kg/ms
M_T	extruder out put rate, i.e., total mass flow rate in the z direction.	kg/s
M	mass flow rate through extruder.	kg/s
m	mass flow rate per unit length, referring to Newtonian flow.	kg/ms
m_{1x}	mass flow rate per unit length in the x direction for Newtonian flow in the upper melt film.	kg/ms
m_{1z}	mass flow rate per unit length in the z direction for Newtonian flow in the upper melt film.	kg/ms
N	screw speed.	r.p.m.
N_A	screw speed used as datum in the scale-up simulations.	r.p.m.
n	'power law' index or iteration number.	
P	pitch of screw.	m
P_e	Peclet number.	
p	pressure.	N/m^2
Q	volumetric flow rate.	m^3/s
Q^*	non-dimensional flow rate.	
Q^*_j	non-dimensional flow rate in the j direction.	
Q^*_{1j}	non-dimensional flow rate in the j direction for the upper melt film.	
Q^*_{2j}	non-dimensional flow rate in the j direction for the lower melt film.	
Q^*_{1x}	non-dimensional flow rate in the x direction for the upper melt film.	

Q^*_{1z}	non-dimensional flow rate in the z direction for the upper melt film.	
r	radial coordinate direction.	
T	temperature.	deg C
T_b	barrel temperature.	deg C
T_D	datum temperature for viscosity measurements.	deg C
T_m	melting point temperature.	deg C
T_o	initial temperature.	deg C
T_R	screw temperature.	deg C
T_S	solid bed temperature.	deg C
T_w	boundary temperature in melt film analysis.	deg C
T_1	upper melt film temperature.	deg C
T_2	lower melt film temperature.	deg C
T_1^*	non-dimensional upper melt film temperature.	
T_2^*	non-dimensional lower melt film temperature.	
T_S^*	non-dimensional solid bed temperature.	
T	mean periodicity of bed break-up.	sec
U	maximum velocity of the solid bed after fracture.	m/s
V	non-dimensional velocity.	
V_b	barrel velocity.	m/s
V_{bx}	barrel velocity component in the x direction.	m/s
V_{bz}	barrel velocity component in the z direction.	m/s
V_j	boundary velocity in the melt film analysis.	m/s
V_s	solid bed velocity.	m/s
V_{sy}	solid bed velocity component in the y direction.	m/s
V_{sz}	solid bed velocity component in the z direction.	m/s
V	solid bed velocity in the z direction calculated from the solids flow equation.	m/s
v_j	velocity in the j direction.	m/s
v_x	velocity component in the x direction.	m/s
v_y	velocity component in the y direction.	m/s
v_z	velocity component in the z direction.	m/s

W	channel width .	m
W_m	width of the melt pool .	m
W	solid bed velocity in the z direction at the point of fracture .	m/s
X	solid bed width .	m
x	coordinate direction across the channel .	
Y	non-dimensional y coordinate direction.	
Y_s	non-dimensional y coordinate direction in the solid bed .	
Y_1	non-dimensional y coordinate direction in the upper melt film .	
Y_2	non-dimensional y coordinate direction in the lower melt film	
y	coordinate direction .	
y_s	coordinate direction in the solid bed .	
y_1	coordinate direction in the upper melt film .	
y_2	coordinate direction in the lower melt film .	
Z	non-dimensional down-channel coordinate direction .	
z	down channel coordinate direction .	

Greek Symbols

α_s	thermal diffusivity of the solid .	m^2/s
β	angle of the resultant velocity between the solid bed and the barrel, to the z coordinate axis.	
γ_D	datum shear rate for the viscosity measurements .	sec^{-1}
$\bar{\gamma}$	mean shear rate .	sec^{-1}
δ	melt film thickness .	m
δ_1	upper melt film thickness .	m
δ_2	lower melt film thickness .	m
δ_A	analytically computed lower melt film thickness .	m
Δz	z direction step length in the numerical solution .	m

ΔY_S	non-dimensional Finite Difference grid spacing in the Y_S direction for the solid bed energy analysis.	
η	viscosity .	Ns/m^2
η_D	datum viscosity calculated at shear rate $\dot{\gamma}_D$ and temperature $\bar{T}_D$.	Ns/m^2
η_N	Newtonian constant viscosity .	Ns/m^2
Θ	Helix angle .	
λ	latent heat of fusion .	J/kg
λ_1	adjusted latent of fusion for the upper melting interface .	J/kg
λ_2	adjusted latent of fusion for the lower melting interface .	J/kg
μ	coefficient of coulomb friction between plastic and metal .	
ξ	ratio of adjacent grid spacings, ΔY_S , in the Finite Difference grid used in the solid bed energy analysis .	
π_H	non-dimensional viscous heating parameter .	
π_P	non-dimensional pressure gradient .	
π_Q	non-dimensional flow rate .	
ρ_m	density of molten material .	kg/m^3
ρ_s	density of solid material .	kg/m^3
τ	shear stress .	N/m^2
τ_{23}	shear stress in the z direction on the lower surface of the solid bed .	N/m^2
τ_{13}	shear stress in the z direction on the upper surface of the solid bed .	N/m^2
$\bar{\tau}$	mean shear stress .	N/m^2
$\bar{\tau}_1$	mean shear stress for the upper melt film.	N/m^2
$\bar{\tau}_2$	mean shear stress for the lower melt film .	N/m^2
τ^*_{1j}	non-dimensional shear stress in the j direction for the upper melt film .	

τ^*_{1x}	non-dimensional shear stress in the x direction for the upper melt film .	
τ^*_{1z}	non-dimensional shear stress in the z direction for the upper melt film	
τ^*_{2j}	non-dimensional shear stress in the j direction for the lower melt film ,	N/m^2
Ψ	general variable .	
$[\Psi]$	matrix of the general variables .	
ω	mass melting rate per unit area .	kg/m^2
ω_1	mass melting rate per unit area at the upper interface	kg/m^2
ω_2	mass melting rate per unit area at the lower interface	kg/m^2

Subscripts

Symbol	Description
A	refers to the 'scale-up' simulation .
b	refers to the barrel .
c	refers to the channel .
D	refers to a datum value .
f	refers to the screw flight clearance .
i	refers to a nodal point of the Finite Difference grid .
j	refers to the j coordinate direction .
k	refers to a nodal point of the Finite Difference grid .
m	refers to the molten material .
o	refers to an initial value .
R	refers to the screw .
s	refers to the solid material .
x	refers to the x coordinate direction.
y	refers to the y coordinate direction .
z	refers to the z coordinate direction .
1	refers to the upper melt film .
2	refers to the lower melt film .

Superscripts

Symbol	Description
$'$	refers to the first derivative with respect to z.
$\bar{}$	refers to mean value.
$*$	denotes non-dimensional quantity.

References

1. Street, L., Modern Plastics, 30, 130 (1953)

2. Maddock, B.H.; 'A visual Analysis of Flow and Mixing in Extruder Screws.' SPE J., 15, 383 (1959)

3. Street, L.; 'Extrusion Plastification'. International Plastics Eng., 1, 289 (1961)

4. Tadmor,Z.; 'Fundamentals of Plasticating Extrusion'. Polymer Eng. Sci., 6, 185 (1966)

5. Tadmor,Z., Duvdevani, I.J., and Klein, I.; 'Melting in Plasticating Extruders-Theory and Experiments.' Polymer Eng. Sci., 7, 198 (1967)

6. Menges,G. and Klenk, P.; 'Melting and Plasticization of Unplasticized PVC Powder in the Single Screw Extruder.' Kunststoffe, 57, 598 (1967)

7. Chung, Chan I. 'A New Theory for Single Screw Extrusion - Part 1'. Modern Plastics, 45, 178 (1968)

8. Tadmor, Z. and Klein, I.; 'The effect of Design and Operating Conditions on Melting in Plasticating Extruders'. Polymer Eng. Sci., 9, 1 (1969)

9. Martin, G.; 'The Determination of Melting Zone Length in a Single Screw Extruder'. Kunststofftechnik, 7, 238 (1969) RAPRA translation number 1716.

10.Donovan, R.C.; 'A Theoretical Melting Model for Plasticating Extruders'. Polymer Eng. Sci., 11, 247 (1971)

11.Hinricks, D.R. and Lilleleht, L.U.; 'A Modified Melting Model for Plastifying Extruders'. Polymer Eng. Sci., 10, 268 (1970)

12.Donovan, R.C.; 'Pressure Profiles in Plasticating Extruders'. Polymer Eng. Sci., 11, 484 (1971)

13.Vermeulen, J.R., Scargo, P.G. and Beek, W.J.; 'The Melting of a Crystalline Polymer in a Screw Extruder'. Chem. Eng. Sci., 26, 1457 (1971)

14. Ingen Housz,J.F.and Gorissen,W.C.M.Private Communication, 1972

15.Tadmor,Z and Klein,I.; 'Engineering Principles of Plasticating Extrusion'. Published by Van Nostrand Reinhold, 1970.

16.Rousselet, J.P.; 'Analysis of Melting Processes in Single Screw Extruder'. 30th ANTEC SPE, 1972

17.Van Leevan,J., 'Stock Temperature Measurement in Plastifying Equipment'.

Polymer Eng. Sci., 7, no2, 98 (1967)

18. Marshall, D.I., Klein,I. and Uhl, R.H. Plastics Eng. J., 21 , 1192 (1965)

19. Klein, I. SPE J., 28, No 8, 47 (1972)

20. Stevens, M.J.; 'The Melting Process in Screw Extruders'. Plastics and Polymers, April 1970, 107

21. Pearson, J.R.A., 'Mechanical Principles of Polymer Melt Processing' Pergamon Press Ltd., 1966.

22. Palit.K, 'Melt Flow in Polymer Processing'. Ph.D. Thesis, Imperial College, London University, 1972

23. Darnell,W.H. and Mol, E.A.J. 'Solids Conveying in Extruders'. S.P.E. J, 12, no. 4, 20 (1956)

24. Lovegrove, J. 'Solids Flow in a Polymer Extruder' Ph.D. Thesis, Imperial College, London University, 1972

25. Broyer, E. and Tadmor, Z.; 'Solids Conveying in Screw Extruders. Part 1: A Modified Isothermal Model'. Polymer Eng. Sci., 12,12 (1972)

26. Tadmor,Z. and Broyer, E.; 'Solids Conveying in Screw Extruders Part 2: Non Isothermal Model'. Polymer Eng. Sci., 12 , 378, (1972)

27. Zamodits, H.T. 'Extrusion of Thermoplastics' Ph.D. Thesis Cambridge University, 1964.

28. Martin, B. 'Numerical Studies of Steady State Extrusion Process'. Ph.D. Thesis, Cambridge University, 1969.

29. Fenner, R.T. 'Extruder Screw Design'. Published by Iliffe, 1970.

30. Maddock, B.H. SPE J., 23 , July 1967

31. Kosel, U.M., Plastics and Polymers, Oct. 1971

32. Gale, G.M.; 'Dry-Blend Extrusion of rigid PVC'. Plastics and Polymers, June 1970

33. Martin, B. Int. J. Non-Linear Mechanics, 2, 285 (1967)

34. Shapiro, J. private Seminar, Cambridge University, 1970.

35. Martin, B.; 'Heat Transfer Coupling Effects between a Dissipative Fluid Flow and its Containing Metal Boundaries'. (With particular reference to problem in the screw extrusion of polymer melts.) Report for the European Working Party on Polymer Processing, 1970

36. Rowell, H.S. and Finlayson, D. Engineering, 126 , 249 (1928)

37. Özişik, M.N. 'Boundary Value Problems of Heat Conduction'. Published by the International text book company 1968

38. Sundstrom, D.W. and Young, Chi-Chang. 'Melting Rates of Crystalline Polymers under Shear Conditions'. Polymer Eng. Sci., 12 , 59 (1972)

39. Fenner, R.T., private communication.

40. Fenner, R.T. and Williams, J.G. 'Some Melt Flow and Mechanical Design Aspects of Large Extruders'. Polymer Eng. Sci., 11, 474 (1971)

41. Tadmor, Z. and Broyer, E. 'Solids Conveying in Screw Extruders Part 2: Non Isothermal Model'. Polymer Eng. Sci., 12 , 378, 1972

42. Kacir, L. and Tadmor,Z. 'Solids Conveying in Screw Extruders Part 3: The Delay Zone'. Polymer Eng. Sci., 12, 387, 1972

43. Chung, Chan I.; 'New ideas about Solids Conveying in Screw Extruders'. SPE J., 26, 32 (1970)

44. Van Wazer, J.R., Lyons, J.W., Kim, K.Y. and Colwell, R.E.;'Viscosity and Flow Measurement'. Interscience, New York, 1963

45. Tharmalingham, R. 'A Transient Method of Measuring Thermal Contact Conductance between metal-plastic surfaces'. M.Sc. Thesis, University of Aston in Birmingham, 1972.

Appendix A

A Calculation of the melting rate of plastic by conduction of residual heat in the extruder during the cooling down period.

The problem whose solution is developed here is a simplified approximation to the real situation. The simplified problem is defined as follows. Initially a semi-infinite solid at uniform temperature, T_o, is in contact with a boundary at temperature T_{bo}, which is greater than the melting temperature of the solid T_m. It is required to find at what rate the melting interface advances from the boundary, given that at time $t = 0$, the thickness of the molten layer is zero and the temperature of the boundary, T_b, decreases exponentially as t increases. It is assumed that the temperature profile in the molten layer is always linear. The situation is illustrated in figure A1.

The symbols used in this appendix are defined as they are introduced. For the most part they are consistant with the main text but are not necessarily so.

The position of the interface in y_m co-ordinate direction whose zero is taken at the fixed boundary, is given by $y_m = S$, where S is a function of t.

A heat balance at the melting interface at time t gives

$$\omega \lambda' = k_m \left. \frac{dT}{dy_m} \right|_{y_m = S} \qquad (A1)$$

where ω is the mass of material melting per unit area per unit time at the interface

k_m is the thermal conductivity of the melt

T is the temperature of the melt

$$\lambda' = \lambda + c_s (T_m - T_o) \qquad (A2)$$

where λ is the latent heat of fusion

c_s is the specific heat of the solid

The temperature gradient in the molten layer is given by

$$\frac{dT}{dy_m} = \frac{T_b(t) - T_m}{S(t)} \qquad (A3)$$

Also $$\omega = \frac{dS'}{dt} \cdot \rho_s \qquad (A4)$$

where ρ_s is the solid density

Substituting equations (A2), (A3) and (A4) into equation (A1) gives

$$S \frac{dS'}{dt} = \frac{k_m (T_b - T_m)}{\rho_s (\lambda + c_s (T_m - T_o))} \qquad (A5)$$

The exponential decay of the boundary temperature T_b is assumed to be of the following form

$$T_b = T_{bo} \exp(Bt) + T_o (1 - \exp(Bt)) \qquad (A6)$$

where $$B = \frac{1}{\tau} \ln \left(\frac{T_m - T_o}{T_{bo} - T_o} \right) \qquad (A7)$$

where τ is the time taken for the boundary temperature to drop from T_{bo} to T_m

Substituting into equation (A5) for T_b from equation (A6) gives

$$S \frac{dS}{dt} = K \exp(Bt) (T_{bo} - T_o) + K(T_o - T_m) \qquad (A8)$$

where $$K = k_m / \rho_s (\lambda + c_s (T_m - T_o)) \qquad (A9)$$

performing the integration in equation (A8) yields

$$S^2 = - \frac{2K (T_{bo} - T_o) \exp(Bt)}{B} + 2K(T_o - T_m)t + 2K(T_{bo} - T_o)/B \qquad (A10)$$

as $S = 0$ at $t = 0$

The results of this calculation are best presented showing S as a function of τ, that is, how the thickness of the molten layer that is generated in the time taken to cool the boundary down from its initial temperature to the melting temperature of the material, varies with this cooling down time.

Thus equation (A10) becomes

$$S^2(\tau) = 2K(T_{bo} - T_m)/B + 2K\tau(T_o - T_m) \qquad (A11)$$

Substituting into equation (A11) for B from equation (A7) and for K from equation (A9) gives

$$S^2(\tau) = \frac{2.k_m \tau}{\rho_s(\lambda + c_s(T_m - T_o))}\left[\frac{T_m - T_{bo}}{\ln\left(\frac{T_m - T_o}{T_{bo} - T_o}\right)} + T_o - T_m\right] \quad (A12)$$

which may be written as

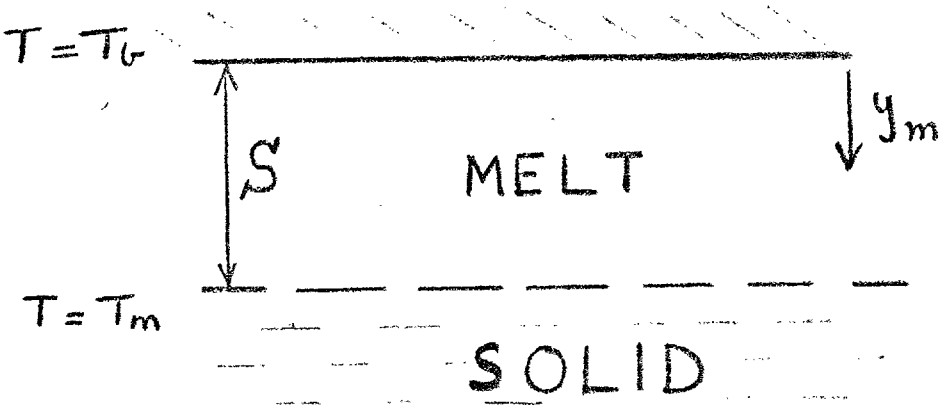
$$S(\tau) = K_1 \tau^{1/2} \quad (A13)$$

where,

$$K_1 = \left\{\frac{2.k_m}{\rho_s(\lambda + c_s(T_m - T_o))}\left[\frac{T_m - T_{bo}}{\ln\left(\frac{T_m - T_o}{T_{bo} - T_o}\right)} + T_o - T_m\right]\right\}^{\frac{1}{2}} \quad (A14)$$

The results of this calculation are shown in figure 2.14 of the main text for a low density polyethylene experiment.

A1 The solution domain



Appendix B:

An analytical Solution for Non-Newtonian, Non-isothermal, drag flow between infinite parallel plates.

The problem is, given a drag flow (zero pressure gradient) with constant shear stress, τ , power law viscosity with exponential temperature dependence, find τ , the boundary temperature gradients and the volumetric flow rate in fully developed flow.

The method of solution is based on that developed by Martin (33).

In the melting application the upper boundary (see figure B.1) is the metal surface, screw or barrel,and the lower boundary is the solid bed whose surface temperature is the melting point, T_m . The normal to the solid bed is the co-ordinate y , and j is the direction of the resultant velocity of the upper surface relative to the lower, V_j . The gap between the surfaces is H , and $v_j(y)$ is the velocity in the j direction.

The boundary conditions are,

$$\begin{aligned} &\text{velocity : } v_j(0) = 0 \;\; ; \;\; v_j(H) = V_j \\ &\text{temperature } T(0) = T_m \;\; ; \;\; T(H) = T_w \end{aligned} \qquad (B1)$$

The simplified form of the power law constitutive equation with temperature dependence, applicable to the present problem is,

$$\tau = \eta_D \left| \frac{1}{\gamma_D} \cdot \frac{dv_j}{dy} \right|^{n-1} \cdot \frac{dv_j}{dy} \cdot \exp\left[-b(T-T_D)\right] \qquad (B2)$$

It should be noted that the nomenclature of this appendix does not consistently follow that used in the main text.

The form of the energy equation applicable here is

$$k \cdot \frac{d^2T}{dy^2} = -\tau \frac{dv_j}{dy} \qquad (B3)$$

In the present solution; $\operatorname{sgn}\left(\frac{dv_j}{dy}\right) = \operatorname{sgn}(V_j)$ (B4)

The following dimensionless variables are introduced

$$\left.\begin{aligned} Y &= y/H \\ V &= v_j/V_j \\ T^* &= b(T-T_m) \\ S &= \tau/\bar{\tau} \end{aligned}\right\} \qquad (B5)$$

where,

$$\bar{\tau} = \eta_D \left| \frac{1}{\gamma_D} \cdot \frac{V_j}{H} \right|^{n-1} \cdot \frac{V_j}{H} \exp\left(-b(T_m - T_D)\right) \qquad (B6)$$

Hence the non-Dimensional shear stress, S , is written as

$$S = \left(\frac{dV}{dY}\right)^n \exp(-T^*) \qquad (B7)$$

And equation (B3) becomes

$$\frac{k}{b H^2} \cdot \frac{d^2T^*}{dY^2} = -S \cdot \bar{\tau} \cdot \frac{dV}{dY} \cdot \bar{\gamma} \qquad (B8)$$

where $\bar{\gamma} = V_j/H$

Defining the 'Griffith Number', G , as

$$G = b H^2 \bar{\tau} \bar{\gamma} / k \qquad (B9)$$

and substituting for this in equation (B8) gives

$$\frac{d^2T^*}{dY^2} = -G \cdot S \cdot \frac{dV}{dY} \qquad (B10)$$

From equation (B7)

$$\frac{dV}{dY} = S^{\frac{1}{n}} \exp(T^*/n) \qquad (B11)$$

Hence equation (B10) becomes

$$\frac{d^2T^*}{dY^2} = -G \cdot S \cdot S^{\frac{1}{n}} \cdot \exp(T^*/n)$$

$$= \frac{dT^*}{dY} \cdot \frac{d}{dT^*}\left(\frac{dT^*}{dY}\right) \qquad (B12)$$

Hence,

$$\left(\frac{dT^*}{dY}\right)^2 = 2 G n S^{\frac{1+n}{n}} \left[\exp(T_T^*/n) - \exp(T^*/n)\right] \qquad (B13)$$

where $dT^*/dY = 0$ at $T^* = T_T^*$

Following the method of Martin, the following substitution is used

$$\cosh^2 \phi = \exp\left(\frac{T_T^* - T^*}{n}\right) \qquad (B14)$$

Thus equation (B13) becomes

$$\frac{d\phi}{dY} = \pm \sqrt{\frac{G}{2n}} \cdot S^{\frac{1+n}{n}} \exp\left(T_T^*/2n\right) \qquad (B15)$$

The sign of $d\phi/dY$ is arbitrary because the sign of ϕ is arbitrary and one may choose the positive root, thus

$$\frac{d\phi}{dY} = B.S^{\frac{1+n}{n}}.A \tag{B16}$$

where,

$$B = \sqrt{G/2n} \tag{B17}$$

$$A = \exp(T_T^*/2n)$$

Thus integrating equation (B16) gives

$$\phi = B.S^{\frac{1+n}{2n}}.A.Y + C \tag{B18}$$

Back substituting into equation (B14) to regain the original variable gives,

$$A^2 \exp(-T^*/n) = \cosh^2(B S^{\frac{1+n}{2n}} A.Y + C) \tag{B19}$$

Substituting from equation (B19) into equation (B11) gives,

$$\frac{dV}{dY} = \frac{S^{\frac{1}{n}} A^2}{\cosh^2(B S^{\frac{1+n}{2n}} A Y + C)} \tag{B20}$$

let

$$F_Y = B.S^{\frac{1+n}{2n}} A Y + C \tag{B21}$$

and

$$F = [F_Y]_{Y=1}$$

Therefore,

$$V = \frac{S^{\frac{1}{n}} A}{B.S^{\frac{1+n}{2n}}} .\tanh F_y + \text{constant} \tag{B22}$$

and since $V(0)=0$ and $V(1)=1$

$$1 = \frac{A}{B}.S^{\frac{1-n}{2n}}(\tanh F - \tanh C) \tag{B23}$$

There are three unknowns, S, A and C, and so far only equation (B23) relating them. The other two equations are obtained from the boundary conditions.

From (B1), $T(0) = T_m$

Therefore, $T^*(0) = 0$

Hence from Equation (B19),

$$A^2 = \cosh^2 C \tag{B24}$$

From Equation (B17) A is positive, thus

$$A = \cosh C \tag{B25}$$

Eliminating A from Equations (B23) and (B25) gives

$$B = S^{\frac{1-n}{2n}} \cosh C \left(\tanh F - \tanh C \right) \qquad \text{(B26)}$$

where, now

$$F = B \, S^{\frac{1+n}{2n}} \cosh C + C \qquad \text{(B27)}$$

Again from B1,

$$T^*(1) = b(T_w - T_m) = T_1^*, \text{ say.} \qquad \text{(B28)}$$

Applying this boundary condition to Equation (B19) gives

$$A^2 \exp(-T_1^*/n) = \cosh^2 F \qquad \text{(B29)}$$

Let $$E = \exp(-T_1^*/n) \qquad \text{(B30)}$$

Therefore,

$$E \cosh^2 C = \cosh^2 F = \frac{1}{1 - \tanh^2 F} \qquad \text{(B31)}$$

Re-arranging Equation (B26) gives

$$\tanh F = \frac{B}{\cosh C \, S^{\frac{1-n}{2n}}} + \tanh C \qquad \text{(B32)}$$

Combining Equations (B31) and (B32) gives, after suitable manipulation

$$\sinh C = \frac{S^{\frac{1-n}{2n}}}{2B} \left[1 - E^{-1} - \frac{B^2}{S^{\frac{1-n}{n}}} \right] \qquad \text{(B33)}$$

This equation, given S, finds C uniquely.

From Equation (B31)

$$\sqrt{E} \cosh C - \cosh F = 0 \qquad \text{(B34)}$$

where F and C are given by Equations (B27) and (B33).

Thus Equation (B34) can be written in terms of constants, boundary conditions and S only. However it cannot be analytically solved for S but is amenable to the Newton Raphson numerical method provided reasonable initial estimates of S are available. Such estimates are available from the Newtonian solution, which is a special case of the above results.

For $n = 1$, Equation (B33) becomes,

$$C = \sinh^{-1} \left[\frac{1}{2B} \left(1 - E^{-1} - B^2 \right) \right] \qquad \text{(B35)}$$

and from Equation (B27)

$$S = \frac{F - C}{B.\cosh C} \tag{B36}$$

where,

$$F = \tanh^{-1}\left[\frac{B}{\cosh C} + \tanh C\right] \tag{B37}$$

Thus the Newtonian value of the shear stress is calculated from the above relationships and is used as the starting value for the Newton Raphson numerical solution for the required non-Newtonian shear stress. It remains now to derive expressions for the other relevant quantities.

Firstly, the temperature gradient at the solid bed, i.e., at the stationary boundary,

$$T^*_{Y_o} = \left(\frac{dT^*}{dY}\right)_{Y=0}$$

From Equation (B19)

$$-\frac{A^2}{n}.\exp\left(-T^*_m/n\right)\left(\frac{dT^*}{dY}\right) = A.B.S^{\frac{1+n}{2n}}\sinh(2C) \tag{B38}$$

Therefore,

$$T^*_{Y_o} = -\frac{n\,B\,S^{\frac{1+n}{2n}}.\sinh(2C)}{A} \tag{B39}$$

Using Equation (B25),

$$T^*_{Y_o} = -2n\,B\,S^{\frac{1+n}{2n}}\sinh C \tag{B40}$$

Secondly, the volumetric flow rate Q^*, defined as

$$Q^* = \int_0^1 V\,dY \tag{B41}$$

From Equation (B22)

$$V = \frac{A}{B}S^{\frac{1-n}{2n}}\left[\tanh\left(B.S^{\frac{1+n}{2n}}.A.Y + C\right) - \tanh(C)\right] \tag{B42}$$

Hence,

$$Q^* = \frac{A}{B}.S^{\frac{1-n}{2n}}.\left[\frac{1}{A.B.S^{\frac{1+n}{2n}}}\ln\left(\frac{\cosh F}{\cosh C}\right) - \tanh(C)\right] \tag{B43}$$

Lastly, the mean convected temperature, $\bar{T}^*$, defined as

$$\bar{T}^* = \frac{\int_0^1 V T^* dY}{\int_0^1 V dY} = \frac{\int_0^1 V T^* dY}{Q^*} \qquad (B44)$$

From Equations (B42) and (B19)

$$\bar{T}^* = \left\{ -n \int_0^1 \frac{A}{B} \cdot S^{\frac{1-n}{2n}} \left[\tanh\left(B \cdot S^{\frac{1+n}{2n}} A Y + C\right) - \tanh C \right] \cdot \ln\left[\frac{\cosh^2\left(B \cdot S^{\frac{1+n}{2n}} A Y + C\right)}{\cosh^2 C} \right] \right\} \Big/ Q^* \qquad (B45)$$

A numerical technique is employed to evaluate the integral.

Finally the dimensional quantities corresponding to the non-dimensional ones calculated in the analysis are as follows

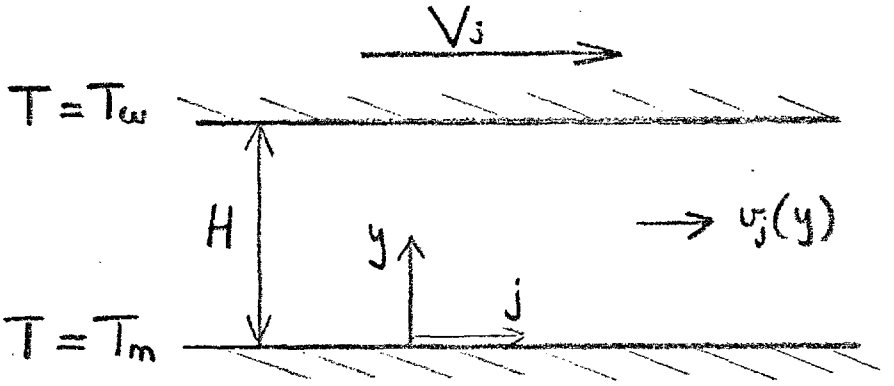
$$\tau = \bar{\tau} S \qquad (B46)$$

$$\left(\frac{dT}{dy}\right)_{y=0} = \frac{T_{vo}^*}{b H} \qquad (B47)$$

$$Q = \int_0^H v_j \, dy = V_j H Q^* \qquad (B48)$$

$$\bar{T} = \frac{\bar{T}^*}{b} + T_m \qquad (B49)$$

B1 The flow domain



Appendix C:

A simple analytical calculation of the initial developement of a melt film.

The situation is illustrated in Figure C1. The assumption is made that the fluid is Newtonian constant viscosity, and that the fluid flow is thermally fully developed so that the non-dimensional temperature profile is not a function of the thickness of the molten layer. The analysis is presently applied to the lower melt film and it is assumed that the solid bed velocity is constant for the purposes of this analysis.

The temperature profile in a constant viscosity fluid between two parallel plates at different velocities and temperatures may be derived as

$$\frac{T - T_m}{T_R - T_m} = \frac{\eta_N \cdot V_{sz}^2}{2 k_m (T_R - T_m)} \cdot \frac{y_2}{\delta_2}\left(1 - \frac{y_2}{\delta_2}\right) + \frac{y_2}{\delta_2} \qquad (C1)$$

where the boundary conditions are given as

$$\left.\begin{array}{lll} \text{Temperature :} & T = T_m \text{ at } y_2 = 0 \\ & T = T_R \text{ at } y_2 = \delta_2 \\ \text{Velocity} & v_z = 0 \text{ at } y_2 = 0 \\ & v_z = -V_{sz} \text{ at } y_2 = \delta_2 \end{array}\right\} \qquad (C2)$$

Assuming the solid bed to be at a uniform temperature, T_o, then an energy balance at the melting interface gives

$$\omega \lambda_2 = k_m \left(\frac{dT}{dy_2}\right)_{y_2 = 0} \qquad (C3)$$

From Equation (C1) we have

$$\left(\frac{dT}{dy_2}\right)_{y_2 = 0} = \frac{(T_R - T_m)}{\delta_2} + \frac{\eta_N V_{sz}^2}{2 \delta_2 k_m} \qquad (C4)$$

Combining Equations (C3) and (C4) gives

$$\omega \lambda_2 = \frac{k_m}{\delta_2}(T_R - T_m) + \frac{\eta_N V_{sz}^2}{2 \delta_2} \qquad (C5)$$

Now, ω, may be written as

$$\omega = \rho_s \cdot \frac{d\delta_2}{dt} \qquad (C6)$$

Substituting into Equation (C5) for ω gives

$$\frac{d\delta_z}{dt} = \frac{1}{\rho_s \lambda_z \delta_z}\left[k_m (T_R - T_m) + \frac{\eta_N \cdot V_{sz}^2}{2}\right] \qquad (C7)$$

Integrating this equation, assuming that only δ_z is a function of t gives

$$\delta_z(t) = \left[\frac{2 k_m (T_R - T_m) + \eta_N V_{sz}^2}{\rho_s \lambda_z}\right]^{\frac{1}{2}} \cdot t^{\frac{1}{2}} \qquad (C8)$$

as $\delta_z = 0$ at $t = 0$

C1 The solution domain

